Albert-Ludwigs Universität Freiburg

Chair of Hydrology

Master Thesis

Influence of bioeconomy-based landuse on different soilhydrological functions

Anneke Okka Döring

First supervisor:

Prof. Dr. Markus Weiler

Second supervisor:

Prof. Dr. Friederike Lang

Freiburg im Breisgau, December 2015

Ehrenwörtliche Erklärung

Hiermit erkläre ich, Anneke Okka Döring, dass die vorliegende Arbeit mit dem Titel „Influence of bioeconomy-based landuse on different soilhydrological functions", selbständig und nur unter Verwendung der angegebenen Hilfsmittel angefertigt wurde.

Ort, Datum: _____

Unterschrift: _____

Abstract

Influence of bioeconomy-based landuse on different soilhydrological functions

In order to examine soil hydraulic properties of short rotation coppices (SRCs) in comparison to grassland or intensively cultivated arable sites, an inverse modeling approach is applied on seven sampling sites in Baden-Wuerttemberg. Soil drilling cores were taken and the pore water stable isotope composition (oxygen-18 and deuterium) was analyzed via direct equilibration, desorption and cryogenic vacuum extraction.

The inverse model SWIS fits simulations to pore water stable isotopes as an optimization target. Because of soil heterogeneity is was difficult to conclude on general patterns of soil hydraulic properties like evaporation and transpiration depth, saturated hydraulic conductivity and porosity. Nevertheless, observed isotope composition of pore water in different depths gave insights into the local water cycle. Depletion horizons till a depth of 50 cm and subsequent enrichment horizons were observed for all profiles drilled in 2015. Thus, precipitation events could be traced into the ground and gave rough ideas on infiltration depth and climatic conditions of previous winters and summers. In conclusion, isotope depth profiles are a great tool for the understanding of the water cycle, but sensitivity analysis and parameter optimization need some improvements to achieve proper simulation results.

Keywords: short rotation coppice; SRC; inverse model; soil hydraulic properties; water cycle; unsaturated zone; direct equilibration; cryogenic vacuum extraction; desorption

Zusammenfassung

Einfluss von Kurzumtriebsplantagen auf verschiedene Bodenfunktionen

In dieser Arbeit werden Kurzumtriebsplantagen (KUP) mit intensiv bewirtschafteten, weniger stark durchwurzelten Referenzflächen verglichen, um Rückschlüsse zu Bodenfunktionen, die den Wasserhaushalt beeinflussen, ziehen zu können. Dazu wurden Bodenbohrkerne auf sieben Versuchsstandorte in Baden-Wuerttemberg extrahiert und hinsichtlich der stabilen Isotope im Porenwasser untersucht. Die Isotopenanalyse wurde auf drei verschiedene Arten durchgeführt: mit direkter Equilibrierung, Desorption und kryogener Vakuum-Extraktion.

Anhand von inverser Modellierung der Isotopentiefenprofile sollen Rückschlüsse auf Bodenfunktionen getroffen werden. Allerdings stellt die Heterogenität der Böden bei diesem Ansatz eine große Herausforderung dar, sodass in dieser Arbeit keine Rückschlüsse auf Bodenfunktionen wie die Evaporations- und Transpirationstiefe, die gesättigte hydraulische Leitfähigkeit oder die Porosität getroffen werden konnten. Trotzdem geben beobachtete Werte der Isotopenzusammensetzung im Porenwasser Aufschlüsse über den lokalen Wasserkreislauf. Bei allen, der in 2015 gebohrten Profile, ist bis zu einer Tiefe von 50 cm eine Abreicherung der schweren Isotope sichtbar, darunter eine Anreicherung. Aus diesen Horizonten können sowohl Rückschlüsse auf die ungefähre Infilrationstiefe, als auch auf klimatische Bedingungen während vergangener Sommer und Winterniederschläge gezogen werden. Zusammenfassend lässt sich sagen, dass Isotopenprofile sehr hilfreich für das Verständnis von Wasserflüssen in der ungesättigten Zone sind, allerdings müssen hinsichtlich der Modellierung die Sensitivitätsanalyse und die damit verbundene Parameteroptimierung noch verbessert werden.

Stichworte: Kurzumtriebsplantagen; KUP; inverse Modellierung; Bodenfunktionen; Wasserhaushalt; ungesättigte Zone; direkte Equilibrierung; kryogene Vakuum-Extraktion; Desorption

Acknowledgements

I like to thank Barbara Herbstritt and Hannes Leistert for the support in the laboratory and modeling work. Further I like to thank Helmer Schack-Kirchner for lending me the construction for extracting desorption solutions. Moreover, I thank Markus Weiler and Friederike Lang for supervising my work. A big thank you to Torsten for everything.

Contents

Ehrenwörtliche Erklärung **i**

Abstract **iii**

Zusammenfassung **v**

Acknowledgements **vii**

Contents **vii**

List of Figures **xi**

List of Tables **xv**

Abbreviations **xvii**

Symbols **xix**

1 Introduction **1**
1.1 Research purpose 5

2 Theoretical background **7**
2.1 Isotope hydrology 7
2.2 Soil physics and properties 10

3 Methods **15**
3.1 Sampling sites and sampling method 15
3.1.1 Soil drilling cores 17
3.2 Isotope analysis 19
3.2.1 Direct equilibration 20
3.2.2 Desorption solution 20
3.2.3 Cryogenic vacuum extraction 22
3.3 Calculation of soil water content 23
3.4 Modeling soil profiles 23
3.4.1 Model input data: time series 25
3.4.1.1 Precipitation, relative humidity and air temperature . . . 26
3.4.1.2 Isotope composition of precipitation 27
3.4.1.3 Evaporation, transpiration, interception 30
3.4.2 Parameter estimation 34

3.4.3 Sensitivity and uncertainty analysis . . . 36
3.4.4 Model efficiency index . . . 37

4 Results **41**
4.1 Isotope analysis . . . 41
4.2 Input data of isotopes in precipitation . . . 44
4.3 Comparison of evapotranspiration methods . . . 46
4.4 Model steps I to V . . . 49
4.4.1 Model step I: Leaf area index at all sites . . . 50
4.4.2 Model steps II-V: Kupferzell . . . 51
4.4.3 Model steps II-V: Kraichtal . . . 55
4.4.4 Model steps II-V: Forchheim . . . 60
4.4.5 Model steps II-V: Marbach . . . 65
4.4.6 Model steps II-V: Laufen . . . 68
4.4.7 Model steps II-V: Buggingen . . . 74
4.4.8 Model steps II-V: Welschingen . . . 76
4.5 Comparison of sampling sites . . . 79

5 Discussion **85**
5.1 Methods of isotope analysis . . . 85
5.2 Observed isotope data . . . 88
5.3 Model input data series . . . 89
5.4 Simulations and sensitivity analysis . . . 91

6 Conclusion **95**

Bibliography **106**

A Detailed description of the sampling sites **107**

B Model step I - sensitivity analysis **109**

C Model step III to V - depth plots **121**

D Model step II - IV - selected sensitivity plots **165**

List of Figures

1.1 Trends of soil erosion due to water. 2

2.1 Conceptualization of the processes affecting pore water stable isotope composition in the vadose zone. 9

3.1 Map of vegetation of sampling sites. 18
3.2 Scheme of a drill core. 19
3.3 Scheme of a pressure chamber used for desorption solution. 21
3.4 Scheme of construction for cryogenic extraction. 22
3.5 Overview of sampling sites, climate stations and GNIP stations. 27
3.6 Schematization of the approach to incorporate sensitivity and uncertainty analysis. 38

4.1 Comparison of cryogenic extraction, desorption and equilibrium methods with measurements of Kraichtal profile 2. 43
4.2 Linear and 3rd order polynomial correlation with oxygen-18 and temperature measurements of Weil data. 44
4.3 Comparison of approaches to model isotope input data for St. Wilhelmer Tal. 46
4.4 Comparison of approaches to model isotope input data for Schauinsland. . 47
4.5 Comparison of potential evapotranspiration methods in Forchheim. 47
4.6 Water balance in Forchheim. 48
4.7 Scheme of depletion and enrichment horizon. 50
4.8 Scheme of a best practice sensitive parameter in sensitivity analysis. . . . 50
4.9 Residual plot of profile 1 in Kupferzell. 54
4.10 Residual plot of profile 3 in Kupferzell. 54
4.11 Residual plot of profile 2 in Kupferzell. 55
4.12 Residual plot of profile 1 in Kraichtal. 58
4.13 Residual plot of profile 2 in Kraichtal. 59
4.14 Residual plot of profile 3 in Kraichtal. 59
4.15 Residual plot of profile 4 in Kraichtal. 60
4.16 Residual plot of profile 1 in Forchheim. 63
4.17 Residual plot of profile 2 in Forchheim. 63
4.18 Residual plot of profile 3 in Forchheim. 64
4.19 Residual plot of profile 4 in Forchheim. 64
4.20 Residual plot of profile 5 in Forchheim. 64
4.21 Residual plot of profile 6 in Forchheim. 65
4.22 Residual plot of profile 1 in Marbach. 67

4.23 Residual plot of profile 2 in Marbach. 68
4.24 Residual plot of profile 3 in Marbach. 68
4.25 Residual plot of profile 2 sampled in autumn 2014 in Laufen. 71
4.26 Residual plot of profile 2 sampled in spring 2015 in Laufen. 71
4.27 Residual plot of profile 3 sampled in spring 2015 in Laufen. 72
4.28 Residual plot of profile 6 sampled in spring 2015 in Laufen. 72
4.29 Residual plot of profile 1 sampled in spring 2015 in Buggingen. 76
4.30 Residual plot of profile 3 sampled in spring 2015 in Buggingen. 76
4.31 Residual plot of profile 2 sampled in autumn 2014 in Welschingen. 78
4.32 Residual plot of profile 2 sampled in spring 2015 in Welschingen. 78
4.33 Relation of saturated hydraulic conductivity and vegetation category. . . . 80
4.34 Relation of porosity and vegetation category. 80
4.35 Relation of saturated hydraulic conductivity and vegetation age. 80
4.36 Relation of porosity and vegetation age. 81
4.37 Relation of saturated hydraulic conductivity and soil texture. 81
4.38 Relation of porosity and soil texture. 82
4.39 Relation of evaporation depth and vegetation category. 82
4.40 Relation of transpiration depth and vegetation category. 83

5.1 Extraction methods. 86

B.1 Sensitivity analysis of model step I at sampling site Kupferzell. 110
B.2 Sensitivity analysis of model step I at sampling site Kraichtal. 111
B.3 Sensitivity analysis of model step I at sampling site Forchheim. 112
B.4 Sensitivity analysis of model step I at sampling site Marbach. 113
B.5 Sensitivity analysis of model step I at sampling site Buggingen in autumn 2015. 114
B.6 Sensitivity analysis of model step I at sampling site Buggingen in spring 2015. 115
B.7 Sensitivity analysis of model step I at sampling site Laufen in autumn 2015. 116
B.8 Sensitivity analysis of model step I at sampling site Laufen in spring 2015. 117
B.9 Sensitivity analysis of model step I at sampling site Welschingen in autumn 2014. 118
B.10 Sensitivity analysis of model step I at sampling site Welschingen in spring 2015. 119

C.1 Depth profile of observed and modeled values from model step V for profile 1 at Kupferzell. 122
C.2 Depth profile of observed and modeled values from model step IV for profile 2 at Kupferzell. 123
C.3 Depth profile of observed and modeled values from model step V for profile 3 at Kupferzell. 124
C.4 Depth profile of observed and modeled values from model step IV for profile 1 at Kraichtal. 125
C.5 Depth profile of observed and modeled values from model step IV for profile 2 at Kraichtal. 126
C.6 Depth profile of observed and modeled values from model step IV for profile 3 at Kraichtal. 127

C.7 Depth profile of observed and modeled values from model step IV for profile 4 at Kraichtal. . . . 128
C.8 Depth profile of observed and modeled values from model step III for profile 1 at Forchheim. . . . 129
C.9 Depth profile of observed and modeled values from model step III for profile 2 at Forchheim. . . . 130
C.10 Depth profile of observed and modeled values from model III for profile 3 at Forchheim. . . . 131
C.11 Depth profile of observed and modeled values from model step III for profile 4 at Forchheim. . . . 132
C.12 Depth profile of observed and modeled values from model step IV for profile 5 at Forchheim. . . . 133
C.13 Depth profile of observed and modeled values from model step IV for profile 6 at Forchheim. . . . 134
C.14 Depth profile of observed and modeled values from model step IV for profile 1 at Marbach. . . . 135
C.15 Depth profile of observed and modeled values from model step IV for profile 2 at Marbach. . . . 136
C.16 Depth profile of observed and modeled values from model step V for profile 3 at Marbach. . . . 137
C.17 Depth profile of observed and modeled values from model step IV for profile 1 sampled in autumn 2014 in Buggingen. . . . 138
C.18 Depth profile of observed and modeled values from model step IV for profile 2 sampled in autumn 2014 in Buggingen. . . . 139
C.19 Depth profile of observed and modeled values from model step IV for profile 3 sampled in autumn 2014 in Buggingen. . . . 140
C.20 Depth profile of observed and modeled values from model step IV for profile 4 sampled in autumn 2014 in Buggingen. . . . 141
C.21 Depth profile of observed and modeled values from model step IV for profile 1 sampled in spring 2015 in Buggingen. . . . 142
C.22 Depth profile of observed and modeled values from model IV for profile 2 sampled in spring 2015 in Buggingen. . . . 143
C.23 Depth profile of observed and modeled values from model IV for profile 3 sampled in spring 2015 in Buggingen. . . . 144
C.24 Depth profile of observed and modeled values from model step IV for profile 4 sampled in spring 2015 in Buggingen. . . . 145
C.25 Depth profile of observed and modeled values from model step IV for profile 1 sampled in autumn 2014 in Laufen. . . . 146
C.26 Depth profile of observed and modeled values from model step V for profile 1 sampled in 2015 in Laufen. . . . 147
C.27 Depth profile of observed and modeled values from model IV for profile 2 sampled in autumn 2014 in Laufen. . . . 148
C.28 Depth profile of observed and modeled values from model step IV for profile 2 sampled in spring 2015 in Laufen. . . . 149
C.29 Depth profile of observed and modeled values from model step IV for profile 3 sampled in autumn 2014 in Laufen. . . . 150
C.30 Depth profile of observed and modeled values from model step IV for profile 3 sampled in spring 2015 in Laufen. . . . 151

C.31 Depth profile of observed and modeled values from model step IV for profile 4 sampled in autumn 2014 in Laufen. 152
C.32 Depth profile of observed and modeled values from model step V for profile 4 sampled in 2015 in Laufen. 153
C.33 Depth profile of observed and modeled values from model step IV for profile 5 sampled in autumn 2014 in Laufen. 154
C.34 Depth profile of observed and modeled values from model step V for profile 5 sampled in 2015 in Laufen. 155
C.35 Depth profile of observed and modeled values from model step IV for profile 6 sampled in autumn 2014 in Laufen. 156
C.36 Depth profile of observed and modeled values from model step IV for profile 6 sampled in spring 2015 in Laufen. 157
C.37 Depth profile of observed and modeled values from model step IV for profile 1 sampled in autumn 2015 in Welschingen. 158
C.38 Depth profile of observed and modeled values from model step III for profile 1 sampled in spring 2015 in Welschingen. 159
C.39 Depth profile of observed and modeled values from model step IV for profile 2 sampled in autumn 2014 in Welschingen. 160
C.40 Depth profile of observed and modeled values from model step IV for profile 2 sampled in spring 2015 in Welschingen. 161
C.41 Depth profile of observed and modeled values from model step IV for profile 3 sampled in autumn 2015 in Welschingen. 162
C.42 Depth profile of observed and modeled values from model step III for profile 3 sampled in spring 2015 in Welschingen. 163

D.1 Sensitivity analysis of transpiration depth at Kupferzell. 166
D.2 Sensitivity analysis of evaporation depth at Kupferzell. 167
D.3 Sensitivity analysis of transpiration depth at Kraichtal. 168
D.4 Sensitivity analysis of evaporation depth at Kraichtal. 169
D.5 Sensitivity analysis of evaporation depth at Forchheim. 170
D.6 Sensitivity analysis of transpiration depth in Laufen 2014. 171
D.7 Sensitivity analysis of transpiration depth in Laufen 2015. 172
D.8 Sensitivity analysis of transpiration depth in Welschingen 2014. 173
D.9 Sensitivity analysis of evaporation depth in Welschingen 2014. 174

List of Tables

3.1 Leaf area indices (A_{LAI}) of different species. 34
3.2 Parameters of the model SWIS and their ranges used for simulation. . . . 35

4.1 Isotope test measurements of desorption after filter conditioning in comparison to equilibrium data. 42
4.2 Best parameter values for Kupferzell obtained from the SWIS model runs. 53
4.3 Best parameter values for Kraichtal obtained from the SWIS model runs. 57
4.4 Best parameter values for Forchheim obtained from the SWIS model runs. 62
4.5 Best parameter values for Marbach obtained from the SWIS model runs. . 67
4.6 Best parameter values for Laufen obtained from the SWIS model runs. . . 73
4.7 Best parameter values for Buggingen obtained from the SWIS model runs. 75
4.8 Best parameter values for Welschingen obtained from the SWIS model runs. 77

A.1 Detailed description of sampling sites. 108

Abbreviations

a.s.l.	**a**bove **s**ea **l**evel
BbodSchG	**B**undes-**Bod**en**sch**utz-**G**esetz
BK 50	**B**oden**k**arte 1: 50,000 (here of Baden-Württemberg)
BwaldG	**B**undes**wald**-**G**esetz
CRDS	**C**avity **R**ing-**D**own **S**pectroscopy
DWD	**D**eutscher **W**etter**d**ienst
ETp	**p**otential **e**vapo**t**ranspiration
FAO	**F**ood and **A**griculture **O**rganization of the United Stated
GMWL	**G**lobal **M**eteoric **W**ater **L**ine
GNIP	**G**lobal **N**etwork of **I**sotopes in **P**recipitation
LAI	**L**eaf **A**rea **I**ndex
LTZ	**L**andwirtschaftliches **T**echnologiezentrum **A**ugustenberg
OAT	**o**ne-**a**t-a-**t**ime
SA	**S**ensitivity **a**nalysis
SRC	**S**hort-**r**otation **c**oppice
UA	**U**ncertainty analysis
UBA	**U**mwelt**b**undes**a**mt
VSMOW	**V**ienna **S**tandard **M**ean **O**cean **W**ater
WRB	**W**orld **R**eference **B**ase

Symbols

A_{LAI}	leaf area index	[-]
C	tracer concentration	[g/l]
D_W	molecular diffusion coefficient in free water	[cm^2/s]
$d^{18}\delta$	change in deuterium isotope ratio	[‰]
$d^2\delta$	change in oxygen-18 isotope ratio	[‰]
D	dispersion coefficient	[cm^2/s]
dh/dx	hydraulic gradient	[-]
$E_{\mathrm{ETp-Har}}$	Hargreaves potential evapotranspiration	[mm]
$E_{\mathrm{ETp-Penm}}$	Penman-Wendling potential evapotranspiration	[mm]
$E_{ETp-FAO}$	FAO56 reference potential evapotranspiration	[mm]
e_a	actual vapor pressure	[kPa]
E_p	potential evaporation	[mm]
e_s	saturated vapor pressure	[kPa]
G	soil heat flux density	[MJ m^-2]
h	pressure head	[hPa] or [cm WC]
I_p	potential interception	[mm]
J_T	julian day	[-]
K_0	saturated hydraulic conductivity	[cm/d]
KGE	Kling- Gupta- Efficiency	[-]
$\mathrm{KGE}_{\mathrm{mean}}(\mathrm{r}+\alpha)$	Kling- Gupta- Efficiency without bias ratio	[-]
KGE_H	deuterium Kling- Gupta- efficiency	[-]
KGE_{mean}	mean Kling- Gupta- efficiency	[-]
KGE_O	oxygen-18 Kling- Gupta- efficiency	[-]
l	flow length	[cm]
L	latent heat of vaporization	$[J \cdot cm^{-2} \cdot mm^{-1}]$

M_{dS}	dry soil mass	[g]
M_{wS}	wet soil mass	[g]
m	Van-Genuchten shape parameter	[-]
n	porosity	[-]
P	precipitation	[mm]
Pearson's r	Pearson's product-moment correlation coefficient	[-]
Q	amount of water percolating through one pore	[cm^3/s]
q	water flux	[cm/s]
R_0/L	evaporation equivalent of extraterrestrial radiation	[mm]
R_0	extraterrestrial radiation	[J/cm^2]
R_G	global radiation	[J/cm^2]
R_n	net radiation at the vegetation surface	[MJ m^{-2}]
r^2	coefficient of determination	[-]
r	radius	[cm]
S_0	astronomically possible duration of sunshine	[h]
S_R	sunshine duration during equinoxes	[h]
S	sink term representing root water uptake	[-]
T_{max}	maximal temperature	[°C] or [K]
T_{mean}	mean daily temperature	[°C] or [K]
T_{min}	minimal temperature	[°C] or [K]
T_p	potential transpiration	[mm]
t	time	[sec]
u_2	wind speed at 2 m height	[m/s]
u	interpolated climate data	depending on climate data
U	mean relative air humidity	%
V_{pores}	volume of pores	[g]
V_{solid}	volume of solids	[g]
v_2	daily mean of wind velocity	[m/s]
v_f	water flow per time and area	[cm/s]
V	total volume of soil	[g]
W_{CWB}	climatic water balance	[mm]
x	sampling site	[-]
z	depth below soil surface	[cm]

α	variability ratio	[-]
β	bias ratio	[-]
Δ	slope of the vapor pressure curve	[kPa/°C]
ϵ	void ratio	[-]
η	viscosity	[cm^2/s]
γ	psychrometric constant	[kPa/°C]
λ_L	longitudinal dispersivity	[cm]
$\partial\psi$	difference of the hydraulic potential	[hPa] or [cm WC]
ϕ	latitude	[°]
τ_W	tortuosity factor	[-]
θ_r	residual volumetric water content	[-]
θ_s	saturated volumetric water content	[-]
θ	volumetric water content	[-]

Chapter 1

Introduction

Soil is considered to be the 'skin of the earth'. It interfaces the lithosphere, hydrosphere, atmosphere and biosphere; therefore, it supplies several essential functions. It is a medium for plant growth, it stores, purifies, buffers and redistributes water, it modifies the atmosphere and it is habitat for organisms (Blum 2005*b*). Since soils constitute the basis of human existence, they face heavy anthropogenic impacts (Blum 2005*a*). Due to intensive agriculture, topsoil is modified in many places. Humus and organic matter are degraded, bare soil is exposed to wind, sun and rain. Additionally, soil is affected by a changing world climate (IPCC 2013) and a change of soil functions effects climatic conditions LABO (2010).

According to climate scenarios of the IPCC the frequency of days with temperatures above 25 °C will increase, whereas that of days below 0 °C will decrease (IPCC 2013). In general, summers will be drier and winters wetter. Especially increasing extreme precipitation events will intensify erosion processes.

Particularly fertile loess regions which tend to slurry seal coating are effected by erosion (LUBW 1995). The soil structure is disturbed by rain drops, which leads to a reduced infiltration rate, thus rain drains at the surface (LUBW 1995). Increasing sediment input to on-site preflooders, rivers and detention reservoirs is a consequence. Loss of soil material, humus and nutrients on arable land accompanied by sediment rearrangements mean not only ecosystem damage but also economic loss.

In Baden-Wuerttemberg, erosion occurs especially in the region Kraichgau, at the edge of the Black Forest and in the lowlands of the Oberrhein. These are regions with a high relief energy and intense agri- or viticulture (Wurbs & Steininger 2011). For example in the region Kraichgau an ablation of 80 tons of soil per hectare and year was measured in 1995 (LUBW 2011). On behalf of the UBA, Wurbs & Steininger (2011) simulated two scenarios, one with a 100 % conservation tillage without plowing, soils remain in their original structure, and another with 100 % conventional tillage with intense plowing. The results indicate most impact on the regions mentioned above, see Fig. 1.1. High ablation rates in the Black forest are less important because cultivation is only partial and most areas are forested. Nevertheless, German legislation has realized the potential harm that climate change might bring. In §§1, 2, 4 and 11 BodSchG it is stated that erosion has to be minimized and soil degradation on cultivated land has to be reduced.

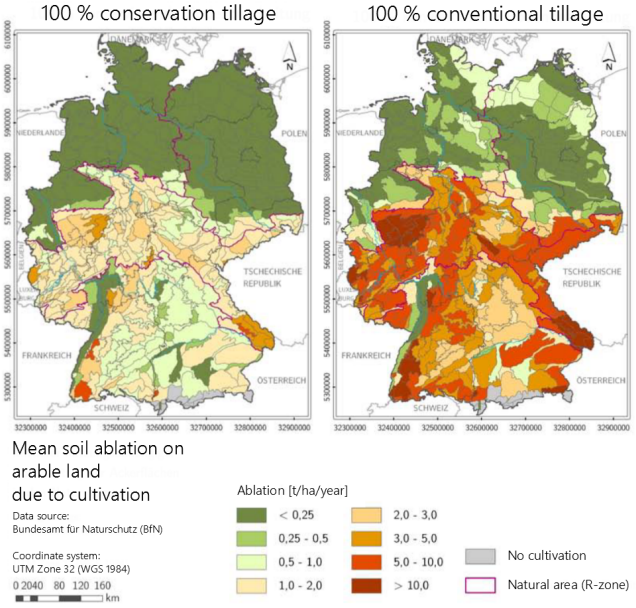

FIGURE 1.1: Trends of soil erosion due to water in two fictitious scenarios: 100 % conservation and 100 % conventional tillage. Both scenarios are fictive and do not take into account intensity of actual cultivation. The figure is taken from Wurbs & Steininger (2011) and translated into English.

Considering the described climatic and antropogenic processes combined with the claims of the 'Bodenschutzgesetz' the need for action becomes clear. One idea of conservation tillage is to plant extensively cultivated short-rotation coppice (SRC). Since 2010, short-rotation coppice (SRC) with a clear cutting every two to twenty years are referred to as agricultural sites and not as woodland in compliance with the BWaldG (MLR 2010). Consequently today SRCs are cultivated on marginal arable sites, fallows or other sites

which are less fertile (Lamersdorf & Schulte-Bisping 2010), with the key objective of woody biomass production. Important characteristics of tree species in short-rotation coppices are fast growing and high biomass production rates during the first years of life time; furthermore, the ability to build stump shots (to coppice) and grow in high density, as well as high reproduction rates, and resistance against biotic and abiotic risks are necessary characteristics (Landgraf et al. 2009). Therefore, especially willow species (*Salix sp.*) like the Swedish clones Tora (*Salix viminalis x Salix Schwerinii*), Tordis (*(Salix viminalis x Salix Schwerinii)x Salix viminalis*) and Jorr (*Salix triandra x Salix viminalis*) and poplar hybrids (*Populus sp.*) like Robusta (*Populus x canadensis = Populus deltoides x Populus nigra*) are cultivated in Germany (Landgraf et al. 2009).

Within the last six years there were several studies examining positive and negative effects of SRCs: for example, DENROM and AGROWOOD in Brandenburg and Saxony, BIODEM in Mecklenburg-Western Pomerania, NOVALIS in Hesse, PROBIOPA in Baden-Wuerttemberg and ProLoc at different sites all over Germany (Murach & Knur 2008, Bemmann & Knust 2010, Aust 2012, Lamersdorf et al. 2010, Hofmann-Schielle et al. 1999). Most of them showed an improvement of soil infiltration capacity and thus an increased protection against erosion (Lamersdorf et al. 2010, Lamersdorf & Schulte-Bisping 2010, Petzold et al. 2009, Dimitriou et al. 2009).

Summarizing the findings of the projects AGROWOOD and Novalis, Lamersdorf et al. (2010) listed positive and negative effects of SRCs on soil ecology. Generally there is only little soil cultivation on SRC stands, thus natural structures in soil physics and chemistry can develop. When activity of soil organisms increases, a continuous pore system can develop. Further, soil water storage capacity is increased, resulting in an increase of infiltration capacity and finally less soil erosion. Moreover, percolating water quality is increased, due to a high root penetration and efficient nutrient absorption. Nevertheless, there are some negative aspects as well. High transpiration and interception lead to reduced groundwater recharge. Depending on cutting frequency, soil compaction in wheel ruts might counteract with the named benefits (Lamersdorf et al. 2010).

More research and measurements are required to specify the influence of SRCs on the local water cycle in different regions. A detailed analysis of soil hydraulic properties usually implies a time consuming and costly experimental setup, which is not always

possible. Soil physics models are widely used to describe water flow and solute transport in the unsaturated zone. For example, Vanclooster et al. (2004) and Christiansen et al. (2006) applied soil physics models to identify the flow and transport of solutes and to estimate percolation rates beneath the root zone. Furthermore, Strasser & Mauser (2001) analyzed climatic effects by using physics based models for evaporation and transpiration and determining spatial and temporal variations of water balance components at catchment scale. Climate change effects on the hydrological regime were also quantified by Bormann (2009) in five different regions in Germany. However, models of water movement in unsaturated soils require accurate calculations of the soil moisture retention and hydraulic conductivity curves (Gribb et al. 2009), which remains a challenge because of the pronounced spatial and temporal soil heterogeneity (Corwin et al. 2006). Most common approaches are either measuring the parameters of interest or calculating them by pedotransfer functions based on grain size distribution (Vereecken et al. 2010). Moreover, inverse model approaches allow optimizing soil hydraulic parameters by fitting model simulations to observed data (Durner et al. 1999). Inverse model parameter identification can be improved further by combining hydrometric and hydrochemical data, hence, water flow and transport mechanisms can be detected (Inoue et al. 2000, Jacques et al. 2002).

Besides hydrometric and hydrochemical data, several studies showed that pore water stable isotopes (deuterium, tritium and oxygen-18) also give insights into hydrological processes in the vadose zone of temperate regions (reviewed by Vitvar (2005)). For example, stable isotopes are used to get information on: the water balance of forest soils and thus insights into flow processes in the unsaturated zone and groundwater recharge mechanisms (Eichler 1964, Blume et al. 1967, Smith et al. 1970, Wenninger et al. 2005); infiltration and percolation processes (Darling & Bath 1988, Gazis & Feng 2004, Koeniger et al. 2010); on the influence of vegetation on evaporation (Eichler 1964, Zimmermann et al. 1966); on root water uptake (Gehrels et al. 1998, Allison et al. 1984, Tang & Feng 2001) and fractionation processes within the plant (Allison et al. 1985, Koeniger et al. 2010); and finally on subsurface hydrological processes in hillslopes (Blume et al. 1967, Garvelmann et al. 2012).

Sprenger, Volkmann, Blume & Weiler (2015) and Stumpp et al. (2012) used the fact that the shape of isotopes over depths includes information on processes that depend on

seasonal variability and take place over years, like infiltration, evaporation and transpiration. While Sprenger, Volkmann, Blume & Weiler (2015) took drilled soil core samples to extract pore water stable isotopes in the field, Stumpp et al. (2012) extracted pore water of different depth using lysimeters. In both studies pore water stable isotope ratios were simulated with a modified version of Hydrus 1D, using pore water stable isotopes for calibration of soil physics parameters for the vadose zone. Hydrus 1D considers variably saturated water flow, root growth, root water uptake, heat transport, and solute transport. The solute transport model was modified to account for isotope transport by Stumpp et al. (2012). They assumed that the fractionation processes can be neglected and that relative concentration of isotopes does not accumulate at the upper boundary condition due to evaporation (Stumpp et al. 2012). A similar approach with a lumped parameter model was applied by Stumpp et al. (2009). The results obtained with the lumped dispersion model were compared with more complex and exact numerical transient flow models. Both modeling approaches defined similar system parameters, indicating that lumped parameter dispersion model achieved satisfying results.

1.1 Research purpose

As mentioned earlier more research and measurements are required to specify the influence of SRCs on the local water cycle in different regions in order to develop distinct management plans. Nine SRCs distributed in Baden-Wuerttemberg and agricultural sites nearby were sampled. Because experimental setups, which give insights into soil hydraulic properties, are time consuming and costly, a new measuring system is applied, which was developed at the Chair of Hydrology at the University of Freiburg.

Similarly to the inverse model approach in Sprenger, Volkmann, Blume & Weiler (2015), pore water stable isotope profiles are taken and simulated with a soil physics model in order to get insights into to soil hydraulic properties (like saturated hydraulic conductivity, porosity and transpiration depth). Instead of Hydrus 1D, another soil physics model, called SWIS (not published yet), is applied. Referring to the two-water world hypothesis of one mobile and one tightly bound water reservoir in the soil (Brooks et al. 2010) (see next chapter), two versions of the SWIS model will be applied. One single pore model under the assumption that the whole pore water underlies the same binding force and

a second multi-pore model where different binding forces are defined. Additionally, the infiltration experiments by Hollmann (2015) provide reference information.

In this thesis, first the question whether it is possible to draw conclusions on soil hydraulic properties using pore water stable isotope profiles and second whether the profiles can correctly be simulated with SWIS, shall be answered. If so, the following questions shall be examined:

a) How do soil functions vary with (1) a changing vegetation (comparison of SRC with agricultural reference site); (2) with a changing vegetation age; and (3) in different soil textures?

b) Does a differentiated multi-pore model display soil-functions better than a single pore model?

This thesis is part of the BioChance project of the Albert-Ludwigs-University Freiburg, funded by the MWK Baden-Wuerttemberg. All field data used in this thesis were collected within the BioChance project.

Chapter 2

Theoretical background

2.1 Isotope hydrology

To draw conclusions on hydrological processes in the vadose zone, natural variations of stable isotopes (deuterium and oxygen-18) in precipitation are used as input signals. To understand the natural variations of stable isotopes at a global scale, one needs to start with the oceans. Water is evaporating from the sea, is transported to cooler regions where it cools down and condenses. Part of the vapor is brought to the continents where it precipitates, infiltrates into the ground or recharges in rivers (Gat et al. 2001). Vapor masses keep moving and progressively rain out when they come to regions with lower temperatures (higher altitudes and latitudes) due to adiabatic expansion (Dansgaard 1964). Meteoric waters (e.g., precipitation, air moisture) are depleted in heavy isotopes (^{18}O, ^{2}H) in comparison to the average ocean composition. The average ocean composition, VSMOW, is 0 ‰ by definition. Delta notations in ‰ always describe the ratio of heavy to light isotope in comparison to the standard VSMOW as the following equation describes:

$$\delta_{\text{sample}} = \left(\frac{R_{\text{sample}} - R_{\text{VSMOW}}}{R_{\text{VSMOW}}} \right) \cdot 1000 \tag{2.1}$$

with

$$R = \frac{^{18}O}{^{16}O} \tag{2.2}$$

or

$$R = \frac{^{2}H}{^{1}H} \tag{2.3}$$

and $R_{\mathrm{VSMOW}} \approx 0$ [‰] for both oxygen and hydrogen.

The main reason for depletion is the Rayleigh rain-out regime. The scenario assumes that precipitation is formed in isotopic equilibrium with the vapor; moreover, water has a higher ^{18}O and ^{2}H content at thermodynamic equilibrium between vapor and water, leading to a progressive depletion of the remaining vapor in the cloud (Gat et al. 2001). Isotopic equilibrium is established between water in falling droplets and the ambient air when the air is not saturated given the prevailing temperature. When the air is under- or over-saturated, evaporation or condensation occurs, respectively, depending on the saturated vapor pressure. Thus, droplets can be enriched or depleted in heavy isotopes in comparison to the in-cloud composition. Hence, light isotopes evaporate first when it comes to evaporation, water droplets are enriched in comparison to the in-cloud composition. During snow or hail events isotopic equilibrium is not established, because evaporation does not occur due to the crystalline structure. Thus, these events result in a more depleted signature than in equilibrium. Seasonal variations in isotope composition in precipitation follow seasonal variations in temperature, depending on precipitable water content and saturated vapor pressure. Due to a decrease in temperature and a lower saturated water vapor pressure, the condensation temperature is lower during winter than during summer, resulting in depletion of heavy isotopes in winter precipitation and enrichment of heavy isotope in summer precipitation in comparison with the mean annual isotope composition of precipitation (Gat et al. 2001). A similar effect is observed with increasing altitude. Condensation increases due to a the temperature drop with increasing altitude; furthermore, atmospheric pressure decreases with increasing height and a larger temperature decrease is required to reach the saturated water vapor pressure than for isobaric condensation processes. Additionally, heavy isotopes precipitate first because of their mass; therefore, precipitation is depleted in heavy isotopes with increasing altitude.

Isotopes of the global precipitation are described by the Global Meteoric Water Line (GMWL). The GMWL is an approximate relation between δ^2H and δ^{18}O found by Craig (1961) in Gat et al. (2001). It takes the following form:

$$\delta^2 H = 8\delta^{18} O + 10 \tag{2.4}$$

The intersection with the y-axis at 10 ‰ is called deuterium-excess. Small or even

negative deuterium-excess values describe a depletion of heavy deuterium isotopes, and indicate non-equilibrium fractionation due to evaporation.

Isotope processes on a local scale of atmosphere, plant and soil are similar to those on a global scale. In winter, precipitation is depleted in heavy isotopes compared to summer months. In the vegetation period, water is absorbed by plant roots (root water uptake), moves through the plant and evaporates from aerial parts, such as leaves and stems (transpiration). During evaporation through aerial parts, fractionation processes occur. Leaves or stems are enriched in heavy isotopes because light isotopes evaporate first. Beyond the growing season in winter, transpiration is reduced to a minimum. The same fractionation occurs at evaporation from the soil surface. Further, water precipitating on leaves or stems remains there for a while and evaporates completely (interception) or falls to the ground as isotopically enriched throughfall. Water infiltrates into the ground and presses older water deeper into the ground. Only during root water uptake water layers mix (Fig. 2.1) (Gat et al. 2001, Gehrels et al. 1998).

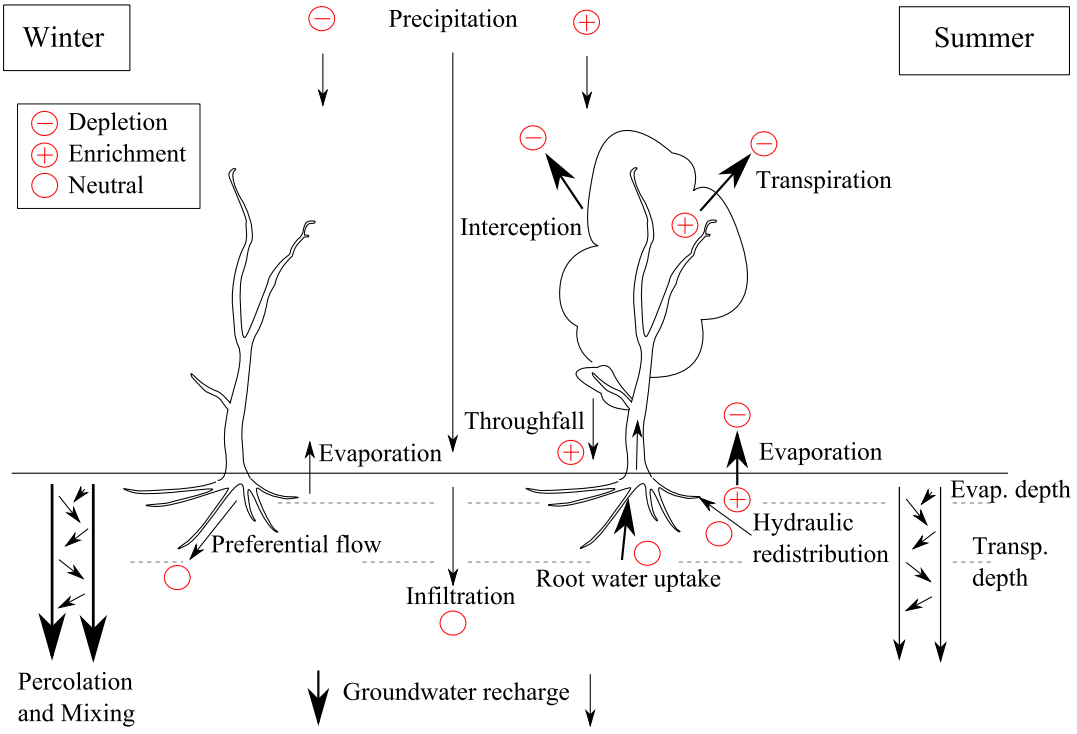

FIGURE 2.1: Conceptualization of the processes affecting pore water stable isotope composition in the vadose zone during summer and winter in a temperate climate. (Figure is drawn according to an idea by Sprenger, Herbstritt & Weiler (2015))

Brooks et al. (2010) established the idea of two seperated 'water worlds'. One pore space

with tightly bound water which is only available to plant roots and in which precipitation is 'layered'. And a second with mobile water which recharges into ground water when the pore space is saturated. In autumn precipitation first fills the dry soil first the tightly bound water reservoir and then the mobile water reservoir. In winter percolation and mixing and groundwater recharge occur only in or from the mobile water reservoir and due to preferential flow. During the dry season in summer, plants take up their water from the tightly bound reservoir. Under drought conditions capillary rise of ground water might occur. However, Brooks et al. (2010) did their study at a Mediterranean climate, so it remains unclear whether those effects also occur in a temperate climate.

2.2 Soil physics and properties

Processes of physical weathering, like wind and water erosion or freezing and melting of water, crush and modify solid rock. In this way, small particles, of different shapes and sizes emerge. The basis for soil is generated. Small particles either occur free and unconnected or joined in aggregates. Diameters of unconnected small particles vary by several powers (2 dm cobbles - 63 nm clay). Grain size distribution is often shown in cumulative curves and is referred to as soil texture in the following. Due to properties like plasticity, roughness, rolling and lubricating capacity, soil texture can be determined during field work (Blume et al. 2010).

Due to granularity and porosity, spaces emerge in which water and air can be stored, plant roots can grow and soil organisms can live. In the following those spaces are referred to as pore spaces or pores. To quantify the proportion of pores (V_{pores}) and total soil volume ($V_{\text{pores}} + V_{\text{solid}}$), porosity ($n$) is calculated (Blume et al. 2010):

$$n = \frac{V_{\text{pores}}}{V_{\text{pores}} + V_{\text{solid}}} \tag{2.5}$$

To quantify a change in volume of the whole system, void ratio (ϵ) is calculated, as a proportion of pore volume (V_{pores}) and volume of solids (V_{solid}) (Blume et al. 2010):

$$\epsilon = \frac{V_{\text{pores}}}{V_{\text{solid}}} \tag{2.6}$$

Depending on size and water storage capacity, pores can be differentiated into micro, meso, and macro pores. The distribution of pores is related to granularity, particle shape and soil structure. General correlations are: the greater the pore diameter, the higher the proportion of macro pores. In turn, the smaller the particles are, the higher the proportion of micro pores is. Thus, the proportion of macro pores is high in sandy soils and decreases with increasing clay content (Blume et al. 2010).

Not all water that is stored in pores is mobile, a certain amount is more or less tightly bound to the soil matrix. One part of precipitation, infiltrating into the ground, is stored in pores against gravity. Another part of infiltrated water is allocated in deeper soil layers as percolating water. During this process, 'older' water, already stored in the soil matrix, is displaced and percolates deeper into the ground. Water remaining in the soil is referred to as soil moisture and can be measured as gravimetric or volumetric water content (Blume et al. 2010).

Water which is stored in the soil matrix against gravity can be divided into adsorbed water and capillary water. Adsorbed water is water which is influenced by Van-der-Waals forces and osmotic forces and covers the surface of soil particles, without the formation of menisci. The amount of adsorption water is correlated to water vapor pressure of the surrounding air; therefore, air-dried soils still contain an amount of water, which increases with increasing relative water vapor pressure. Soils whose water content is not in balance with the water vapor pressure of the surrounding air take up water from the air. Water absorbed during that process is named hygroscopic water (Blume et al. 2010).

Capillary water is water which is stored in the soil matrix due to adhesion and cohesion in order to reduce the surface tension between water and air. During this process, menisci are formed, based on adhesion forces between solid soil particles and pore water, in combination with cohesion between the water molecules (Blume et al. 2010).

The above mentioned forces, from soil matrix on pore water, are summarized as matrix potential (ψ_m). General principles are: (1) the less water is in the soil, the tighter it will be bound to the soil matrix, and the more difficult it will be to extract it from the soil; and (2) water will be stored even tighter to the soil matrix the bigger the distance to the ground water surface is, given a steady state in which water is not in movement.

Because matrix potential and gravity potential are two opposing forces, matrix potential is defined with a negative sign (Blume et al. 2010).

Soil water content at a certain matrix potential is correlated to pore volume and depends on grain size distribution. Therefore, the interaction of water content and matrix potential is characteristic for every soil horizon, and is named pF-curve or moisture retention curve. The pF-value equals the logarithmic absolute matrix potential. In order to determine moisture retention curves, time consuming measurements are required; thus, functions were developed by which moisture retention curves can be calculated, based on grain size distribution, bulk density and some other parameters (Blume et al. 2010).

Due to precipitation and evapotranspiration, a balance between water potentials almost never exists. Rather, soil water is continuously in movement towards the lowest potential. The amount of water movement depends on the potential gradient and the hydraulic conductivity of the soil (Blume et al. 2010). Darcy's law describes the amount of water flow per time and area (v_f) in cm/s as a function of saturated hydraulic conductivity (K_0) and a hydraulic gradient (dh/dx), as follows:

$$v_f = K_0 \cdot \frac{dh}{dx} \tag{2.7}$$

Hydraulic conductivity K_0 in m/s depends on the amount, size, and structure of pores in which water movement occurs. The Hagen-Poiseuille equation describes the amount of water percolating through one pore (Q) as a function of pore radius (r), the difference of the hydraulic potential ($\partial\psi$), the viscosity (η), and the flow length (l):

$$Q = \frac{\pi r^4 \partial\psi}{8\eta l} \tag{2.8}$$

When pores include air instead of water, the area through which water flow can occur decreases; thus, hydraulic conductivity decreases, as well. The biggest pores transport the biggest amount of water; moreover, they drain first. Accordingly, hydraulic conductivity decreases rapidly when big pores drain; furthermore, it depends on water content in the pore space.

Precipitation, temperature and linked plant metabolism vary over the year and influence the soil water balance. These effects of different saturation states can be observed in hydraulic conductivity. Water content at a saturation state close to a balanced hydraulic

potential ($\psi = 0$) is called field capacity. This state is reached two to three days after a heavier rainfall event. A saturation state at which transpiration is greater than soil water content and plants begin to wilt, is called permanent wilting point.

Chapter 3

Methods

3.1 Sampling sites and sampling method

Nine different study sites in Baden-Wuerttemberg were sampled, located in five different natural regions according to the classification in the 'Bodenkarte' 1:50,000 of Baden-Wuerttemberg (BK 50): the Upper Rhine plains, the 'Neckar-Tauber-Gäuplatten', the pre-alpine hills and wetlands, the Middle Black Forest and the Swabian Alp.

In the **Upper Rhine Plain** Laufen, Buggingen and Forchheim were examined. The southern part of the Upper Rhine Plain, with Laufen and Buggingen, is shaped by the eastern plains of the Rhine and hilly slopes at the edge of the Black Forest, with a mean annual temperature of 9 °C and mean annual precipitation of 580 - 800 to 1000 mm close to the Black Forest (MLR 2015). More precisely Buggingen is located in the flat 'Markgräfler Rheinebene' shaped by former gravelly Rhine floodplains and covered by a loess layer which in combination with the mean annual temperature supplies ideal condition for agriculture. On the other hand, Laufen is placed in the hilly 'Markgräfler Hügelland' shaped by loamy loess layers which are partly well aerated and used for viticulture and partly tend to become waterlogged and badly aerated. Especially in Laufen, groundwater level is high, approximately 30-40 cm below soil surface. According to the German soil classification system in BK 50, the dominant soil type in Laufen is Pararendzina (Ah/eC), whereas in Buggingen colluvium occurs due to its relatively low age. Forchheim near Karlsruhe is located in the northern Upper Rhine plain, more

precisely in the 'Hardtebenen', with mean annual temperatures of 10 °C and mean annual precipitation of 530 to 980 mm (MLR 2015). Covered by eolian sand fields the soils in this region are nutrient-poor and permeable. According to BK 50 and German soil classification, the dominant soil type is sandy 'Braunerde', which translates to Brunic Arenosols according to the World Reference Base (WRB).

The sampling sites Kupferzell and Kraichtal are situated in the **'Neckar-Tauber-Gäuplatten'**, which are characterized by a hilly landscape made of tertiary shell limestone. Mean annual temperature is around 8 to 9 °C and mean annual precipitation varies between 700 to 830 mm (MLR 2015). Both 'Kraichgau' with sampling site Kraichtal and Kocher-Jagst-plains with sampling site Kupferzell have fertile soils with shell limestone and Keuper covered by loess. Dominant soil in Kraichtal is 'Pararendzina' and in Kupferzell 'Pelosol' according to BK 50. In 'Pelosol', dry cracks can emerge due to clay minerals which swell when water is available and shrink when there is drought.

The **pre-alpine hills and wetlands** with Aulendorf and Welschingen cover the part of the pre-alpine landscape glaciated during the Würm glacial period and made up of Tertiary molasse. Mean annual temperature is between 7 and 8 °C (MLR 2015). Mean annual precipitation varies depending on the region between 700 and 1000 mm (MLR 2015). Welschingen, west of the 'Bodensee', is located in the 'Hegau'. Shaped by tectonical movement, shallow soils cover stone runs and rocks. The sampling site in Aulendorf is part of the 'Oberschwäbisches Hügelland' and placed in a fen.

Biederbach is situated in the **Middle Black Forest**. Shallow podzols and cambisols derived from crystalline and sedimentary bedrock are dominant soil types (BK 50). The whole region is characterized by more or less steep slopes. In the valleys at 200 m a.s.l., mean annual temperature is around 9 °C, whereas with elevation temperature decreases and is around 6.5 °C at 700 m a.s.l.(MLR 2015). Similar patterns can be observed for mean annual precipitation, which varies between 980 and 2000 mm depending on elevation (MLR 2015).

Limestone and lime marl from the late Jurassic period build the **Swabian Alb** with sampling site Marbach. More precisely Marbach is situated in the 'Mittlere Kuppenalb'. The climate of the 'Mittlere Kuppenalp' varies a lot; thus, mean annual temperature is between 8 and 5.5 °C and mean annual precipitation between 770 and 1100 mm (MLR

2015). Un-layered limes and clays result in karstification. Shallow 'Rendzina' consisting of limestone and dolomite is the dominant soil type (BK 50).

All study sites examined in this thesis were taken from short-rotation coppices (SRC) located in the sampling sites described above. The SRC differ in soil type and plant species. There are 12 samples from poplar plantations and 10 from willow plantations, the distribution among the sites is shown in Fig. 3.1. Furthermore, paulownia, sida and sudangrass plantations were sampled. In most of the sites grassland was sampled for comparison, except Welschingen, Kraichtal and Marbach. In the latter three reference sites agrarian land with maize and oat or uncultivated fields serve as comparison.

3.1.1 Soil drilling cores

Within SRCs soil drilling cores were taken between the planted rows. Sampling was performed by percussion drilling using a Cobra percussion hammer. The drilled depth differed from site to site depending on soil structure. Maximal drilling depth was 3 m. In order not to contaminate soil samples with soil material from other depths, for each meter of depth a smaller size of drill bar was utilized (exact diameters in section 3.3). To examine the stable isotopes in pore water from different seasons, two field campaigns took place: one in autumn (October 2014) and one in spring (April 2015). However, in the first campaign in October 2014 only four sites, Buggingen, Laufen, Welschingen and Biederbach, were sampled. In March and April 2015 the remaining sites, Aulendorf, Marbach, Forchheim, Kraichtal and Kupferzell were added and the sites of 2014 sampled a second time. A third campaign was carried out in October and November 2015. Because of time issues these data are not part of this thesis. Thus, in total 63 drilling cores are part of this thesis. They are divided into 21 cores on 4 different stands in 2014 and 42 cores on 9 different stands in spring 2015. Exact drilled depth can be seen in table A. Drilling cores were divided into subsamples resulting in one sample per 10 cm depth (Fig. 3.2). Subsamples were in turn halved, to get equal samples for nitrate and isotope analysis. During percussion drilling, soil compaction occurred. Measured compaction in cm was split and proportionally added to the depth steps, when calculating a mean depth per 10 cm of soil sample.

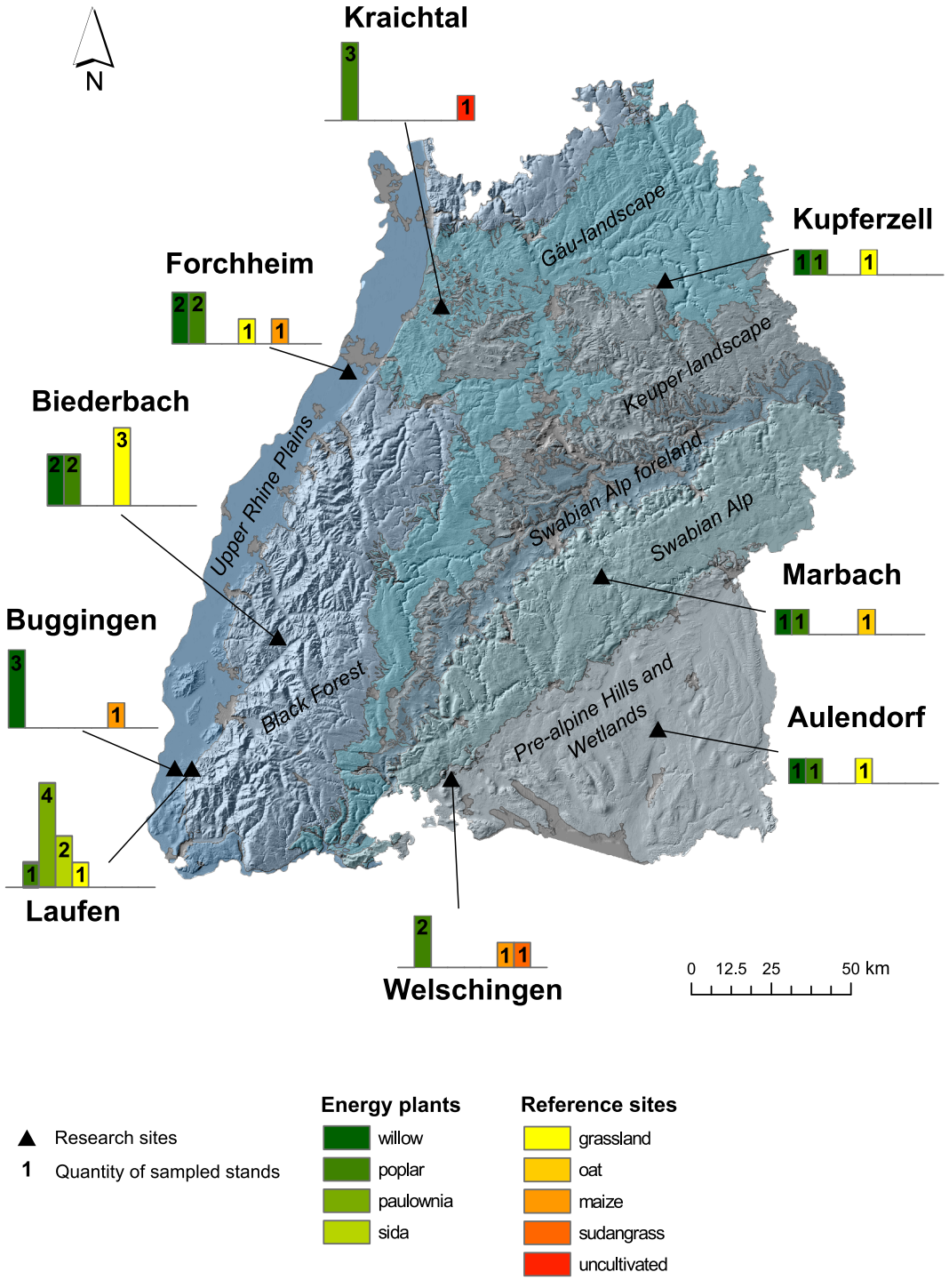

FIGURE 3.1: Map of plantations which were sampled. Plantations with mixed vegetation are counted twice. In Laufen one stand has a mixed plantation of poplar and paulownia. In total 7 stands were sampled in Laufen. In Welschingen sudangrass and maize were mixed at one stand. In total 3 stands were sampled in Welschingen.

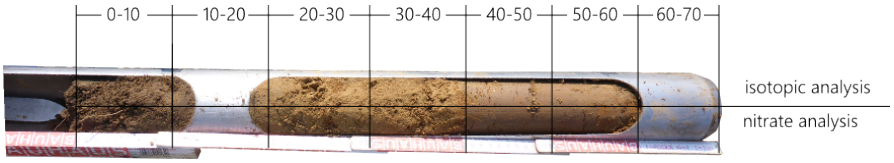

FIGURE 3.2: Scheme of a drill core in Kraichtal illustrating segmentation in 10 cm of depth (0-10, 10-20 ...) and segmentation for analysis.

3.2 Isotope analysis

Sprenger, Herbstritt & Weiler (2015) summarized approaches to analyze the signature of stable isotopes ($\delta^{18}O$, $\delta^{2}H$) in pore water. He grouped the methods by the following criteria: (a) the way to access information (extraction of pore water in the field, laboratory or via equilibration); (b) the related pore sizes that are sampled; and (c) the type of information (resident or flux information). In this thesis, pore water 18-Oxygen and Deuterium analysis was performed in three ways: in the gas phase by **direct equilibration**, in the extracted soil solution first after **desorption at 1.7 bar** and second after **cryogenic vacuum extraction**. These three methods were selected in order to verify pore space analyzed by direct equilibration described in former studies and summarized in Sprenger, Herbstritt & Weiler (2015). Because of time issues, only direct equilibration was applied on all samples. The other two methods were tested on a selection of samples (see in the next subsections).

All samples of the three methods were measured on a Picarro Cavity Ring-Down Spectrometer (CRDS). This technique measures the adsorption of light of specific near-infrared wavelenghts by H_2O gas molecules from the samples at subatmospheric pressure. In CRDS the beam from a single-frequency laser diode enters a cavity which is made of three highly reflecting mirrors (Picarro 2015) and which contains the gas molecules. A continuous traveling light wave is produced; thus, an effective path length of many kilometers is used. A small amount of light leaking through one of the mirrors is detected by a photodetector. The light signal is proportional to the intensity in the cavity. After reaching a certain threshold the continuous wave laser is turned off and light already in the cavity bounces between the mirrors before it exponentially decays to zero, partly because the light leaves the cavity through the mirror and partly because it is absorbed by the gas molecules. This is named "ring down", for different wavelengths of light. Final concentration data is derived from the difference between these ring down

times. Ring down times are then converted into adsorption intensity (Picarro 2015) and further to relative gas concentrations. In the following subsections the three methods are described in detail.

3.2.1 Direct equilibration

Sampling bags from the field are filled with dry air and heat sealed to avoid non-equilibrium fractionation processes. Within this closed system and under constant room temperature, pore water of soil samples equilibrates with dry air. Equilibration was done for approximately 2 days. After equilibration, water vapor of the saturated headspace is directly sampled with a needle connected to a continuous flow Picarro CRDS. After reaching a constant water vapor content the isotope composition of the subsequent two minutes are averaged. To identify isotopic drift of the instrument and calibrate the method to reference concentrations (VSMOW) three standard waters (North Sea water, tap water, deuterated water) of known isotope composition are analyzed.

3.2.2 Desorption solution

Originally Blattner et al. (2000) developed an approach to obtain soil solution and measure water soluble ions. Field moist soil is desorbed in a pressure chamber at 170 kPa (pF 3.2), with a cellulose acetate membrane filter as a capillary bridge between interior and exterior of the chamber (Blattner et al. 2000). Fig. 3.3 illustrates the construction of the pressure chambers used in this thesis. Schlotter et al. (2012) compared the desorption solution with other extraction methods. They found that the desorption solution contains quasi-stationary water from the intra-aggregate pore space (gröbere Mittelporen). These results correspond to the results for squeezing methods at this pressure reviewed by Sprenger, Herbstritt & Weiler (2015). In this thesis pressure chambers constructed in the Department of Soil Science of the University of Freiburg and described in Blattner et al. (2000) were used.

It was ensured that during the desorption the soil sample was not contaminated with other water. Pressure was applied by using a compressed dry air connection. By using an airtight sealed distribution unit, 9 pressure chambers could be used at once. Soil water solution directly dripped through the cannula into Picarro vials closed with a

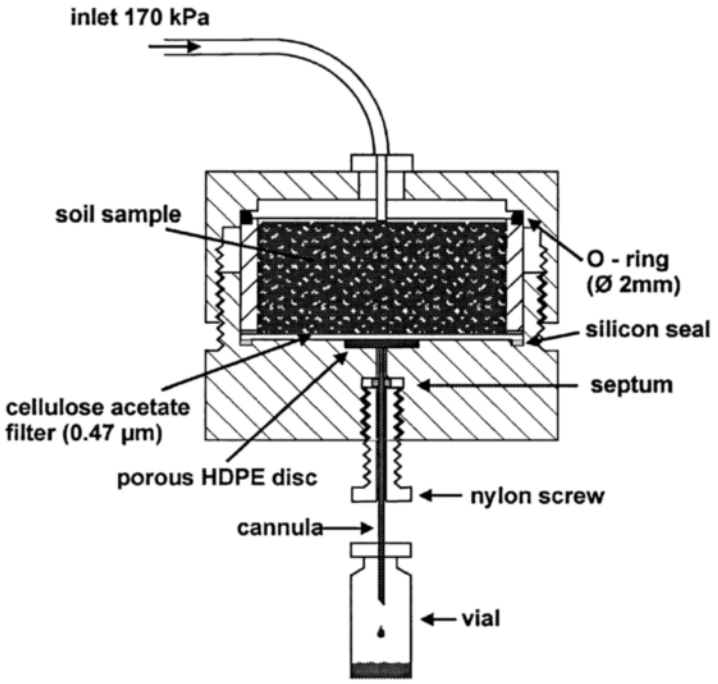

FIGURE 3.3: Scheme of a pressure chamber used for desorption solution (figure is taken from Blattner et al. (2000)).

membrane. Acetate membrane filters had to be moistened to be permeable; therefore, the filter was moistened and afterwards conditioned by squeezing the soil sample for two hours. Especially at low soil water content filter conditioning was necessary; otherwise, the non-permeable acetate filter sealed the cannula and soil water was pressed over the thread.

Desorption was performed for 15 hours. However, after the first 3 hours vials were changed because vials were filled with soil water or to ensure that no water evaporates during the following hours. Within the remaining 12 hours most of the soil samples did not drain any longer. Especially at low water content when microvials were used, vials were set under pressure. A thin cannula had to be applied for pressure compensation, enabling gas exchange between the vial and the the laboratory atmosphere. (Further advantages and disadvantages of the approach discussed later.)

At first, desorption was performed on a selection of one sample per sampling site (Biederbach, Forchheim, Laufen, Kraichtal, Kupferzell, Buggingen) in order to test the approach with different soil textures. Then a whole profile (Kraichtal profile 2) was measured and compared with the other approaches.

3.2.3 Cryogenic vacuum extraction

Cryogenic vacuum extraction is a widespread technique in isotope analysis because of its simplicity (for instance Araguás-Araguás et al. (1995), West et al. (2006), Orlowski et al. (2013, 2015)). With this method, soil samples are boiled, the evaporating water is cooled in liquid nitrogen and collected. The whole process proceeds under vacuum conditions (Figure 3.4). Araguás-Araguás et al. (1995) showed that extracted soil water is depleted in deuterium and oxygen-18, when compared to percolating water; moreover, the depletion depends on the soil type. Whereas in sandy soils a complete recovery of the soil water can be achieved, in clayey soils care is required when the isotope composition of interstitial water is to be investigated. Further Araguás-Araguás et al. (1995) stated that the temperature should be kept as low as possible to ensure the extraction of tightly bound water and to avoid the mix with other water pools (mix with weakly bound water). West et al. (2006) figured out that depending on the soil texture 30 to 40 min are required to obtain an unfractionated soil water sample. When applying distillation under high temperatures both hygroscopic and biologically bound water are likely to be mobilized (Koeniger et al. 2011).

For this thesis cryogenic vacuum extraction was done with the desorbed Kraichtal soil samples. Extraction time varied between 1 to 2 hours, depending on water content of the soil layer. Extraction temperature was at 115 °C, liquid nitrogen had a temperature of -190 °C and the system was set under a vacuum of less than 0.03 mbar. After the extraction, samples were weighed, oven-dried at 180 °C for 2.5 days and weighed again.

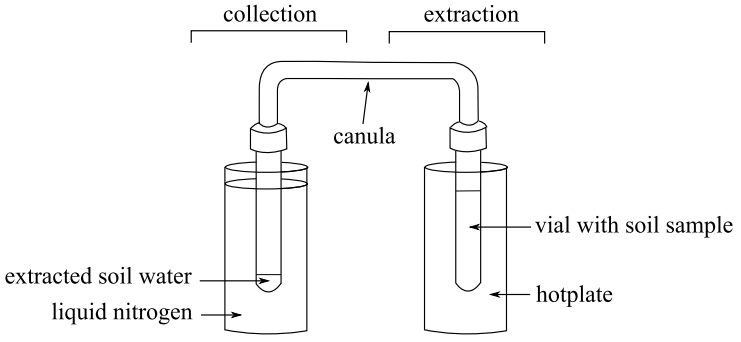

FIGURE 3.4: Scheme of construction of one unit for cryogenic extraction, consisting of one vial with soil sample for extraction and a second vial for collection. The whole system is set under vacuum before hotplate is heating. Ten units can be run simultaneously.

3.3 Calculation of soil water content

Gravimetric soil water content [g] of the samples was determined by weighing wet soil (M_{wS}) and soil after drying (M_{dS}) at 105 °C in the laboratory. It is expected that at this temperature all water evaporates, except water bound in minerals or organic substances (Blume et al. 2010). By dividing the gravimetric water content by the total volume of soil (V), the volumetric watercontent (θ in cm^3 water per cm^3 soil) is calculated:

$$\theta = \frac{(M_{wS} - M_{dS}) \cdot \frac{1}{\rho_w}}{V}. \tag{3.1}$$

When calculating the volume of soil within the core (V) some problems occurred. Approximately 10 cm of soil in drilling core were divided into two approximately equal parts and filled into two bags, one for isotope analysis, the other for nitrate analysis. The exact proportion (p) was calculated and is part of the calculation:

$$V = (10\text{cm} \cdot \pi r^2) \cdot p. \tag{3.2}$$

For the samples from 2014, the initial weight of the nitrate bags was not determined; therefore, p could not be calculated correctly and was calculated by doubling the initial weight of the bag for isotope analysis. Three different drilling cores were used in the field, depending on drilling depth. The biggest one with 6.6 cm diameter, the medium one with 4.57 cm diameter and the smallest one with 3.56 cm diameter; therefore, r varies depending on drilling core.

3.4 Modeling soil profiles

In this thesis the unpublished model SWIS is applied and tested. SWIS is a one dimensional physical soil model developed at the Chair of Hydrology at Freiburg University. SWIS simulates the movement of water and isotope concentrations in the unsaturated zone.

Unsaturated water flow is simulated by numerically solving the Richards equation:

$$\frac{\partial \theta}{\partial t} = -\frac{\partial q}{\partial z} = \frac{\partial}{\partial z}\left[K(h)\frac{\partial h}{\partial z} + K(h)\right] - S \tag{3.3}$$

where a change of the volumetric water content θ over time t is defined by a change of the the water flux q over depth below soil surface z, which is defined by a function of soil hydraulic conductivity $K(h)$, a sink term representing root water uptake S [T^{-}1] and a change of pressure head h over depth z. The Mualem-van-Genuchten model (van Genuchten 1980) is used to define the water retention characteristics $\theta(h)$ and the unsaturated hydraulic conductivity function $K(h)$:

$$\theta(h) = \begin{cases} \theta_r + \dfrac{\theta_s - \theta_r}{(1 + |\alpha_{VG} h|^n)^m} & h \leq 0 \\ \theta_s & h \geq 0 \end{cases} \tag{3.4}$$

$$K(h) = K_0 \frac{[[1 - (\alpha_{VG} h)^{n-1}][1 + (\alpha_{VG} h)^n]^{-m}]^2}{[1 + (\alpha_{VG} h)^n]^{\frac{m}{2}}} \tag{3.5}$$

where θ_r is the residual volumetric water content and θ_s is the saturated volumetric water content, α_{VG}, n and m (=1-1/n) are parameters defining the shape of the retention curves. K_0 is the saturated hydraulic conductivity. In this thesis n is referred to as porosity (this is discussed in section 5 in detail).

Van-Genuchten empirically defined values for the described parameters θ_r, θ_s, α_{VG}, n and m for different soil textures, in the following they are referred to as van-Genuchten-parameter (van Genuchten 1980, Hartke & Horn 2014). During modeling, values for the van-Genuchten Parameter are selected according to the texture of soil layer.

As mentioned earlier Richards flow equation includes a sink term S to account for water uptake by plant roots. In SWIS, S is defined by a daily transpiration amount and rooting depth (see section 3.4.1.3). Similarly, evaporation loss from the upper soil layers is calculated, with a given rate per day and a defined depth as lower boundary condition. Furthermore, three different methods to calculate changes in evapotranspiration rate with depth are implemented: (1) evapotranspiration only in the upper layers, (2) a constant evapotranspiration rate with depth, or (3) linearly declining with depth. In this thesis evapotranspiration is calculated according to the third method.

Initial atmospheric conditions like temperature, relative humidity, precipitation amount and isotope composition of precipitation are defined by input data time series. Interception is implemented as well and subtracted from total precipitation amount. As bottom boundary condition either soil, a non-permeable layer or groundwater can be selected.

Isotope transport in the unsaturated zone is either simulated for a single porous medium, assuming all water to be mobile, or for two pore spaces, assuming that a certain amount of water is tightly bound in micro-pores and that only the remaining amount in meso- and macropores is mobile. In both cases isotope transport is described using the advection-dispersion equation:

$$\frac{\partial(\theta C)}{\partial t} = \frac{\partial}{\partial z}\left(\theta D \frac{\partial C}{\partial z}\right) - \frac{\partial(qC)}{\partial z} - SC \tag{3.6}$$

with the tracer concentration C, the dispersion coefficient D, and the root water uptake S from Eq. 3.3. D is defined by:

$$D = \frac{\lambda_L \cdot q}{\theta} + D_W \cdot \tau_w \tag{3.7}$$

with the longitudinal dispersivity λ_L, the molecular diffusion coefficient in free water D_W and a tortuosity factor τ_W. In order to simulate isotope transport, delta notations were translated into concentrations.

All spatially distributed climatic parameters, such as initial condition for precipitation amount and composition of isotopes in precipitation, temperature, relative humidity as well as evaporation, transpiration and interception are specified by **input data time series** and described in the following. **Input parameters** such as transpiration and evaporation depth as well as definition of texture of soil layers are estimated in a defined range (section 3.4.2). In the time series all days before sampling took place serve as model calibration. At most sampling sites two years of input data are provided, thus the calibration period is around 730 days.

3.4.1 Model input data: time series

As mentioned above SWIS, requires time series of (1) the climate parameters precipitation, relative humidity and air temperature, (2) isotope composition in precipitation and (3) plant and soil parameters like evaporation, transpiration and interception. Ideally

time series of daily measurements over two years before sampling was started would be used. None of these time series were measured during the BioChance project nor during this thesis, thus public climate stations, approximations and equations were consulted.

3.4.1.1 Precipitation, relative humidity and air temperature

For each sampling site, precipitation, relative humidity and air temperature data were taken from the nearest climate station which provided daily values over the two years before sampling took place. All selected climate stations are run by the Landwirtschaftliches Technologiezentrum Augustenberg (LTZ). While in Forchheim, Welschingen, Buggingen and Laufen climate stations where nearby and almost at the same elevation, Kupferzell and Kraichtal needed a special treatment; moreover, climate data of Marbach have to be evaluated carefully because there was no nearby climate station at a similar elevation (Fig. 3.5). The height difference between the sampling site Marbach and the climate station St. Johann is around 300 m. In Kupferzell no climate station was nearby; therefore, climate data were inverse distance weighted using the data of Ilshofen, Zweiflingen and Renzen-Pferdelberg. Interpolated data (u) in Kupferzell (x) are calculated based on input climate data ($u_i = u(x_i)$) of the three climate stations mentioned before (i = 1,2,3) using the following equation:

$$u(x) = \sum_{i=1}^{3} \frac{w_i(x) u_i}{\sum_{j=1}^{3} w_i(x)} \tag{3.8}$$

with

$$w_i(x) = \frac{1}{d(x, x_i)}. \tag{3.9}$$

The linear distance between the climate stations and sampling site Kupferzell is described by $d(x, x_i)$.

Climate station Stifterhof could be detected as the nearest climate station to the sampling site in Kraichtal. Because Stifterhof did not provide data for the whole period, inverse distance weighted data of climate stations in Helmheim and Stetten were taken to fill missing values.

In Biederbach no climate station of the LTZ or DWD is nearby, except weekly measurements from St. Wilhelmer Tal. Weekly measurements could be accessed too late; thus, Biederbach is excluded in this thesis.

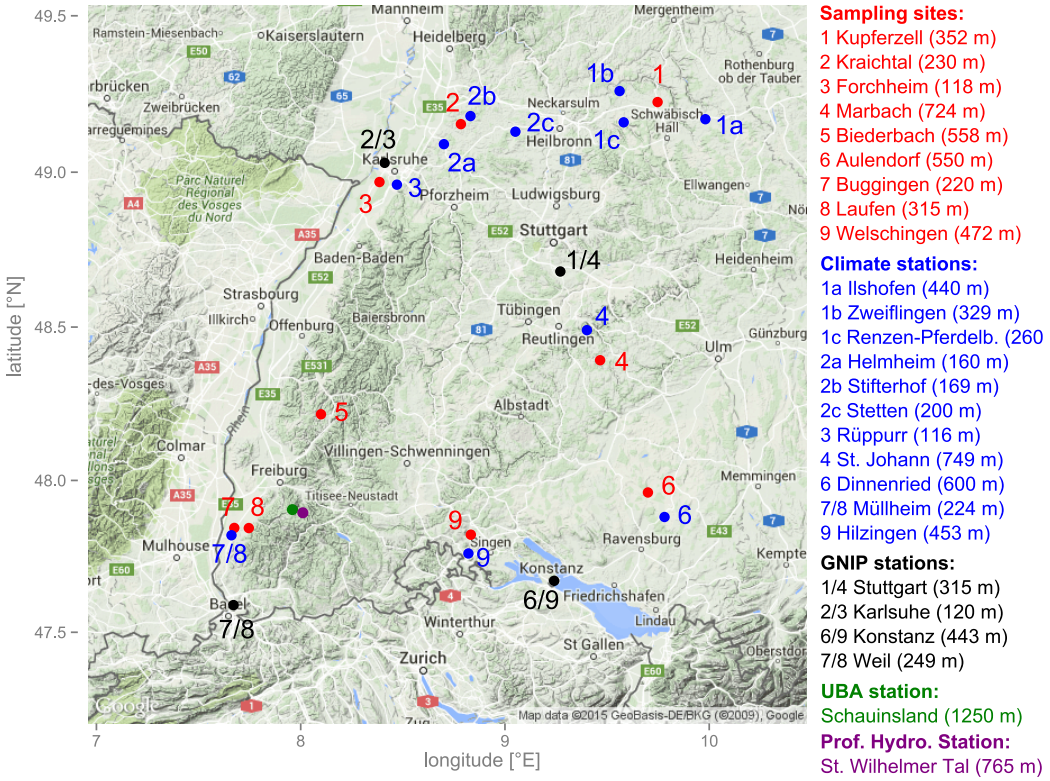

FIGURE 3.5: Overview of sampling sites (red), climate stations (blue) and GNIP stations (black) with elevation data in m a.s.l.. Numbers of sampling sites are repeated at climate and GNIP stations to clarify of which station climate data was taken from for modeling. For example, for the modeling in Kupferzell (1), climate stations 1a, 1b and 1c are taken and GNIP station in Stuttgart (1).

3.4.1.2 Isotope composition of precipitation

For the years 1970 and 2013 monthly data on isotope composition in precipitation is available from climate stations within the Global Network of Isotopes in Precipitation (GNIP), they are referred to as GNIP stations in the following. Closest GNIP stations to the sampling sites in this study are located in Karlsruhe, Stuttgart, Konstanz and Weil (Fig. 3.5).

Furthermore, daily measurements on isotopes in precipitation are supplied by the Umweltbundesamt (UBA) at Schauinsland and weekly values are supplied by the Chair of

Hydrology at St. Wilhelmer Tal. Missing values in both time series were linearly interpolated. However, high resolution data from Schauinsland and St. Wilhelmer Tal are specific for the Black Forest.

For the modeling in this thesis daily isotope data for the years 2012 to 2015 are required. Because there are not enough climate stations in the area that offer daily isotope data, ten approaches to model daily isotope composition from monthly GNIP values were tested. In the following the ten approaches are described:

1. Monthly mean GNIP: Isotope data at GNIP Stations (Weil am Rhein, Konstanz, Karlsruhe, Stuttgart) is available for the years 1980 (± 2–5 years depending on the station) to 2013. Because more recent data is not available yet, longtime monthly means were aggregated. For each day of a month the same value is assumed, daily variations are neglected in this approach.

1a) Monthly mean altitude corrected: Monthly GNIP data were corrected by a height factor by Siegenthaler & Oeschger (1980). They calculated the following factors for the Swiss alps:

$$\frac{d^{18}\delta}{dT} = +0.4‰/°\mathrm{C} = -0.2‰/100\mathrm{m} \tag{3.10}$$

for oxygen-18 and

$$\frac{d^{2}\delta}{dT} = +3‰/°\mathrm{C} = -1.5‰/100\mathrm{m} \tag{3.11}$$

for deuterium. According to Gat et al. (2001), the factors for Central German Uplands like the Black forest are higher. In this work the above mentioned factors are applied, because there were not found plausible values for both oxygen-18 and deuterium in the Black forest. After altitude correction, the longtime monthly means were aggregated as in approach 1.

2. Ten years monthly mean: Within the last ten to fifteen years an increase in temperature and a shift of yearly means of oxygen-18 and deuterium could be observed (Stumpp et al. (2014)); therefore, monthly means of the last ten (from 2003 till 2013) years were taken. Daily variations are neglected in this approach.

2a) Ten years monthly mean with altitude correction: GNIP isotope data was corrected by altitude factor as in approach 1a). Afterwards monthly means of the last 10 years were aggregated like in approach 2.

3. Linear temperature regression: Linear regression of the relative concentration of deuterium and oxygen-18 as a function of temperature was performed with monthly values of GNIP stations. Using the given function, daily values for deuterium and oxygen-18 were calculated for the sampling sites from the available daily temperature data. Further analysis of the correlation of isotope values and temperature is given in section 4.2.

3a) Linear temperature regression with altitude correction: Approach 3 was performed after GNIP isotope data were corrected by an altitude factor (approch 1a).

4. 3rd order temperature regression: Similarly to approach 3, third-order polynomial regression of deuterium and oxygen-18 relative concentrations as a function of temperature was performed with monthly values from the GNIP station. Using the obtained function, daily values for the relative concentrations of deuterium and oxygen-18 were calculated for the sampling sites.

4a) 3rd order temperature regression with altitude correction: Similarly to approach 3a), 3rd order temperature regression was applied on altitude corrected GNIP data.

5. Volume weighted: Linear regression of deuterium and oxygen-18 relative concentrations as a function of temperature was performed with monthly values from the GNIP station. Using the obtained function daily values for deuterium and oxygen-18 were calculated for the sampling sites (see approach 3). Daily values were corrected by the difference between ten year monthly isotope mean from the GNIP station (see approach 2) and precipitation volume weighted monthly isotope means at the sampling site.

5a) Volume weighted and altitude corrected: Approach 5 was repeated with altitude corrected GNIP data.

The ten approaches were tested with monthly data from the GNIP station in Weil and compared to measurements from Schauinsland and St. Wilhelmer Tal (Fig. 3.5). Residuals from simulated isotope time series from the ten approaches were consulted to find the approach which performed best. The approach with the best performance was selected to model daily isotope time series for all sampling sites. Selected respective GNIP station was the nearest station as illustrated in Fig. 3.5.

3.4.1.3 Evaporation, transpiration, interception

Three approaches to model evapotranspiration were tested in this thesis. Equations of Hargreave and Penman are taken from DVWK (1996). In 1975 **Hargreave** developed a simplified approach to calculate potential evapotranspiration without radiation data, making the following assumptions:

$$E_{\mathrm{ETp-Har}} = \frac{0.0023 \cdot R_0}{L} \cdot (T_{\max} - T_{\min})^{0.5} \cdot (T_{\mathrm{mean}} + 17.8) \tag{3.12}$$

with the potential evapotranspiration $E_{\mathrm{ETp-Har}}$ in mm, and the daily evaporation equivalent of extraterrestrial radiation (R_0/L) in mm, daily maximal ($T_{\max}$), minimal ($T_{\min}$) and mean (T_{mean}) temperatures in °C. Extraterrestrial radiation R_0 in J/cm^2 is approximated from the following equations with the date as a continuous number of days (J_T) and the latitude (ϕ) in degree of latitude:

$$R_0 = 245 \cdot (9.9 + 7.08 \cdot \sin(\zeta) + 0.18 \cdot (\phi - 51.0) \cdot (sin(\zeta) - 1)) \tag{3.13}$$

and

$$\zeta = 0.0172 \cdot J_T - 1.39 \tag{3.14}$$

The latent heat of vaporization L in $J/cm^2/mm$ is calculated as follows:

$$L = 249.8 - (0.242 \cdot T_{\mathrm{mean}}) \tag{3.15}$$

Additionally, a simplification by **Wendling (1991)** of an approach by **Penman (1956)** is tested in this thesis (DVWK 1996). The potential evapotranspiration $E_{\mathrm{ETp-Penm}}$ is calculated from the daily sum of global radiation R_G in J/cm^2, the latent heat of vaporization L in J/cm^2/mm (as described in equation 3.15), the proportion of astronomically possible duration of sunshine (S_0) and sunshine duration during equinoxes $S_R = S_0/12$ in hours, daily means of temperature T_{mean} in °C, daily mean relative air humidity U in % and daily mean of wind velocity v_2 in m/s:

$$E_{\mathrm{ETp-Penm}} = g(T) \cdot \left(\frac{0.60 \cdot R_G}{L} + 0.66 \cdot (1 + 1.08 \cdot v_2) \cdot \left(1 - \frac{U}{100}\right) \cdot S_R \right) \tag{3.16}$$

with

$$g(T) = 2.3 \cdot \frac{T_{\text{mean}} + 22}{T_{\text{mean}} + 123} \tag{3.17}$$

Both approaches mentioned above have their disadvantages. On the one hand, the Hargreaves equation is a broad approximation without taking into account radiation measurements. On the other hand, the approach due to Penman-Wendling is more complex and requires a lot of measured time series (radiation, sunshine duration, humidity and wind velocity) which are not available for all sampling sites in this thesis. Thus, the following third approach is chosen to calculate potential evapotranspiration in this thesis:

All selected climate stations provide daily data of climatic water balance. **Climatic water balance** (W_{CWB}) in mm according to DIN 4049-3 is defined as the difference between precipitation (P) and potential evapotranspiration ($E_{\text{ETp-FAO}}$):

$$W_{\text{CWB}} = P - E_{\text{ETp-FAO}}. \tag{3.18}$$

Evapotranspiration ($E_{\text{ETp-FAO}}$) in the climatic water balance (W_{CWB}) is modeled according to the FAO-56 Penman-Monteith equation. Penman Monteith equation is a method from Penman, which was further developed by Monteith by introducing resistance factors, and standardized in 1990 by the FAO as follows:

$$E_{\text{ETp-FAO}} = \frac{0.408 \cdot \Delta(R_n - G) + \gamma \cdot \frac{900}{T_{\text{mean}}+273} \cdot u_2 \cdot (e_s - e_a)}{\Delta + \gamma \cdot (1 + 0.34 \cdot u_2)} \tag{3.19}$$

where $E_{\text{ETp-FAO}}$ is the reference potential evapotranspiration in mm; R_n is the net radiation at the vegetation surface in MJ m^{-2}; G is the soil heat flux density in MJ $\text{m}^{-}2$; T_{mean} is the mean daily air temperature at 2 m height in °C; u_2 is the wind speed at 2 m height in m/s, e_s is the saturated vapor pressure in kPa; e_a is the actual vapor pressure in kPa, accordingly; $e_s - e_a$ is the saturation vapor pressure deficit in kPa; Δ is the slope of the vapor pressure curve in kPa/°C; and γ is the psychrometric constant in kPa/°C.

When calculating potential evapotranspiration ($E_{\text{ETp-FAO}}$) from climatic water balance (W_{CWB}) and precipitation is smaller than climatic water balance, evapotranspiration

values are set to zero, to avoid negative evapotranspiration values. These values are assumed to be outliers.

For the SWIS model applied in this thesis, daily time series of evaporation (E_p), transpiration (T_p) and interception (I_p) are needed. The part of of the total potential evapotranspiration ($E_{ETp-FAO}$) due to transpiration (T_p) is obtained from the coverage with vegetation (β) in percent which in turn is calculated from the leaf are index (A_{LAI}):

$$T_p = E_{\mathrm{ETp-FAO}} * \beta \tag{3.20}$$

$$\beta = 1 - e^{-0.5 \cdot A_{\mathrm{LAI}}} \tag{3.21}$$

This approach of calculating transpiration is applied in the MONICA- model by Nendel et al. (2011). MONICA, simulation model for nitrogen and carbon dynamics in agro-ecosystems, was developed for the assessment of climatic change impact on agricultural production (Nendel et al. 2011, 2014). The model is based on former approaches by McVoy et al. (1995), Diekkrüger et al. (1995), Kersebaum (1995). One part of MONICA was designed to describe plant growth processes, including transpiration, and is used in this thesis (ZALF Leibniz-Zentrum für Agrarlandschaftsforschung 2012).

Daily potential evaporation (E_p) in mm was calculated as the difference between potential evapotranspiration ($E_{\mathrm{ETp-FAO}}$) and transpiration (T_p):

$$E_p = E_{\mathrm{ETp-FAO}} - T_p \tag{3.22}$$

Daily potential interception (I_p) in mm was calculated with a non-linear regression according to von Hoyningen-Huene (1983), with precipitation P in mm and leaf area index A_{LAI}:

$$I_p = -0.42 + 0.245P + 0.2A_{\mathrm{LAI}} - 0.0111P^2 + 0.0271P \cdot A_{\mathrm{LAI}} - 0.0109A_{\mathrm{LAI}}^2. \tag{3.23}$$

Although this approach was proposed for crops based on field experiments, several studies found that the equation performed well on non-crop systems (Bulcock & Jewitt 2009,

Kozak et al. 2007, Tesfuhuney et al. 2013). For instance, Schulze (1995) in Bulcock & Jewitt (2009) suggested the Hoyningen-Huene approach for an agrohydrological model. However, other studies like Gómez et al. (2001) and de Jong & Jetten (2007) found deviating relationships for olive and coniferous trees. Just to give an overview of possible methods they are introduced in the following.

Based on the findings of Aston (1979), Valante et al. (1997), Llorens & Gallart (2000), Dijk & Bruijnzeel (2001), de Jong & Jetten (2007) were able to define the following relationship between interception (I_p) and leaf area index (A_{LAI}) for conifers (Pinus species, Douglas Fir and Spruce):

$$I_p = 0.282 \cdot A_{\mathrm{LAI}} \tag{3.24}$$

Doing field experiments on leaf area index of olive trees combined with the measurements of average storage capacity of an olive leaf done by Leon & Bukovac (1978), Gómez et al. (2001) obtained the following equation:

$$I_p = 1.184 + 0.490 \cdot A_{\mathrm{LAI}} \tag{3.25}$$

Besides the mentioned studies there were no particular studies done in broad-leafed deciduous forests with willow or poplar; therefore, the most common and widespread approach of von Hoyningen-Huene (1983) is used in this thesis under the assumption that it fits well in agroforest systems.

Interception and transpiration are calculated only for days during the growing season. In the non-growing season, interception and transpiration are considered to be negligible and set to zero.

Because leaf area indices for the calculation of interception and transpiration and are not measured in this thesis, they are selected from literature. Since von Hoyningen-Huene (1983) tested their model with measurements on maize, wheat and turnip, a mean of leaf area indices of maize measured by von Hoyningen-Huene (1983) is used for maize samples in this thesis. In 2000, Tharakan et al. (2005) measured different morphological traits on 30 three-years-old willow clones in a short-rotation coppice in Tully, New York. Barigah et al. (1994) did a similar study in Orsay, France, with five

one-year-old poplar clones. They examined morphological traits on two fast-growing and high-producing interamerican *Populus trichocarpa x Populus deltoides* hybrid clones (Raspalje and Beaupré); two native American clones *Populus trichocarpa* (Columbia River and Fritzi Pauley) and one *Populus deltoides x Populus nigra* clone (Robusta) (Barigah et al. 1994). As explained in the introduction, especially willow species like the Swedish clones Tora, Tordis and Jorr and poplar hybrids like Robusta are cultivated in Germany (Landgraf et al. 2009). Considering for instance that poplar stands sampled in this thesis are twice as high as poplar stands mentioned in Barigah et al. (1994), a modification of the literature values is necessary. In Table 3.1, leaf area indices from the literature are listed. They establish the range within which the leaf area index is varied in this thesis.

TABLE 3.1: Leaf area indices (A_{LAI}) of different species.

Species/ Clone	Age [yrs]	Height [m]	A_{LAI} [m^2/m^2]	Studysite	Reference
Salix alba	3	1.88	1.6	Tully, New York	Tharakan et al. (2005)
Salix purpurea	3	2.46 (mean)	3.5 (mean)	Tully, New York	Tharakan et al. (2005)
Robusta (*P. deltoides x P. nigra*)	1	1.8	0.82	Orsay, Paris, France	Barigah et al. (1994)
Maize	1	-	3.5	Braunschweig, Germany	von Hoyningen-Huene (1983)

3.4.2 Parameter estimation

Parameter estimation was performed on LAI and seven parameters that can vary between sampling sites, and are not measured during field work:

1. The input parameter **transpiration depth** is based on rooting depth of the vegetation. Because rooting depths of willow and poplar or crops vary a lot depending on species, clone, soil texture and age, it could not easily be defined. In Kutschera & Lichtenegger (2002), rooting depth for willow and poplar species vary between 1 m to 2.3 m. Taking into account that measurement was performed between the rows and grassland was sampled as well, values between 10 to 250 cm were used in the parameter estimation (Tab. 3.2).

2. Similarly to transpiration depth, a definition of **evaporation depth** was not possible either. Furthermore, variations of evaporation depth should be compared between SRC and open sites like grassland and crops or uncultivated sites. Smallest

TABLE 3.2: Parameters of the model SWIS and their ranges used for simulation. Notes: [1] all textures defined in Van-Genuchten-parameter are possible; [2] depending on field notes and BK50; [3] saturated hydraulic conductivity [cm/d] and porosity [-] are varied in relation to the value given in Van-Genuchten-parameter for soil texture.

Model Step	Parameter	Unit	Explanation	Min	Max	step size
I.	leaf area index	-		0.8	3.5	0.1
II./III.	Transpiration depth	cm	depth to which transpiration occurs depending on rooting depth	10	250	10
II./III.	Evaporation depth	cm	depth to which evaporation occurs	10	50	10
II./III.	Upper soil layer	-	soil texture near the surface	-	-	[1] [2]
II./III.	Bottom soil layer	-	if multiple layers occur, texture of second soil layer	-	-	[1] [2]
II./III.	Depth of bottom soil layer	cm	depth at which second/bottom soil layer begins	10	100	[2]
IV.	K_0	%	saturated hydraulic conductivity	-20 [3]	+20 [3]	10
IV.	n	%	porosity	-10 [3]	+10 [3]	5

possible values were defined as 10 cm depending on cell size of the model and highest values were approximated based on average plowing depth of 30 cm to 50 cm.

3. Possible values for **soil texture and layers** were obtained via field analysis and from BK50. If both specifications differ from each other, a combination of both was tested (Tab. 3.2).

4. In case of two soil layers, the **depth of the second soil layer** varied according to information from field analysis and BK50 (Tab. 3.2).

5. To answer the question whether soil hydraulic properties change with a changing vegetation, Van-Genuchten-parameters **saturated hydraulic conductivity** K_0 and **porosity** n were varied within a defined range. In order to achieve comparability, saturated hydraulic conductivity was varied by ±20 % of the original Van-Genuchten value in steps of 10 % and porosity by ±10 % of the original Van-Genuchten values in steps of 5 % (Tab. 3.2). These percentages were chosen arbitrarily, but if they were any bigger, a different soil texture would have to be used.

As described above, Van-Genuchten-parameters are specific to each soil texture. Because the sampling site Aulendorf is situated in a fen, modeling by using Van-Genuchten-parameter was not possible without further treatment, so the sampling site was excluded from the modeling in this thesis.

3.4.3 Sensitivity and uncertainty analysis

Sensitivity analysis (SA) was applied in order to characterize the confidence bounds of the model output and answer the question of how uncertain inferences from the model are; moreover, factors that are mostly responsible for the uncertainty in the prediction were identified (Saltelli & Annoni 2010, Saltelli et al. 2008, Cariboni et al. 2007, Sieber & Uhlenbrook 2005). In conventional Monte Carlo analysis of models, models are run for all possible combinations of model parameter values. Owing to long processing time of the SWIS model, a complete Monte Carlo analysis with millions of randomly sampled parameter values was impossible; therefore, the defined ranges for all parameters (Tab. 3.2) were split into equal intervals and one parameter value was taken from each interval. There are other approaches to achieve a reduced but still random sampling strategy, like Latin hypercube sampling as published by McKay et al. (1979) and applied in hydrological modeling for example by Sieber & Uhlenbrook (2005). But in terms of explanatory gain a more random sampling seemed not to be necessary; furthermore, not all parameter values are numeric.

To analyze the model runs, a graphical sensitivity analysis was done, plotting model efficiency index against value of parameter. Kling-Gupta-efficiency (KGE) was used as model efficiency index, further explanations in section 3.4.4. Uncertainty analysis was performed via residual plots illustrating in percent how well the model fits the observed values at which depths, taking into account a confidence interval of $pm5$ %. The confidence interval of $pm5$ % is defined as an approximation of the standard deviation of the isotope measurements. Additionally, Pearson-r, the variability ratio α and the bias ratio β are given to characterize the relationship between simulations and observations. After finding the parameters that produce the best model fit, they are used to extrapolate to a depth of 3 m.

In Fig. 3.6 the approach to incorporate sensitivity and uncertainty analysis is shown. Modeling and SA were executed in five steps.

Step I. As leaf area indices are not measured and literature values are not available for all species, or species of the same age, leaf area indices are fitted using the SWIS model. Because leaf area index is needed to model transpiration and interception input data series, it is excluded from the fitting of the rest of the parameters and

follows the approach of one-at-a-time (OAT) sensitivity analysis. OAT-SA means analyzing the effect of varying one model input factor at a time while keeping all other factors fixed (Saltelli & Annoni 2010). According to Saltelli & Annoni (2010) OAT-SA is a widespread approach even though it makes several simplifying assumptions that are not always satisfying.

Step II. LAIs found in step I, are implemented in the input data. A limited number of parameter value combinations is used in order to reduce computing time. Non-sensitive and sensitive parameters are detected by the variability of the efficiency index. Those which show an effect on model efficiency are defined as sensitive parameters, those who do not as non-sensitive ones. Non-sensitive parameters are fixed at a plausible value within the defined range (factor fixing). Individual considerations are described in the results

Step III. Sensitive parameters are varied with a higher frequency within the defined range. Sensitivity and uncertainty analysis supply the best fit.

Step IV. With the best fitting parameter set found in step III, two further parameters are optimized: saturated hydraulic conductivity (K_0) and porosity (n). Because of time issues this is not embedded in step III.

Step V. With the best parameter fit of step III, SWIS is run with two compartments (micro-pores, meso-/macro-pores). Because of time issues this step was not performed with optimized saturated hydraulic conductivity (K_0) and porosity (n) from step IV; moreover, dispersivity between the compartments was set to a fix value of no exchange.

3.4.4 Model efficiency index

Several studies showed that correlation-based measures in itself cannot provide sufficient evaluations of the goodness-of-fit of model simulations (Legates & McCabe 1999, Krause et al. 2005, Wagener et al. 2003). For example the coefficient of determination (r^2) should be used in combination with observed and modeled means and standard deviations as well as absolute error measures (Legates & McCabe 1999). Gupta et al. (2009) developed an efficiency index called Kling-Gupta-Efficiency (KGE). It combines Pearson's product-moment correlation coefficient (r), the ratio between the mean of the

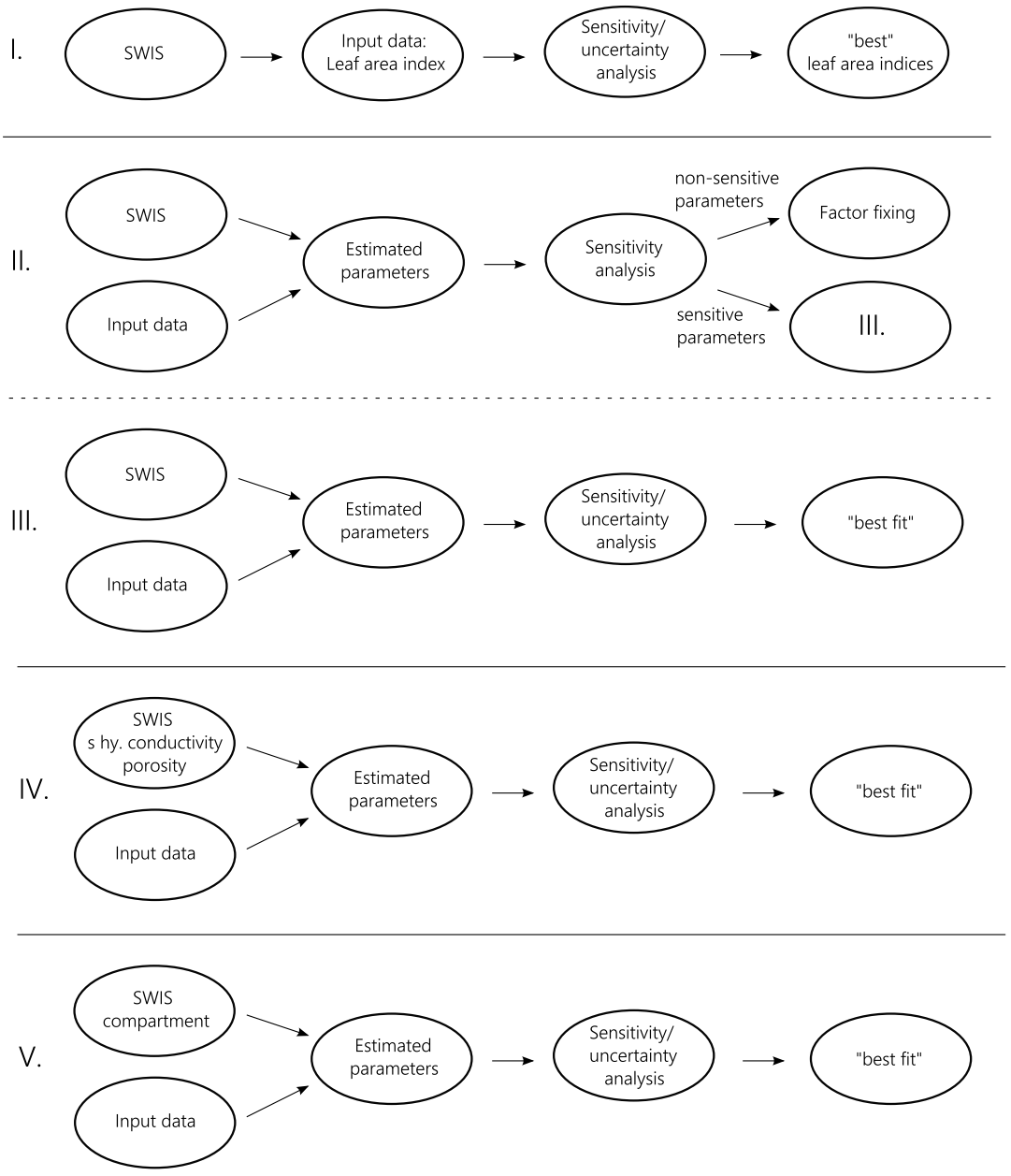

FIGURE 3.6: Schematization of the approach to incorporate sensitivity and uncertainty analysis. Explanations for steps I to V are given in the text above.

simulated values and the mean of the observed ones (bias ratio, β) and the ratio between the standard deviation of the simulated values and the standard deviation of the observed ones (variability ratio, α), as follows:

$$\mathrm{KGE} = 1 - \sqrt{(r-1)^2 + (\alpha-1)^2 + (\beta-1)^2} \tag{3.26}$$

Kling-Gupta-efficiencies range from $-\inf$ to 1. Essentially, the closer to 1, the more accurate the model is. For finding the best parameter value combination, the mean KGE ($\mathrm{KGE}_{\mathrm{mean}}$) of δ^{18}O KGE (KGE_O) and δ^2H KGE (KGE_D) was optimized. To evaluate whether there is a systematically shift between model and observations, KGE was calculated without the bias ration (β):

$$\mathrm{KGE}_{r+\alpha} = 1 - \sqrt{(r-1)^2 + (\alpha-1)^2}. \tag{3.27}$$

Here again mean KGE ($\mathrm{KGE}_{\mathrm{mean}}(\mathrm{r} + \alpha)$) of δ^{18}O KGE ($\mathrm{KGE}_O(\mathrm{r} + \alpha)$) and δ^2H KGE ($\mathrm{KGE}_D(\mathrm{r} + \alpha)$) was calculated. Moreover, Pearson's product-moment r, variability ratio α and bias ratio β are considered separately in the analysis of model runs.

Chapter 4

Results

The following part is structured as follows: first, the results of direct equilibration, desorption and cryogenic extraction are presented and compared; second, the results from the ten approaches to simulate input data of isotopes in precipitation are compared; third, evapotranspiration according to Penman, Hargreave and FAO56 are compared for the example of sampling site Forchheim; fourth, results from LAI optimization in model step I are presented; fifth, model results for model steps III to V are described for each sampling site beginning in Kupferzell, northern Baden-Wuerttemberg, going south to Welschingen, southern Baden-Wuerttemberg; sixth, best fit results from all sampling sites are compared to each other in order to draw conclusion about the research questions.

4.1 Isotope analysis

As described earlier, test measurements of isotope analysis after desorption were performed for samples with sandy, silty and loamy soil texture; moreover, silty profile 2 from sampling site Kraichtal was cryogenically extracted, desorped, and equilibrated.

Isotope values of test measurements in Forchheim (sand), Kraichtal (silt), Biederbach (loam), Buggingen (loam), Laufen (loam) and Kupferzell (loam) show similar patterns for both methods, equilibration and desorption. Variations between the methods are within a range of ± 0.7 ‰ for $\delta^{18}O$ and ± 1.9 ‰ for $\delta^{2}H$ (Tab. 4.1). The smallest difference between the methods was observed in Biederbach with a loamy soil texture

as well as in Kraichtal with a silty soil texture. Sandy soil samples of Forchheim are slightly (+0.5 ‰ for $\delta^{18}O$ and +1.2 ‰ for $\delta^{2}H$) more depleted in isotope signature after desorption (Tab. 4.1). A general influence of soil texture on isotope composition after desorption could not be observed. In other words, differences between the methods are not correlated to soil texture.

Desorption duration times depend strongly on the water content of the soil sample. Laufen and Buggingen had highest water contents and drained most rapidly. Within the first 30 min, 1 ml of soil water was collected; whereas, barely 1 ml could be collected from the soil sample of Kupferzell after 7.5 hours. To get an idea if evaporation occurs or if isotope signature changes over time, samples from Buggingen, Laufen and Kraichtal were measured twice. First after 30 min to 1 hour and second after 2.5 hours in Buggingen, 4.5 hours in Laufen and 17 hours in Kraichtal. No decrease of deuterium-excess after desorption could be observed between the time intervals (Tab. 4.1). In Kraichtal, deuterium-excess even increases. Therefore, evaporation from the vials seems not to be relevant.

TABLE 4.1: Isotope test measurements of desorption (des) after filter conditioning in comparison to equilibrium (equi) data, with deuterium-excess of desorption (d-ex$_{des}$) and desorption time.

soil texture	site	profile	depth [cm]	$\delta^{18}O_{\text{equi}}$ [‰]	$\delta^{2}H_{\text{equi}}$ [‰]	$\delta^{18}O_{\text{des}}$ [‰]	$\delta^{2}H_{\text{des}}$ [‰]	d-ex$_{\text{des}}$ [-]	desorption duration [h]
sand	Forchheim	3	50-60	-7.5	-57.99	-8.05	-59.2	5.17	15
silt	Kraichtal	3	30-40	-9.44	-67.43	-9.58	-67.9	8.74	1
						-9.62	-66.92	10.05	17
loam	Biederbach	1	30-40	-11.53	-81.35	-11.52	-81.51	10.61	14
loam	Buggingen	3	40-50	-11.2	-87.86	-11.13	-84.84	4.19	0.5
						-11.34	-86.08	4.62	2.5
loam	Laufen	4	60-70	-7.58	-57.21	-8.37	-59.74	7.77	0.5
						-8.3	-59.13	7.24	4.5
loam	Kupferzell	2	50-60	-7.73	-60.09	-7.06	-51.43	5.02	7.5

Desorption and equilibrium measurement results of Kraichtal profile 2 are in the same range as well. In the first 40 cm depth, deuterium values of desorption are slightly more positive than deuterium values of direct equilibration; furthermore, desorption values for $\delta^{18}O$ are slightly more negative in the first 100 cm depth (Fig. 4.1). The huge difference between isotope values of 10 and 20 cm depth after direct equilibration could neither be observed after desorption nor cryogenic extraction. Besides these differences, both methods yield values within the same range. Isotope values from cryogenic extraction have a depleted signature in comparison to the other two methods, especially below 100 cm. Gravimetric water content is assumed to be 0 after cryogenic extraction. In some

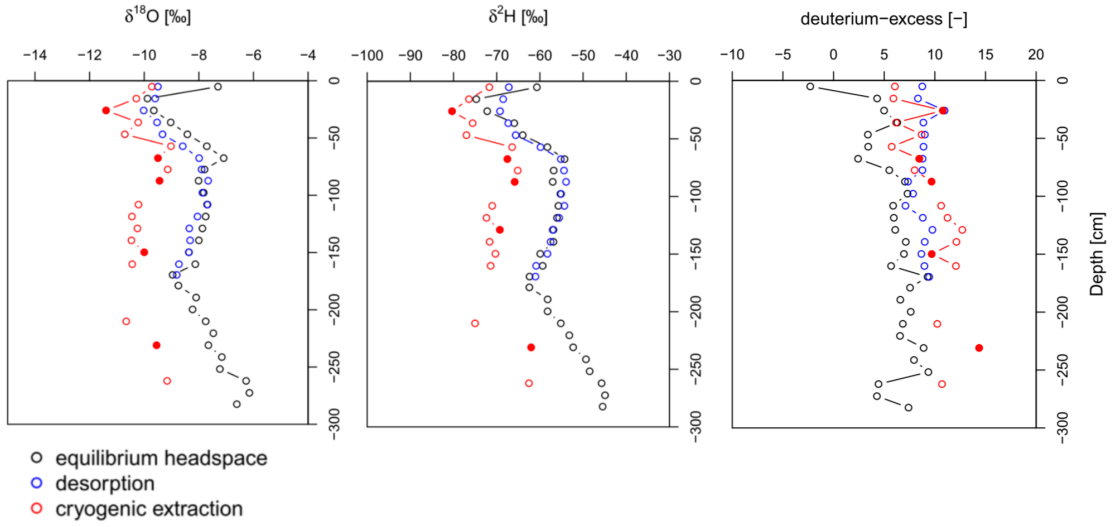

FIGURE 4.1: Comparison of cryogenic extraction, desorption and equilibrium methods with measurments of Kraichtal profile 2. Filled dots symbolize values were residual water content after drying was > 0.01 g.

depths cryogenic extraction did not completely extract pore water. Isotope analysis in these depth might be inaccurate, because is does not represent the isotope signature of the whole pore water (filled red dots in Fig. 4.1). However, only deuterium-excess in 220 cm depth seems to be an outlier.

Differences between all three methods can be observed in deuterium-excess. While equilibrium has comparably lowest deuterium-excess values around 5, desorption deuterium-excess is almost constant at 10 with exception of values at 100 cm depth. Deuterium-excess of cryogenic extraction lies between 5 and 10 till 100 cm depth and increases below 100 cm.

In conclusion, cryogenic vacuum extraction had a significantly more depleted isotope composition in comparison to the other two methods. However, the isotope signatures of direct equilibration and desorption were almost identical for all soil textures; thus, both methods seem to extract water from the same pore space. Further elaborations on this in the discussion.

4.2 Input data of isotopes in precipitation

For the years 1970 and 2013 monthly data on isotope composition in precipitation is available from GNIP-stations. Furthermore, daily measurements on isotopes in precipitation are supplied by the Umweltbundesamt (UBA) at Schauinsland and weekly values are supplied by the Chair of Hydrology at St. Wilhelmer Tal. For the modeling in this thesis daily isotope data for the years 2012 to 2015 are required; therefore, ten approaches were tested with monthly data from the GNIP station in Weil and compared to measurements from Schauinsland and St. Wilhelmer Tal in order to classify the performance of each approach. The ten approaches are: (1) monthly mean GNIP; (1a) monthly mean GNIP with altitude correction; (2) 10 years monthly mean; (2a) 10 years monthly mean with temperature correction; (3) linear temperature regression; (3a) linear temperature regression with altitude correction; (4) 3rd order temperature regression; (4a) 3rd order temperature regression with altitude correction; (5) volume weighted; (5a) volume weighted and altitude corrected. Because the UBA station at Schauinsland did not provide precipitation data, approach 5 was only applied on St. Wilhelmer Tal data.

The basis for daily approaches is an approximation of the relationship from temperature and isotope value. The relationship was obtained by fitting a linear (approach 3) and a 3rd order polynomial function (approach 4) to δ^{18}O and δ^{2}H as a function of temperature. An example for the performance of this fitting for GNIP data in Weil is shown in (Fig. 4.2). Both approaches result in proper fits with an R^2 of 0.5 and standard deviations of $\pm$ 1.9 for both functions (Fig. 4.2).

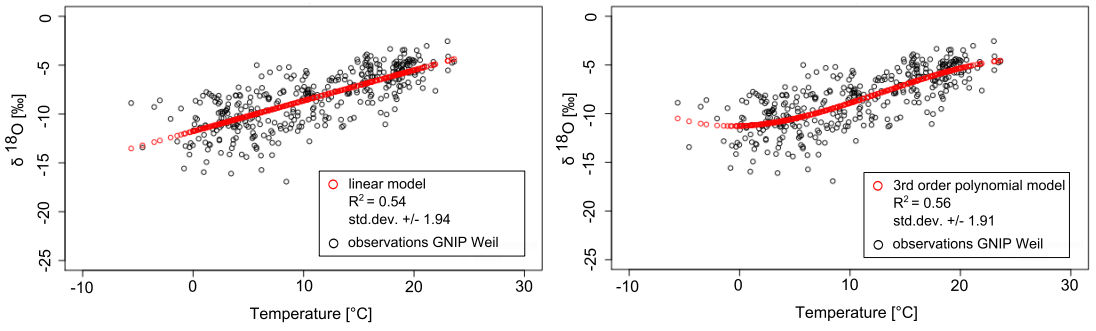

FIGURE 4.2: Linear and 3rd order polynomial correlation with oxygen-18 and temperature measurements of Weil data.

In Fig. 4.3 and Fig. 4.4, boxplots of the residuals of $\delta^{18}O$ illustrate the performance of the applied approaches. Approaches which model daily values (3,4,5) could not achieve a better fit than those modeling monthly means (1,2). Particularly when using daily measurements from Schauinsland, daily approaches (3 + 4) fit less. When applied to data of St. Wilhelmer Tal, altitude corrected approaches produce generally better fits than those without height correction; whereas, when applied to data of Schauinsland, those approaches fit less well.

As mentioned in section 3.4.1.2 altitude correction factors depend on the absolute altitude difference between two sampling points. Hence, the altitude difference between Weil and Schauinsland with around 1000 m is much bigger than between Weil and St. Wilhelmer Tal with around 300 m, altitude correction factors have to be adapted. Different values for the altitude correction factor found by Siegenthaler & Oeschger (1980) were tested. A reduction of altitude correction factor leads to a smaller median of the residuals at Schauinsland data; thus, the variance of simulated to observed values is smaller and the model fits better. However, an optimal altitude correction factor could not be found, models without altitude correction still performed better.

To conclude, while approach 1a 'longtime monthly mean of GNIP data with altitude correction' performed best on weekly St. Wilhelmer Tal data, approach 1 'longtime monthly mean of GNIP data' showed the best performance for daily Schauinsland data. Because the altitude difference between the remaining sampling sites and GNIP stations is marginal, except Marbach, altitude correction is of minor importance; therefore, approach 1: longtime monthly mean is performed for all sampling sites, except Marbach, in the following. In Marbach altitude difference to the nearest GNIP station in Stuttgart is around 300 m. This altitude difference is similar to that between Weil and St. Wilhelmer Tal; thus, approach 1a 'longtime monthly mean of GNIP data with altitude correction' is applied at Marbach.

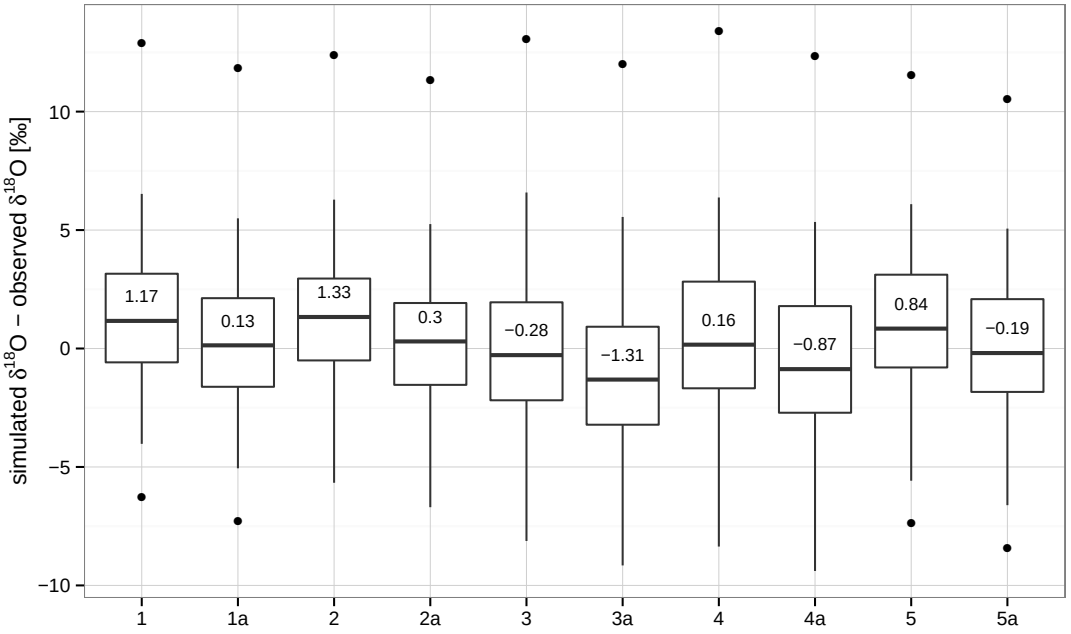

FIGURE 4.3: Comparison of approaches to model isotope input data for St. Wilhelmer Tal. (1) monthly mean GNIP; (1a) monthly mean GNIP with altitude correction; (2) 10 years monthly mean; (2a) 10 years monthly mean with altitude correction; (3) linear temperature regression; (3a) linear temperature regression with altitude correction; (4) 3rd order temperature regression; (4a) 3rd order temperature regression with altitude correction; (5) volume weighted; (5a) volume weighted and altitude corrected. Notes: values and solid black line given in the boxplots simulate the median, black dots are outliers.

4.3 Comparison of evapotranspiration methods

Evapotranspiration methods of Hargreaves, Penman and FAO56 were applied on data of Forchheim to exemplify the differences between them: see Figure 4.5. In the summer months of the years 2013 and 2014, Penman evapotranspiration is almost double the ETp by Hargreveas or by the FAO56. While in 2013 Hargreaves and FAO56 model similar values, in summer 2014, Hargreave ETp is around 40 mm higher than ETp by FAO56. FAO56 method is the current standard taking into account energy flows, aerodynamics and surface resistance; therefore, it is assumed that the method of FAO56 is most precise in comparison to the other two methods. However, it is the only one which can be calculated for all sampling sites in this thesis.

As described earlier, FAO56 evapotranspiration was calculated from the climatic water balance. The calculated water balance of sampling site Forchheim is illustrated in Fig. 4.6, with measured precipitation and calculated transpiration, evaporation, interception

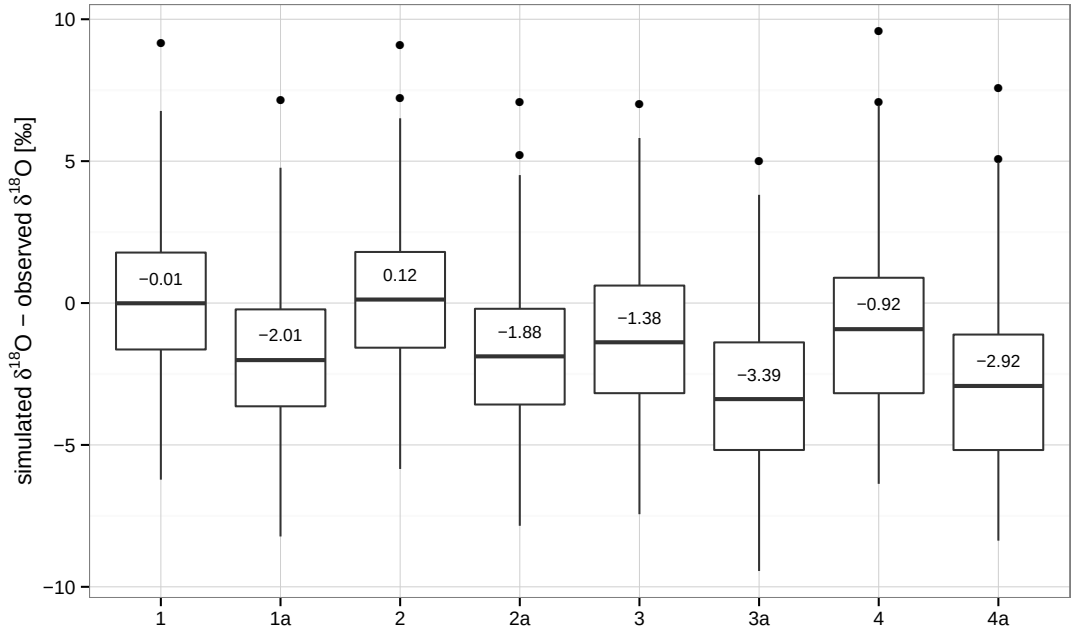

FIGURE 4.4: Comparison of approaches to model isotope input data for Schauinsland. (1) monthly mean GNIP; (1a) monthly mean GNIP with altitude correction; (2) 10 years monthly mean; (2a) 10 years monthly mean with altitude correction; (3) linear temperature regression; (3a) linear temperature regression with altitude correction; (4) 3rd order temperature regression; (4a) 3rd order temperature regression with altitude correction. Notes: values and solid black line given in the boxplots simulate the median, black dots are outliers.

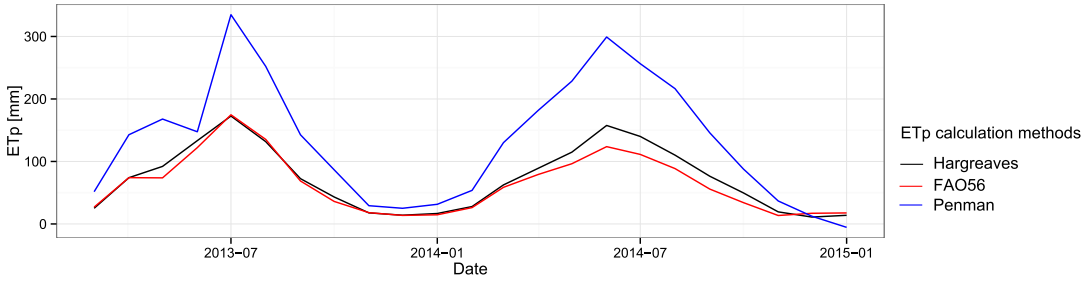

FIGURE 4.5: Comparison of potential evapotranspiration methods in Forchheim.

and storage. Precipitation during March 2013 to March 2015 indicate a wet summer and dry winter. In March, lowest precipitation amount was measured. Calculated evaporation, transpiration and interception show plausible variations over the course of the year, high values in summer and low values in winter. Knowing the water fluxes out of the soil and into the vegetation, like evaporation, transpiration and interception and precipitation which refills the water reservoir in the soil, storage of soil water was calculated. A negative flux means that plants take in more water than precipitates in

that month, a positive storage flux means that water is stored in the soil, or recharges into groundwater without being uptaken by plants immediately. To conclude fluxes seem to be plausible and solely FAO56 evapotranspiration is applied in the following.

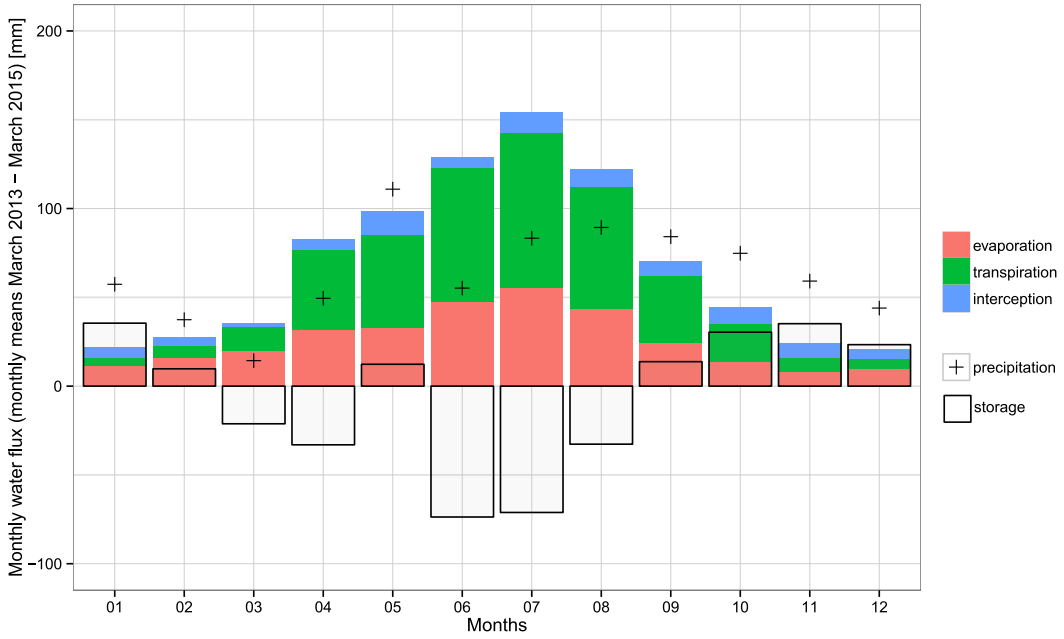

FIGURE 4.6: Water balance in Forchheim with water fluxes over two years. Evaporation, transpiration, interception and storage are calculated potential fluxes. Precipitation is measured. Negative storage means that water flux into plants is greater than flux into the soil.

4.4 Model steps I to V

In this section, first, best fit leaf area indices for the simulation of transpiration rates are described for all 7 sampling sites (model step I); second, observations and best fit simulations of SRC and reference site are compared within one sampling site and between years of one sampling site (model step II to V); and third, model results and soil hydraulic properties are compared between the sampling sites.

More detailed, the second part is structured as follows: First general information on the sampling site itself are given, followed by a description of the observations. Then the performance of the different model steps is described. Starting with the results of the sensitivity analysis (model step II and III), proceeding with a comparison of (a) the model efficiency after fitting soil hydraulic properties (K_0 and n) in model step IV and (b) the results of the multi-pore model step V. Afterwards a detailed description of the best fit simulation follows and a conclusion is drawn from the differences between SRC and reference site is drawn. The sampling sites are described in the order of their geographical location in Baden-Wuerttemberg, beginning north in Kupferzell and finishing south in Welschingen.

Beforehand some explanations of terms used in the following:

1. A depletion horizon is a depth range within which the isotope concentration is relatively low. Depth ranges with relatively high isotope concentrations are referred to as enrichment horizon. Figure 4.7 exemplifies the shape of isotopes over depth and the ranges which are referred to as depletion and enrichment horizons. As described earlier, infiltrating precipitation presses pore water which is already in the pores deeper into the ground. To some extent this depth is modified by mixing and evaporation. Nevertheless, depletion and enrichment horizons give at least an approximation of the infiltration depth of precipitation of winter and summer months.

2. As mentioned earlier, sensitive parameters influence model efficiency, therefore, a distinct maximum for one parameter value should be visible when comparing model efficiency of parameter values. Figure 4.8 exemplifies how the shape of a best practice sensitive parameter should look like, when plotting model efficiency

over parameter values. Every dot in the sensitivity plot Figure 4.8 is one model run. Moreover, during model runs one parameter value is fixed while all other parameters and their values vary. The latter explains the range of model efficiencies of model runs for one parameter value. The box of the violin plot drawn around the dots, illustrates a smoothed probability density of the model runs at different model efficiencies.

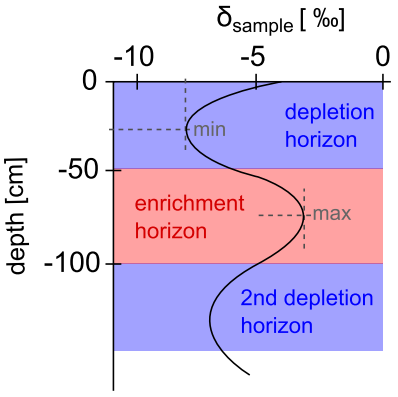

FIGURE 4.7: Scheme of depletion and enrichment horizon with minimum and maximum depletion and enrichment, respectively.

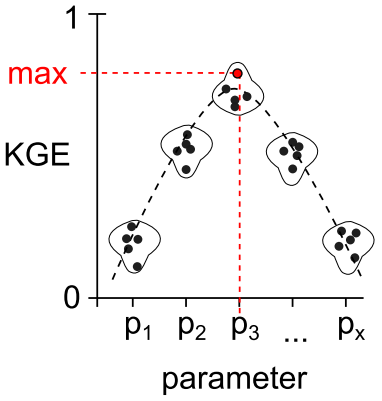

FIGURE 4.8: Scheme of a best practice sensitive parameter in sensitivity analysis, with model efficiency (KGE) over parameter (p) values (1...x).

4.4.1 Model step I: Leaf area index at all sites

Model step I was performed in order to select leaf area indices for the calculation of interception and transpiration. LAI was varied between 0.8 to 3.5 by 0.1 as defined in section 3.2. All other parameters were fixed at the following values:

- transpiration depth at 100 cm
- evaporation depth at 10 cm
- soil texture top layer, soil texture bottom layer and depth of the bottom layer were fixed to the textures given in BK50
- saturated hydraulic conductivity and porosity were fixed at the values given in Van-Genuchten-parameters.

A sensitive behavior of leaf area index as described in Fig. 4.8 could only be observed at willow profiles 2 and 3 in Buggingen (2015) (Fig. B.6), and willow profile 4 in Forchheim (Fig. B.3). From these three profiles it is concluded that a leaf area index around 2 seems to fit well at willow plantation sites. Grassland and poplar profiles in Kupferzell had best model efficiency at leaf area index of 1.9 (Fig. B.1). Furthermore, poplar and uncultivated profiles from sampling site Kraichtal achieved best fits at leaf area index of 1.8 (Fig. B.2). In the latter two cases of Kupferzell and Kraichtal local maxima are used, because the global maximum is not plausible when referring to the leaf area indices from literature. Simulations for profiles 1 to 3, 4 and 6 in Forchheim perform equally well for leaf area indices from 0.8 to 1.9, performance decreases with LAI bigger than 1.9 (Fig. B.3). The remaining profiles are either not sensitive to leaf area index or do not have a local or global maximum (Fig. B.5, B.4, B.7, B.8, B.9, B.10). Because of these unreliable results and the uncertainties brought by the equations of interception and transpiration as explained in section 3.4.1.3, leaf area index is set to a mean of 1.9 for further modeling steps.

4.4.2 Model steps II-V: Kupferzell

Sampling in Kupferzell was performed mid of April 2015, in an area which is flat to slightly prone. Profile 1 and 3 are placed in extensively cultivated SRCs, profile 1 in a willow plantation and profile 3 in a poplar plantation. The willow plantation was cut down once, hence plants are at least 4 years old. SRCs were planted with 180 cm space between the rows and 2.5 trees per square meter within rows. The reference, profile 2, was drilled on grassland next to the SRCs. Drilled profile depths in Kupferzell are 125, 76, and 92 cm for profiles 1 to 3. Observed data of $\delta^{18}O$ and $\delta^{2}H$ from all sites show only marginal variations in the upper 10 to 30 cm (Fig. C.1, C.2, C.3). Below 30 cm, isotope values are almost constant. Thus, no seasonal variations are displayed in depth and the data does not support the hypothesis mentioned in the introduction. Observed volumetric water content varies between 0.2 and 0.5 in all profiles and no trend can be detected (Fig. C.1, C.2, C.3). Deuterium-excess shows especially in the first 20 cm of depth evaporation effects, these effects decrease with depth for profile 1 and 3 (Fig. C.1, C.3). For profile 2 deuterium-excess decreases to 5, showing evaporation effects till 70 cm of depth (Fig. C.2).

In the following the results from the sensitivity analysis are described:

Soil texture: The soil texture parameter from the top soil layer was the same in BK50 and field notes; thus, only texture of bottom soil layer (Tu2 and Lt2) and depth of bottom layer were altered in the model runs. Bottom soil layer alteration did not impact model efficiency. Therefore, top soil texture could be defined as silty loam (Lu). Below 30 cm clay content increases in field notes, hence texture from bottom soil layer is defined as slightly silty clay (Tu2).

Transpiration and evaporation depth: When varying the transpiration depth, no clear maximum in model efficiency could be detected. The changes in model efficiency between sets of model runs with different transpiration depths are much smaller than the changes within each set with a fixed transpiration depth (Fig. D.1). However, evaporation depth could be detected as a sensitive parameter with best fit values at 50 cm depth (Fig. D.2). It was concluded that transpiration depth did not have a major impact on model efficiency, and alterations can be better explained by a change in evaporation depth. However, both parameters were set to the value showing a maximum in KGE_{mean} (Tab. 4.2).

Saturated hydraulic conductivity K_0 and porosity n: When adjusting K_0 and n in model step IV, model efficiency (KGE_{mean}) increased, hence these parameters are sensitive. While in the reference profile 2 and poplar profile 3, best fit was achieved with increasing saturated hydraulic conductivity (K_0) and porosity (n), for profile 1 it was achieved with a decrease in both (Tab. 4.2).

Multiple compartments: At SRC profiles 1 and 3, model step V simulates observed isotope signature over depth even better.

Best model runs: However, model efficiency (KGE_{mean}) of profiles 1 and 3 is below 0 for all model steps; therefore, the validity of the model results is limited (Tab. 4.2). A best model efficiency (KGE_{mean} (r + α)) of 0.25 is achieved for profile 2 which is still a poor efficiency (Tab. 4.2). Comparing KGE_{mean} with KGE_{mean} (r + α) almost no shift is measured (Tab. 4.2), this is illustrated as well in the depth plots (Fig. C.1, C.2, C.3).

In the following, the best model runs (profile 1 and 3: model step V, profile 2: model step IV) are described in detail. Pearson's r for profile 1 and 3 indicates a weak linear

TABLE 4.2: Best parameter values for Kupferzell obtained from the SWIS model runs. Notes: [1] Texture of topsoil layer was equal in BK50 and field notes; thus, it was fixed from the beginning.

	Unit	Profile 1	Profile 2	Profile 3
Profile characteristics				
Vegetation	-	willow	grassland	poplar
Age	[yrs]	4	-	4
Sampling time	-	spring 2015	spring 2015	spring 2015
Model step II: insensitive parameter				
Texture top soil layer [1]	-	Lu	Lu	Lu
Texture bottom soil layer	-	Tu2	Tu2	Tu2
Depth of bottom soil layer	[cm]	30	30	30
Transpiration depth	[cm]	90	250	250
Model step III: sensitive parameter				
Evaporation depth	[cm]	50	50	50
Model step III: model efficiency				
KGE_{mean}	-	-1.87	0.08	-0.6
KGE_{mean} (r + α)	-	-1.87	0.09	-0.6
Model step IV: parameter				
K_0	[%]	-20	10	20
n	[%]	-10	5	5
Model step IV: model efficiency				
KGE_{mean}	-	-0.94	0.24	-0.4
KGE_{mean} (r + α)	-	-0.94	0.25	-0.4
Model step V: model efficiency				
KGE_{mean}	-	-0.16	0.01	-0.33
KGE_{mean} (r + α)	-	-0.16	0.02	-0.33

relationship of simulated and observed oxygen-18 values ($0 < r < 0.4$) and inverse proportional relationship of deuterium values ($-0.9 < r < 0$) (Fig. C.1, C.3). For profile 2, a linear relationships for both simulated and observed oxygen-18 values and deuterium values can be measured ($0 < r < 0.7$) (Fig. C.2).

The bias ratio of isotope values of all three profiles is almost one, indicating that the mean values of simulations is almost equal to the mean value of observations (Fig. C.1, C.2, C.3). To analyze the shift indicated by β, the residuals of the model runs can be examined. For profile 1, residuals of isotopes over depth indicate model over-predictions of up to 10 % till 50 cm of depth and under-predictions of up to 10 % between 60 and 120 cm depth. A few values lie within the confidence interval of ± 5 %. The residuals for oxygen-18 tend to be smaller than those for deuterium, except at depths 10, 30 and 50 cm (Fig. 4.9 left plot). Similar patterns can be observed for profile 3. Differences are that values are over-estimated till a depth of 40 cm and that under-estimations of deuterium values are higher, further, no outlier of oxygen-18 occurs (Fig: 4.10). For profile 2 oxygen-18 outlier in 10 cm depth occurs again. Over-estimations are within the +/-5 % confidence interval. Under-estimations occur below 30 cm depth and are

around 15 % to 20 % (Fig. 4.11).

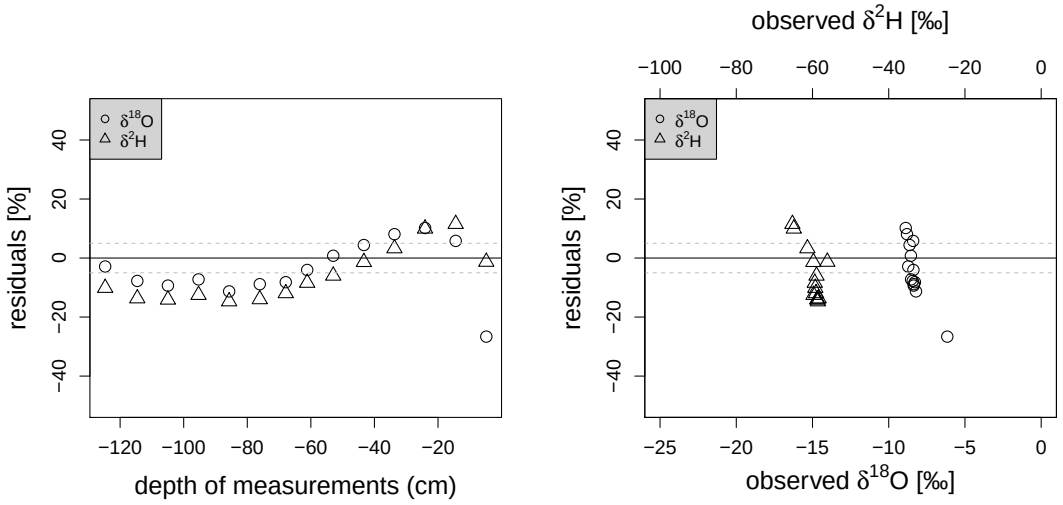

FIGURE 4.9: Residual plot from best fit run of model step V of profile 1 in Kupferzell.

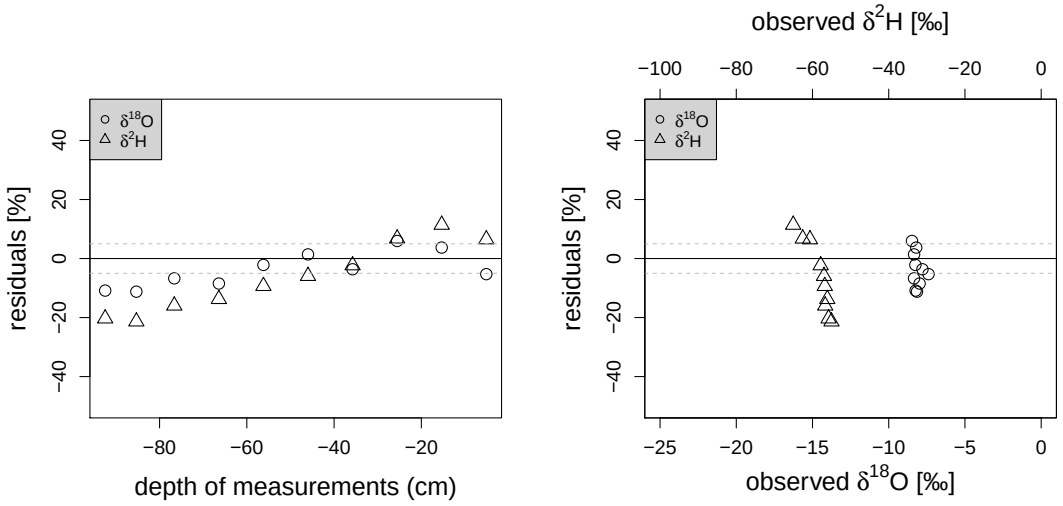

FIGURE 4.10: Residual plot from best fit run of model step V of profile 3 in Kupferzell.

When comparing deuterium values, variability ratio (α) of greater 1 is calculated, indicating that standard deviation of simulations is bigger than that of measurements (Fig. C.1, C.2). In contrast, variability ratio of oxygen-18 for profile 1 and 2 indicates higher standard deviations of observed values. Plots of residuals over observed isotope values indicate that the biggest residuals occur at small deuterium values and for the oxygen-18 outlier, the former being over-estimated and the latter being under-estimated by the simulations (Fig. 4.9, right plot). For profile 3, oxygen-18 values vary more than simulated ones ($1 > \alpha > 1.6$) (Fig. C.3). Variability ratio of volumetric water content ($0 > \alpha > 0.2$) and deuterium-excess describes the above mentioned great variability of measurements ($0 > \alpha > 0.3$) which the model fails to reproduce.

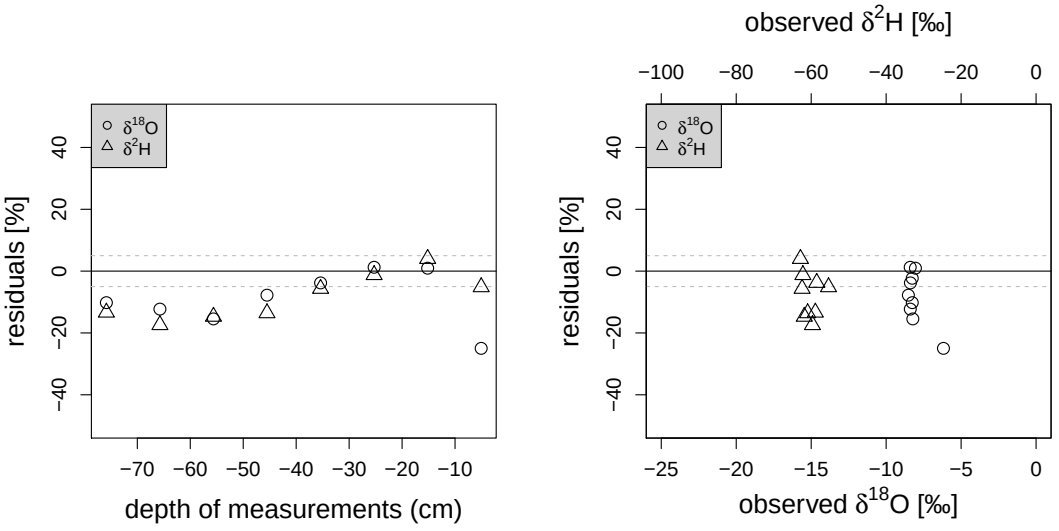

FIGURE 4.11: Residual plot from best fit run of model step IV of profile 2 in Kupferzell.

In conclusion, best model fits were achieved at the reference site (grassland, profile 2). Model predictions for willow and poplar stands achieve poor model efficiency ($KGE_{mean} < 0$) and inverse proportional relationships between simulations and observations. The biggest difference between model step IV at the reference site and model step V at SRC sites is that model step V simulates almost constant isotope values with depth, thus observed seasonal effects are not reproduced. Without taking into account model efficiency, profile 2 at grassland and profile 3 in poplar plantation behave similarly concerning fitted parameter values. To sum up, no clear trend can be observed concerning an increase of permeability of soil at SRC stands, nor do differences between poplar in willow profiles occur.

4.4.3 Model steps II-V: Kraichtal

In Kraichtal, sampling was performed mid of March 2015, within three recently cut down poplar plantations of different age. Poplar plantation of profile 1 is the youngest (2 years), followed by profile 4 (4 years) and profile 2 (7 years). The area is slightly prone to prone. Control site, profile 3, was located within an uncultivated former maize field below the plantations (same height as profile 4). SRCs underlie intensive cultivation associated with rotations, nitrate fertilization and soil cultivation every two years. All SRC sites were used for crop production before poplar was planted. Space between rows is 2 m, within rows 2-3 trees are planted per m^2. In the silty soil, drilling was possible to

almost 3 m depth, more exact drilled depth were 285, 282, 191 and 223 cm for profiles 1 to 4.

Especially for profile 2 and 3, isotope values ($\delta^{18}O$ and $\delta^{2}H$) are depleted in the upper 50 cm depth compared to values below. This is an indication for infiltration depth of winter precipitation. In 150 to 200 cm depth a similar isotope depletion horizon occurs for profiles 2 and 3 (Fig. C.5, C.6). For profile 1 it occurs in a shallower depth of 100 to 150 cm (Fig. C.4). Profile 3 is too short to detect a second isotope depletion horizon (Fig. C.6). Nevertheless, coming deeper in soil, isotope variations become smaller; therefore, isotopic enrichment during summer below 50 cm and above second isotope depletion horizon is hardly detectable. Generally, measured volumetric soil water content varies from 0.1 to 0.5 between profiles and depths; additionally, a decrease in volumetric water content can be observed below 150 cm with a varying extent for all profiles. Deuterium-excess of profile 2, 3 and 4 varies between 5 and 10, except for one outlier in 10 cm depth, which indicates evaporation (Fig. C.5, C.6, C.7). For profile 1, deuterium-excess shows greater evaporation effects compared to the other profiles. It varies around 5, except for outliers in 10 and 70 cm depth. To sum up, no major differences can be observed comparing SRC profiles with the reference profile. Quite the contrary can be observed, the shape of the oldest poplar profile 2 is even more like the shape of the reference profile than like the shape of the other poplar profiles.

In the following the results of the sensitivity analysis shown in Tab. 4.3 are described:

Soil texture: The declining water content below 150 cm can not be associated with soil texture. Best fit of soil texture comparing field notes and BK 50 is achieved with a mono-layered silty silt (Uu).

Evaporation depth: Evaporation depth is not a sensitive parameter for the model; thus, evaporation effects, like those seen in the deuterium-excess of the observations were not detected in model step II.

Transpiration depth: Transpiration depth was detected to be a sensitive parameter and was set to 30 and 40 cm, with exception of profile 1.

TABLE 4.3: Best parameter values for Kraichtal obtained from the SWIS model runs. Notes: [1] Transpiration depth was not sensitive for profile 1.

	Unit	Profile 1	Profile 2	Profile 3	Profile 4
Profile characteristics					
Vegetation	-	poplar	poplar	uncultivated	poplar
Age	[yrs]	2	7	-	4
Sampling time	-	spring 2015	spring 2015	spring 2015	spring 2015
Model step II: insensitive parameter					
Texture bottom soil layer	-	-	-	-	-
Depth of bottom soil layer	[cm]	-	-	-	-
Evaporation depth	[cm]	40	10	10	20
Model step III: sensitive parameter					
Texture top soil layer	-	Uu	Uu	Uu	Uu
Transpiration depth	[cm]	80[1]	30	30	40
Model step III: model efficiency					
KGE_{mean}	-	0.41	0.47	0.69	-0.17
KGE_{mean} (r + α)	-	0.44	0.49	0.7	-0.16
Model step IV: parameter					
K_0	[%]	-20	20	20	-10
n	[%]	-5	0	-10	0
Model step IV: model efficiency					
KGE_{mean}	-	0.71	0.52	0.84	0.29
KGE_{mean} (r + α)	-	0.77	0.54	0.85	0.30
Model step V: model efficiency					
KGE_{mean}	-	0.33	-0.18	-0.05	-0.13
KGE_{mean} (r + α)	-	0.33	-0.18	-0.05	-0.13

Saturated hydraulic conductivity (K_0) and porosity (n): When optimizing soil hydraulic properties (K_0 and n) model efficiency increases, with the greatest increase for profile 1. Comparing K_0 and n between the profiles no trend can be observed.

Multiple compartments: Applying model step V does not improve model efficiency, model efficiency is even lower than at model step III.

Best model runs: Model efficiency $KGE_{mean}(r+\alpha)$ is in all model steps not remarkably better than KGE_{mean}. To conclude model step IV achieved highest model efficiency (KGE_{mean}) at all profiles. Comparing KGE_{mean}, best fit was performed at the uncultivated site, profile 3 ($KGE_{mean} = 0.84$).

A detailed description of best fit runs of model step IV follows: Pearson's r between 0.59 and 0.9 describe strong linear relationships between simulated and observed isotope values (Fig. C.4, C.5, C.6, C.7). Maximal r of 0.9 appears at reference profile 3 (Fig.

C.6). Bias ratio β of isotope values lies between 0.8 and 0.96, indicating that mean of simulations is almost equal to mean of observations. Again highest values are calculated for profile 3. Variability ratio α of isotope values for profiles 1 and 3 is between 0.79 and 0.92, indicating slightly greater standard deviation of observations. On the contrary, profiles 2 and 4 have α values greater 1 for isotope simulations, indicating that simulated variability is greater than observed. Modeled water content of all profiles is considered to be constant at around 0.4; thus, the measured variability is not reproduced correctly. The simulated deuterium-excess variability does not agree with the measurements, either.

To further quantify and classify the differences between model and observations, residuals are calculated and described in the following. Generally oxygen-18 values are less over-predicted than deuterium values in all profiles. For profile 1, the plot of residuals over depth of measurements demonstrates that the model over-predicts constantly more than 20 % with exception of the depth to 50 cm and between 150 and 200 cm (Fig. 4.12, left plot). Findings on variability ratio are also supported by the shape of figure 4.12 (right plot). As heavy and light isotope values are less over-predicted than values in between, the shape suggests that a model with higher variability should be introduced for a better fit (Fig. 4.12, right plot).

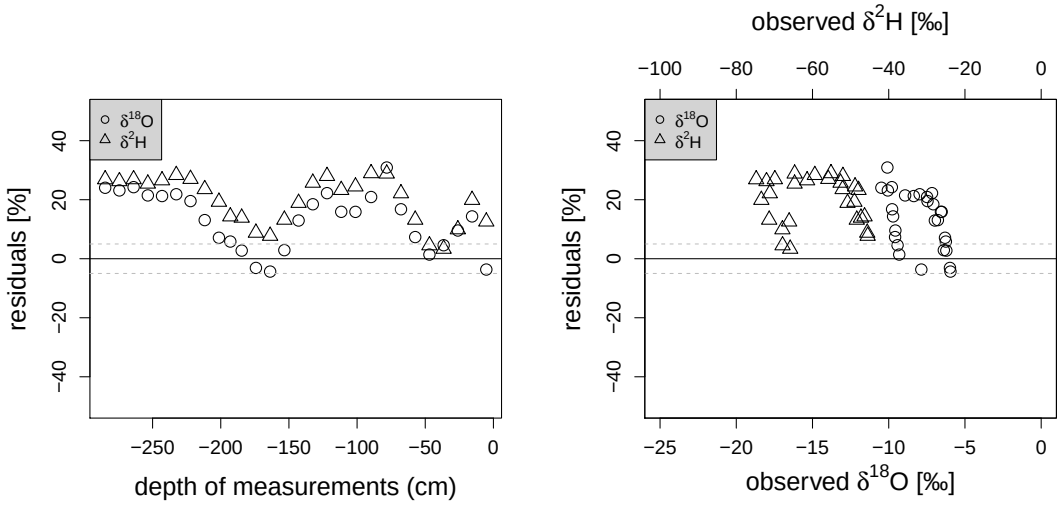

FIGURE 4.12: Residual plot from best fit runs of model step IV of profile 1 in Kraichtal.

For profile 2 residual plot in figure 4.13 (left plot) shows an under-estimation around 50 cm depth and over-estimations up to 30 % in all other depth, occurring at the range of all isotope values (4.13 (right plot)). For profile 3 residuals are within the confidence interval of ± 5 % except around 100 cm depth, where the model over-estimates (Fig.

4.14 (left plot). Again low and high isotope values are overestimated in the simulations (Fig. 4.14 (right plot)). Isotope values of profile 4 are continuously over-estimated, between 70 and 190 cm by around 20 % (Fig. 4.15).

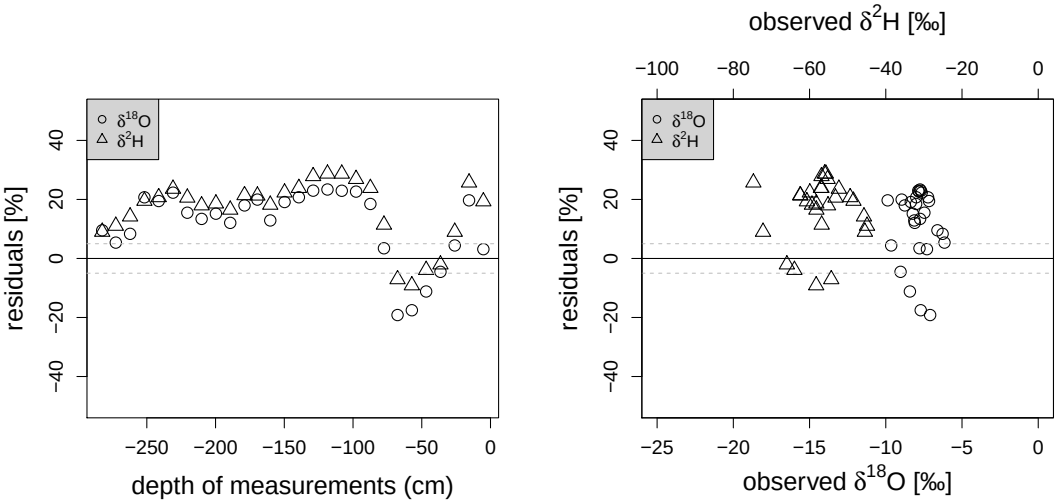

FIGURE 4.13: Residual plot from best fit runs of model step IV of profile 2 in Kraichtal.

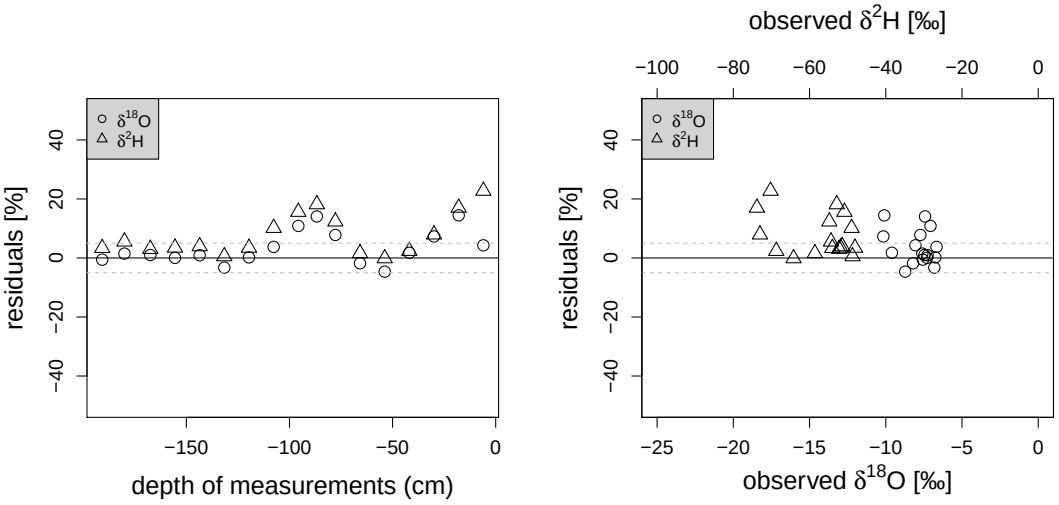

FIGURE 4.14: Residual plot from best fit runs of model step IV of profile 3 in Kraichtal.

In conclusion, model efficiency was greater than or equal to 0.3 for all profiles, with highest values at uncultivated site (profile 3). Neither between SRC profiles and reference site, nor between the poplar profiles of different age, significant differences occurred. Depletion horizon reaches a depth of approximately 60 cm for all profiles. Below that, isotope values of profiles are either constant or vary a lot; therefore, no conclusions can be drawn on an enrichment or second depletion horizon.

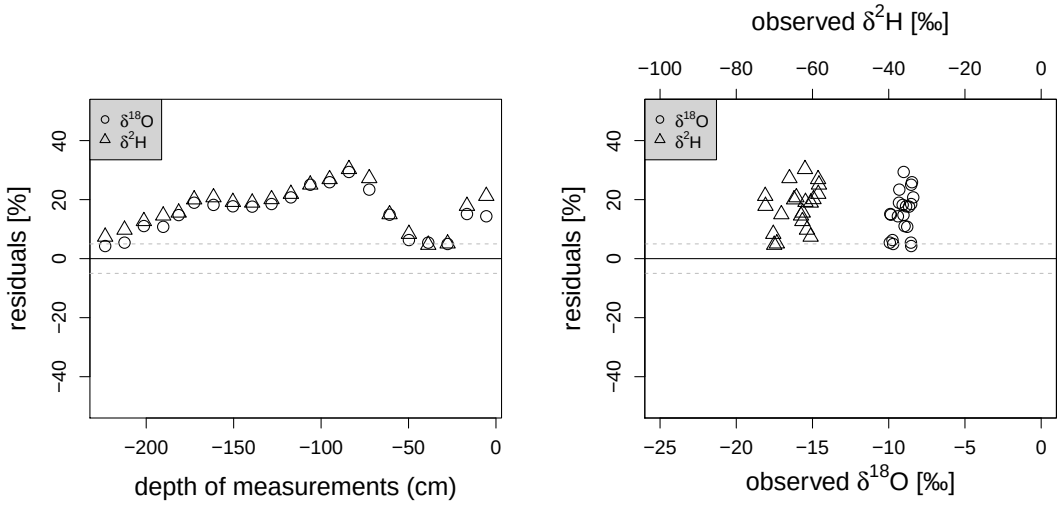

FIGURE 4.15: Residual plot from best fit runs of model step IV of profile 4 in Kraichtal.

4.4.4 Model steps II-V: Forchheim

SRCs of the Landwirtschaftliches Technologie Zentrum (LTZ) in Forchheim near Rheinstetten were sampled mid of March 2015. In total 6 depth profiles were drilled, two within poplar stands, two in willow stands and two reference profiles on grassland and in maize. Since the plantations are cultivated for tests on growth behavior and other characteristics of species in short rotation, there are different clones of poplar and willow planted next to each other. Cultivation is performed extensively. Furthermore, the age of plantations differs a lot, from 2 to 6 years. The whole area is flat and soils are sandy, thus drilling to 3 m of depth was possible. Drilling depths are 175, 176, 195, 282, 189, 180 cm for profiles 1 to 6.

Observations of isotope values for profiles 1 and 2 with 6-year-old poplar and 2-year-old willow show similar patterns (Fig. C.8, C.9). Depletion in heavy isotopes occurs till a depth of 50 cm, indicating infiltration of precipitation during winter months. From 100 to 150 cm depth another depletion horizon is visible, but less distinct than the first one. Volumetric water content varies between 0.2 and 0. Deuterium-excess for profile 1 shows high evaporation in the first 20 cm of depth, below that it varies between 5 and 10 (Fig. C.8). For profile 2 deuterium-excess varies a lot in the first 50 cm depth and is around 4, below that slight evaporation effects occur (Fig. C.9). Isotope observations of poplar profile 5 differ slightly from profile 1 and 2 by almost linearly decreasing values below 60 cm depth (Fig. C.12). Volumetric water content has a peak in 50 cm depth and

decreases to a constant value 0.05 below 100 cm (Fig. C.12). Deuterium-excess varies around 5 except in the first 20 cm, where strong evaporation effects occur (Fig. C.12).

Observed isotope values of willow profile 4 show much higher variations with depth than the other profiles (Fig. C.11). Winter depletion occurs till a depth of 60 cm, below an enriched horizon till 120 cm is visible indicating summer precipitation of 2014. Below 120 cm smaller variations occur with different amplitudes, till a depth of 220 cm, where a second enrichment horizon occurs. Volumetric water content is below 0.1. Deuterium-excess varies with depth, with values smaller than 10, which indicate evaporation. Isotopes, volumetric water content and deuterium-excess of the reference profiles 3 and 6 (Fig. C.10, C.13) significantly differ from those of willow and poplar profiles 1 and 2. To summarize, first depletion horizons occur to a depth of 50 cm, between 100 and 150 and below 220 cm. Between these horizons either enrichment horizons occur, or isotopes show smaller variations.

In the following the findings of the sensitivity analysis are summarized (Tab. 4.4):

Soil texture: During drilling, in poplar profile 1 and reference profile 6, a change of soil texture from sandy sand to a sandy loam could be observed for a layer of 5 to 10 cm between 120 and 145 cm of depth. This was not observed while fitting soil texture parameters. A mono-layered sandy sand (Ss) achieved best model efficiency results.

Evaporation depth: Sensitivity analysis (model step II and III) identified evaporation depth as sensitive parameter with best fits for depths of 10 cm for profiles 1 to 5 and 50 cm in the maize profile.

Transpiration depth: The model was not sensitive to transpiration depth.

Saturated hydraulic conductivity (K_0) and porosity (n): A reduction of K_0 and n, in model step IV, leads to an increase of variability of isotope simulation over depth. However, the simulated variability in model step IV increases model efficiency only for profile 5 and 6.

Multiple compartments: By seperating micro- from meso- and macropores, model V achieved worst efficiency. A distinction between pore spaces does not play a major rule in sandy soils with almost no micro pores. As higher KGE_{mean} (r + α) than

TABLE 4.4: Best parameter values for Forchheim obtained from the SWIS model runs.

	Unit	Profile 1	Profile 2	Profile 3	Profile 4	Profile 5	Profile 6
Profile characteristics							
Vegetation	-	poplar	willow	grassland	willow	poplar	maize
Age	[yrs]	6	2	-	6	6	-
Sampling time	-	spring 2015	spring 2015	spring 2015	spring 2015	spring 2015	spring 2015
Model step II: insensitive parameter							
Texture bottom soil layer	-	-	-	-	-	-	-
Depth of bottom soil layer	[cm]	-	-	-	-	-	-
Transpiration depth	[cm]	30	30	30	30	30	30
Model step III: sensitive parameter							
Texture top soil layer	-	Ss	Ss	Ss		Ss	Ss
Evaporation depth	[cm]	10	10	10	10	10	50
Model step III: model efficiency							
KGE_{mean}	-	0.08	0.29	0.27	0.27	-0.35	0.21
KGE_{mean} (r + α)	-	0.1	0.33	0.29	0.32	-0.32	0.24
Model step IV: parameter							
K_0	[%]	-10	-10	-10	-10	-10	-10
n	[%]	5	-10	5	-10	-10	-5
Model step IV: model efficiency							
KGE_{mean}	-	-0.46	-0.13	-0.01	-0.01	-0.22	0.49
KGE_{mean} (r + α)	-	-0.41	-0.06	0.05	0.08	-0.15	0.51
Model step V: model efficiency							
KGE_{mean}	-	-0.06	0.18	0.17	0.26	-0.45	0.13
KGE_{mean} (r + α)	-	-0.05	0.22	0.19	0.31	-0.43	0.16

KGE_{mean} values show there is a slight systematical shift between simulations and observations.

Best model runs: Comparing KGE_{mean} of model steps III, IV, and V, model step III achieved the best fit for profiles 1 to 4 and model step IV for profile 5 and 6.

In the following, best fit model runs for each profile are described in detail (Fig. C.8, C.9, C.10, C.12, C.13). Pearson's r of around 0.5 describes linear relationships between simulated and observed isotope values at all profiles except profile 5. For poplar profile 5 almost no linear relationship can be detected ($-0.15 < r < 0$) (Fig. C.12). Bias ratio between 0.5 to 0.93 for all profiles shows that mean of simulated values is bigger than mean of observed values. Over-estimations of up to 50 % are as well illustrated in the residual plots (Fig. 4.16, 4.17, 4.18, 4.19, 4.20). Simulated values are in almost all depth and all isotope value ranges twice as high as observed ones. Only for profile 6 over-estimations decline to 10 % with depth (Fig. 4.21). Variability ratio (α) is in all profiles, except willow profile 4, greater than 1, indicating that simulated variation is bigger than observed. For profile 4 observed and simulated variation ($0.9 < \alpha < 1$) are equal. Looking at the depth plots (Fig. C.8, C.9, C.10, C.12, C.13) significant variation

in simulated isotope values does only occur in the first 100 cm while observed values vary over the whole profile.

For profiles 1,2,3 and 6, simulated volumetric water content and deuterium-excess are in the same range as observed values, but their variability does not agree with the measured one. For profile 4 and 5, deuterium-excess also behaves like this, but simulated volumetric water content is twice the measured water content.

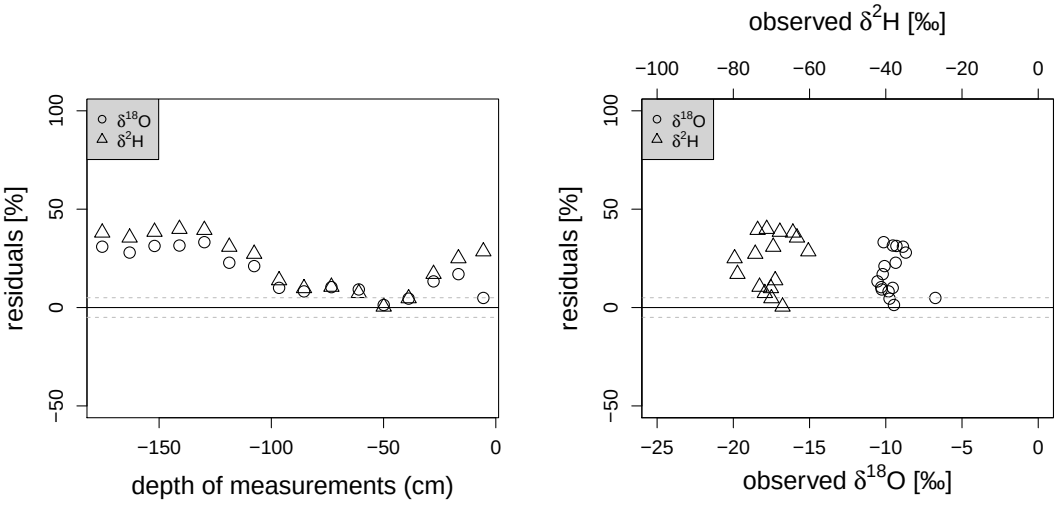

FIGURE 4.16: Residual plot from best fit run of model step III of profile 1 in Forchheim.

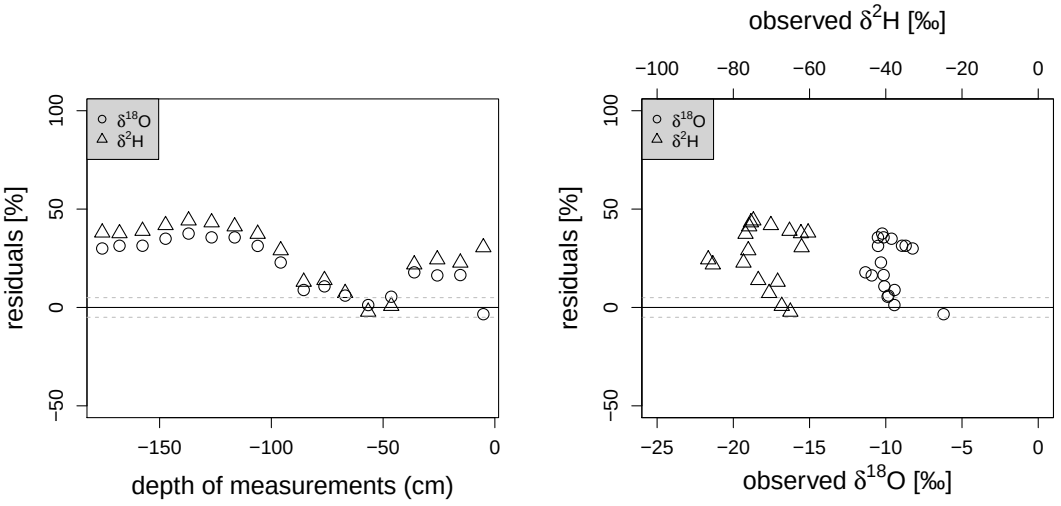

FIGURE 4.17: Residual plot from best fit run of model step III of profile 2 in Forchheim.

In conclusion, simulations in Forchheim do not display the variability of the measurements. Model step III simulates almost stable values below 100 cm. Model step IV with reduced K_0 and n, and evaporation depth of 10 cm, simulates greater variability with depth, but is not able to reproduce measurements either. The best-fit evaporation depth was highest at the reference profile in maize, due to the the type of cultivation

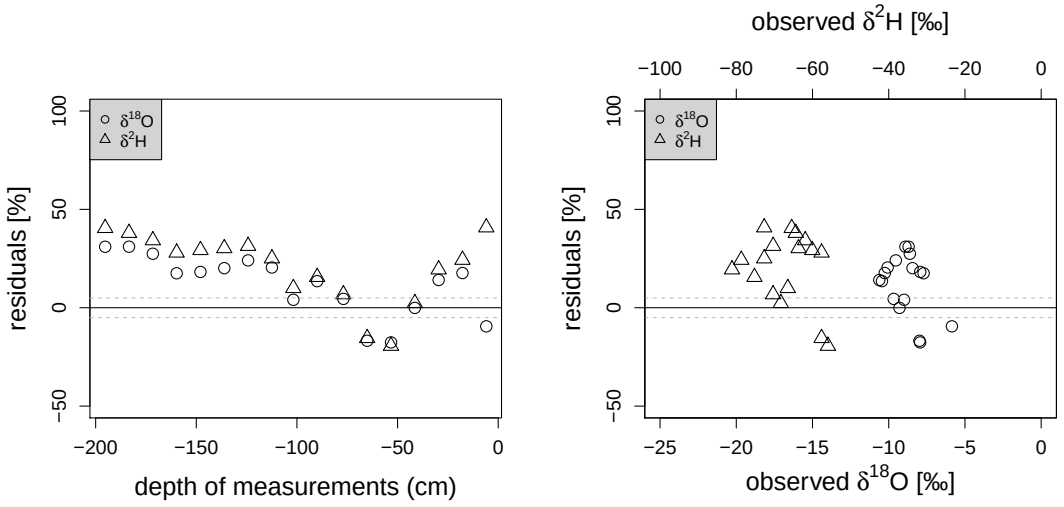

FIGURE 4.18: Residual plot from best fit run of model step III of profile 3 in Forchheim.

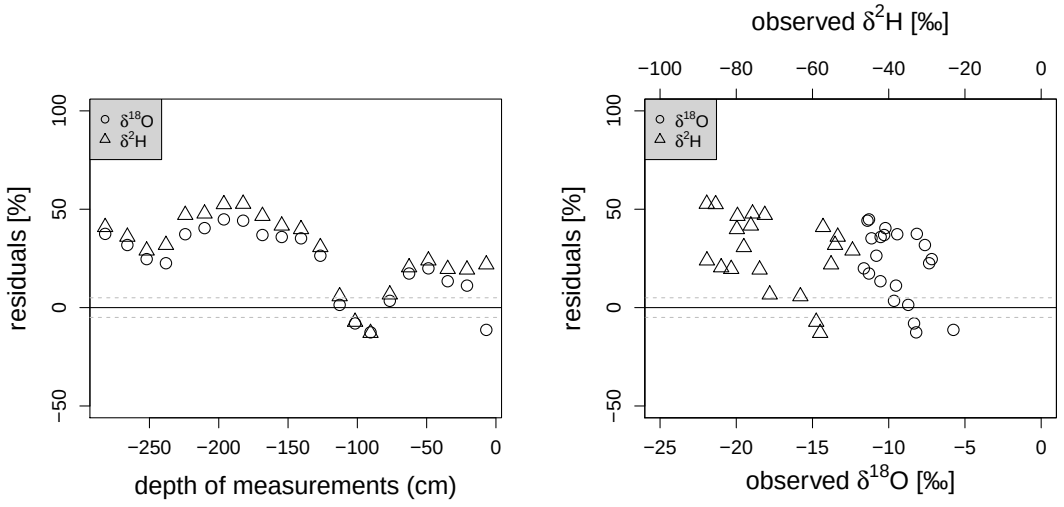

FIGURE 4.19: Residual plot from best fit run of model step III of profile 4 in Forchheim.

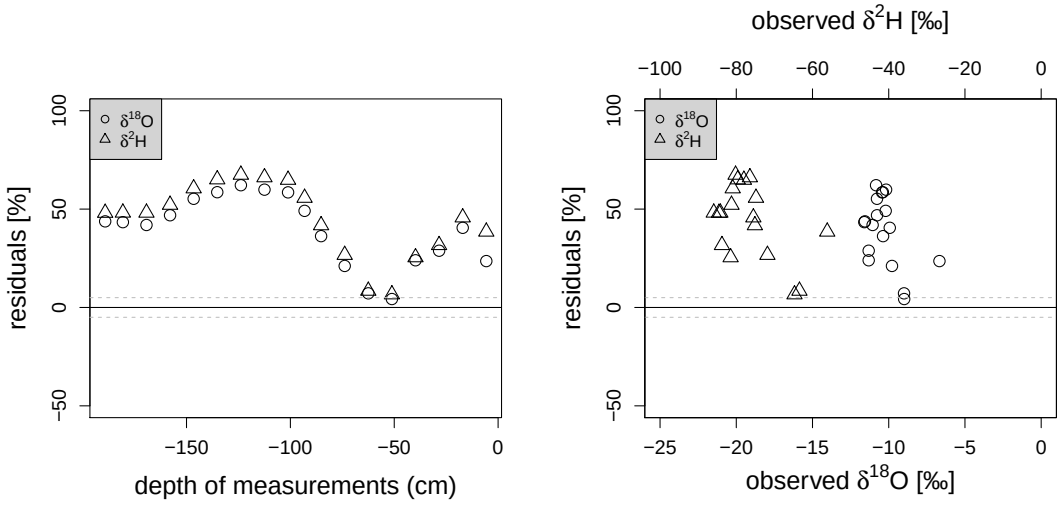

FIGURE 4.20: Residual plot from best fit run of model step IV of profile 5 in Forchheim.

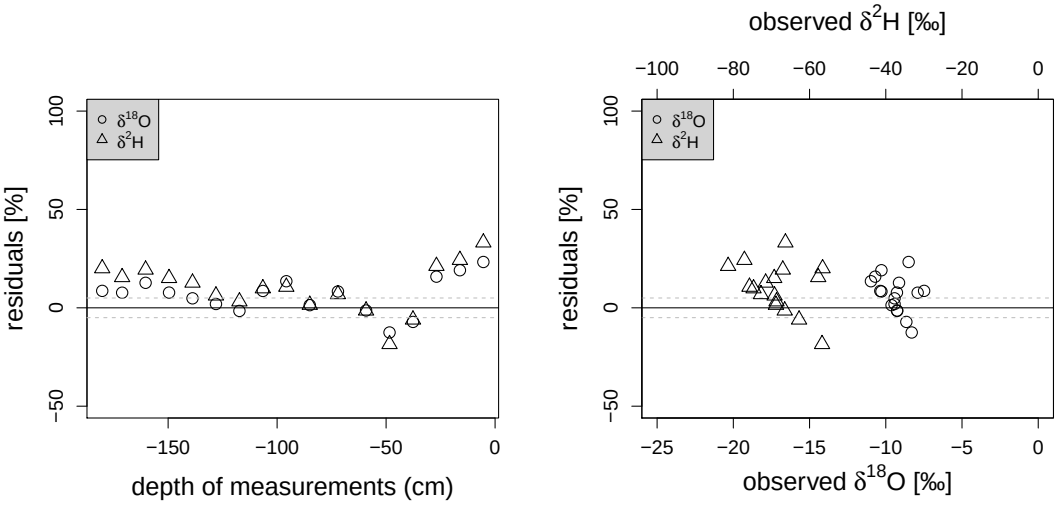

FIGURE 4.21: Residual plot from best fit run of model step IV of profile 6 in Forchheim.

and plowing horizon this was expected. Although model efficiency ($KGE_{mean} = 0.33$) is equal to profile 2 in Kupferzell the shape of simulations seem to fit less in Forchheim. Some of the observed and inexplicable variation in the measurements might come from problems during sampling. When pulling the drilling core out of the ground, mixture and soil loss could not be avoided due to the sandy soil texture. Furthermore, there might have been complications during isotope analysis within the direct equilibration, because water content was below 0.1.

4.4.5 Model steps II-V: Marbach

In Marbach, sampling was done in the beginning of April 2015. In a flat to slightly prone terrain, extensively cultivated poplar and willow plantations were sampled. Space between rows is 2 m and within rows 1 m. As reference, a third profile was drilled in an intensively cultivated oat field. Drilled depth of profile 1 to 3 are 155, 83 and 135 cm.

While isotope values of profile 1 and 2 are depleted in the first 50 cm of depth, they are enriched till 100 cm of depth, indicating seasonal variations of winter and summer (Fig. C.14, C.15). Reference profile 3 shows the same depletion pattern in the first 50 cm but constantly decreases below (Fig. C.16). Volumetric water content of all profiles is highly variable with depth. While deuterium-excess of profiles 2 and 3 varies around 5, indicating some evaporation, it varies around 10 for profile 1, indicating no evaporation.

Tab. 4.5 summarizes the results of the sensitivity analysis which are described in the following:

Soil texture: Texture of topsoil was identified as silty clay (Tu3). Model efficiency was not sensitive to the texture of the second soil layer and its depth. However, field analysis and BK50 showed a layering; therefore, soil texture of bottom layer is set to clayey loam (Lt3).

Transpiration and evaporation depth: Both, transpiration and evaporation depth, effected model efficiency with best results at depth of 140, 30, 250 cm for transpiration depth and 10 cm for evaporation depth, respectively.

Saturated hydraulic conductivity and porosity: Model efficiency for profile 1 and 2 could be improved by a decrease of porosity and saturated hydraulic conductivity.

Multiple compartments: For oat profile 3 model step V resulted in an improvement, but the model efficiency of profile 3 is still around 0.

Best model runs: To conclude, best model efficiency of KGE_{mean} $(r + \alpha) = 0.71$ and 0.82 can be achieved by model step IV for profile 1 and 2. Model efficiency of profile 3 is below 0 for all model steps.

Looking at best fit model runs, model step IV for profile 1 has a linear relationship to the observations ($0.3 < r < 0.9$) (Fig. C.14), but over-predicts observations by 20 to 40 % at the whole range of isotope values (Fig. 4.22); moreover, it over-estimates variability of measurements ($1 < \alpha < 1.3$). Simulated volumetric water content and deuterium-excess do not mirror the great variability in measurements.

For poplar profile 2, model step IV performed very well for oxygen-18 values with r, α and β of 0.9; however, simulations do still over-predict by up to 20 %. Modeled deuterium-excess fits better than for profile 1 and 3 (Fig. C.15, 4.23).

Model step V for profile 3 over-predicts especially low deuterium values up to 20 %. Generally the variability of the observations is not simulated well for isotopes, volumetric water content and deuterium-excess (Fig. C.16, 4.24).

In conclusion, neither parameter fitting nor observation data showed specific trends of increased infiltration capacity at the SRC sites. Simulations did continuously over-estimated observed isotope data. Contrary to the expectations, best fit was achieved

TABLE 4.5: Best parameter values for Marbach obtained from the SWIS model runs. Notes: [1] texture of bottom soil layer is Lt3 according to BK50 and field notes; thus, it is fixed from the beginning.

	Unit	Profile 1	Profile 2	Profile 3
Profile characteristics				
Vegetation	-	willow	poplar	oat
Age	[yrs]	5	5	-
Sampling time	-	spring 2015	spring 2015	spring 2015
Model step II: insensitive parameter				
Texture bottom soil layer [1]	-	Lt3	Lt3	Lt3
Depth of bottom soil layer	[cm]	30	30	30
Model step III: sensitive parameter				
Texture top soil layer	-	Tu3	Tu3	Tu3
Transpiration depth	[cm]	140	30	250
Evaporation depth	[cm]	10	10	10
Model step III: model efficiency				
KGE_{mean}	-	-0.29	-0.24	-0.47
KGE_{mean} (r + α)	-	-0.26	-0.23	-0.44
Model step IV: parameter				
K_0	[%]	-10	0	-10
n	[%]	-5	-5	-5
Model step IV: model efficiency				
KGE_{mean}	-	0.58	0.71	-0.41
KGE_{mean} (r + α)	-	0.71	0.82	-0.36
Model step V: model efficiency				
KGE_{mean}	-	-0.31	-0.75	0.04
KGE_{mean} (r + α)	-	-0.30	-0.75	0.07

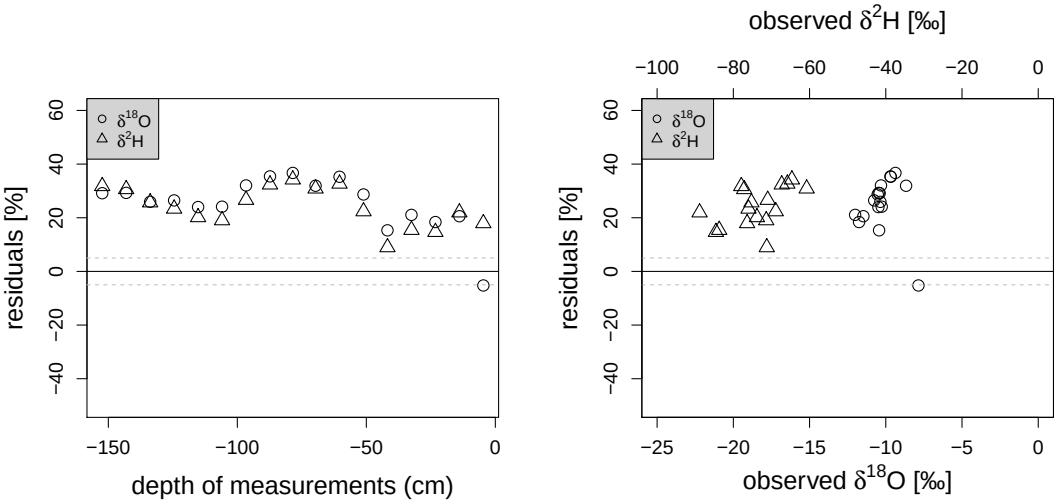

FIGURE 4.22: Residual plot from best fit runs of model step IV of profile 1 in Marbach.

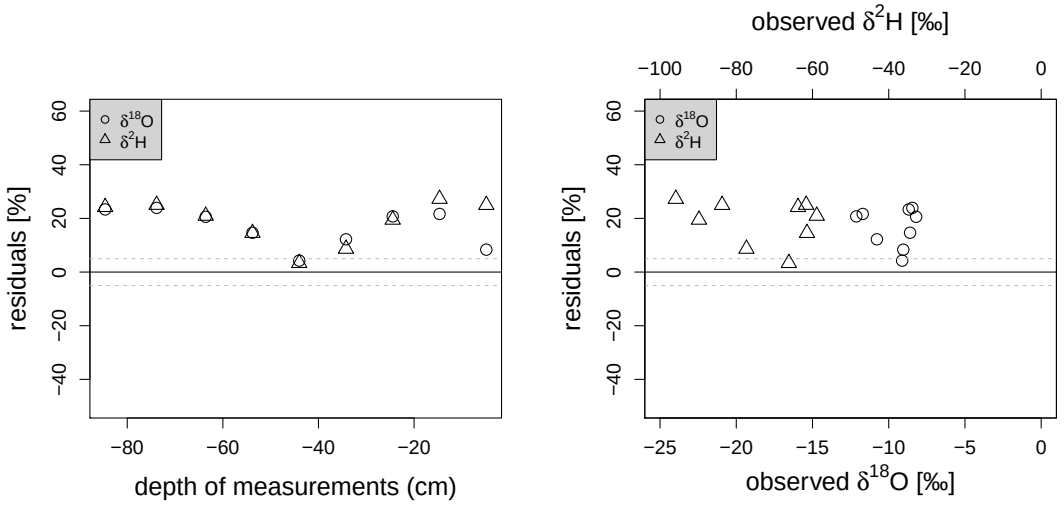

FIGURE 4.23: Residual plot from best fit runs of model step IV of profile 2 in Marbach.

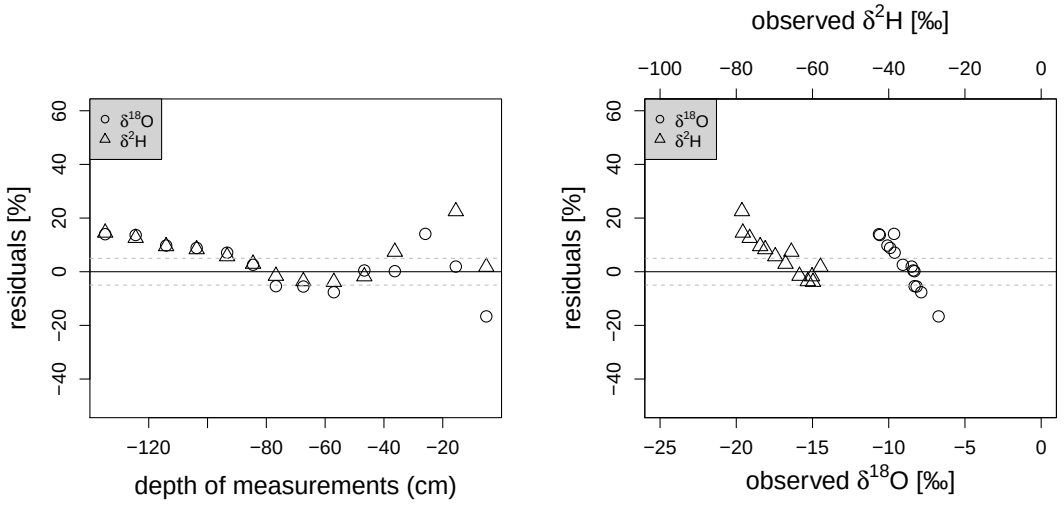

FIGURE 4.24: Residual plot from best fit runs of model step V of profile 3 in Marbach.

with reduced porosity values. So, no trend towards increased saturated hydraulic conductivity or porosity at SRC sites could be observed. Poorest model efficiency was observed at the reference site with oat. A depletion horizon till a depth of approximately 50 cm indicated infiltration depth of winter precipitation in all profiles.

4.4.6 Model steps II-V: Laufen

In Laufen, sampling was done twice, mid of October 2014 and in the beginning of March 2015, in a slightly prone to prone area. Species in short rotation differ from those of the other sampling sites. There are two profiles in sida plantations and three sites in paulownia plantations, whereby there was a mixture of paulownia and poplar on profile 5.

For comparison, one profile was drilled in grassland. All sites are extensively cultivated and fertilized with manure. Sites with sida were harvested in 2015. The age of SRCs differs from 2 to 4 years. Drilled depth in 2014 for profile 1 to 6 are 92.21, 177.02, 143.18, 96.63, 94.1 and 64.39 cm. In 2015 most drilling cores were less deep: depth profile 1 to 6 are 93.18, 131.68, 90.68, 67.94, 87.29, 83.05 cm. Profile 4 and 5 are below profiles 1 to 3 near an old riverbed; therefore, groundwater level is around 40 cm below ground. Taking into account drilling depth of approximately 1 m, drilling cores were influenced by ground water. However this effect was only observed in 2014.

It is expected that isotope values over depth of October 2014 are enriched in the first few cm of depth indicating infiltrated summer precipitations, while isotope values over depth of March 2015 are expected to be depleted in the first few cm of depth indicating infiltrated winter precipitations. Isotopes for profile 1, 4 and 5 show only marginal to no variations with depth and between the years; thus, no seasonal variations are visible (Fig. C.25, C.26, C.31, C.32, C.33, C.34). For profile 2, 3 and 6, variations between the years are visible (Fig. C.27, C.28, C.29, C.30, C.35, C.36). While a distinct depletion horizon in the first few cm of depth in the profile taken in March 2015 is detectable, enrichment horizon in 2014 is not that distinct. This might be due to the wet and cold summer in 2014 (see section 5.2). Volumetric water content of 2014 could not be calculated correctly (see section 3.3); thus, variations are not taken into account here. In 2015, volumetric water content varies around 0.4. Expected differences in deuterium-excess between the years do not occur.

Results of the sensitivity analysis are summarized in Tab. 4.6 and described in the following:

Soil texture: A mono-layered soil gave the best fit in both years. Whereas for profiles taken in 2014 a clayey silt (Ut2) achieved best model efficiency, for profiles taken in 2015 it was a silty loam (Lu).

Transpiration and evaporation depth: Transpiration and evaporation depth were detected as sensitive parameters, except transpiration depth of profiles 4 and 5 in 2015 (Fig. D.6, D.7). Values of best fit are mentioned in Tab. 4.6. Generally, evaporation depth was higher in spring 2015 than in autumn 2014; furthermore, transpiration depth was higher in autumn 2014 than in spring 2015, except for profiles 5 and 6.

Saturated hydraulic conductivity and porosity: In 2014, model step IV achieved best fits, with a reduction of K_0 by 20 % and a reduction of n by 10 %, with one exception for profile 2. In 2015, model step IV performed best for profiles 2, 3 and 6 with the same reduction of K_0 and n like in 2014.

Multiple compartments: For profiles 1, 4 and 5, model step V described the observations best.

Best model runs: All in all, model efficiency (KGE_{mean}) of model step IV for profile 2 paulownia, profile 3 paulownia (in 2015), and profile 6 grassland (in 2015) are the only ones exceeding 0. The other model fits must be viewed with caution and are neglected from the following description because of their poor model efficiency.

KGE_{mean} smaller 0 are calculated due to r almost equal to 0, or $r < 0$, or α values around 2 which means that, variability of simulations is greater than of observations and relationship between simulations and observations is inverse linear. [1]

In the following, profiles with $KGE_{mean} > 0$ are described in detail. Model step IV for profile 2 achieved a best fit of $KGE_{mean} = 0.36$ in 2014 and $KGE_{mean}(r + \alpha) = 0.54$ in 2015, with a reduction in saturated hydraulic conductivity and porosity. Modeled variability of isotopes over depth is in 2014 higher than the observed one (Fig. C.27, 4.25); nevertheless, bias ratio of almost 1 indicates that simulations and observations cover the same range of relative isotope concentration (Fig. C.27).

Furthermore, residuals illustrate that large values are over- or under-estimated within the upper 90 cm of depth. Simulations of profiles 2 and 3 fit particularly well at $\delta^{18}O$ observations of the first 60 cm depth (Fig. 4.26, 4.27). Enrichment horizon below 50 cm is over-predicted by around 40 %. While variability of simulations and observations for profiles 2 and 3 in 2015 is equal, means of δ^2H observations are lower than the observed (Fig. 4.26, 4.27). Simulations of short profile 6 in 2015 behave like for profiles 2 and 3 in 2015.

In conclusion, enrichment during summer 2014 is over-estimated by model step IV. This might be due to poor input data. Climate data were taken from Müllheim and isotope data from Weil, both are located in the Rhine plains and not at the edge of the Black

[1] Residual plots are only shown for profiles with $KGE_{mean} > 0$. The remaining residual plots are stored on the attached CD.

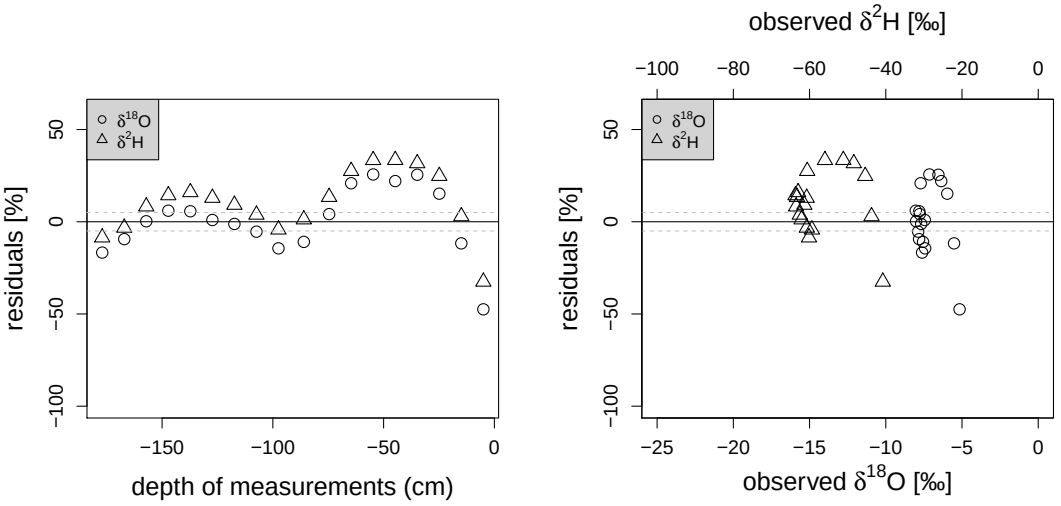

FIGURE 4.25: Residual plot from best fit runs of model step IV of profile 2 sampled in autumn 2014 in Laufen.

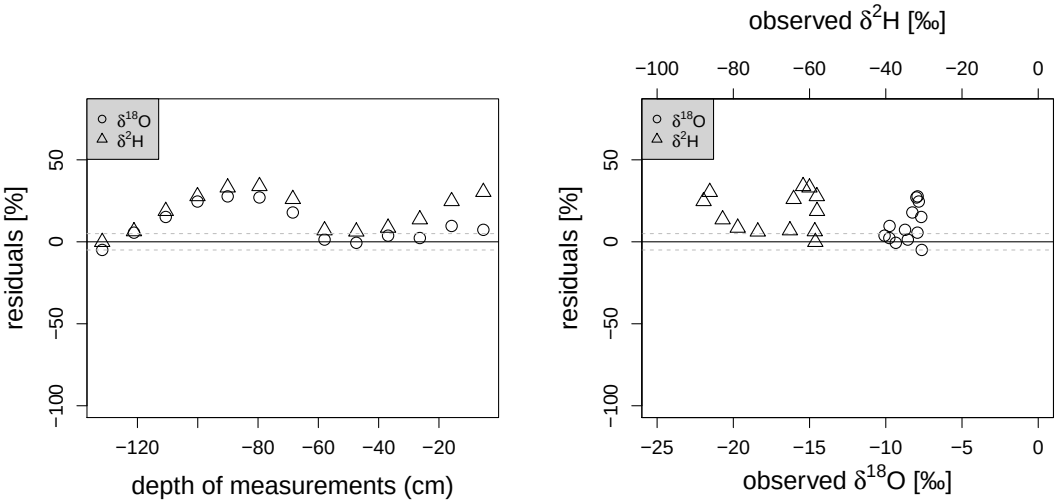

FIGURE 4.26: Residual plot from best fit runs of model step IV of profile 2 sampled in spring 2015 in Laufen.

forest where the sampling site is located. In that area there are huge climatic differences as described in section 3.1. Thus precipitation and temperature effects in Laufen might not be accounted for correctly. Because most profiles have poor model efficiencies, a comparison of soil hydraulic properties of SRC and reference site is not possible.

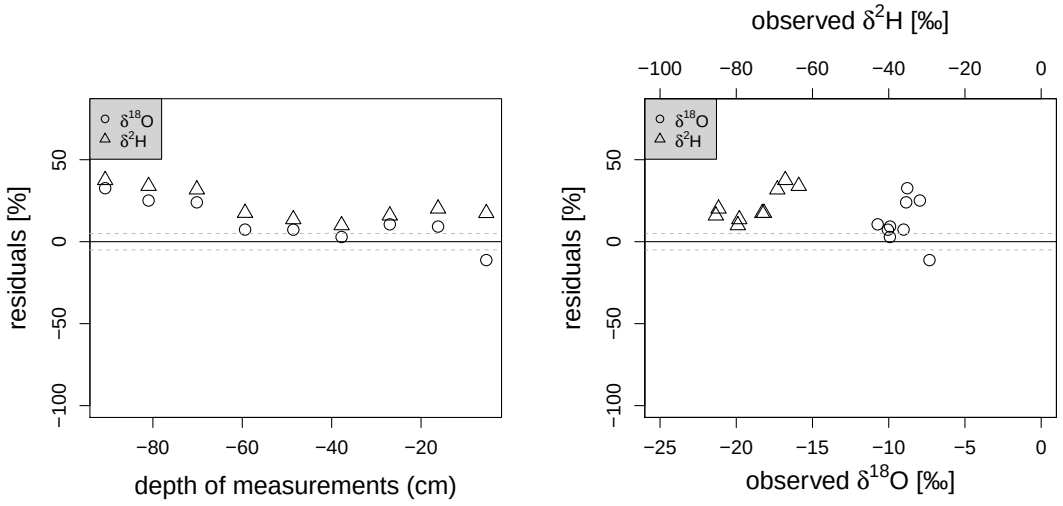

FIGURE 4.27: Residual plot from best fit runs of model step IV of profile 3 sampled in spring 2015 in Laufen.

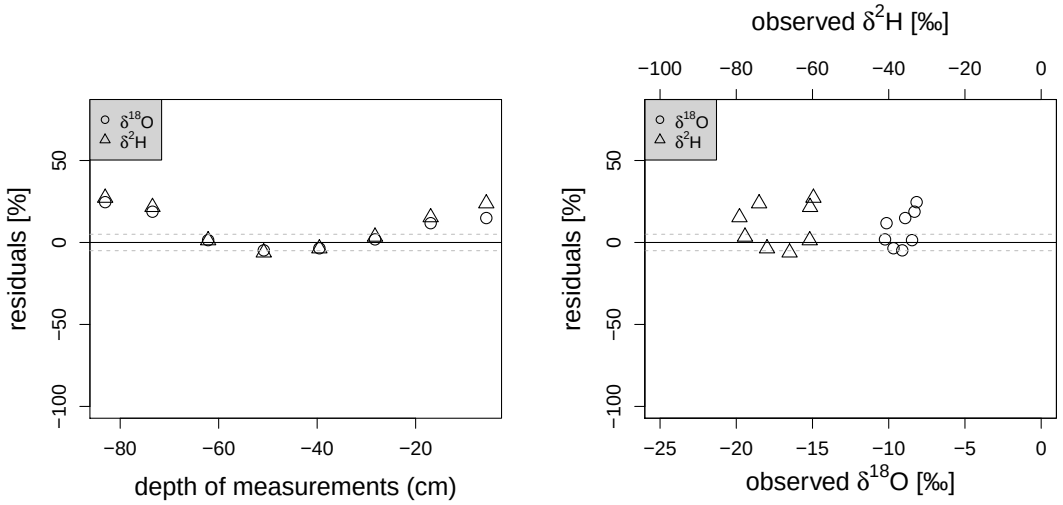

FIGURE 4.28: Residual plot from best fit runs of model step IV of profile 6 sampled in spring 2015 in Laufen.

TABLE 4.6: Best parameter values for Laufen obtained from the SWIS model runs. Notes: [1] Transpiration depth not sensitive for profiles 4 and 5.

	Unit	Profile 1		Profile 2		Profile 3		Profile 4		Profile 5		Profile 6	
Profile characteristics													
Vegetation	-	sida		paulownia		paulownia		sida		poplar/ paulownia		grassland	
Age	[yrs]												
Sampling time	-	autumn 2014	spring 2015	autumn 2014	spring 2015	autumn 2014	spring 2015	autumn 2014	spring 2015	autumn 2014	spring 2015	autumn 2014	spring 2015
Model step II: insensitive parameter													
Texture bottom soil layer	-	Ut2	Lu	Ut2	Lu	Ut2	Lu	Ut2	Lu	Ut2	Lu	Ut2	Lu
Depth of bottom soil layer	[cm]	50	50	50	50	50	50	50	50	50	50	50	50
Model step III: sensitive parameter													
Texture top soil layer	-	Ut2	Lu	Ut2	Lu	Ut2	Lu	Ut2	Lu	Ls3	Lu	Ut2	Lu
Transpiration depth	[cm]	30	250	70	60	40	30	30 [1]	30 [1]	50 [1]	30 [1]	30	30
Evaporation depth	[cm]	10	50	10	50	10	50	10	50	50	50	10	10
Model step III: model efficiency													
KGE_{mean}	-	-0.74	-2.18	-0.17	0.07	-0.13	0.39	-0.57	-1.2	-0.93	-0.81	-0.62	-0.15
KGE_{mean} (r + α)	-	-0.72	-2.18	-0.16	0.1	-0.12	0.41	-0.57	-1.2	-0.9	-0.81	-0.6	-0.15
Model step IV: parameter													
K_0	[%]	-20	10	-10	-20	-20	-20	-20	10	-20	-10	-20	-20
n	[%]	-10	5	0	-10	-10	-10	-10	-10	-10	5	-10	-10
Model step IV: model efficiency													
KGE_{mean}	-	-0.07	-1.55	0.36	0.50	-0.09	0.42	-0.11	-1.17	-0.58	-0.49	0.01	0.27
KGE_{mean} (r + α)	-	-0.07	-1.56	0.37	0.54	-0.10	0.45	-0.11	-1.17	-0.58	-0.50	0.02	0.29
Model step V: model efficiency													
KGE_{mean}		-0.95	-0.62	-0.17	-1.01	-0.46	-0.83	-0.97	-0.60	-0.72	-0.38	-0.83	-0.93
KGE_{mean} (r + α)		-0.95	-0.62	-0.17	-1.02	-0.46	-0.83	-0.97	-0.60	-0.72	-0.38	-0.83	-0.93

4.4.7 Model steps II-V: Buggingen

Sampling in Buggingen was performed twice, mid October 2014 and end of April 2015. The sampling area within three willow plantations of different ages is flat. Profiles are taken in 3-, 4- and 5-year-old stands in 2014, as well as half a year later in 2015. SRCs are cultivated extensively and fertilized with manure. In comparison to sampling site Kraichtal, rows are planted relatively densely with space of 1 m within and between rows. Reference profile was drilled in a maize field nearby. Drilled profile depths range from 57 to 90 cm in 2014 and from 59 to 89 cm in 2015.

Isotope observations of profiles 1 and 3 in 2014 show a depletion horizon between 50 and 100 cm, above that heavy isotopes are more abundant, indicating enriched summer precipitation (Fig. C.17, C.19). Profiles 2 and 4 are shorter and measurements end in a depth of 50 cm; thus, depletion horizon is not monitored in 2014 (Fig: C.18, C.20). In 2015, isotope values of all measured profiles indicate a depletion horizon to a depth of almost 1 m depending on the drilled depth (Fig. C.21, C.22, C.23, C.24).

A summary of the results of the sensitivity analysis shown in Tab. 4.7 follows:

Soil texture: A two-layered soil consisting of 60 cm silty loam (Lu) over silty clay (Tu3) was identified as best fit soil texture.

Transpiration and evaporation depth: In 2014, transpiration depth was sensitive for profiles 1 and 3, while evaporation depth was sensitive for profiles 2 and 3. In contrast, in 2015, transpiration depth was not significantly sensitive but evaporation depth was sensitive with a maximum in model efficiency at 10 cm depth for the willow profiles and 50 cm depth at the maize plantation.

Saturated hydraulic conductivity and porosity: In most profiles, unchanged or slightly increased K_0 values in combination with a lower porosity (n) improved model step III efficiency.

Multiple compartments: Model step V did not achieve better fits than the other model steps.

Best model runs: Model step IV achieved at all profiles and in both years maximum efficiency in comparison to the other model steps.

TABLE 4.7: Best parameter values for Buggingen obtained from the SWIS model runs. Notes: [1] solely these profiles are sensitive to transpiration depth, [2] solely these profiles are sensitive to evaporation depth.

	Unit	Profile 1		Profile 2		Profile 3		Profile 4	
Profile characteristics									
Vegetation	-	willow		willow		willow		maize	
Age	[yrs]	3	4	5	-				
Sampling time	-	autumn	spring	autumn	spring	autumn	spring	autumn	spring
	-	2014	2015	2014	2015	2014	2015	2014	2015
Model step II: insensitive parameter									
Texture top soil layer	-	Lu	Lu	Lu	Lu	Lu	Lu	Lu	Lu
Texture bottom soil layer	-	Tu3	Tu3	Tu3	Tu3	Tu3	Tu3	Tu3	Tu3
Depth of bottom soil layer	[cm]	60	60	60	60	60	60	60	60
Model step III: sensitive parameter									
Transpiration depth	[cm]	40[1]	250	30	30	40 [1]	30	30	30
Evaporation depth	[cm]	30	10[2]	10[2]	10[2]	30[2]	10[2]	10	50[2]
Model step III: model efficiency									
KGE_{mean}		-0.57	0.74	-2.03	0.73	-0.63	0.67	-0.88	0.09
KGE_{mean} (r + α)		-0.54	0.83	-0.61	0.79	-0.59	0.72	-0.88	0.11
Model step IV: parameter									
K_0	[%]	0	10	0	0	0	10	-20	0
n	[%]	5	-10	5	0	5	-10	-10	5
Model step IV: model efficiency									
KGE_{mean}	-	0.54	0.74	-1.86	0.73	0.58	0.67	0.57	0.53
KGE_{mean} (r + α)	-	0.56	0.83	0.54	0.80	0.60	0.72	0.60	0.55
Model step V: model efficiency									
KGE_{mean}	-	-1.08	0.06	-3.23	0.24	-1.06	0.26	-1.04	-0.64
KGE_{mean} (r + α)	-	-1.08	0.08	-0.96	0.27	-0.58	0.29	-1.03	-0.65

In the following, results of best fit model runs are described in detail. Especially in spring 2015 a shift of means of simulations and measurements is visible expressed in bias ratio ($0.8 < \beta < 0.95$) and leading to higher $KGE_{mean}(r + \alpha)$ than KGE_{mean} (Fig. C.21, C.22, C.23, C.24). In autumn 2014 the first 10 to 20 cm depth are under-estimated by the model; however, the remaining depths observations are reproduced well (Fig. C.17, C.18, C.19, C.20). Residuals illustrate an over-estimation of around 20 % for all profiles in 2015. In 2014 it is a bit lower, but has a similar patter; therefore, two residual plots from 2015 are shown for exemplary visualization (Fig. 4.29, 4.30).

In conclusion, Buggingen was the only sampling site showing a trend of lower evaporation depth at the SRC plantations than at the maize cultivation site. Furthermore, Buggingen achieved overall good model efficiency compared to the other sampling sites even though observations are in most profiles under-estimated. Nevertheless, profiles are shallow in relation to Forchheim and Kraichtal and there is no information below 100 cm depth.

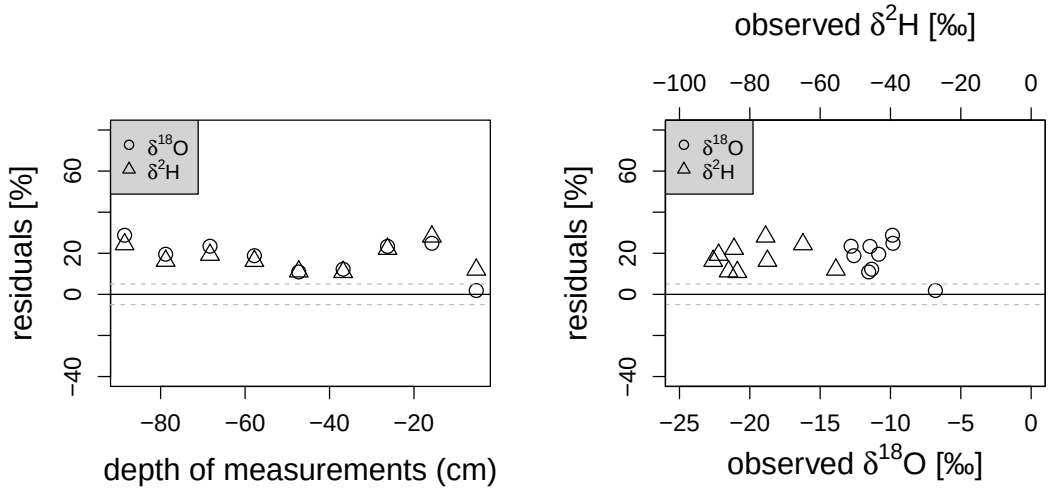

FIGURE 4.29: Residual plot from best fit run of model step IV of profile 1 sampled in spring 2015 in Buggingen.

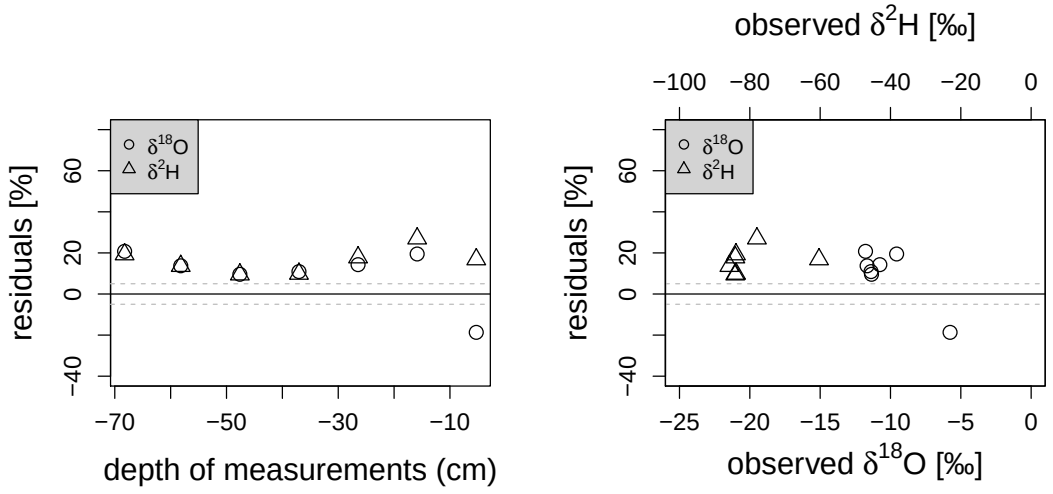

FIGURE 4.30: Residual plot from best fit run of model step IV of profile 3 sampled in spring 2015 in Buggingen.

4.4.8 Model steps II-V: Welschingen

Sampling in Welschingen was performed twice in the end of October 2014 and mid of April 2015 in a poplar short rotation coppice. With an age of 8 years poplar in short rotation is quite old in comparison to the other sampling sites. Cut-down is performed every 4 years. Between harvesting times, sites are cultivated extensively. Sampling in 2015 was done after cut-down. The reference profile was taken within a sudangrass cultivation. The whole sampling area is flat. Drilling cores in poplar plantations (profile 1 and 3) are comparably short. For profile 1 drilling was performed to a depth of 56 cm in 2014, and 42 cm in 2015. For profile 3 depth was even shallower with 37 and 26 cm. Therefore, only 5 isotope measurements could be done for profile 1 and 3 for profile 3.

TABLE 4.8: Best parameter values for Welschingen obtained from the SWIS model runs.

	Unit	Profile 1		Profile 2		Profile 3	
Profile characteristics							
Vegetation	-	poplar		sudangrass/maize		poplar	
Age	[yrs]						
Sampling time	-	autumn 2014	spring 2015	autumn 2014	spring 2015	autumn 2014	spring 2015
Model step II: insensitive parameter							
Texture top soil layer [1]	-	Ls2	Ls2	Ls2	Ls2	Ls2	Ls2
Texture bottom soil layer	-	-	-	-	-	-	-
Depth of bottom soil layer	[cm]	-	-	-	-	-	-
Transpiration depth [2]	[cm]	30	100	40	30	240	100
Model step III: sensitive parameter							
Evaporation depth [3]	[cm]	10	10	10	10	50	10
Model step III: model efficiency							
KGE_{mean}	-	-0.79	0.46	0.34	0.49	-0.1	0.38
KGE_{mean} (r + α)	-	-0.78	0.51	0.34	0.5	-0.91	0.39
Model step IV: parameter							
K_0	[%]	-5	-5	-5	5	5	5
n	[%]	1	1	1	0	1	1
Model step IV: model efficiency							
KGE_{mean}	-	-0.77	0.45	0.52	0.55	-0.95	0.35
KGE_{mean} (r + α)	-	-0.85	0.52	0.42	0.56	-0.90	0.37
Model step V: model efficiency							
KGE_{mean}	-	-1.22	0.31	-1.02	-0.72	-1.01	0.26
KGE_{mean} (r + α)	-	-1.14	0.35	-1.03	-0.72	-0.85	0.28

As SRC depth profiles 1 and 3 in 2015 and 2014 have only a few data points, a proper sensitivity analysis and fitting of simulations is impossible; therefore, these profiles are excluded from further analysis (Fig. C.37, C.38, C.41, C.42). Isotope observations of control profile 2 in 2014 show a jump in 70 cm depth by -5 in $\delta^{18}O$ and by -30 in $\delta^{2}H$ (Fig. C.39). Observed isotope values of profile 2 in 2015 indicate a depletion horizon till 50 cm and almost constant values below (Fig. C.40). Volumetric water content shows huge variations in both years. Deuterium-excess indicates more evaporation effects in 2014 than 2015 within the first 100 cm of depth (Fig. C.39, C.40).

In the following the results of the sensitivity analysis and modeling of profile 2 are described (Tab. Tab. 4.8): Both BK50 and field notes define soil texture as a mono-layered sandy loam (Ls2); thus, it was fixed before modeling. Both, transpiration depth and evaporation depth, were sensitive for profile 2 (Fig. D.8, D.9); moreover, transpiration depth was a bit higher in autumn 2014 than in spring 2015. Best fits were achieved after optimization of K_0 and n in model step IV.

However, the best fit run of model step IV under-estimates isotope values in the upper 40 cm in 2014. Variability ratio and bias ratio are almost equal ($\beta \approx 1$ and $\alpha \approx 1$); therefore, good model fits of $\mathrm{KGE}_{mean} = 0.52$ can be achieved. In 2015 similar model efficiency can be obtained with $\mathrm{KGE}_{mean} = 0.55$; however, the residual plots in 2015

show an over-estimation in the first and last 50 cm of the profile and an under-estimation between 50 and 100 cm (Fig. 4.32). Comparing that to the residual plots in 2014 (Fig. 4.31), it can be seen that the model fit in 2014 is actually better than in 2015.

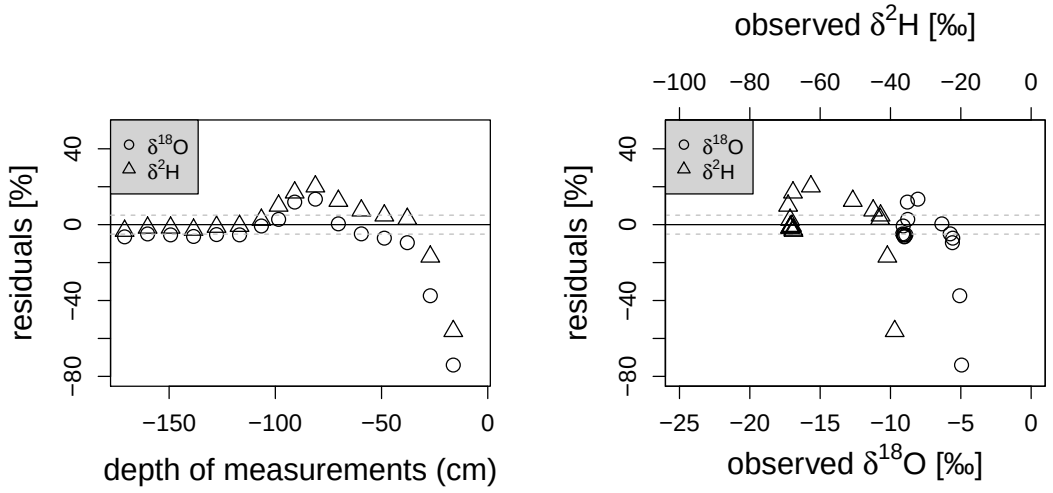

FIGURE 4.31: Residual plot from best fit run of model step IV of profile 2 sampled in autumn 2014 in Welschingen.

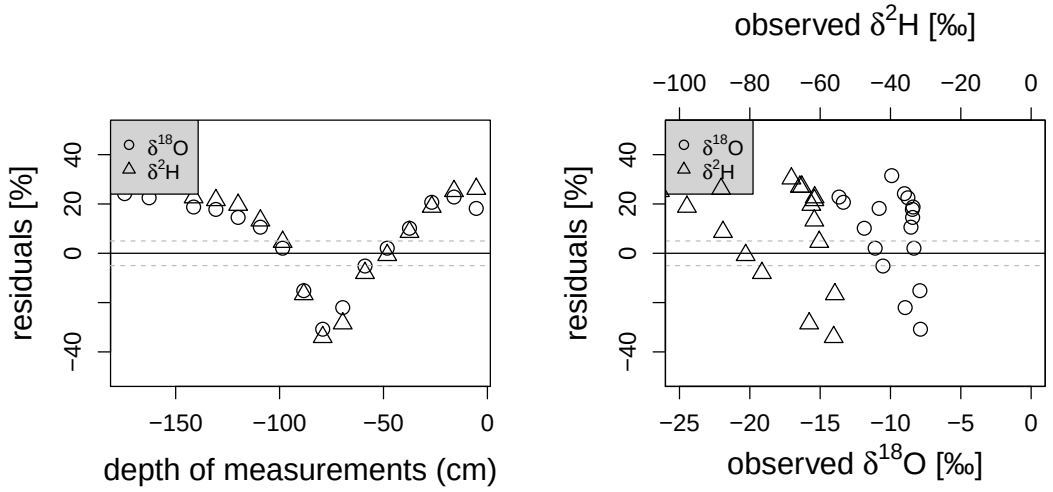

FIGURE 4.32: Residual plot from best fit run of model step IV of profile 2 sampled in spring 2015 in Welschingen.

In conclusion, because drilled depths in SRCs were only a few cm, a comparison between SRCs and reference site is not possible for Welschingen. Anyway, model step IV performed well at the reference profile number 2 for both years.

4.5 Comparison of sampling sites

To refer back to the research question whether soil functions vary with a changing vegetation, with vegetation age or between the soil textures of the sampling sites, the results from model steps II to IV described above are summarized and compared in the following. (The results from model step V are discussed in section 5.)

All in all, model step IV (after fitting of K_0 and n) performed best on the observations, with the best model efficiency in Kraichtal. Figures 4.33 - 4.38 show the values of K_0 and n obtained from the best runs from model step IV for all profiles at all stands except for profiles 1 and 3 of Welschingen and profiles 1 to 4 of Forchheim. The former pair is excluded because there are too few observations to fit a proper model and the latter because these profiles were not sensitive on variations of K_0 and n. The results of the remaining profiles still have to be treated with caution, because model efficiencies are often below 0.2, as described in the previous sections. Only the results from Kraichtal, Buggingen (2015) and the SRC profiles in Marbach have reasonably high model efficiencies with $\mathrm{KGE}_{\mathrm{mean}} > 0.5$.

In any case, no distinct trends can be observed in the variation of K_0 or n. Figure 4.33 and Figure 4.34 illustrate the relation between the K_0 and n values obtained from the best model run and the vegetation. If a trend towards an increase in hydraulic permeability within SRCs can be detected, one would expect K_0 and n being high at vegetation category of paulownia, poplar, willow and sida, or at least at one of them. However, no such trends can be shown, neither for K_0 nor n. Moreover, huge variations of increases and decreases in K_0 and n occur within one sampling site. Overall decreases in porosity occur slightly more often than increases in porosity.

Figures 4.35 and 4.36 illustrate whether changes of hydraulic conductivity and porosity from the best model runs for SRCs are correlated to vegetation age. This correlation data has some uncertainties, because vegetation age of most profiles is estimated; moreover, there are only few profiles within plantations older than 4 years. Still, no trend can be observed. Neither an increase nor a decrease of saturated hydraulic conductivity or porosity with increasing age. In general there are slightly more observations with a decrease of saturated hydraulic conductivity and porosity, but they are not correlated to age.

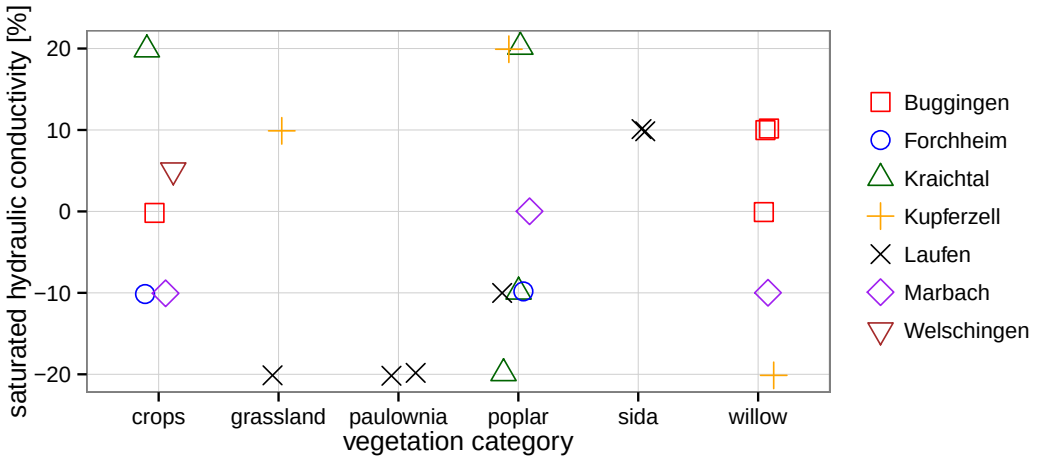

FIGURE 4.33: Relation of saturated hydraulic conductivity K_0 and vegetation category at the different sampling sites.

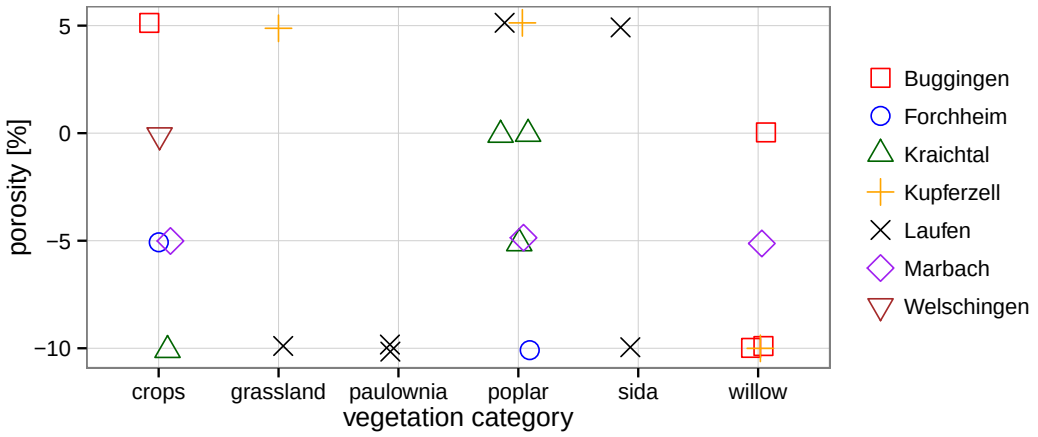

FIGURE 4.34: Relation of porosity (n) and vegetation category at the different sampling sites.

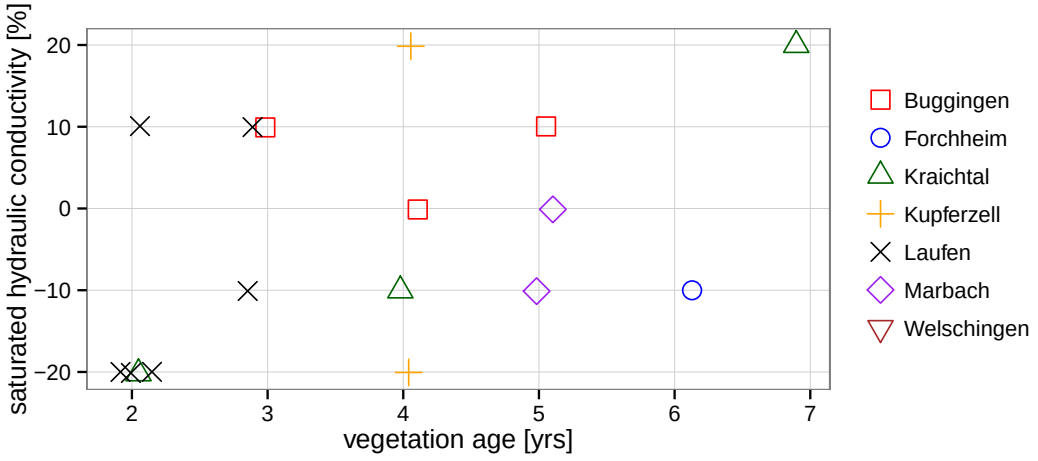

FIGURE 4.35: Relation of saturated hydraulic conductivity (K_0) and vegetation age at the different sampling sites. Only for SRC sites.

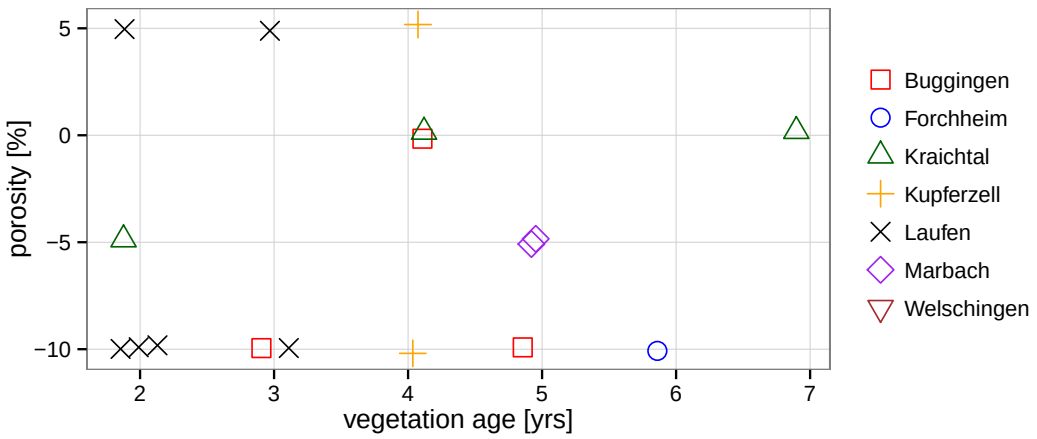

FIGURE 4.36: Relation of porosity (n) and vegetation age at the different sampling sites. Only for SRC sites.

To analyze the relation between soil texture and saturated hydraulic conductivity and porosity the soil textures are roughly organized into three categories: loam (L), sand (S) and silt (U). Figures 4.37 and 4.38 show that porosity and saturated hydraulic conductivity vary over the whole range for all categories. No correlation can be detected.

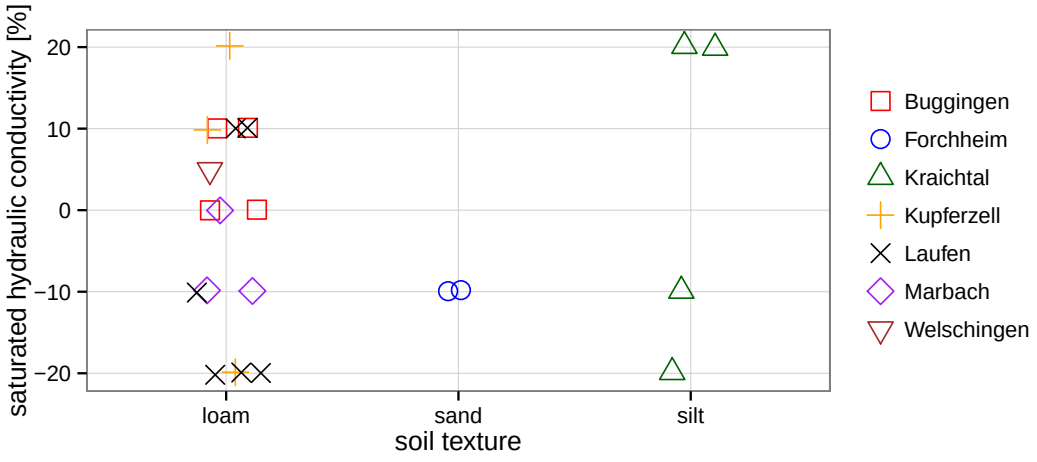

FIGURE 4.37: Relation of saturated hydraulic conductivity (K_0) and soil texture at the different sampling sites.

In figure 4.39 and 4.40 all profiles sensitive to evaporation depth or transpiration depth, respectively, are compared. The following profiles are sensitive to changes in transpiration depth: Buggingen 1 and 3, Kraichtal 2 to 4, Welschingen 2, Marbach 1 to 3, Laufen 1 to 6; moreover, Buggingen 2 and 4, Forchheim 1 to 6, Welschingen 2, Kupferzell 1 to 3, Marbach 1 to 3, Laufen 1 to 6 are sensitive towards changes in evaporation depth. While almost all sites had best fits at low transpiration depths, best fit of evaporation depth is either low (10 cm) or high (50 cm). Evaporation depth differs between sampling

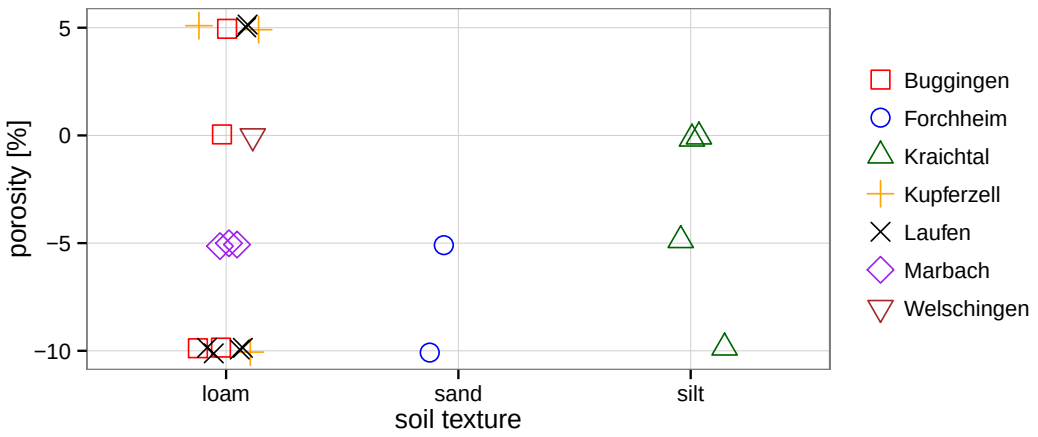

FIGURE 4.38: Relation of porosity (n) and soil texture at the different sampling sites.

sites but not within the vegetation of one sampling site; thus, best-fit evaporation depth seems to be site specific and not dependent on vegetation.

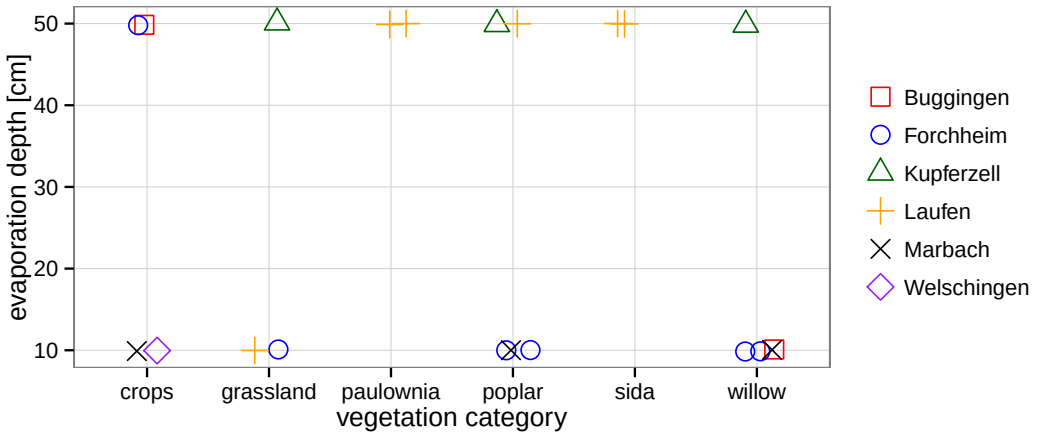

FIGURE 4.39: Relation of evaporation depth and vegetation category.

In the previous subsections the isotope observation data shown in the Figures in C were described in detail. In this paragraph a summary of general patterns of the observations follows. Even though observed relative isotope concentrations over depths have different shapes, it can be summarized that: depletion horizon in the upper 50 cm depth of profiles taken in 2015 reaches minimum values 20 to 30 cm below ground; moreover, enrichment horizon occurred till a depth of 100 cm with a maximum in 50 to 60 cm depth.

In all profiles, enrichment effects in the upper soil layers of sampled profiles in spring 2014 are simulated less appropriately than depletion horizon within the first cm of depth of

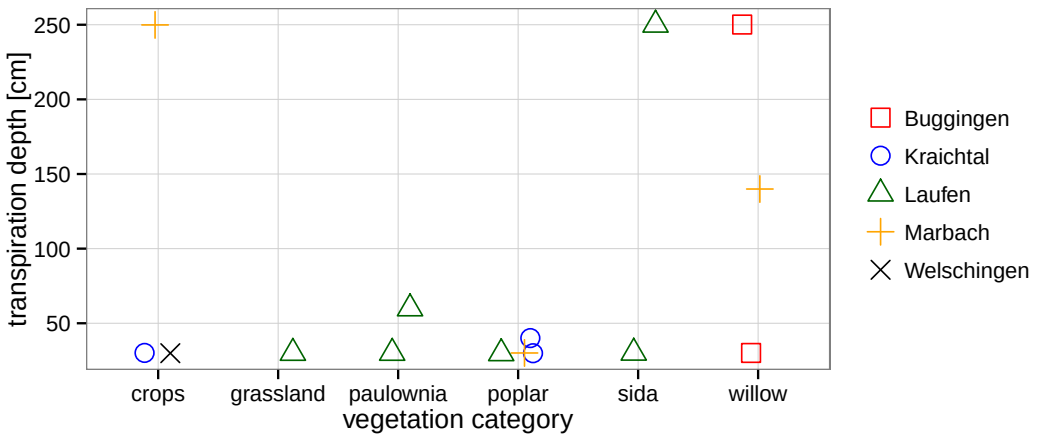

FIGURE 4.40: Relation of transpiration depth and vegetation category.

profiles taken in spring 2015. Deep profiles indicate that in general, enrichment horizons are over-estimated in isotope concentrations and variability.

In conclusion, effects of vegetation on soil hydraulic properties could not be detected with the model under investigation. It remains to discuss whether the chosen parameters K_0 and n, transpiration and interception depth give enough insights to conclude on soil hydraulics.

Chapter 5

Discussion

The applied methods and obtained results are discussed in the following order: (1) methods of isotope analysis, (2) observed isotope values and challenges in taking soil samples, (3) challenges in calculating input data, (4) results of the simulations and challenges in sensitivity analysis.

5.1 Methods of isotope analysis

Soil textures differ from each other in grain size distribution, as explained in detail in the introduction. According to the classification in Blume et al. (2010), micro pores have a diameter smaller than 0.2 μm, meso pores have a diameter between 0.2 and 50 μm and macro pores include all pores with diameter greater than 50 μm. Water retention curves of different soil textures and respective pore diameters illustrate the volumetric water content over characteristic water potentials. According to the findings of the studies reviewed by Sprenger, Herbstritt & Weiler (2015), different extraction methods extract water from different pore spaces. Squeezing methods with a pressure head of -10^3 hPa extract water in meso pores of diameters up to 3 μm. This method is equivalent to a desorption at 1.7 bar, as applied in this thesis. Direct equilibration methods extract water under a pressure head of -10^5 to -10^6 hPa and micro pores till a diameter of 0.03 to 0.003 μm drain (Fig. 5.1). Cryogenic vacuum extraction extracts all water in the soil, even hygroscopic water, when temperatures are high enough (Koeniger et al. 2011).

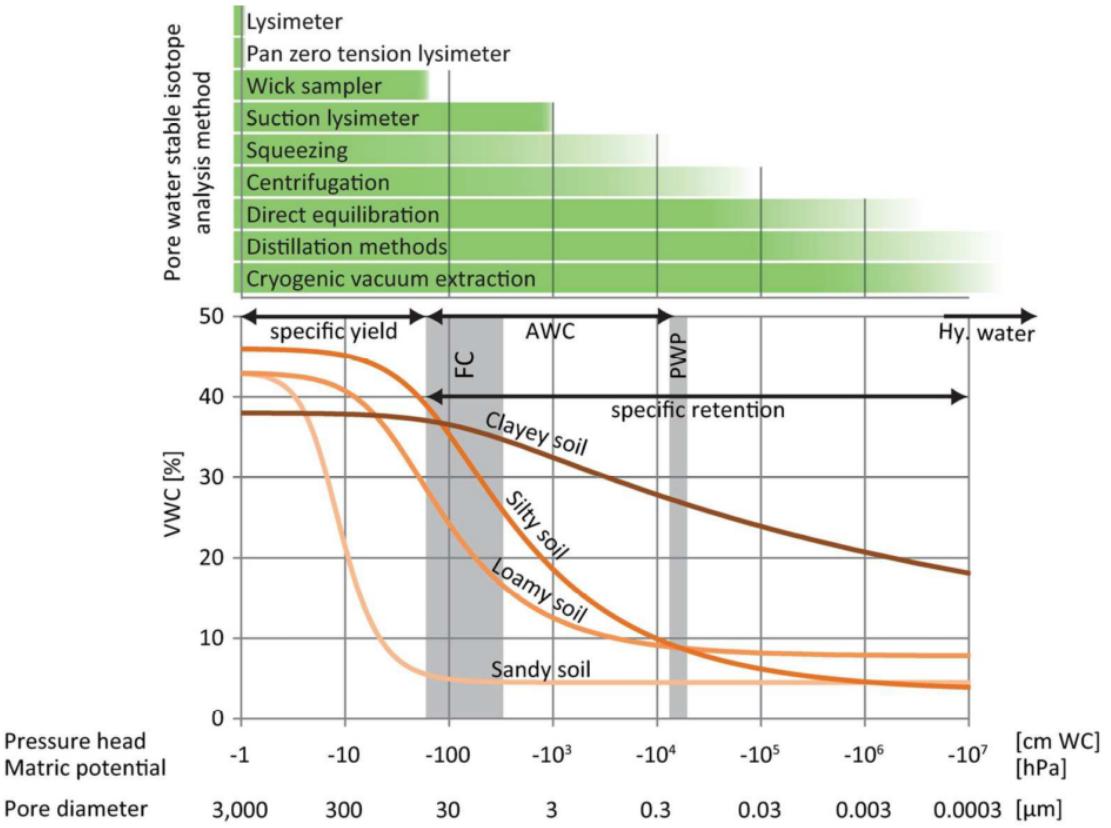

FIGURE 5.1: Extraction methods taken from Sprenger, Herbstritt & Weiler (2015). Bottom: Exemplified water retention curves for four different soil textures, the respective pore diameter described by (Schjonning 1992), and characteristic water potentials as defined by Blume et al. (2010): VWC = Volumetric water content, FC = Field capacity (gray area), AWC = plant available water capacity, PWP = permanent wilting point, Hy. water = hygroscopic water. Top: The most widely used pore water stable isotope analysis methods and their range of pore water extraction in relation to matrix potential and pore diameter.

Given this information one would expect differences in isotope composition depending on the extraction method. Accordingly, isotope composition in pore water after desorption is expected to be significantly different from direct equilibration or cryogenic vacuum extraction. It was shown in this thesis that cryogenic vacuum extraction had a significantly more depleted isotope composition in comparison to the other two methods. Considering that cryogenic vacuum extraction was applied on samples, already drained by desorption, this is not surprising, because pore water after cryogenic extraction contains only water from micro pores.

A major shift between equilibration and desorption was expected in silty soil texture, because pores still drain under a pressure head of more than 1.7 bar (Blume et al. 2010). In loamy soils, a small shift was expected. On the other hand, only in sandy soil the

signatures of both methods are equal, because there are no micro pores in sand that drain at a higher pressure head. However, the isotope signatures of direct equilibration and desorption obtained in this thesis were almost identical for all soil textures.

It has to be examined whether the identical results for equilibration and desorption in this study are effected by the fact that soil material for desorption was frozen and de-frozen at least two times before the measurement. It is conceivable that there is an exchange of pore water and air between micro and meso pores during the defreezing process; thus, the signature of different pore spaces would be lost. Leading to an isotope signature for desorption which displays not only meso pores but also micro pores. An attempt to test this hypothesis was made: field-moist samples from Kraichtal were collected in October 2015 and measured afterwards. Unfortunately, summer 2015 was very dry and no pore water drained under a pressure head of 1.7 bar. An alternative idea for future studies is the following: first, cryogenically extract pore water from dry field moist samples from Kraichtal, then, saturating the original sample with a water of known isotope composition, applying all three methods again, in the end compare both results from cryogenic extraction and conclude whether exchange processes occurred or not.

So, it remains to discuss whether the desorption method is adequate to analyze stable isotope composition at all. Arising due to the fact that desorption is highly depended on soil water content, there are some challenges in making the method consistent. Some samples drain very rapidly, within the first hours, others drip only a few ml and dry samples do not drain at all. Moreover, acetate membranes used in the desorption method are only permeable if they are wetted beforehand. The required wetting is one possible source of error. Another source of error is that sometimes water can be pressed through the screw thread and not the canula of the desorption apparatus. This occurred during the measurement for this thesis. The reason for the leakage could not be identified for certain.

In conclusion, only a few measurements could be performed during this thesis. More measurements are required to generalize the observed effects. All isotope observation data used in the modeling were analyzed via direct equilibration, all measurements on desorption were not considered in the modeling. Hence, this thesis can not provide new results about the equivalence of the applied extraction methods. Therefore, it is

assumed, in the following, that direct equilibration adsorbed mobile and tightly bound pore water from meso and micro pores, because this is the dominating hypothesis.

5.2 Observed isotope data

Soil depth differs a lot between the sampling sites due to different soil structures and textures: between 30 and almost 300 cm. This restricts the comparability of the the isotope observations of profiles and sampling sites. However, depletion and enrichment horizons were detectable in all observed isotope profiles in this thesis. For profile drilled in 2015, depletion horizons occurred till a depth of 50 cm; moreover, enrichment horizons occurred till a depth of 100 cm in profiles from 2015, given they reached a depth of 100 cm or more. These layers of fluctuations in pore water stable isotopes can be associated with annual fluctuations in the isotope signature in precipitation even though the precipitation signal is smoothed with depth (Sprenger, Volkmann, Blume & Weiler 2015, Stumpp et al. 2009, Gehrels et al. 1998, Brooks et al. 2010). Therefore, enrichment and depletion horizons found in this thesis give rough ideas of infiltration depth and climatic conditions of previous winters and summers.

Isotopic depletion is correlated to decreasing temperatures during winter; therefore, winter precipitation events of 2015 infiltrated into a depth of 50 cm. One would expect this depth to differ between the sampling sites due to changing soil hydraulic properties. But only small variations between the sampling sites occurred and major trends towards deeper infiltration of winter precipitation could neither be detected at SRCs, nor between the sampling sites. The enrichment horizon between 50 and 100 cm depth is correlated to summer precipitation in 2014. However, it is less pronounced than the depletion horizon. On the one hand this smoothing of the isotopic signal with depth occurs due to dispersion, which leads to a mixing between the layered water reservoirs (Brooks et al. 2010, Gehrels et al. 1998). On the other hand temperatures were comparably low and precipitation amounts comparably high in Baden-Wuerttemberg in summer 2014; therefore, isotopic signature is not as enriched as expected . Smoothed enrichment horizons were also observed in the profiles of 2014, which is evidence for the second hypothesis.

Hollmann (2015) did infiltration experiments at seven of the nine sampling sites of the BioChance project. The seven sites were: Kupferzell, Marbach, Aulendorf, Welschingen, Biederbach, Laufen, and Buggingen. He did not detect characteristics in the variations of infiltration rates between the sampling sites, either.

Generally it has to be considered which soil hydraulic processes were detected and which were not detected with the drilling method applied in this thesis. Due to feasibility issues, drilling in SRCs was performed between the tree rows and not within the tree rows. Preferential flowpaths in macropores (Gazis & Feng 2004), originating from tree roots, are most likely not considered in this approach. Thus, a degree of uncertainty remains on soil hydraulic properties under a deep well-rooted vegetation cover. In turn, soil compaction originating from harvesters might have an influence on the profiles (Lamersdorf et al. 2010). This is a possible explanation for similar patterns in depletion depths, and hence in infiltration depth, over all profiles and soil textures.

Some of the profiles taken in 2015 had outliers in isotope signature in the first 10 cm of depth. It remains unclear whether this is an artifact of the measurement technique via direct equilibration or has other reasons.

In conclusion, despite these problems isotope depth profiles are still a great tool for the qualitative understanding of water fluxes within the unsaturated zone. It breaks down system heterogeneity to a point where comparisons between different locations and soils are possible.

5.3 Model input data series

As described in section 3.4.1.2, daily data of isotopes in precipitation were required but not available for the years 2012 to 2015; therefore, ten different approaches to simulate proper time series of isotopes in precipitation were tested. The results showed that daily approaches did not achieve better fits than longtime monthly means of isotope values. It was shown that, mean daily temperatures 2 m above the ground could only explain a small part of the variations in the isotope signature. This is most likely due to the fact that isotope signature is characterized not only by near-surface processes but also by processes in higher atmospheric layers (Gat et al. 2001); furthermore, the signature during a single heavy precipitation event changes over the duration of the event. So

far, there is only little research on the variability of the isotope signature during a single precipitation event. In conclusion, to simulate the actual daily isotope signature more climate data like the temperature and relative air pressure and moisture of higher atmospheric layers are required. Therefore, longtime monthly mean is at least a good approximation of the inner-annual variations, though not of the daily variations.

The results in section 4.2 further showed that the altitude correction factor chosen by Siegenthaler & Oeschger (1980) did not fit for all cases. The altitude correction factor by Siegenthaler & Oeschger (1980) is calculated for the Swiss Alps. Factors for the Black Forest might be even higher according to Gat et al. (2001). As it was shown in the results, altitude correction did fit less on Schauinsland data than on St. Wilhelmer Tal data. When altitude correction factor was reduced, simulated data fit better, even though not better than without altitude correction; thus, altitude correction factor by Siegenthaler & Oeschger (1980) did not fit for the Black Forest region and an altitude difference bigger than 700 m. Further, Siegenthaler & Oeschger (1980) stated that with increasing altitude difference, isotope correction factors decrease, which was shown by the Schauinsland data. Because altitude differences between GNIP stations and sampling sites are in almost all sites only a few meters, altitude correction plays a minor role.

As elaborated in the methods (section 3.4.1.3), interception and transpiration were calculated from LAI. Especially the suitability of the interception equation of von Hoyningen-Huene (1983) is limited, because it was developed for crops (more information in section 3.4.1.3). As leaf area indices are not measured and literature values are not available for all species, or species of different age, leaf area indices are fitted using the SWIS model (see model step I in 3.4.3). From the results it can be concluded that the attempt to calibrate LAI by using the model SWIS did not achieve the expected results (see section 4.4.1). Only within a few profiles model efficiency was sensitive to LAI, most profiles were insensitive or showed no clear patterns. Certainly measured LAI would increase the reliability of the input data series of interception and transpiration, nevertheless, the uncertainty of the above mentioned equations still persists. However, including the calculated water fluxes to the water balances yields satisfying results, as exemplarily shown by the sampling site in Forchheim in section 4.3.

In conclusion, the deviations between the simulations and the observations, which are

described in the following, can at least partly be reduced to the described uncertainties in the input data series.

5.4 Simulations and sensitivity analysis

Sensitivity analysis and parameter optimization were done for seven parameters which were selected and estimated in order to describe soil hydraulic properties: transpiration and evaporation depth; single or two-layered soil texture; in case of a two-layered soil, the depth of the bottom soil layer; saturated hydraulic conductivity and porosity.

Evaporation depth was estimated within a certain range via inverse modeling in order to conclude on differences between reference sites, where bare soil is exposed to wind and sun between the growing seasons, and SRC sites with well-rooted soils, which are protected from direct wind and sun radiation by a closed canopy half the year. Thus, evaporation depth for the reference sites is expected to be higher than for SRCs. Furthermore, transpiration depth was estimated because of missing measurements and literature values on rooting depths of species and clones sampled in this thesis. It was expected to be higher for SRCs than for the reference sites in grassland, maize and other crops. For most profiles, model efficiency was sensitive to changes in either evaporation depth or transpiration depth or changes in both. However, expected trends were not observed continuously neither for transpiration nor for evaporation depth.

In some cases model efficiency marginally increases with changes in transpiration depth. However, the variances of model efficiencies within runs for fixed values of the parameter was much bigger than the variance of model efficiencies between runs with different parameter values. When this patterns occurred, transpiration depth is assumed to be an insensitive parameter for the model. But even though changes in transpiration depth do not influence the model significantly, it was still set to the value which produced the maximum efficiency.

In case of a two-layered soil texture the depth of the second soil layer was not a sensitive parameter for the model for any case. It was concluded that this parameter can be excluded from the sensitivity analysis.

No clear trend can be observed concerning an increase in saturated hydraulic conductivity or porosity at SRCs (section 4.5); thus, an improvement of soil infiltration capacity at SRCs in comparison to intensively cultivated arable sites found by former studies can not be observed in this study (Lamersdorf et al. 2010, Lamersdorf & Schulte-Bisping 2010, Petzold et al. 2009, Dimitriou et al. 2009). The questions of whether soil functions vary with a changing vegetation, with a changing vegetation age or in different soil textures can not be answered because such effects were not observed.

In this thesis the Van-Genuchten parameter n is referred to as porosity, which is not quite fitting because it is a shape parameter according to the definition of van Genuchten (1980). It remains to discuss whether a variation of other soil hydraulic parameters might achieve better results, however doing this implies modifications of the SWIS model.

At profiles with only small variations in isotope signature with increasing depth, model step V achieved best model efficiencies. The separated simulation of water flux in micro, meso and macro pores is responsible for an increase in simulated linearity of isotope values with depth. On a random basis dispersivity was altered. Changes in dispersivity did not affect model efficiency. A structured estimation of diffusion and exchange between pore spaces was not conducted.

Quite some time was invested to decide which measurement efficiency index to take. In the end it was a combination of KGE and KGE (r + α), Pearson's r, α, β and residual plots. With this combination variations and shifts between the simulations and observations could be detected in detail.

Generally, SWIS performed best in the first meter of depth of profiles taken in 2015, in depths below that, the simulated smoothing was too big and did not mirror the observed variability. Moreover, SWIS performed better on oxygen-18 values than on deuterium values. These two effects of the simulations indicate that assumptions made in the model might have to be adapted.

Observed water content measurements were not as adequate as required for simulation fitting (see section 3.3 and 4.4). Thus, the adequacy of the simulated water transport could not be verified rigorously, and the performance of the simulated water flow via the Richards equation remains unclear.

In conclusion, an increase in permeability of soils underneath SRCs can not be observed, although it was described in former studies. This is likely due to the shortcomings of the available input data and soil heterogeneity. Some improvements are also likely needed for the parameter selection and a further Monte Carlo analysis might lead to new assumptions on sensitive parameter values.

Chapter 6

Conclusion

A proper simulation of the effect of vegetation on soil hydraulic properties is complicated due to the heterogeneity in soils. Qualitative conclusions on soil hydraulic properties could be drawn from the observed isotope depth profiles. Moreover, quantitative assumptions should be made via inversely model those depth profiles. Major problems in inverse modeling were to calculate input data like transpiration and interception and especially isotope values of precipitation.

To improve the applied methodology it would be useful to measure some more model input data. Some easy and fast to obtain parameters are for instance: (1) the canopy coverage, which can be determined by a Digital Canopy Imager, to calculate leaf area index, transpiration and interception; and (2) more information on the examined poplar and willow clones in short rotation can give insights into the rooting depth and hence on transpiration depths.

It is much more difficult to obtain a better estimation of the isotopes in precipitation, because spatial distribution of isotope measurements is not as widespread as climate stations are. Furthermore, the correlation to other climate parameters is still a challenge as described in section 5.3.

In summary, the simple method of taking soil drilling cores twice a year and estimating all other parameters via inverse modeling was not successful. While qualitative conclusions could be drawn from the isotope depth profiles, quantitative research questions about differences between SRC and reference sites could not be answered.

Bibliography

Allison, G., Barnes, C. J., Hughes, M. & Leaney, F. (1984), Effect of climate and vegetation on oxygen-18 and deuterium profiles in soils, *in* 'Isotopes Hydrology 1983', IAEA, Vienna, pp. 105–137.

Allison, G., Gat, J. & Leaney, F. (1985), 'The relationship between deuterium and oxygen-18 delta values in leaf water', *Chemical Geology: Isotope Geoscience section* **58**(1-2), 145–156.

Araguás-Araguás, L., Rozanski, K., Gonfiantini, R. & Louvat, D. (1995), 'Isotope effects accompanying vacuum extraction of soil water for stable isotope analyses', *Journal of Hydrology* **168**(1-4), 159–171.

Aston, A. R. (1979), 'Rainfall interception by eight small trees', *Journal of Hydrology* **42**, 383–396.

Aust, C. (2012), Abschätzung der nationalen und regionalen Biomassepotentiale von Kurzumtriebsplantagen auf landwirtschaftlichen Flächen in Deutschland, PhD thesis, Albert-Ludwigs-Universität Freiburg i. Brsg.

Barigah, T. S., Saugier, B., Mousseau, M., Guittet, J. & Ceulemans, R. (1994), 'Photosynthesis, leaf area and productivity of 5 poplar clones during their establishment year', *Annales des Sciences Forestieres* **51**, 613–625.

Bemmann, A. & Knust, C., eds (2010), *AGROWOOD - Kurzumtriebsplantagen in Deutschland*, Weißensee Verlag, Berlin.

Blattner, M. S., Augustin, S., Schack-Kirchner, H. & Hildebrand, E. E. (2000), 'The desorption solution — an alternative approach to measure water soluble ions in soils', *Journal of Plant Nutrition and Soil Science* **163**(6), 583–587.

Blum, W. E. H. (2005*a*), 'Functions of soil for society and the environment', *Reviews in Environmental Science and Biotechnology* **4**(3), 75–79.

Blum, W. E. H. (2005*b*), 'Soils and Climate Change', *Journal for Soils & Sediments* **5**(2), 67–68.

Blume, H.-P., Brümmer, G., Horn, R., Kandeler, E., Kögel-Knabner, I., Kretschmar, R., Stahr, K. & Wilke, B.-M. (2010), *Scheffer/Schachtschabel Lehrbuch der Bodenkunde*, Spektrum Akademischer Verlag Heidelberg 2010, Heidelberg.

Blume, H., Zimmermann, U. & Münnich, K. (1967), Tritium tagging of soil moisture: the water balance of forest soils, *in* 'Isotope and Radiation Techniques in Soil Physics and Irrigation Studies', IAEA, Vienna, pp. 315–332.

Bormann, H. (2009), 'Analysis of possible impacts of climate change on the hydrological regimes of different regions in Germany', *Advances in Geosciences* **21**, 3–11.

Brooks, J. R., Barnard, H. R., Coulombe, R. & McDonnell, J. J. (2010), 'Ecohydrologic separation of water between trees and streams in a Mediterranean climate', *Nature Geoscience* **3**(2), 100–104.

Bulcock, H. H. & Jewitt, G. P. W. (2009), 'Improved spatial mapping of leaf area index using hyperspectral remote sensing for hydrological applications with a particular focus on canopy interception', *Hydrology and Earth System Sciences Discussions* **6**(5), 5783–5809.

Cariboni, J., Gatelli, D., Liska, R. & Saltelli, a. (2007), 'The role of sensitivity analysis in ecological modelling', *Ecological Modelling* **203**(1-2), 167–182.

Christiansen, J. R., Elberling, B. & Jansson, P. E. (2006), 'Modelling water balance and nitrate leaching in temperate Norway spruce and beech forests located on the same soil type with the CoupModel', *Forest Ecology and Management* **237**(2006), 545–556.

Corwin, D. L., Hopmans, J. & de Rooij, G. H. (2006), 'From field-to landscape-scale vadose zone processes: scale issues, modeling, and monitoring', *Vadose Zone Journal* **5**(1), 129–139.

Dansgaard, W. (1964), 'Stable isotopes in precipitation', *Tellus A* .

Darling, W. & Bath, A. (1988), 'A stable isotope study of recharge processes in the English chalk', *Journal of Hydrology* **101**, 31–46.

de Jong, S. M. & Jetten, V. G. (2007), 'Estimating spatial patterns of rainfall interception from remotely sensed vegetation indices and spectral mixture analysis', *International Journal of Geographical Information Science* **21**(5), 529–545.

Diekkrüger, B., Söndgerath, D., Kersebaum, K. C. & McVoy, C. W. (1995), 'Validity of agroecosystem models - A comparison of results of different models applied to the same data set', *Ecological Modelling* **81**, 3–29.

Dijk, a. V. & Bruijnzeel, L. (2001), 'Modelling rainfall interception by vegetation of variable density using an adapted analytical model. Part 1. Model description', *Journal of Hydrology* **247**, 230–238.

Dimitriou, I., Busch, G. & Jacobs, S. (2009), 'A review of the impacts of short rotation coppice cultivation on water issues', *Agriculture and Forestry Research* **59**(3), 197–206.

Durner, W., Schultze, B. & Zurmühl, T. (1999), State-of-the-Art in Inverse Modeling of Inflow / Outflow Experiments, *in* 'Reprint from: M. Th. van Genuchten, F. J. Leij, and L. Wu (ed.) Proc. Int. Workshop on Characterization and Measurement of the Hydraulic Properties of Unsaturated Porous Media, October 22-24, 1997', University of California, Riverside, CA.

DVWK (1996), *Ermittlung der Verdunstung von Land- und Wasserflächen Vorwort.*

Eichler, R. (1964), 'Deuterium-Isotopengeochemie des Grund- und Oberflächenwassers', *Geologische Rundschau* **55**(1), 144–159.

Garvelmann, J., Külls, C. & Weiler, M. (2012), 'A porewater – based stable isotope approach for the investigation of subsurface hydrological processes', *Hydrology and Earth System Sciences Discussions* **8**(5), 9089–9112.

Gat, J., Mook, W. & Meijer, H. (2001), 'Environmental isotopes in the hydrological cycle: Principles and applications', *Technical Documents in Hydrology* **2**.

Gazis, C. & Feng, X. (2004), 'A stable isotope study of soil water: Evidence for mixing and preferential flow paths', *Geoderma* **119**(1-2), 97–111.

Gehrels, J. C., Peeters, J. E. M., De Vries, J. J. & Dekkers, M. (1998), 'The mechanism of soil water movement as inferred from O-18 stable isotope studies', *Hydrological Sciences Journal-Journal Des Sciences Hydrologiques* **43**(4), 579–594.

Gómez, J. a., Giráldez, J. V. & Fereres, E. (2001), 'Rainfall interception by olive trees in relation to leaf area', *Agricultural Water Management* **49**(1), 65–76.

Gribb, M. M., Forkutsa, I., Hansen, A., Chandler, D. G. & McNamara, J. P. (2009), 'The Effect of Various Soil Hydraulic Property Estimates on Soil Moisture Simulations', *Vadose Zone Journal* **8**(2), 321.

Gupta, H. V., Kling, H., Yilmaz, K. K. & Martinez, G. F. (2009), 'Decomposition of the mean squared error and NSE performance criteria: Implications for improving hydrological modelling', *Journal of Hydrology* **377**(1-2), 80–91.

Hartke & Horn (2014), *Einführung in die Bodenphysik*, Stuttgart: Schweizerbart.

Hofmann-Schielle, C. ., Jug, a. ., Makeschin, F. . & Rehfuess, K. E. (1999), 'Short-rotation plantations of balsam populars, aspen and willows on former arable land in the FRG I site-growth relationships', *Forest Ecology and Management* **121**, 41–55.

Hollmann, A. (2015), Einfluss von Energiepflanzen auf die Infiltrationseigenschaften und Hochwassergefährdung, PhD thesis, Albert-Ludwigs-Universität.

Inoue, M., Šimůnek, J., Shiozawa, S. & Hopmans, J. W. (2000), 'Simultaneous estimation of soil hydraulic and solute transport parameters from transient infiltration experiments', *Advances in Water Resources* **23**(7), 677–688.

IPCC (2013), Annex I: Atlas of Global and Regional Climate Projections, *in* V. G. Oldenborgh, M. Collins, J. Arblaster, J. Christensen, J. Marotzke, S. Power, M. Rummukainen & T. Zhou, eds, 'Climate Change 2013: The Physical Science Basis. Contribution of Working Group I to the Fifth Assessment Report of the Intergovernmental Panel on Climate Change', Cambridge University Press, Cambridge, United Kingdom and New York, NY, USA., pp. 1311–1394.

Jacques, D., Jirka, S., Timmerman, A. & Feyen, J. (2002), 'Calibration of Richards' and convection–dispersion equations to field-scale water flow and solute transport under rainfall conditions', *Journal of Hydrology* **259**, 15–31.

Kersebaum, K. C. (1995), 'Application of a simple management model to simulate water and nitrogen dynamics', *Ecological Modelling* **81**, 145–156.

Koeniger, P., Leibundgut, C., Link, T. & Marshall, J. D. (2010), 'Organic Geochemistry Stable isotopes applied as water tracers in column and field studies', *Organic Geochemistry* **41**(1), 31–40.

Koeniger, P., Marshall, J. D., Link, T. & Mulch, A. (2011), 'An inexpensive, fast, and reliable method for vacuum extraction of soil and plant water for stable isotope analyses by mass spectrometry', *Rapid Communications in Mass Spectrometry* **25**(20), 3041–3048.

Kozak, J., Ahuja, L., Green, T. & Ma, L. (2007), 'Modelling crop canopy and residue rainfall interception effects on soil hydrological components for semi-arid agriculture', *Hydrological processes* **21**, 229–241.

Krause, P., Boyle, D. P. & Bäse, F. (2005), 'Comparison of different efficiency criteria for hydrological model assessment', *Advances in Geosciences* **5**, 89–97.

Kutschera, L. & Lichtenegger, E. (2002), *Wurzelatlas mitteleuropäischer Walbäume und Sträucher*, Stocker, Graz.

LABO (2010), Bund/Länder-Arbeitsgemeinschaft Bodenschutz-Positionspapier "Boden und Klimawandel", Technical Report June.

Lamersdorf, N., Petzold, R., Schwärzel, K., Feger, K.-h., Köstner, B., Moderow, U. & Bernhofer, C. (2010), 3.4 Bodenökologische Aspekte von Kurzumtriebsplantagen, *in* 'AGROWOOD - Kurzumtriebsplantagen in Deutschland und europäische Perspektiven', pp. 170–188.

Lamersdorf, N. & Schulte-Bisping, H. (2010), 'Zum Wasserhaushalt von Kurzumtriebsplantagen', *Archiv f. Forstwesen u. Landsch.ökol.* **44**(1), 23–29.

Landgraf, D., Böcker, L., Schildbach, M. & Wolf, H. (2009), Baumarten- und Sortenwahl, *in* T. Reeg, A. Bemmann, W. Konold, D. Murach & H. Spiecker, eds, 'Anbau und Nutzung von Bäumen auf landwirtschaftlichen Flächen', chapter 6.2.

Legates, D. R. & McCabe, G. J. (1999), 'Evaluating the use of 'goodness-of-fit' measures in hydrologic and hydroclimatic model validation', *Water Resources Research* **35**(1), 233–241.

Leon, J. & Bukovac, M. (1978), 'Cuticle development and surface morphology of olive leaves with reference to penetration of foliar-applied chemicals', *Journal of the American Society for Horticultural Science* **103**, 465–472.

Llorens, P. & Gallart, F. (2000), 'A simplified method for forest water storage capacity measurement', *Journal of Hydrology* **240**, 131–144.

LUBW (1995), Prognose von Bodenerosion, *in* 'Zentraler Fachdienst Wasser- Boden- Abfall- Altlasten bei der Landesanstalt für Umweltschutz baden-Württemberg', Karlsruhe, pp. 1–144.

LUBW (2011), Merkblatt Gefahrenabwehr bei Bodenerosion, Technical report, Karlsruhe.

McKay, M. D., Beckman, R. J. & Conover, W. J. (1979), 'Comparison of Three Methods for Selecting Values of Input Variables in the Analysis of Output from a Computer Code', *Technometrics* **21**(2), 239–245.

McVoy, C., Kersebaum, K., Arning, M., Kleeberg, P., Othmer, H. & Schröder, U. (1995), 'A data set from north Germany for the validation of agroecosystem models: documentation and evaluation', *Ecological Modelling* **81**(94), 265–300.

MLR (2010), Anlage und Bewirtschaftung von Kurzumtriebsflächen in Baden-Württemberg, Technical report, Stuttgart.

MLR (2015), 'Naturräume in Baden-Württemberg'.
URL: *https://www.landwirtschaft-bw.info/pb/MLR.LaendlicherRaum,Lde/Startseite/Allgemein/Naturraeume*

Murach, D. & Knur, L. (2008), *DENDROM – Zukunftsrohstoff Dendromasse.*

Nendel, C., Berg, M., Kersebaum, K. C., Mirschel, W., Specka, X., Wegehenkel, M., Wenkel, K. O. & Wieland, R. (2011), 'The MONICA model: Testing predictability for crop growth, soil moisture and nitrogen dynamics', *Ecological Modelling* **222**(9), 1614–1625.

Nendel, C., Kersebaum, K., Mirschel, W. & Wenkel, K. (2014), 'Testing farm management options as climate change adaptation strategies using the MONICA model', *European Journal of Agronomy* **52**, 47–56.

Orlowski, N., Frede, H.-G., Brüggemann, N. & Breuer, L. (2013), 'Validation and application of a cryogenic vacuum extraction system for soil and plant water extraction for isotope analysis', *Journal of Sensors and Sensor Systems* **2**(2), 179–193.

Orlowski, N., Kraft, P. & Breuer, L. (2015), 'Exploring water cycle dynamics through sampling multitude stable water isotope pools in a small developed landscape of', *Hydrology and Earth System Sciences Discussions* **12**, 1809–1853.

Petzold, R., Schwärzel, K. & Feger, K.-H. (2009), Wasserhaushalt von Kurzumtriebsplantagen, *in* 'Anbau und Nutzung von Bäumen auf landwirtschaftlichen Flächen', Wiley-VCH Verlag GmbH & Co KGaA, chapter 16, pp. 181–192.

Picarro (2015), 'Cavity Ring-Down Spectroscopy (CRDS)'.
URL: *http://www.picarro.com/technology/cavity_ring_down_spectroscopy*

Saltelli, A. & Annoni, P. (2010), 'How to avoid a perfunctory sensitivity analysis', *Environmental Modelling & Software* **25**(12), 1508–1517.

Saltelli, A., Ratto, M., Andres, T., Campolongo, F., Cariboni, J., Gatelli, D., Saisana, M. & Tarantola, S. (2008), *Sensitivity Analysis: From Theory to Practice*, number November 2015.

Schjonning, P. (1992), 'Size Distribution of Dispersed and Aggregated Particles and of Soil Pores in 12 Danish Soils', *Acta Agriculturae Scandinavica, Section B - Soil & Plant Science* **42**, 26–33.

Schlotter, D., Schack-Kirchner, H., Hildebrand, E. E. & von Wilpert, K. (2012), 'Equivalence or complementarity of soil-solution extraction methods', *Journal of Plant Nutrition and Soil Science* **175**(2), 236–244.

Schulze, R. (1995), Hydrology and Agrohydrology: A Text to Accompany the ACRU 3.00 Agrohydrological Modelling System, Technical report, Water Research Commission, Pretoria.

Sieber, A. & Uhlenbrook, S. (2005), 'Sensitivity analyses of a distributed catchment model to verify the model structure', *Journal of Hydrology* **310**(1-4), 216–235.

Siegenthaler, U. & Oeschger, H. (1980), 'Correlation of 18O in precipitation with temperature and altitude', *Nature* **285**, 314.

Smith, D. B., Wearn, P. L., Richards, H. & Rowe, P. (1970), Water movement in the unsaturated zone of high and low permeability strata by measuring natural tritium, *in* 'Isotope Hydrology 1970', Vol. 73-, IAEA, Vienna, pp. 95–138.

Sprenger, M., Herbstritt, B. & Weiler, M. (2015), 'Established methods and new opportunities for pore water stable isotope analysis', *Hydrological Processes* pp. n/a–n/a.

Sprenger, M., Volkmann, T. H. M., Blume, T. & Weiler, M. (2015), 'Estimating flow and transport parameters in the unsaturated zone with pore water stable isotopes', *Hydrology and Earth System Sciences* **19**(6), 2617–2635.

Strasser, U. & Mauser, W. (2001), 'Modelling the spatial and temporal variations of the water balance for the Weser catchment 1965-1994', *Journal of Hydrology* **254**(1-4), 199–214.

Stumpp, C., Klaus, J. & Stichler, W. (2014), 'Analysis of long-term stable isotopic composition in German precipitation', *Journal of Hydrology* **517**, 351–361.

Stumpp, C., Stichler, W., Kandolf, M. & Šimůnek, J. (2012), 'Effects of Land Cover and Fertilization Method on Water Flow and Solute Transport in Five Lysimeters: A Long-Term Study Using Stable Water Isotopes', *Vadose Zone Journal* **11**(1), 0.

Stumpp, C., Stichler, W. & Maloszewski, P. (2009), 'Application of the environmental isotope δ18O to study water flow in unsaturated soils planted with different crops: Case study of a weighable lysimeter from the research field in Neuherberg, Germany', *Journal of Hydrology* **368**(1-4), 68–78.

Tang, K. & Feng, X. (2001), 'The effect of soil hydrology on the oxygen and hydrogen isotopic compositions of plants' source water', *Earth and Planetary Science Letters* **185**(3-4), 355–367.

Tesfuhuney, W. A., Rensburg, L. D. V. & Walker, S. (2013), 'Surface Treatments Effect on Rainfall Canopy Interception and Runoff-Rainfall Ratio for in-Field Rainwater Harvesting', *Journal of Agricultural Science and Technology* **3**, 423–435.

Tharakan, P. J., Volk, T. a., Nowak, C. a. & Abrahamson, L. P. (2005), 'Morphological traits of 30 willow clones and their relationship to biomass production', *Canadian Journal of Forest Research* **35**(2), 421–431.

Valante, F., David, J. S. & Gash, J. H. C. (1997), 'Modelling interception loss for two sparse eucalypt and pine forests in central Portugal using reformulated Rutter and Gash analytical models', *Journal of Hydrology* **190**(1-2), 141–162.

van Genuchten, M. T. (1980), 'A Closed-form Equation for Predicting the Hydraulic Conductivity of Unsaturated Soils1', *Soil Science Society of America Journal* **44**(5), 892.

Vanclooster, M., Boesten, J., Tiktak, A., Jarvis, N., Kroes, J. G., Munoz-Carpena, R., Clothier, B. E. & Green, S. R. (2004), On the use of unsaturated flow and transport models in nutrient and pesticide management, *in* R. A. Feddes, G. H. de Rooij & J. C. van Dam, eds, 'Unsaturated-zone modeling: progress, challenges and applications', number 6, Springer, New York, chapter 11, pp. 331–361.

Vereecken, H., Weynants, M., Javaux, M., Pachepsky, Y., Schaap, M. G. & Genuchten, M. V. (2010), 'Using Pedotransfer Functions to Estimate the van Genuchten–Mualem Soil Hydraulic Properties: A Review', *Vadose Zone Journal* **9**(4), 795.

Vitvar, T. (2005), A Review of Isotope Applications in Catchment Hydrology, *in* P. K. Aggarwal, J. R. Gat & K. F. O. Froehlich, eds, 'Isotopes in the Water Cycle: Past, Present and Future of a Developing Science', Springer, Dordrecht, Netherlands, chapter 12, pp. 151–168.

von Hoyningen-Huene, J. (1983), 'Die Interzeption des Niederschlages in landwirtschaftlichen Pflanzenbeständen', *DVWK Schriften* **57**, 3–53.

Wagener, T., McIntyre, N., Lees, M. J., Wheater, H. S. & Gupta, H. V. (2003), 'Towards reduced uncertainty in conceptual rainfall-runoff modelling: dynamic identifiability analysis', *Hydrological Processes* **17**(2), 455–476.

Wenninger, J., Königer, P., Leibundgut, C., Schindler, D. & Mayer, H. (2005), 'Untersuchung der Bodenwasserbewegung mit stabilen Isotopen in Hinblick auf die Grundwasserneubildung', *Zbl. Geol. Paläont. Teil I* **Heft 1/2**, 123–139.

West, A. G., Patrickson, S. J. & Ehleringer, J. R. (2006), 'Water extraction times for plant and soil materials used in stable isotope analysis', *Rapid Communications in Mass Spectrometry* **20**(8), 1317–1321.

Wurbs, D. & Steininger, M. (2011), Wirkungen der Klimaänderungen auf die Böden. Untersuchungen zu Auswirkungen des Klimawandels auf die Bodenerosion durch Wasser, Technical report, Umweltbundesamt.

ZALF Leibniz-Zentrum für Agrarlandschaftsforschung (2012), 'monica: Das Modell für Stickstoff und Kohlenstoff in Agrarökosystemen. Transpiration'.
URL: *http://monica.agrosystem-models.com/de/pflanzenprozesse/27-transpiration*

Zimmermann, A. U., Münnich, K. O., Roether, W., Kreutz, W., Schubach, K. & Siegel, O. (1966), 'Tracers Determine Movement of Soil Moisture and Evapotranspiration', *Science* **152**(3720), 346–347.

Appendix A

Detailed description of the sampling sites

TABLE A.1: Detailed description of sampling sites (Soil type, texture and region are taken from BK 50).

Location	Sample	Coordinates		Drilled depth [cm] 2014	Drilled depth [cm] 2015	Vegetation	Slope	Cultivation	BK 50 soil type	BK 50 KE
Aulendorf	AUL 1	3548531	5313798	-	67.5	willow	flat	extensive	Niedermoor, Gley-Niedermoor	U155
	AUL 2	3548537	5313812	-	102	poplar	flat	extensive	Niedermoor, Gley-Niedermoor	U155
	AUL 3	3548541	5313804	-	63.5	grassland	flat	-	Niedermoor, Gley-Niedermoor	U155
Biederbach	BIE 1	3429350	5342470	170	205	willow	slightly prone	extensive	Podsol-Gley und Gley-Stagnogley aus blockschuttreicher Talfüllung	A215
	BIE 2	3429350	5342470	80	103.5	grassland	slightly prone	-	Podsol-Gley und Gley-Stagnogley aus blockschuttreicher Talfüllung	A215
	BIE 3	3429181	5342466	70	108	willow	slightly prone	extensive	Podsol-Gley und Gley-Stagnogley aus blockschuttreicher Talfüllung	A215
	BIE 4	3429350	5342470	90	120	grassland	slightly prone	-	Podsol-Gley und Gley-Stagnogley aus blockschuttreicher Talfüllung	A215
	BIE 5	3430181	5336944	70	72	poplar	flat	extensive	Siedlung	3
	BIE 6	3430211	5336945	120	67	grassland	flat	-	Siedlung	3
	BIE 8	3428751	5342065	90	63.5	poplar	slightly prone	extensive	Braunerde aus Kristallin-Hangschutt und -gestein	A132
	BIE 9	3428751	5342065	94	95	grassland	slightly prone	-	Braunerde aus Kristallin-Hangschutt und -gestein	A132
Buggingen	BUG 1	3397071	5301569	90	88.5	willow	flat	extensive	Kolluvium	Z96
	BUG 2	3397053	5301531	60	56	willow	flat	extensive	Kolluvium	Z96
	BUG 3	3397028	5301471	90	69	willow	flat	extensive	Kolluvium	Z96
	BUG 4	3396760	5301825	56	62	maize	flat	intensive	Parabraunerde und Pseudogley-Parabraunerde	Z92
Kupferzell	KUP 1	3550779	5454426	-	135	willow	flat	extensive	Pelosol, Braunerde-Pelosol	J18
	KUP 2	3550772	5454431	-	89	grassland	flat	-	Pelosol, Braunerde-Pelosol	J18
	KUP 3	3550755	5454444	-	94	poplar	flat	extensive	Pelosol, Braunerde-Pelosol	J18
Marbach	MAR 1	3530787	5361692	-	169	willow	flat	extensive	Rendzina aus Kalk- und Dolomitstein	q14
	MAR 2	3530775	5361694	-	92	poplar	flat	extensive	Rendzina aus Kalk- und Dolomitstein	q14
	MAR 3	3530789	5361707	-	13.5	oat	flat	intensive	Rendzina aus Kalk- und Dolomitstein	q14
Rheinhausen/Forchheim	FOR 1	3451354	5425893	-	164	poplar	flat	extensive	Braunerde, z.T. podsolig	w30
	FOR 2	3451363	5425916	-	173	willow	flat	extensive	Braunerde, z.T. podsolig	w30
	FOR 3	3451343	5425872		170	grassland	flat	-	Braunerde, z.T. podsolig	w30
	FOR 4	3451408	5425875	-	209	willow	flat	extensive	Braunerde, z.T. podsolig	w30
	FOR 5	3451411	5425900	-	169	poplar	flat	extensive	Braunerde, z.T. podsolig	w30
	FOR 6	3451494	5426284	-	171	maize	flat	intensive	Braunerde, z.T. podsolig	w30
Kraichtal/ Neuenbuerg	KRAI 1	3480615	5446363	-	218	poplar	slightly prone	intensive	Pararendzina aus Löss und Sandlöss	e13
	KRAI 2	3480753	5446250	-	273	poplar	prone	intensive	Pararendzina aus Löss und Sandlöss	e13
	KRAI 3	3480768	5446246	-	163	uncultivated	prone	intensive	Pararendzina aus Löss und Sandlöss	e13
	KRAI 4	3480633	5446364	-	207	poplar	slightly prone	intensive	Pararendzina aus Löss und Sandlöss	e13
Laufen/Sulzburg	LAU 1	3402392	5301427	85	85	sida	prone	extensive	Pararendzina	Z33
	LAU 2	3402383	5301417	183	130	paulownia	prone	extensive	Pararendzina	Z33
	LAU 3	3402149	5301354	165	167	paulownia	slightly prone	extensive	Pararendzina	Z34
	LAU 3/2	3402149	5301354		88	paulownia	slightly prone	extensive	Pararendzina	Z34
	LAU 4	3402237	5301482	95	77	sida	slightly prone	extensive	Pararendzina	Z274
	LAU 5	3402238	5301462	93	70	poplar/ paulownia	slightly prone	extensive	Auengley	Z48
	LAU 6	3402228	5301436	82	77	grassland	slightly prone	-	Auengley	Z48
Welschingen	WEL 1	3483735	5298203	40	42	poplar	flat	extensive	Auftragsboden aus unterschiedlichen Substraten	U164
	WEL 2	3483769	5298215	165	169	sudangrass/ maize	flat	intensive	Auftragsboden aus unterschiedlichen Substraten	U164
	WEL 3	3483776	5298153	40	24	poplar	flat	extensive	Auftragsboden aus unterschiedlichen Substraten	U164

Appendix B

Model step I - sensitivity analysis

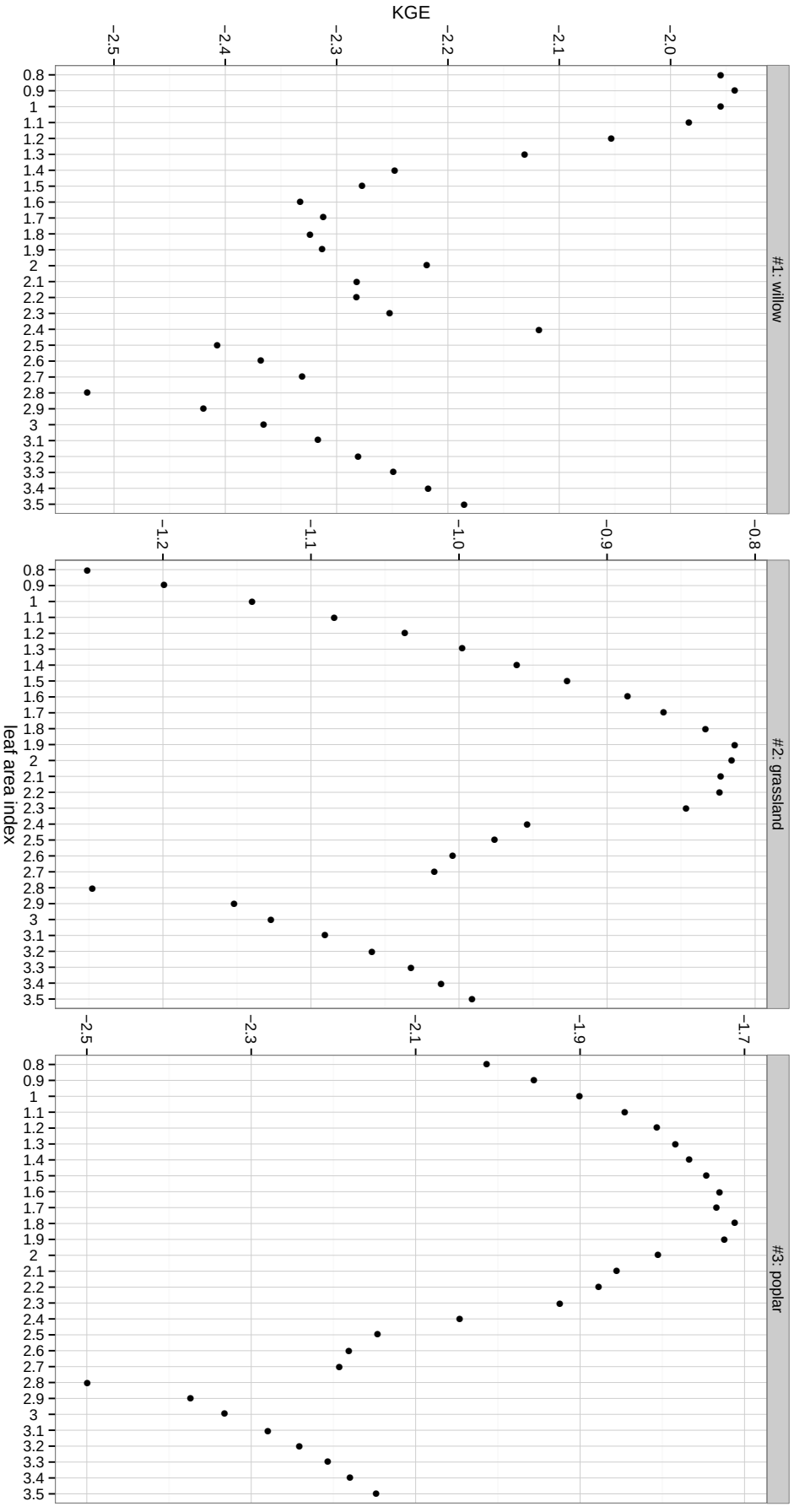

FIGURE B.1: Sensitivity analysis of model step I at sampling site Kupferzell.

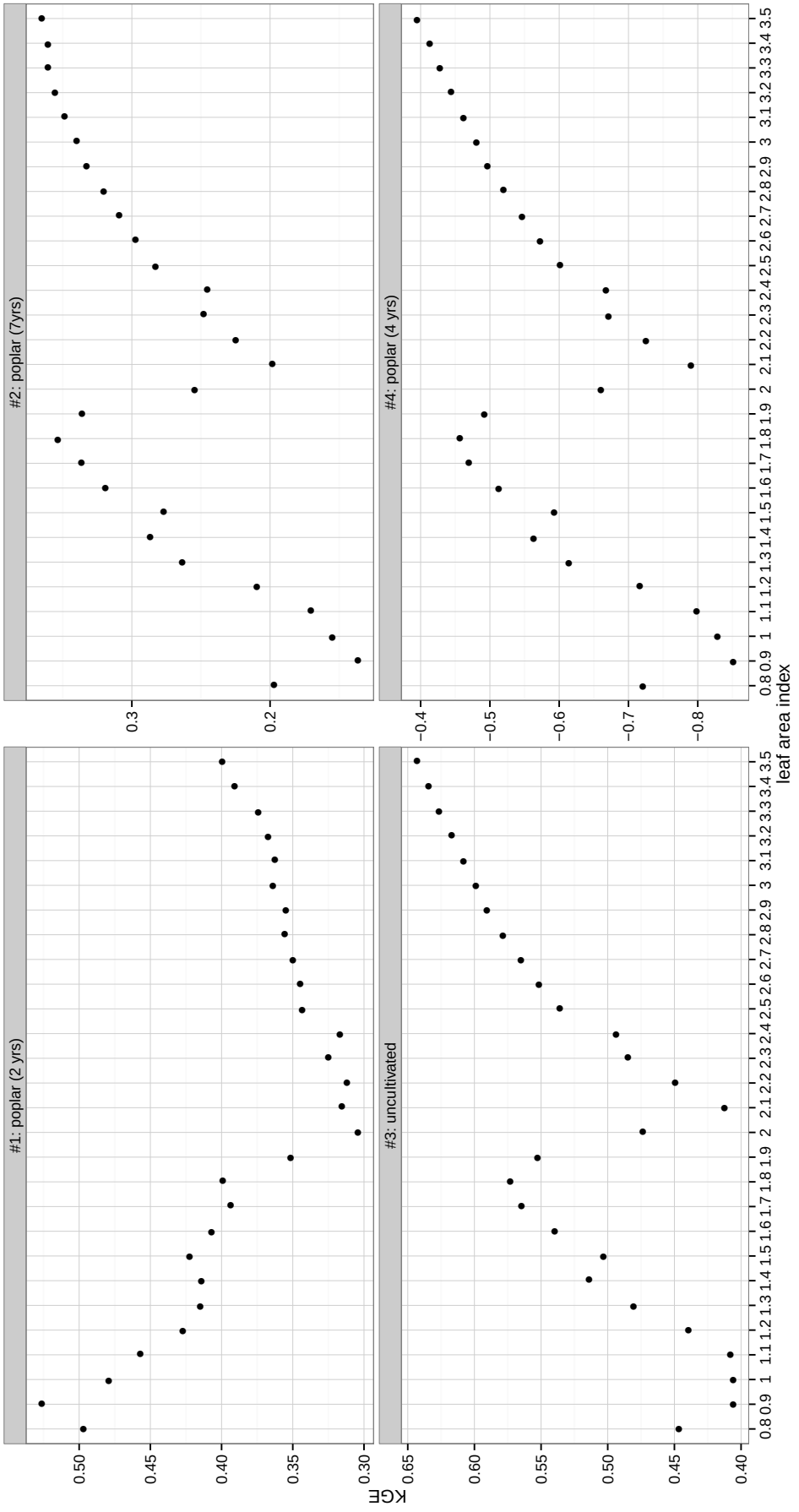

FIGURE B.2: Sensitivity analysis of model step I at sampling site Kraichtal.

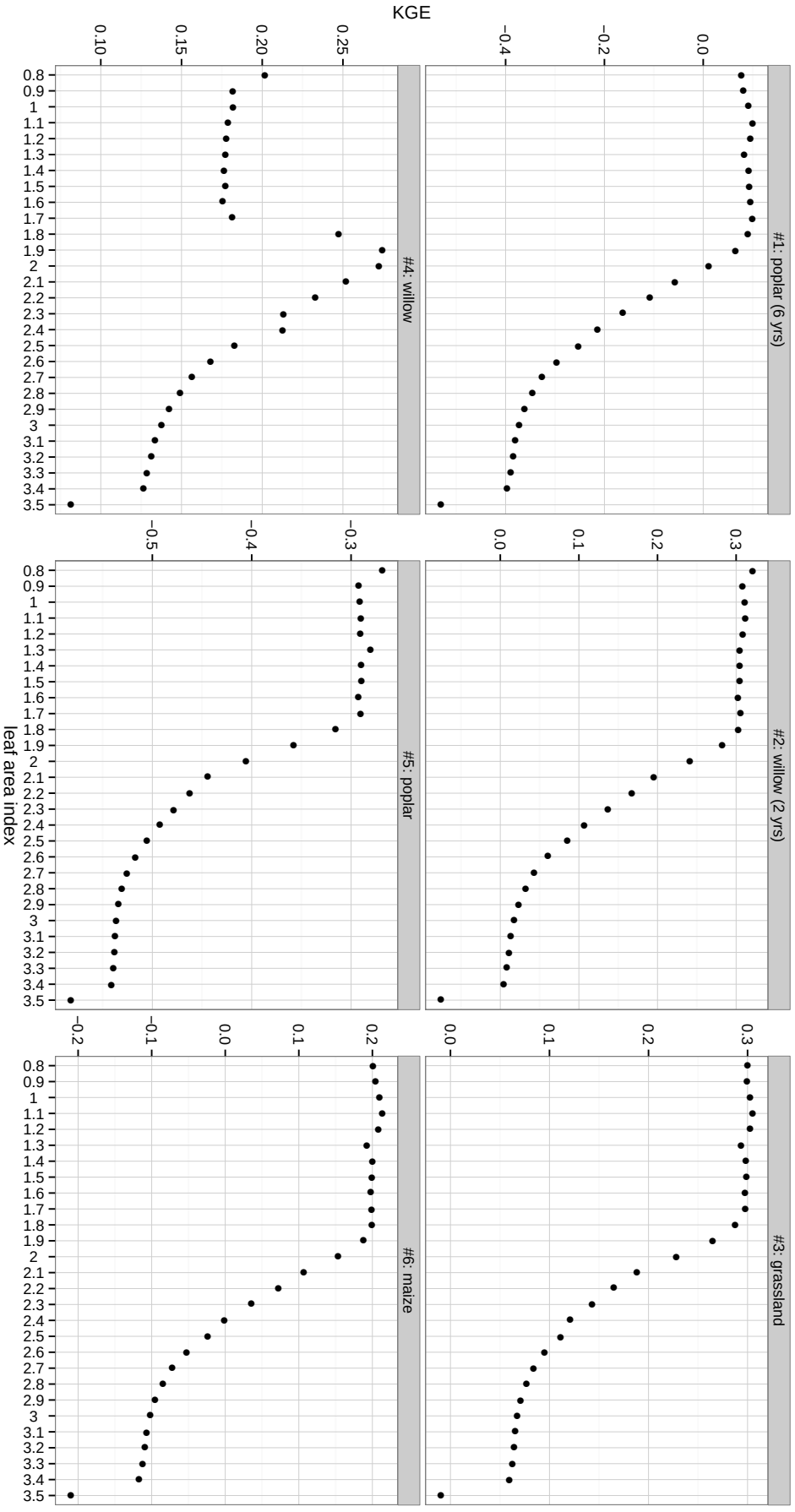

FIGURE B.3: Sensitivity analysis of model step I at sampling site Forchheim.

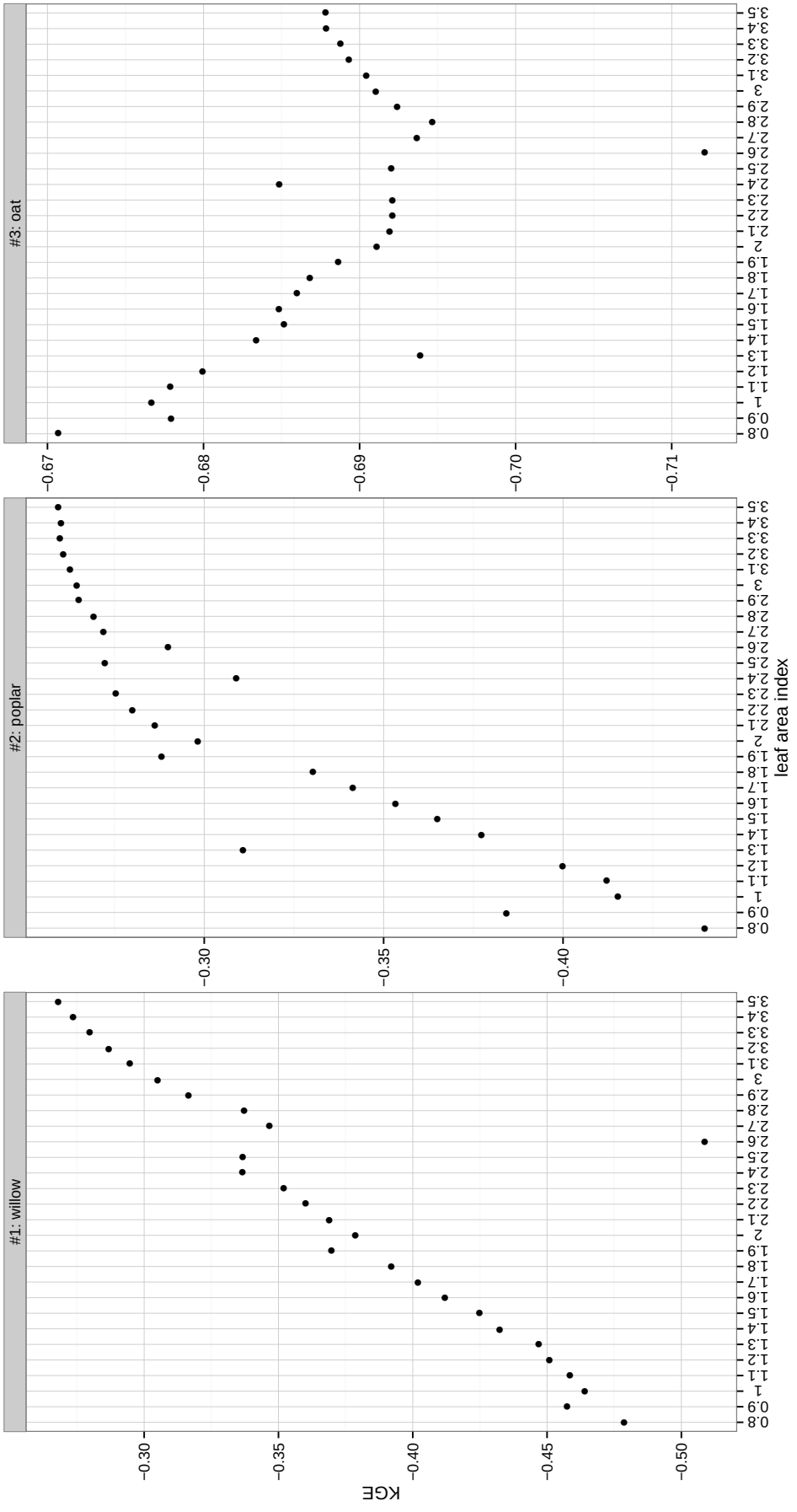

FIGURE B.4: Sensitivity analysis of model step I at sampling site Marbach.

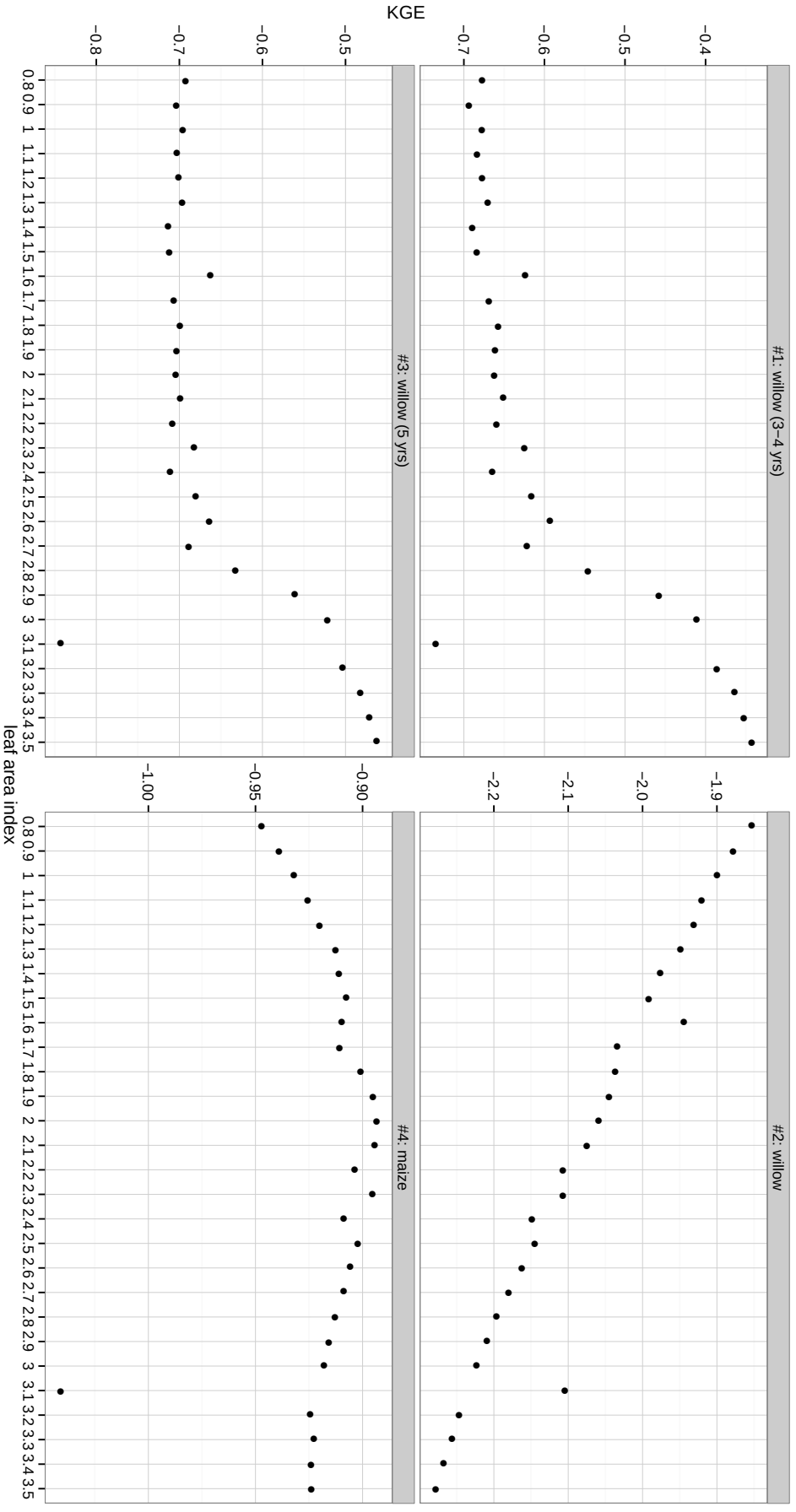

FIGURE B.5: Sensitivity analysis of model step I at sampling site Buggingen in autumn 2014.

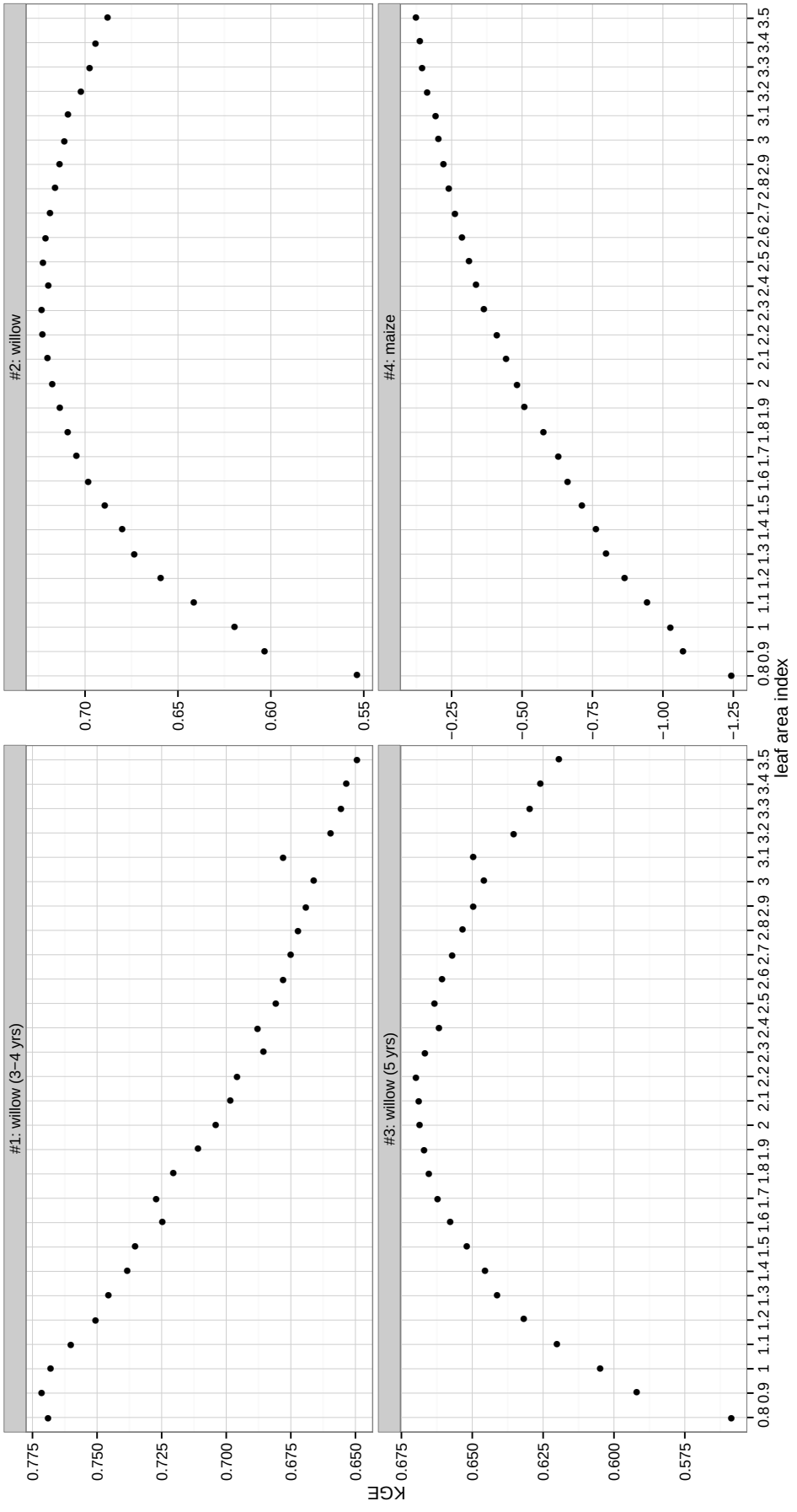

FIGURE B.6: Sensitivity analysis of model step I at sampling site Buggingen in spring 2015.

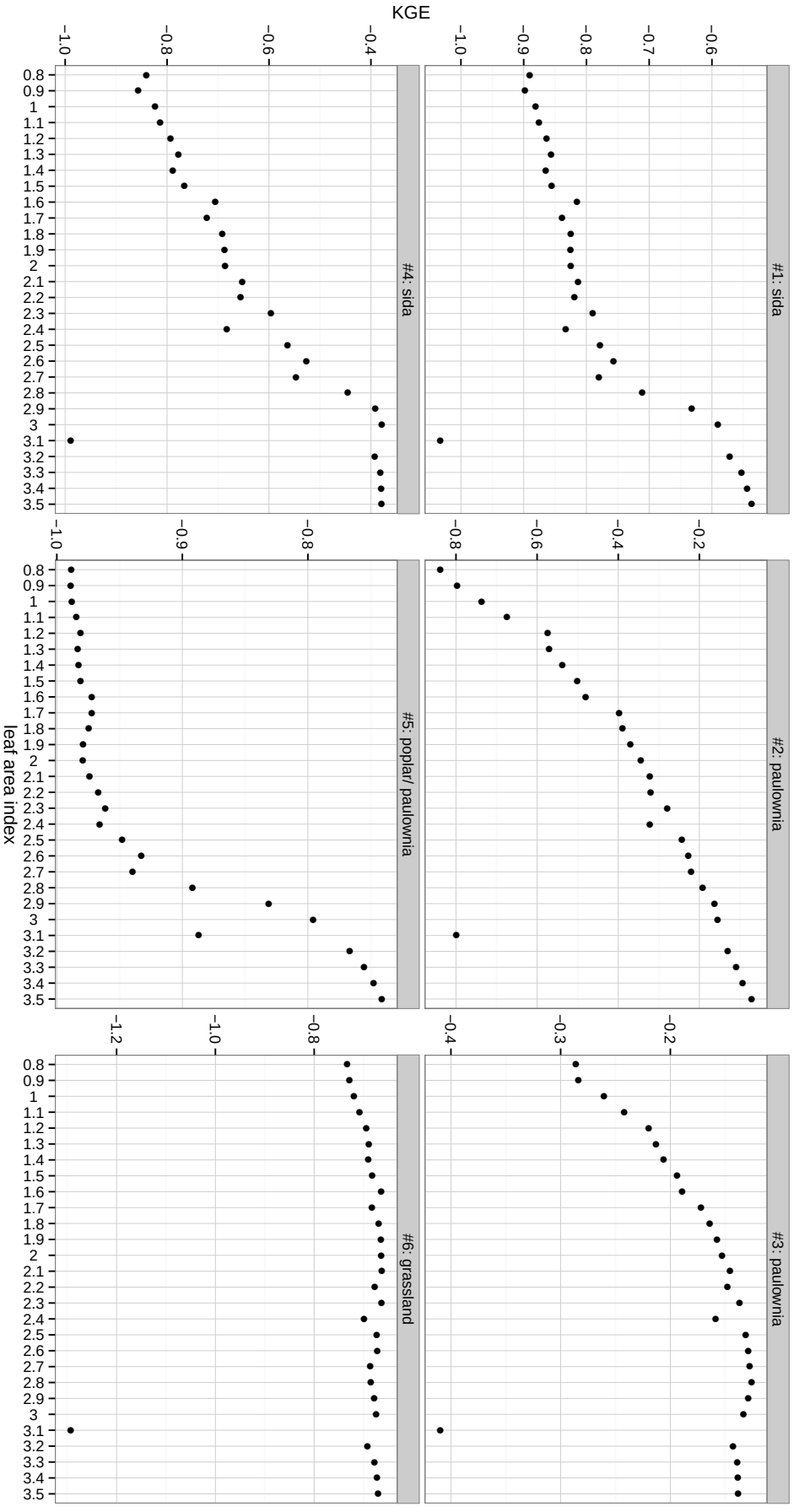

FIGURE B.7: Sensitivity analysis of model step I at sampling site Laufen in autumn 2014.

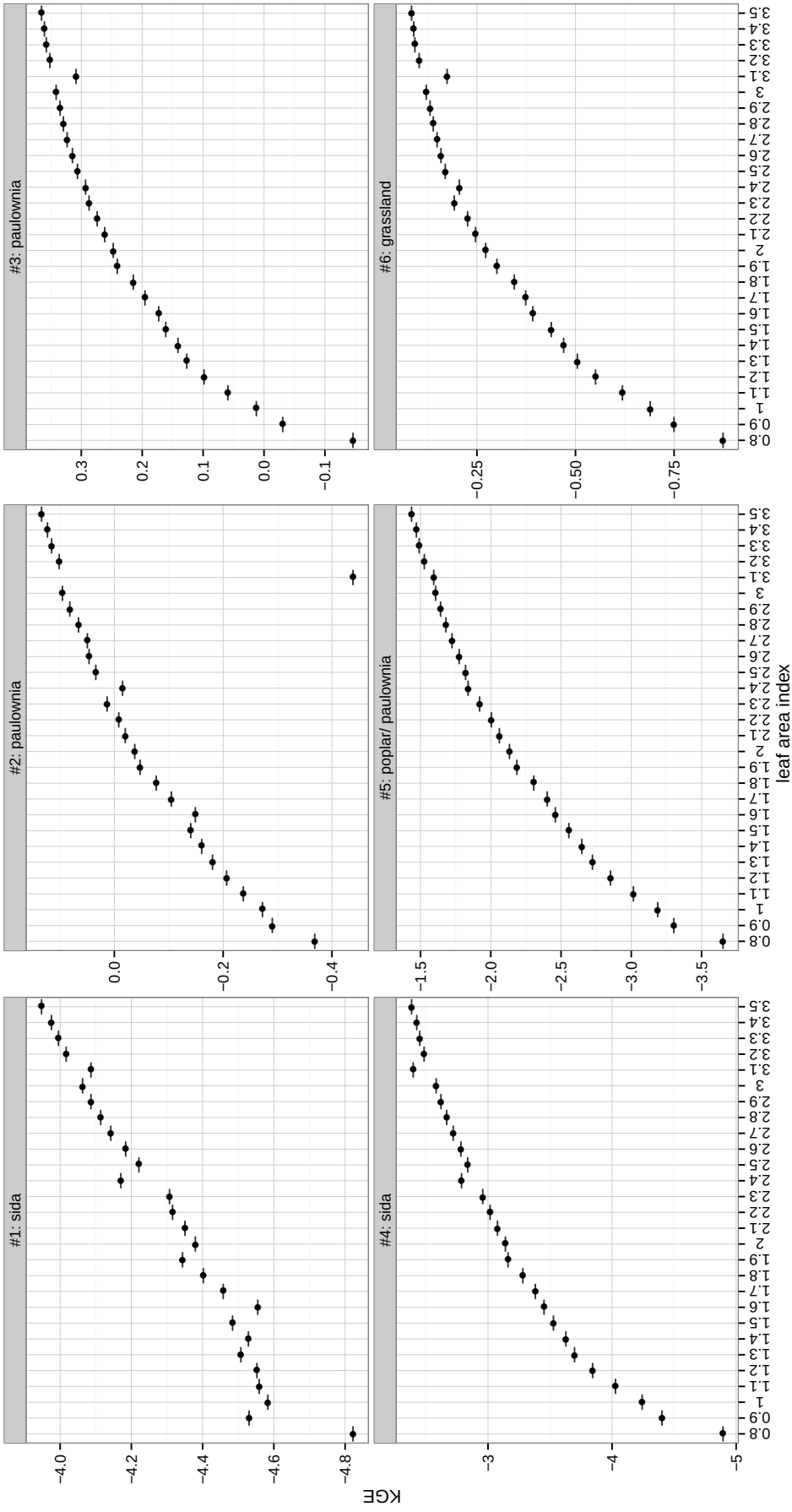

FIGURE B.8: Sensitivity analysis of model step I at sampling site Laufen in spring 2015.

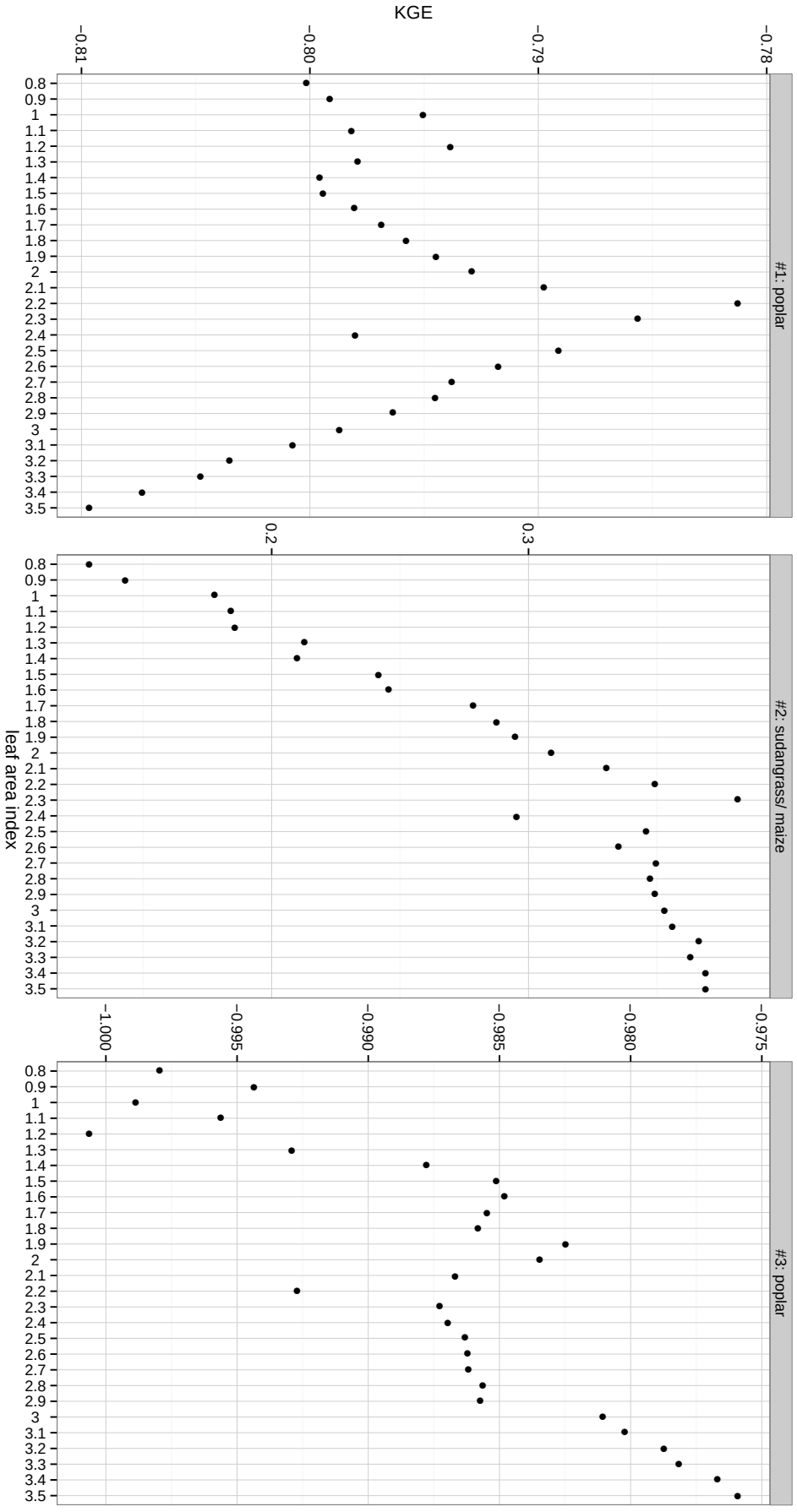

FIGURE B.9: Sensitivity analysis of model step I at sampling site Welschingen in autumn 2014.

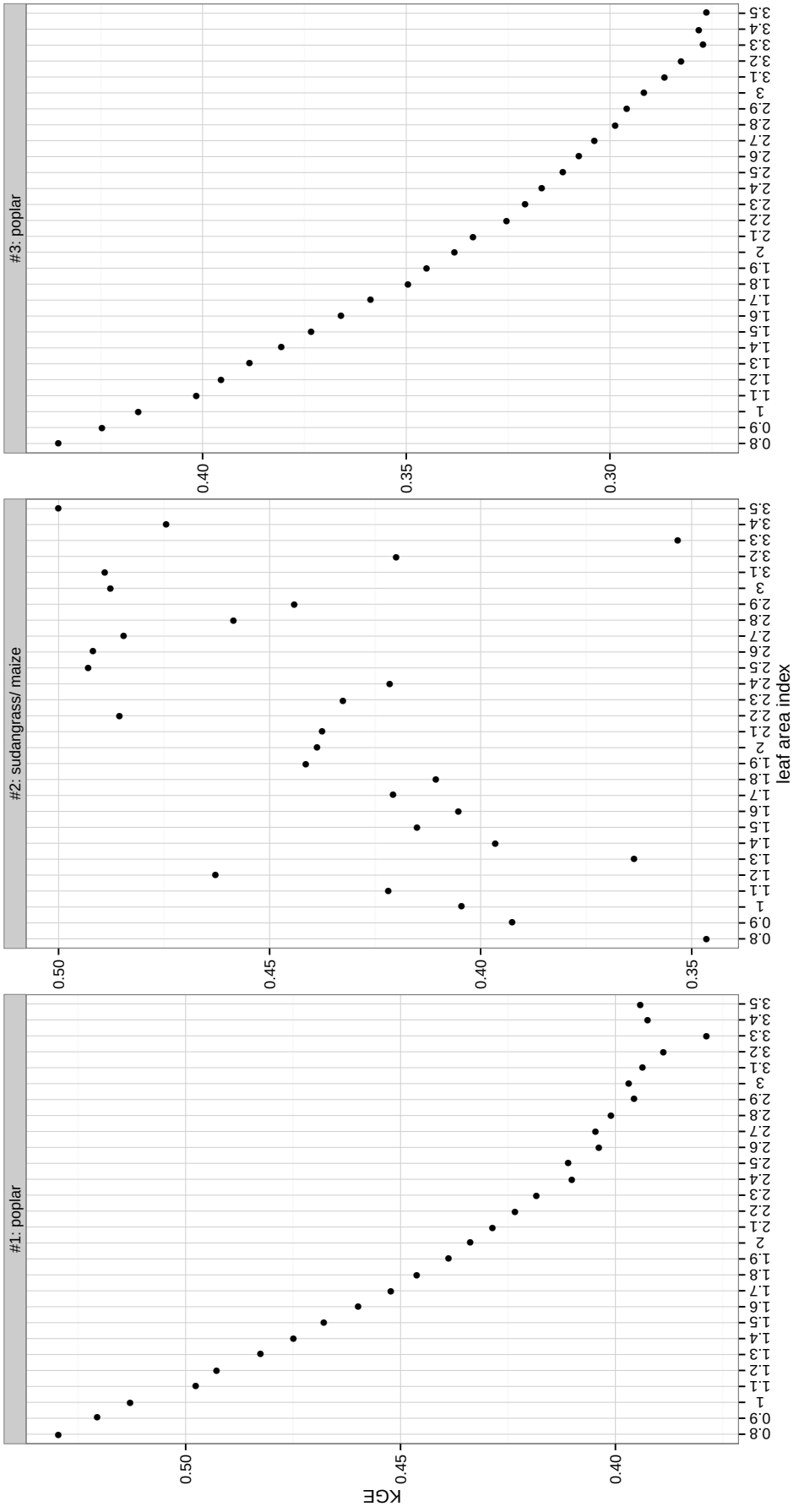

FIGURE B.10: Sensitivity analysis of model step I at sampling site Welschingen in spring 2015.

Appendix C

Model step III to V - depth plots

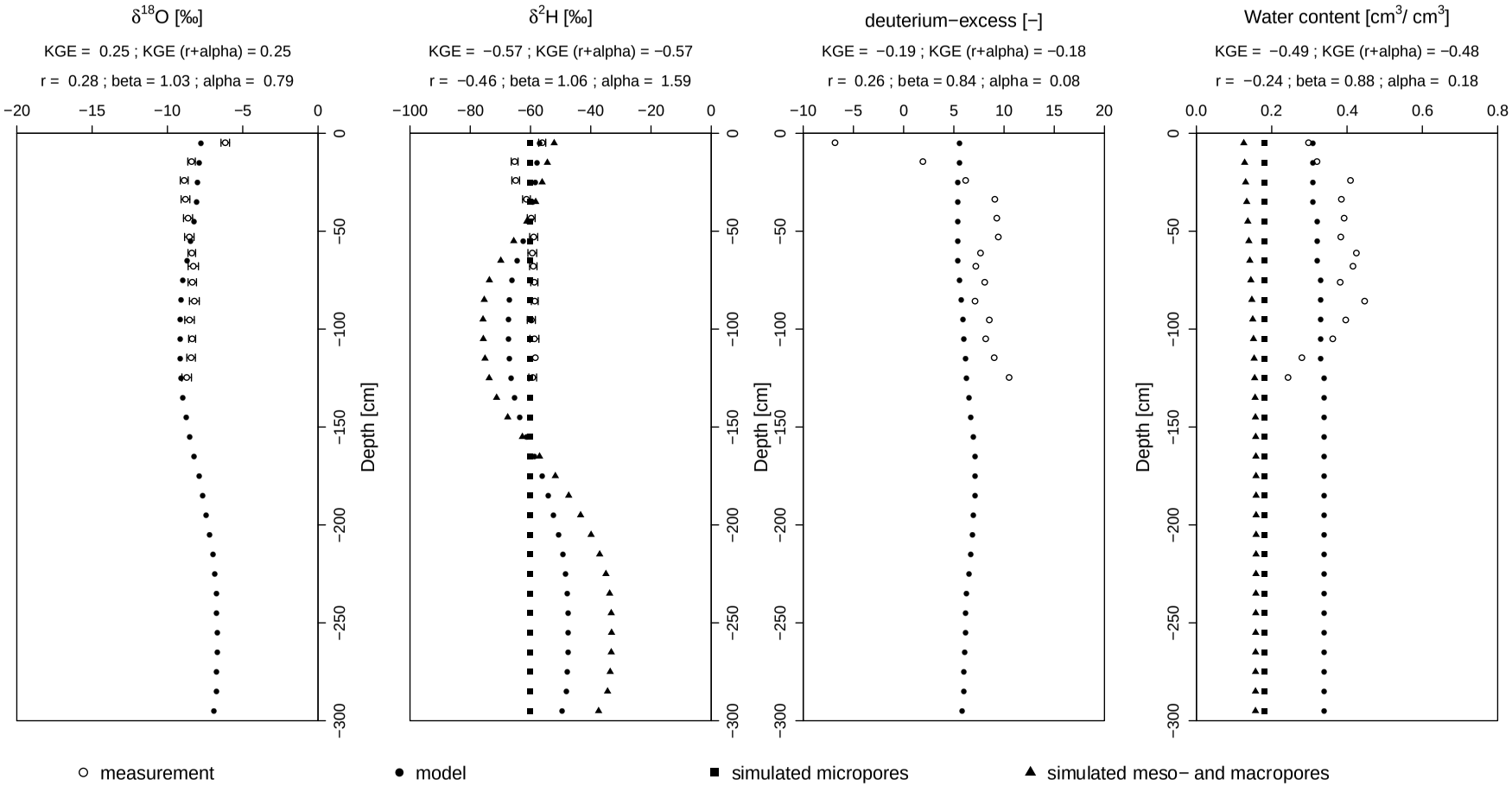

FIGURE C.1: Depth profile of observed and modeled $\delta^{18}O$, $\delta^{2}H$, volumetric water content and deuterium-excess values from best fit run of model step V for profile 1 at Kupferzell. Within model step V water flow is calculated separately in micro-, meso- and macropores. The black model graph shows isotope signature resulting from a combination of both pore spaces; moreover, KGE is calculated from these simulations. For oxygen-18 the output of SWIS is only a combination of pore spaces.

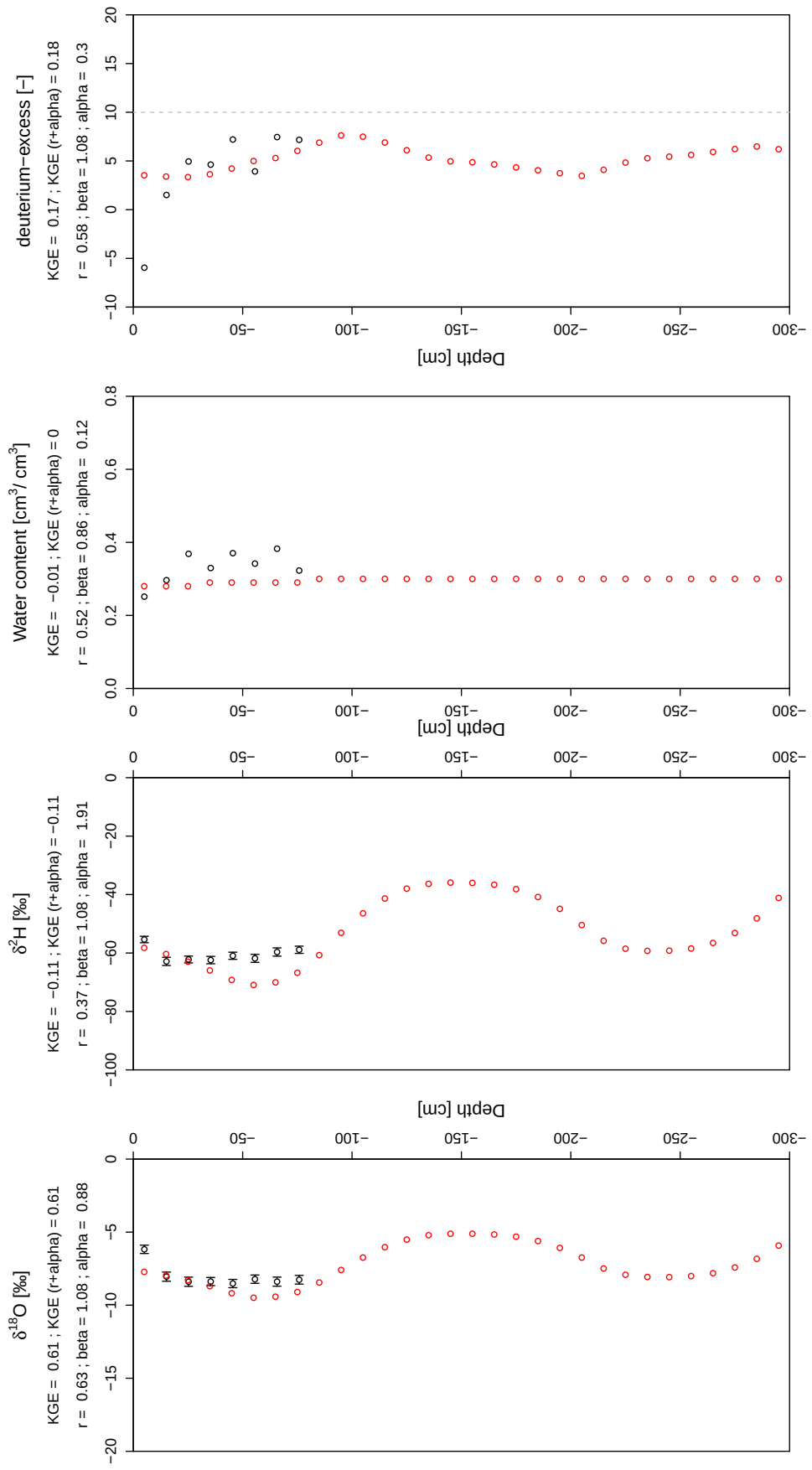

FIGURE C.2: Depth profile of observed (black) and modeled (red) $\delta^{18}O$, $\delta^{2}H$, volumetric water content and deuterium-excess values from best fit run of model step IV for profile 2 at Kupferzell.

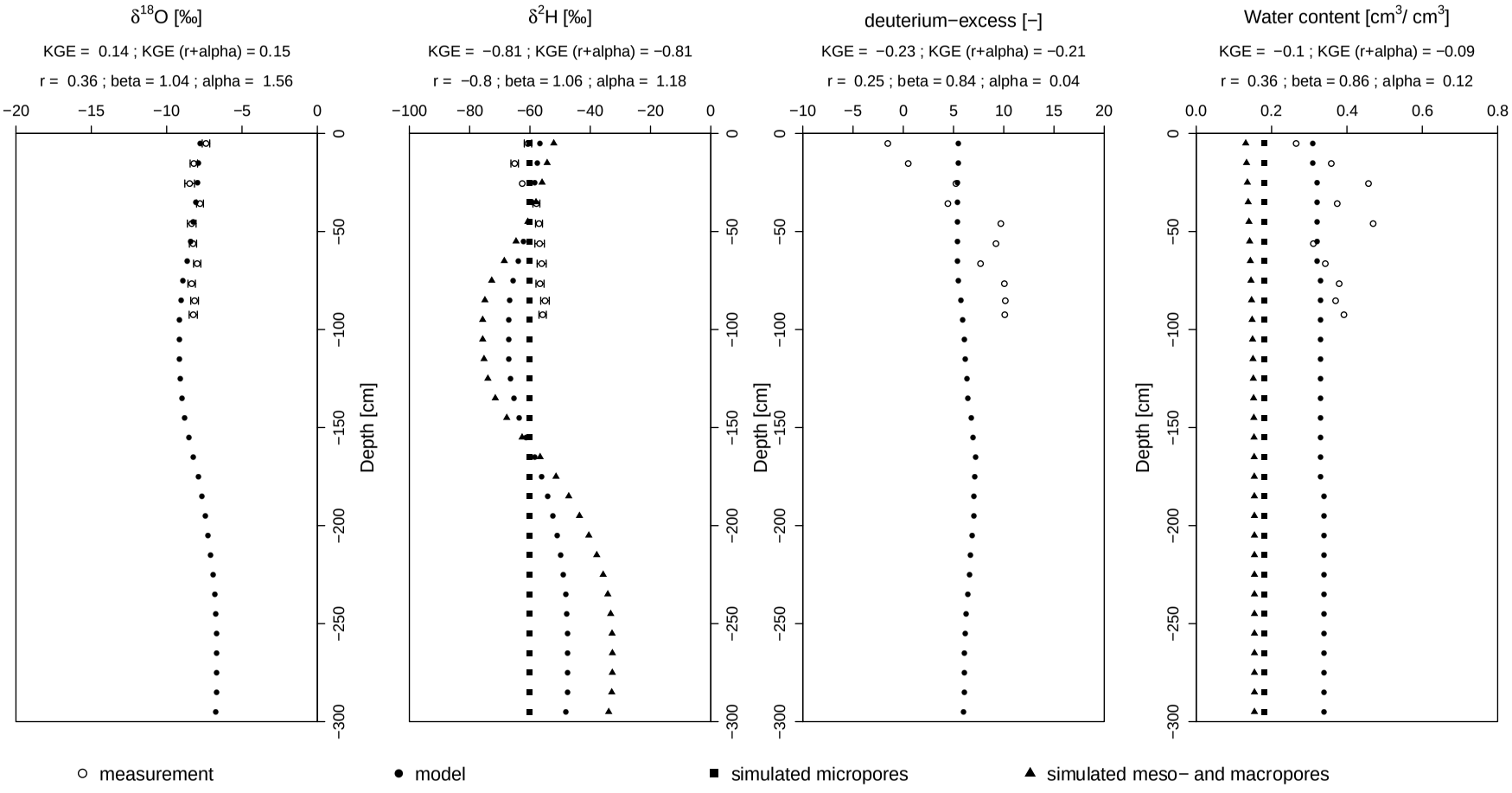

FIGURE C.3: Depth profile of observed and modeled $\delta^{18}O$, $\delta^{2}H$, volumetric water content and deuterium-excess values from best fit run of model step V for profile 3 at Kupferzell. Within model step V water flow is calculated separately in micro-, meso- and macropores. Black model graph shows isotope signature resulting from a combination of both pore spaces; moreover, KGE is calculated from these simulations. For oxygen-18 the output of SWIS is only a combination of pore spaces.

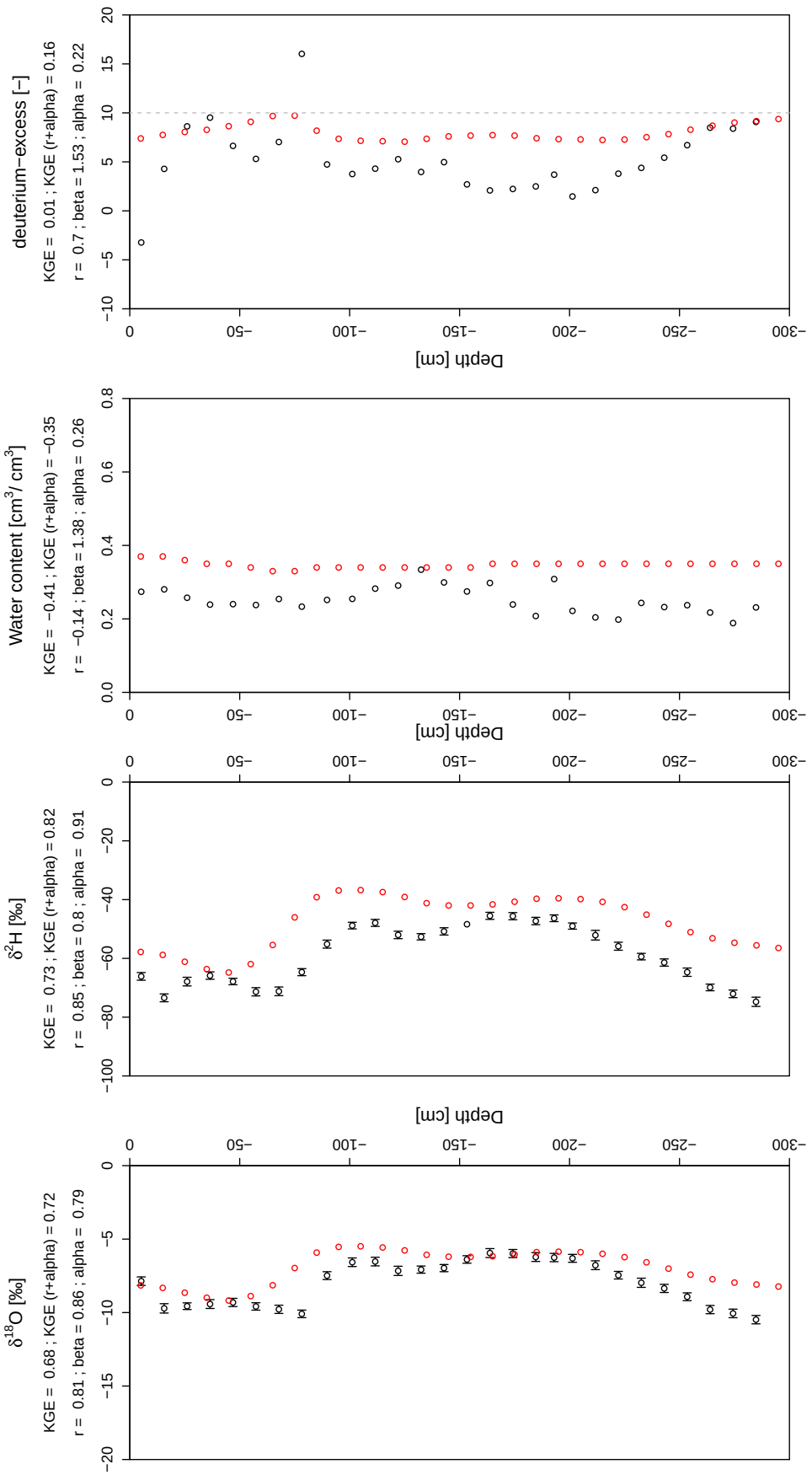

FIGURE C.4: Depth profile of observed (black) and modeled (red) $\delta^{18}O$, $\delta^{2}H$, volumetric water content and deuterium-excess values from best fit run of model step IV for profile 1 at Kraichtal.

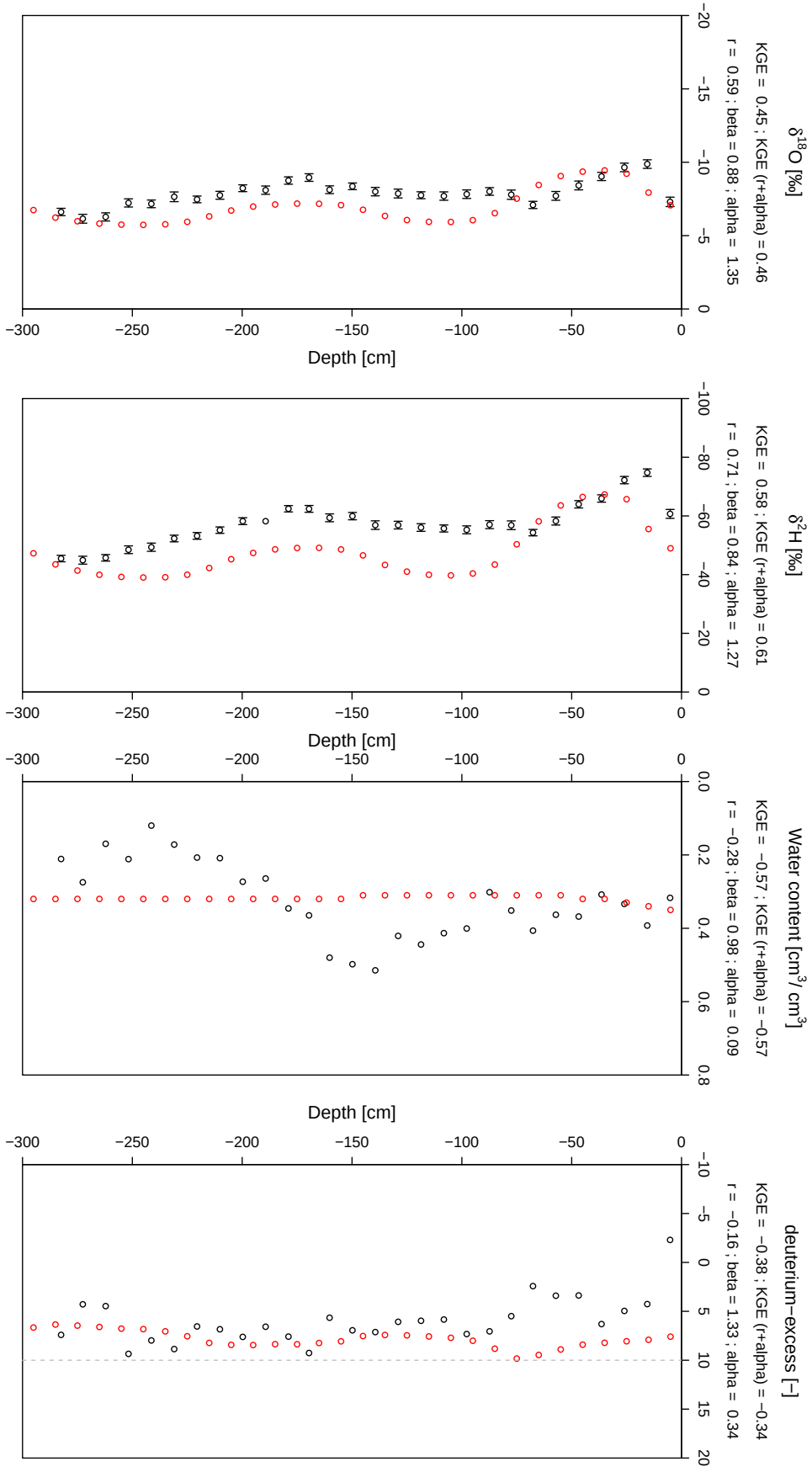

FIGURE C.5: Depth profile of observed (black) and modeled (red) $\delta^{18}O$, $\delta^{2}H$, volumetric water content and deuterium-excess values from best fit run of model IV for profile 2 at Kraichtal.

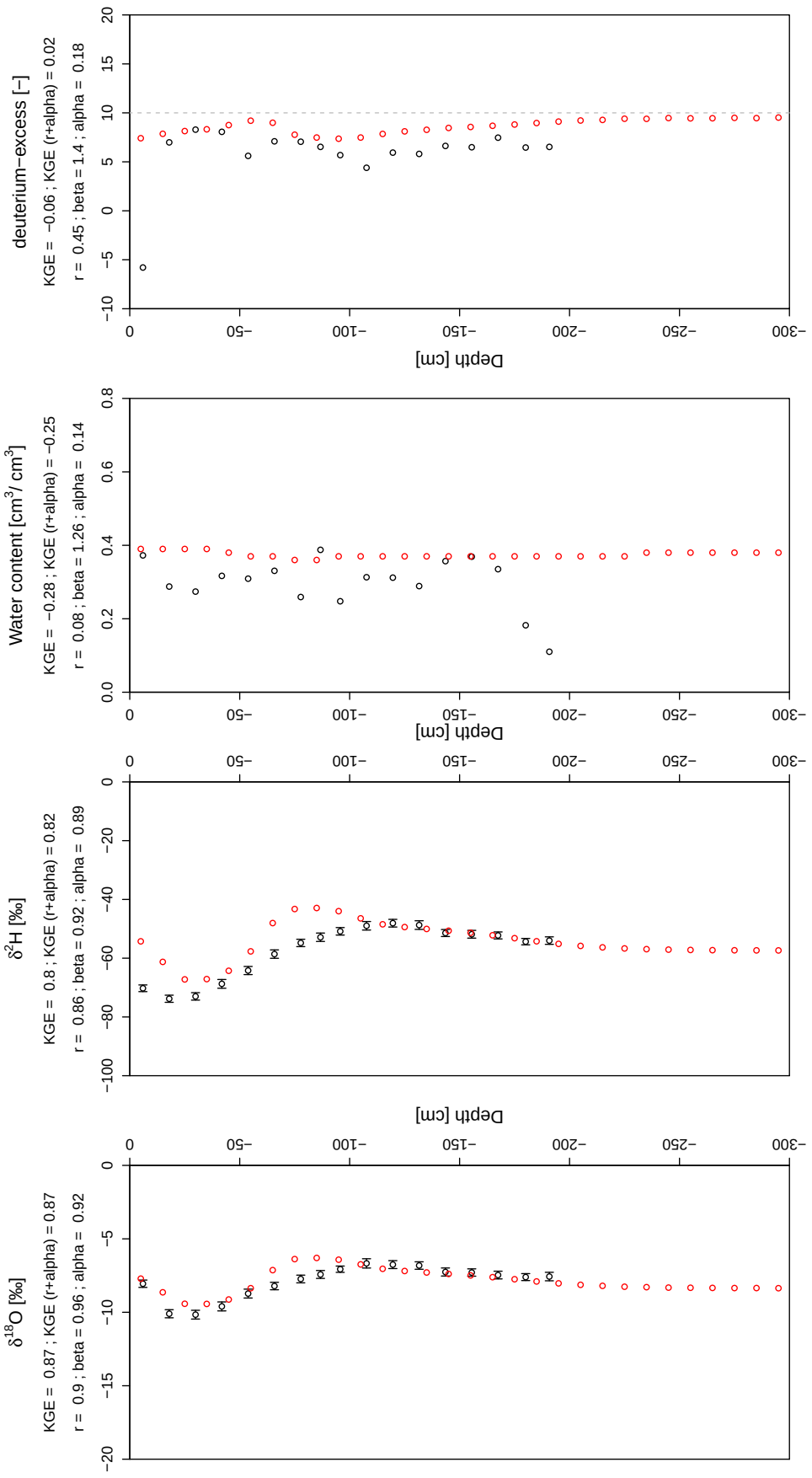

FIGURE C.6: Depth profile of observed (black) and modeled (red) $\delta^{18}O$, $\delta^{2}H$, volumetric water content and deuterium-excess values from best fit run of model step IV for profile 3 at Kraichtal.

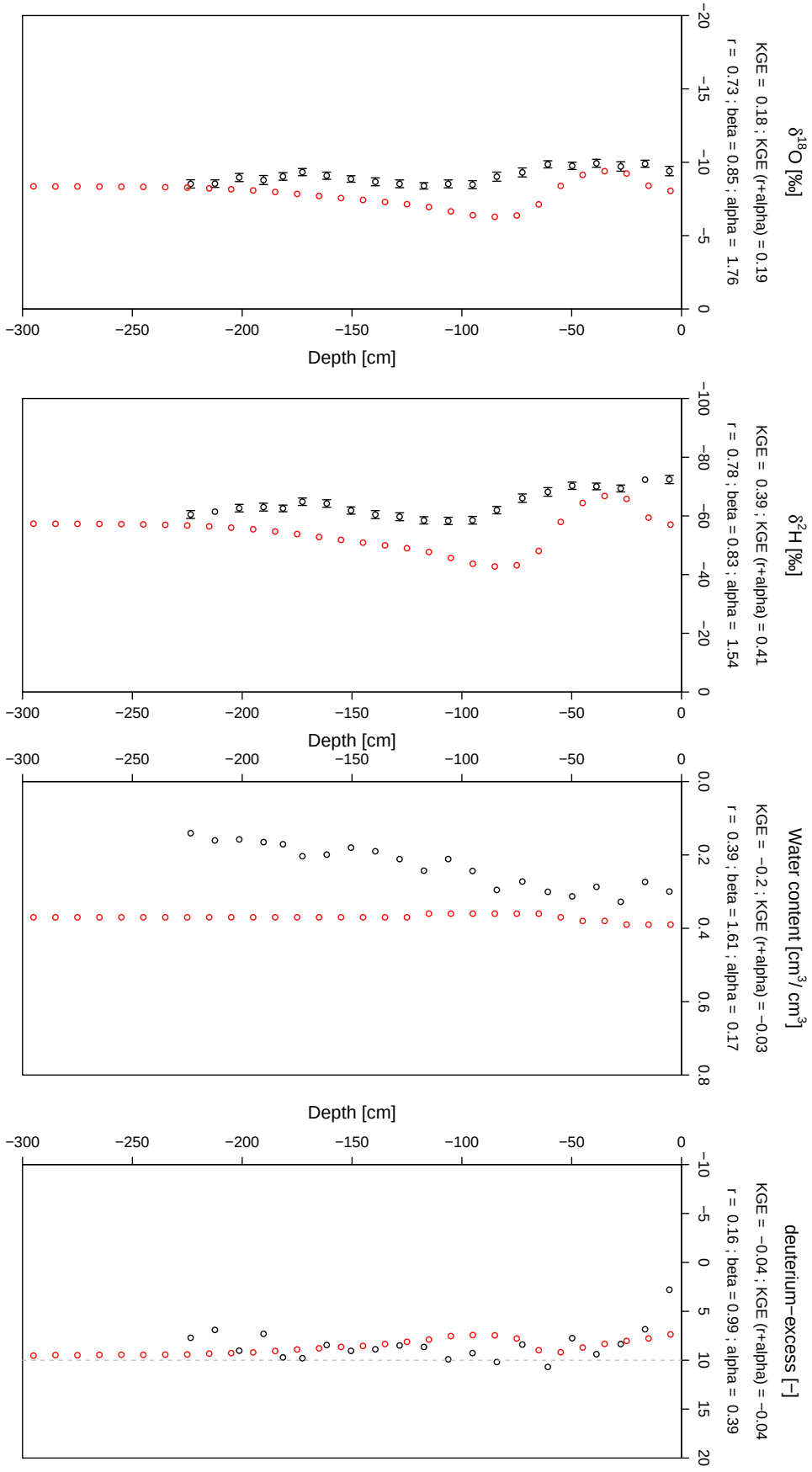

FIGURE C.7: Depth profile of observed (black) and modeled (red) $\delta^{18}O$, $\delta^{2}H$, volumetric water content and deuterium-excess values from best fit run of model step IV for profile 4 at Kraichtal.

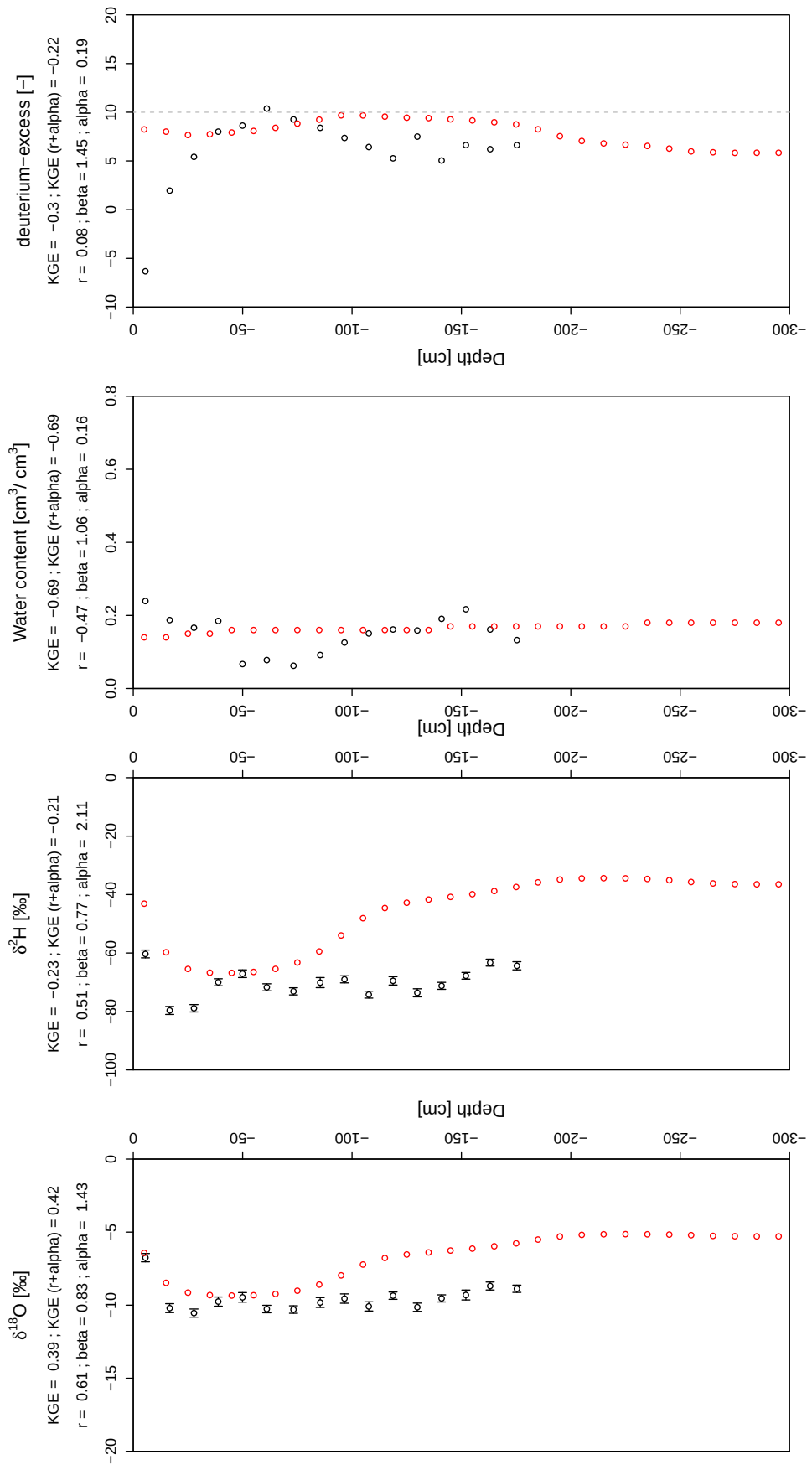

FIGURE C.8: Depth profile of observed (black) and modeled (red) $\delta^{18}O$, $\delta^{2}H$, volumetric water content and deuterium-excess values from best fit run of model step III for profile 1 at Forchheim.

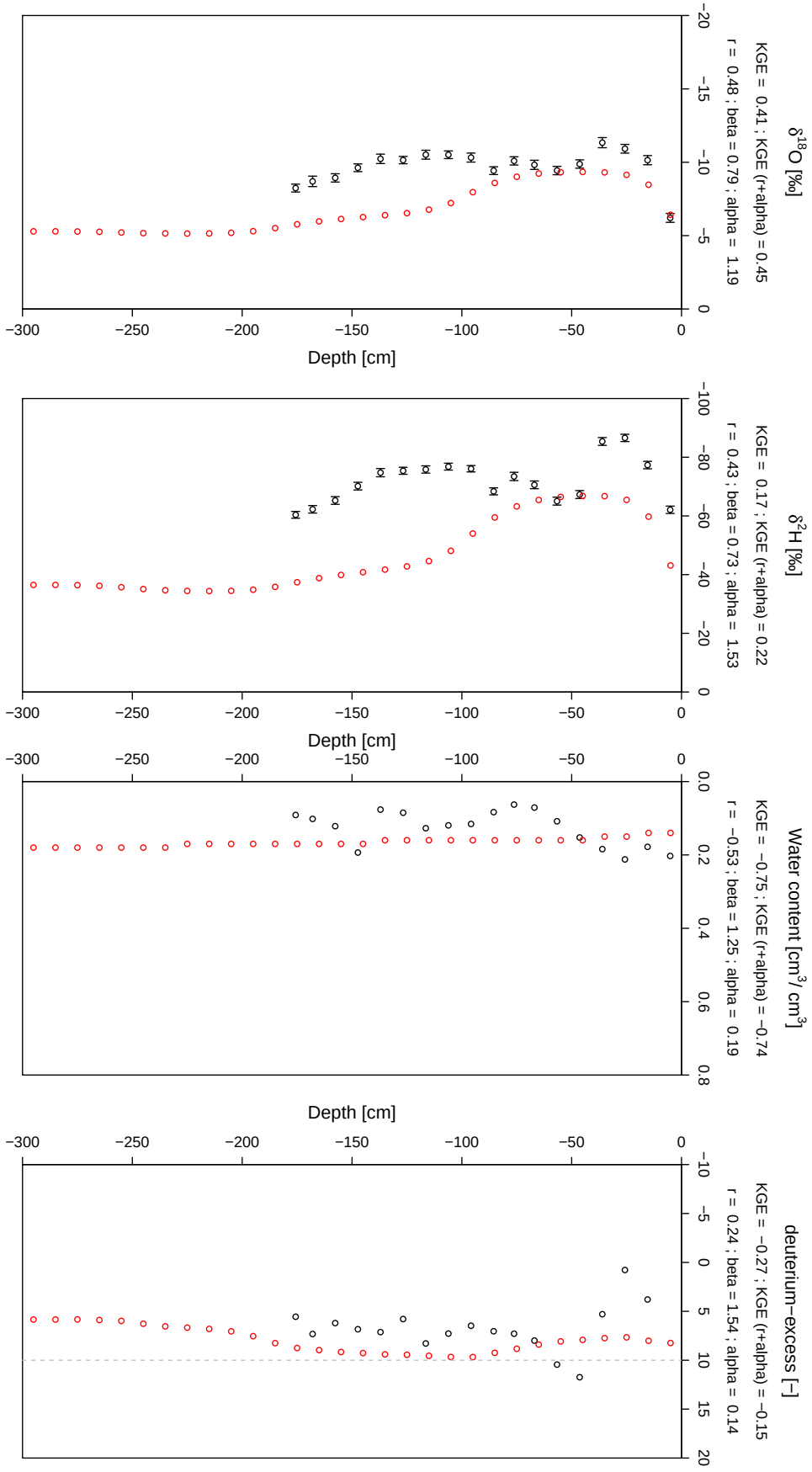

FIGURE C.9: Depth profile of observed (black) and modeled (red) $\delta^{18}O$, $\delta^{2}H$, volumetric water content and deuterium-excess values from best fit run of model step III for profile 2 at Forchheim.

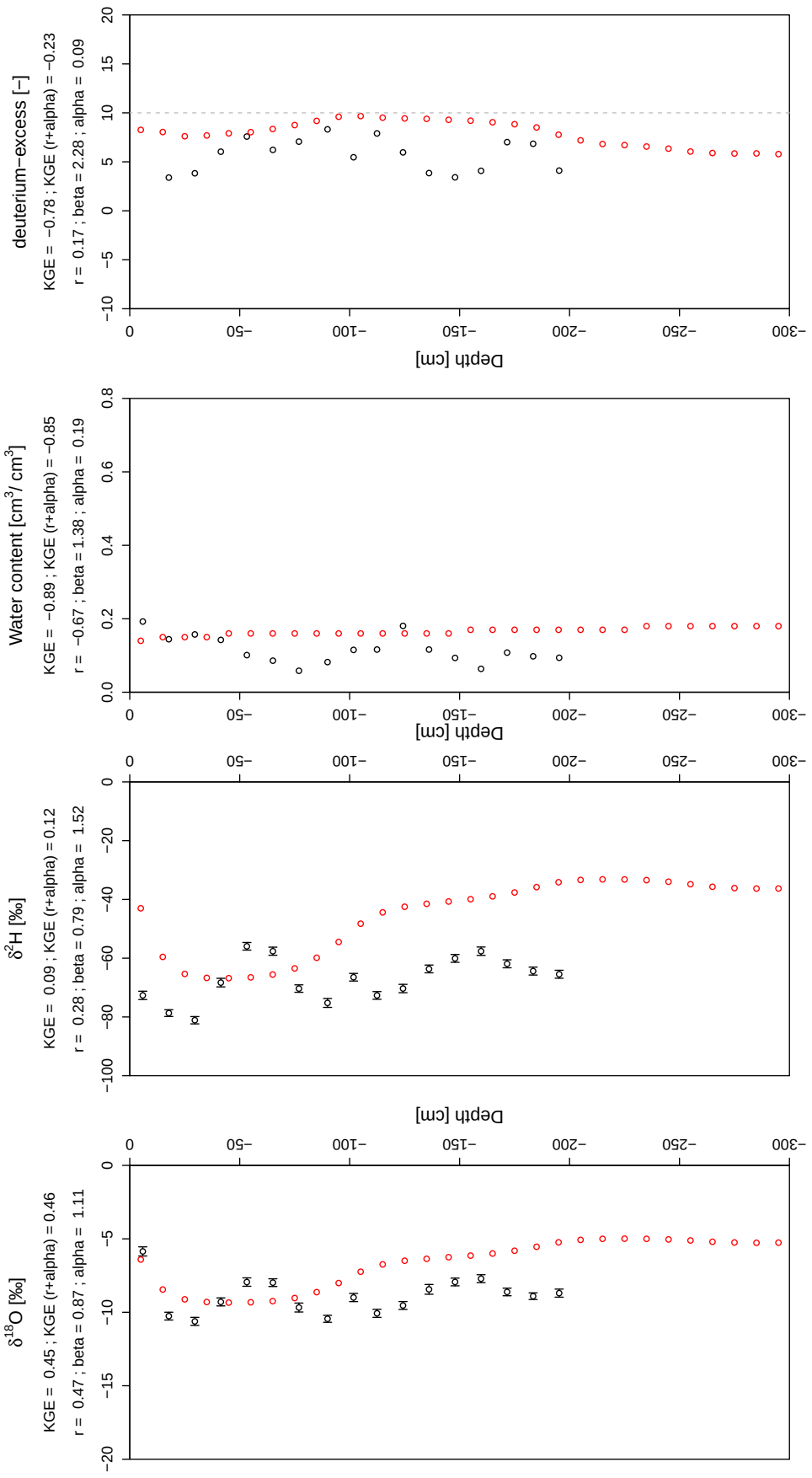

FIGURE C.10: Depth profile of observed (black) and modeled (red) $\delta^{18}O$, $\delta^{2}H$, volumetric water content and deuterium-excess values from best fit run of model step III for profile 3 at Forchheim.

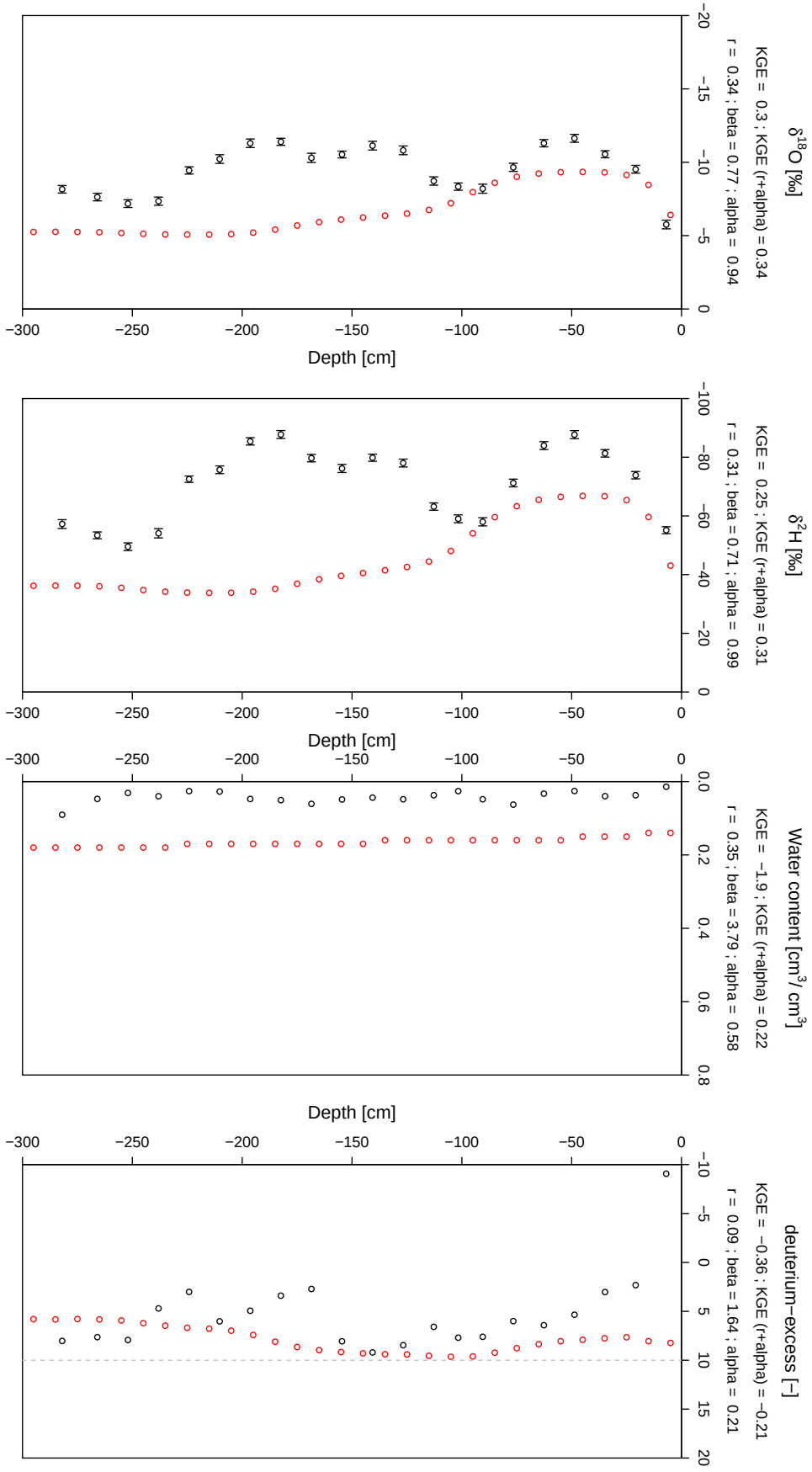

FIGURE C.11: Depth profile of observed (black) and modeled (red) $\delta^{18}O$, $\delta^{2}H$, volumetric water content and deuterium-excess values from best fit run of model step III for profile 4 at Forchheim.

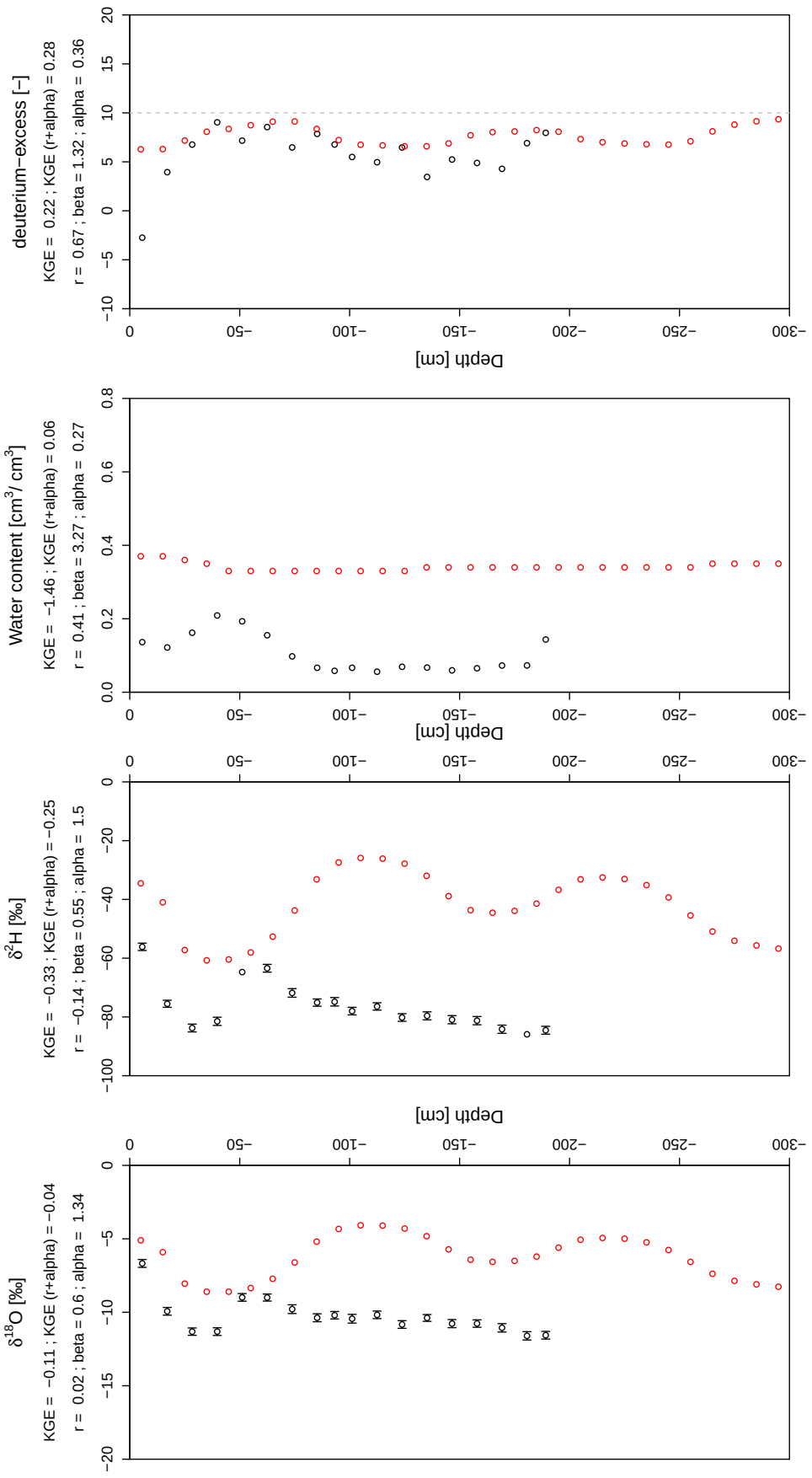

FIGURE C.12: Depth profile of observed (black) and modeled (red) $\delta^{18}O$, $\delta^{2}H$, volumetric water content and deuterium-excess values from best fit run of model step IV for profile 5 at Forchheim.

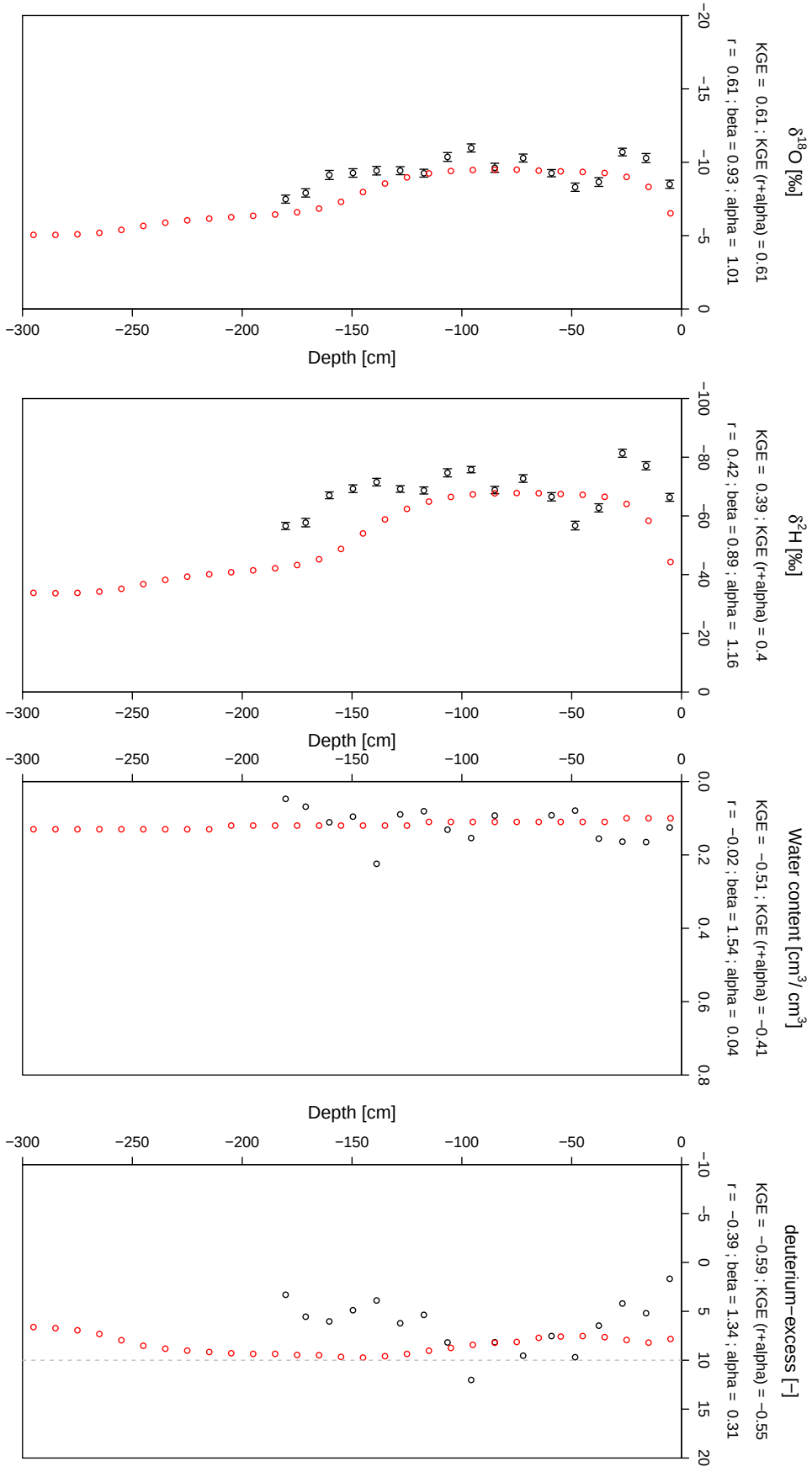

FIGURE C.13: Depth profile of observed (black) and modeled (red) $\delta^{18}O$, $\delta^{2}H$, volumetric water content and deuterium-excess values from best fit run of model step IV for profile 6 at Forchheim.

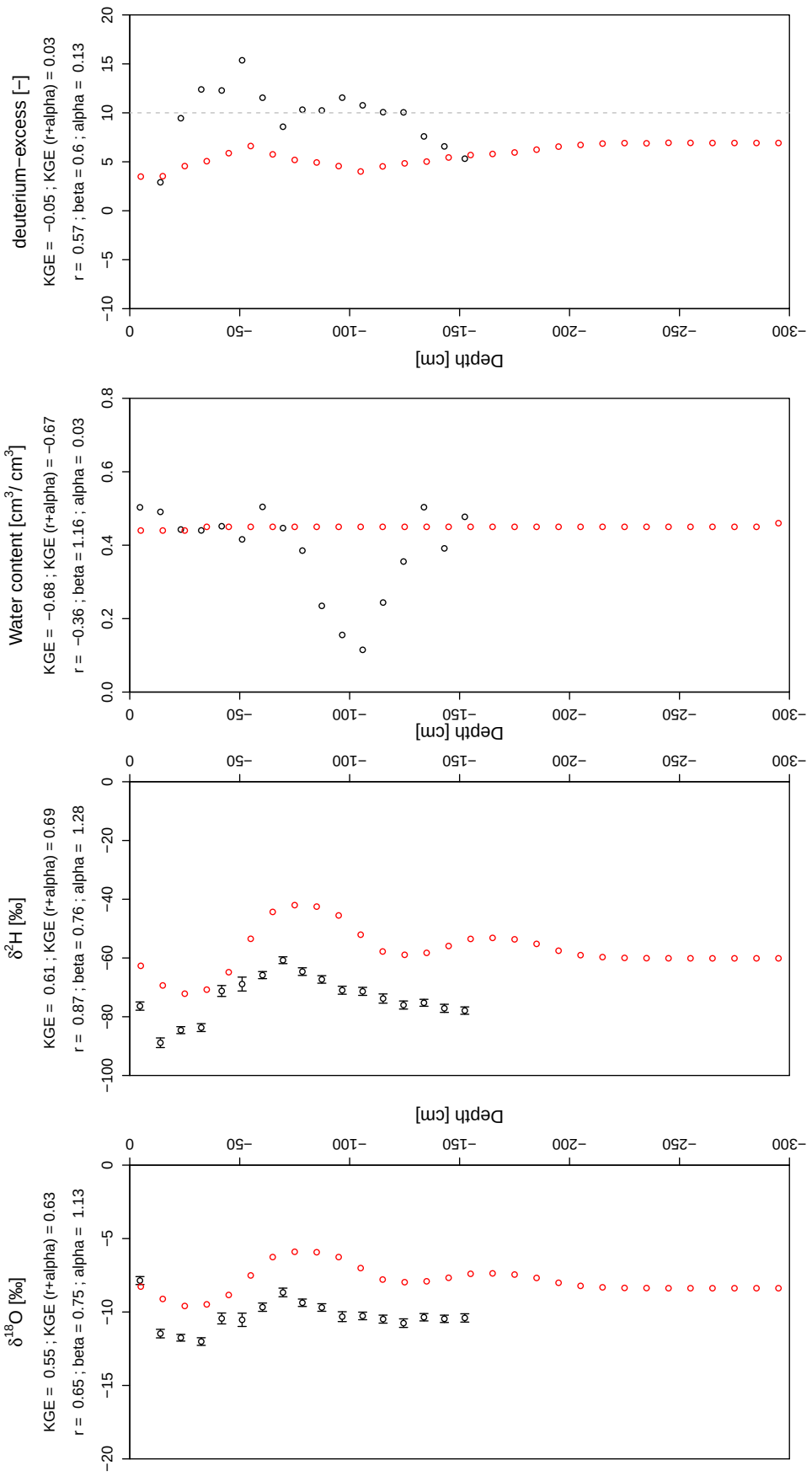

FIGURE C.14: Depth profile of observed (black) and modeled (red) $\delta^{18}O$, $\delta^{2}H$, volumetric water content and deuterium-excess values from best fit run of model step IV for profile 1 at Marbach.

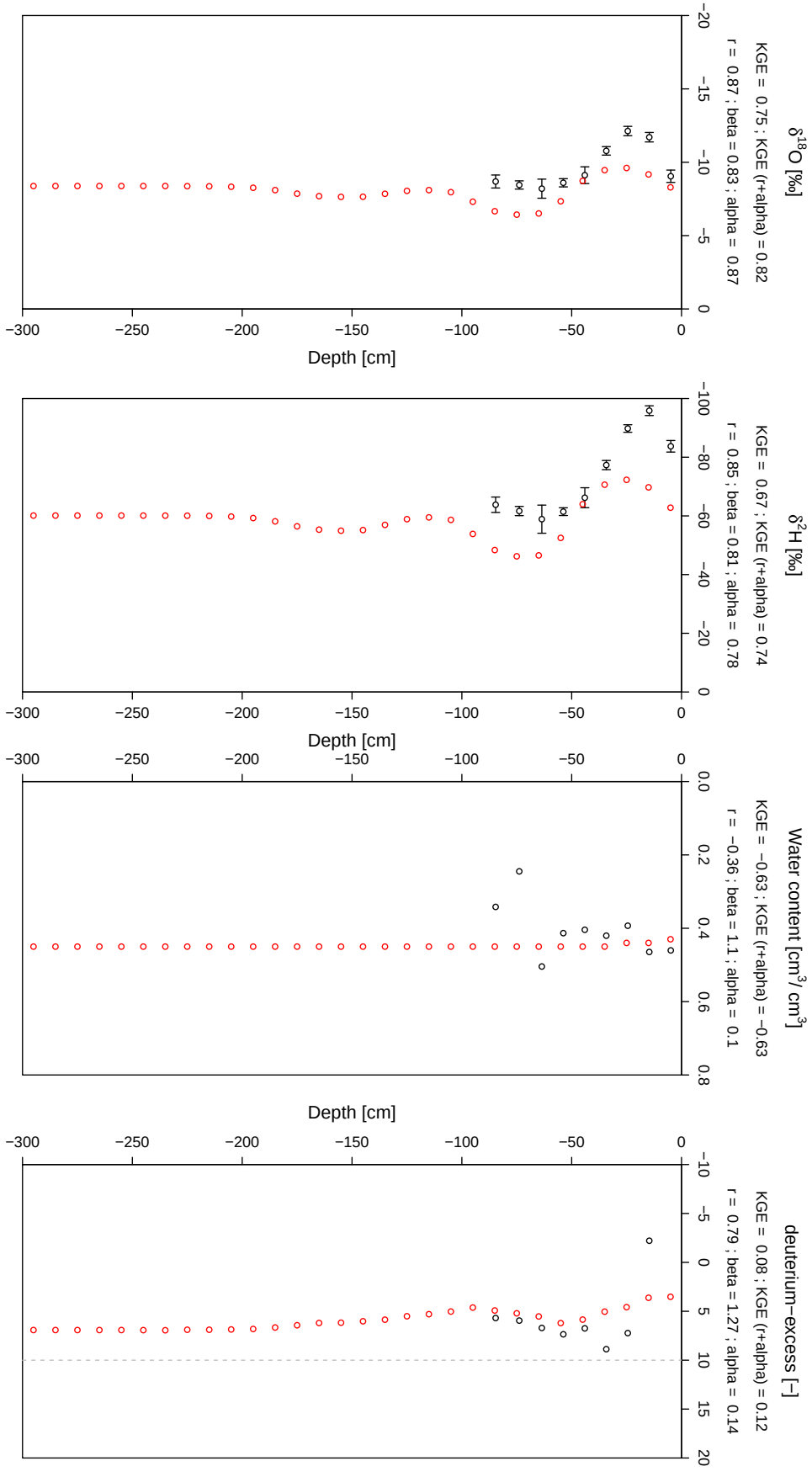

FIGURE C.15: Depth profile of observed (black) and modeled (red) $\delta^{18}O$, $\delta^{2}H$, volumetric water content and deuterium-excess values from best fit run of model step IV for profile 2 at Marbach.

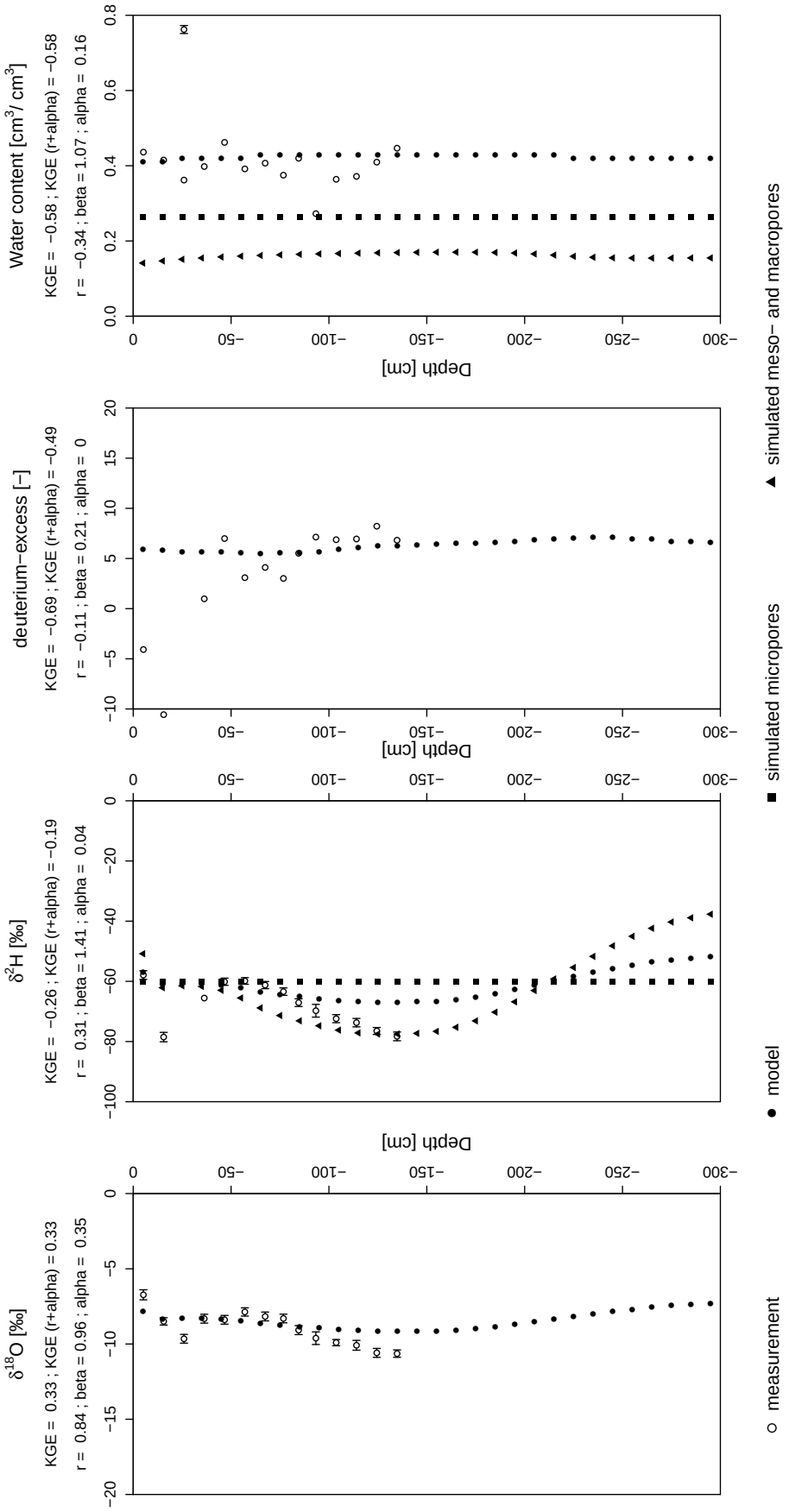

FIGURE C.16: Depth profile of observed and modeled $\delta^{18}O$, $\delta^{2}H$, volumetric water content and deuterium-excess values from best fit run of model step V for profile 3 at Marbach. Within model step V water flow is calculated separately in micro-, meso- and macropores. Black model graph shows isotope signature resulting from a combination of both pore spaces; moreover, KGE is calculated from these simulations. For oxygen-18 the output of SWIS is only a combination of pore spaces.

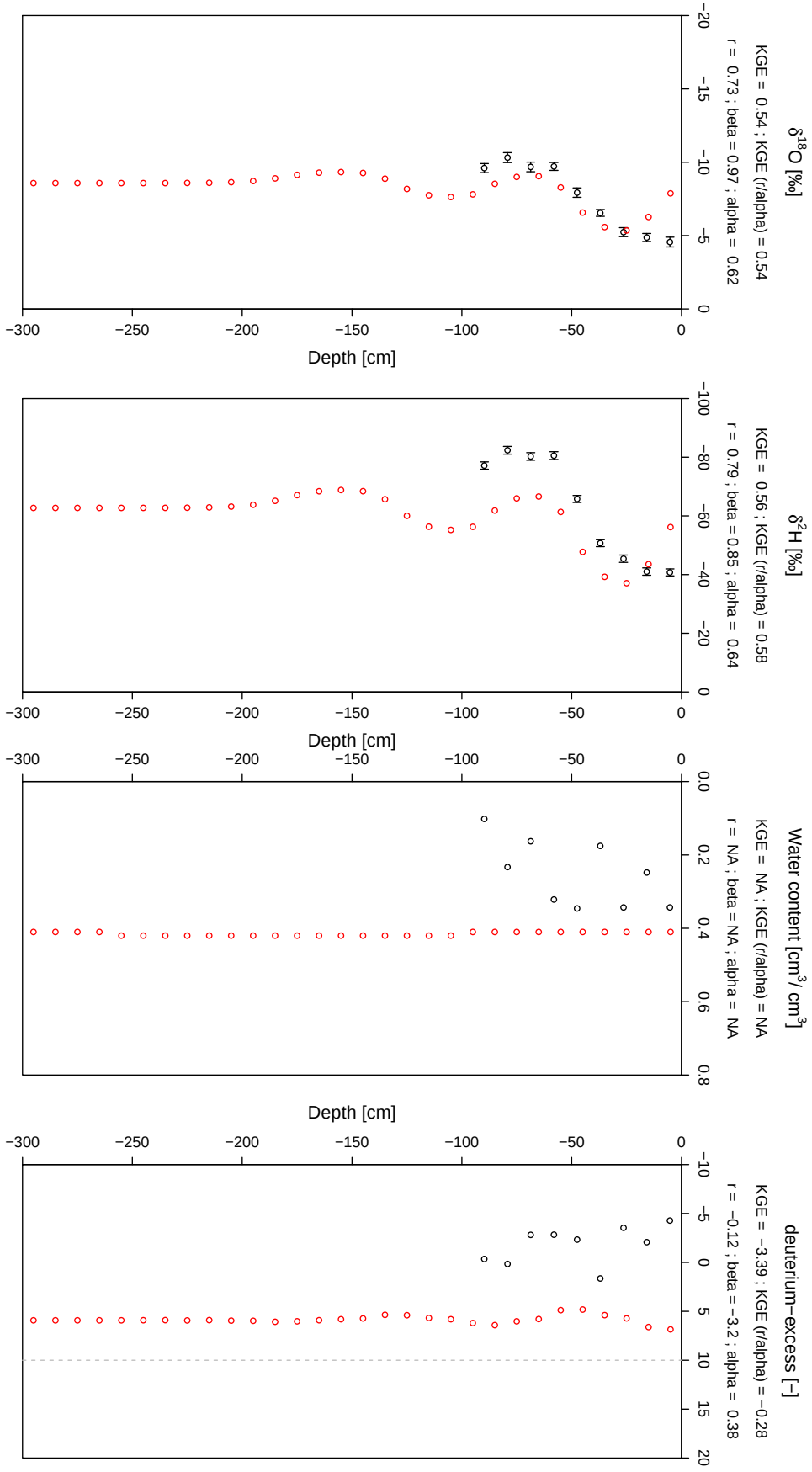

FIGURE C.17: Depth profile of observed (black) and modeled (red) $\delta^{18}O$, $\delta^{2}H$, volumetric water content and deuterium-excess values from best fit run of model step IV for profile 1 sampled in autumn 2014 in Buggingen.

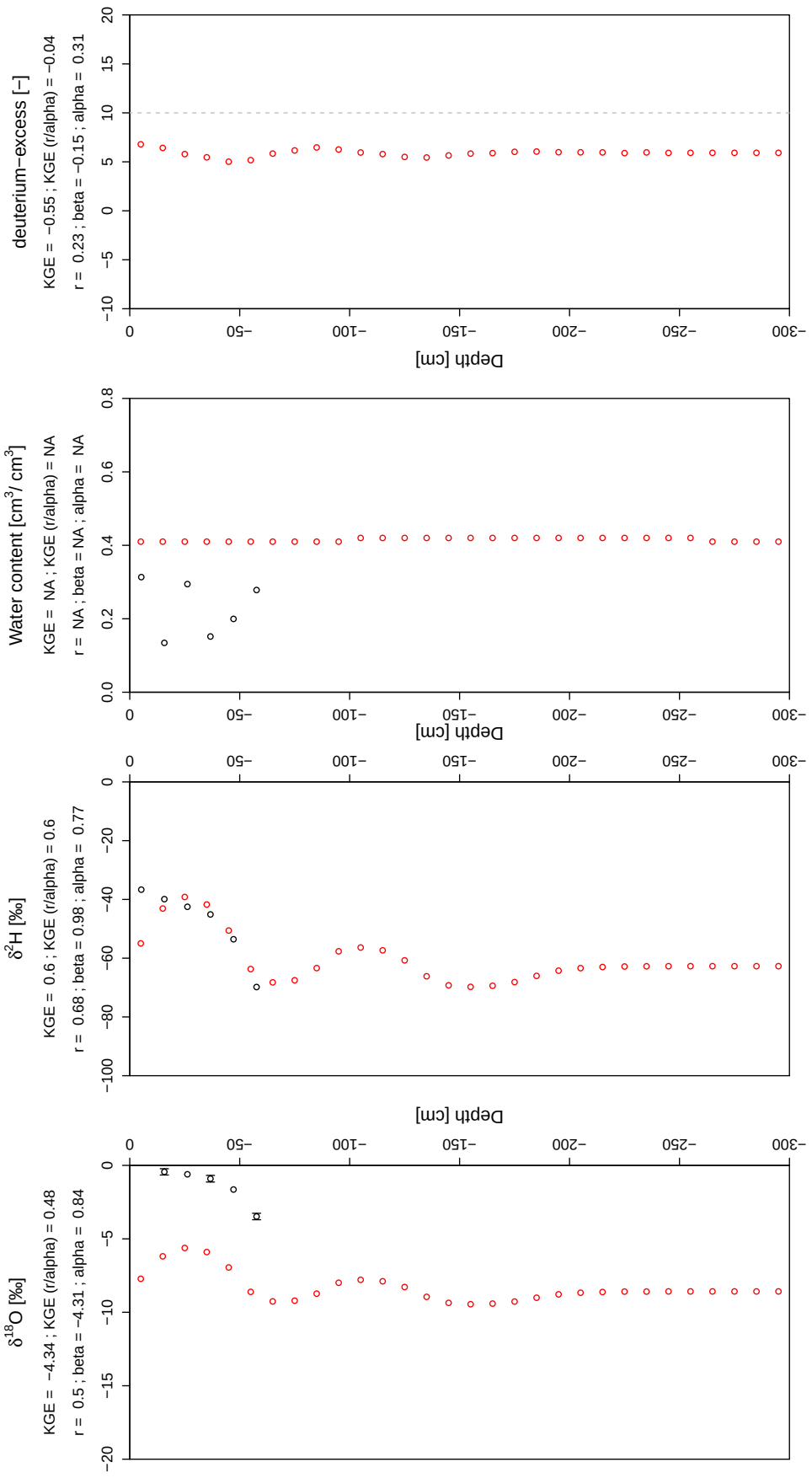

FIGURE C.18: Depth profile of observed (black) and modeled (red) $\delta^{18}O$, $\delta^{2}H$, volumetric water content and deuterium-excess values from best fit run of model step IV for profile 2 sampled in autumn 2014 in Buggingen.

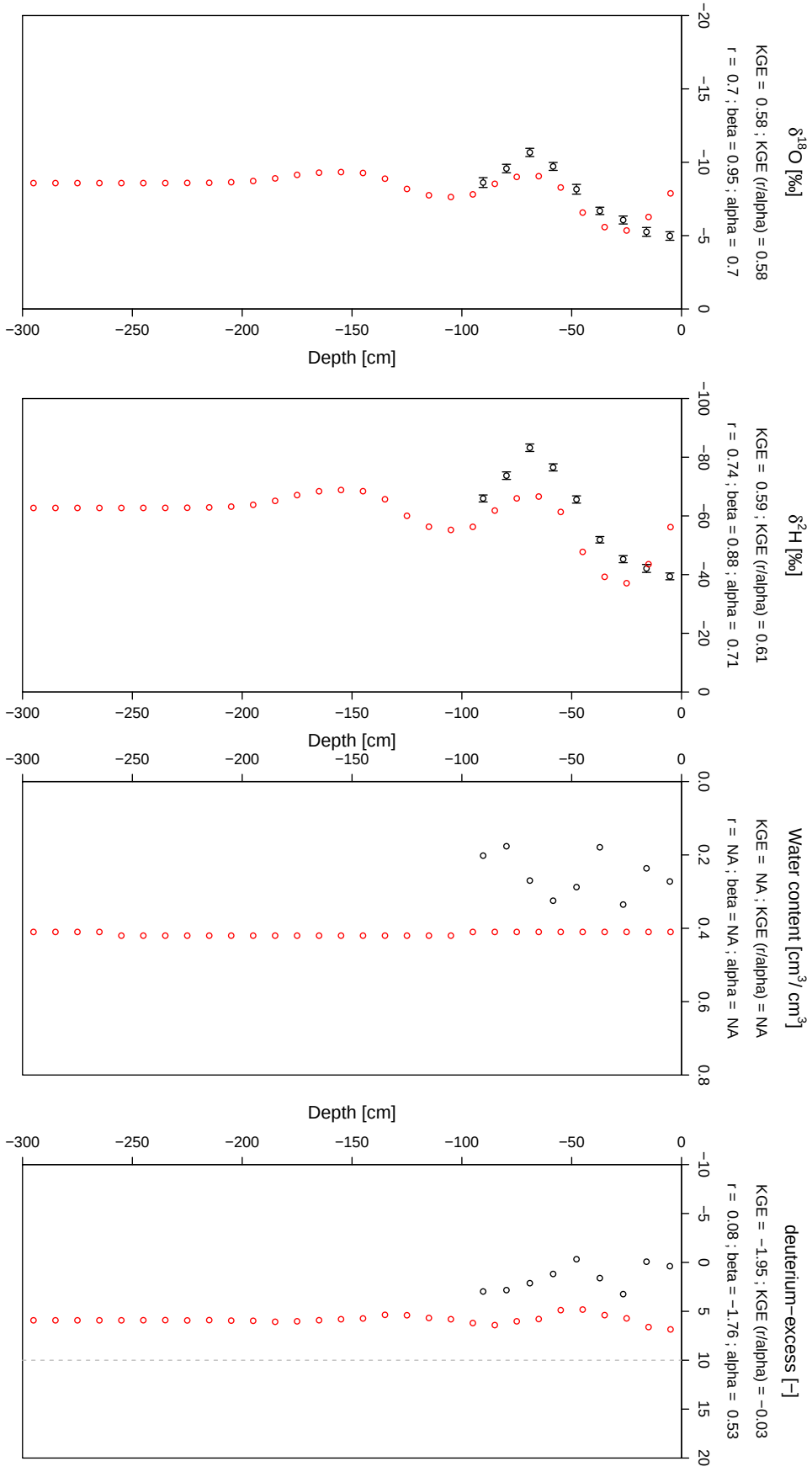

FIGURE C.19: Depth profile of observed (black) and modeled (red) $\delta^{18}O$, $\delta^{2}H$, volumetric water content and deuterium-excess values from best fit run of model step IV for profile 3 sampled in autumn 2014 in Buggingen.

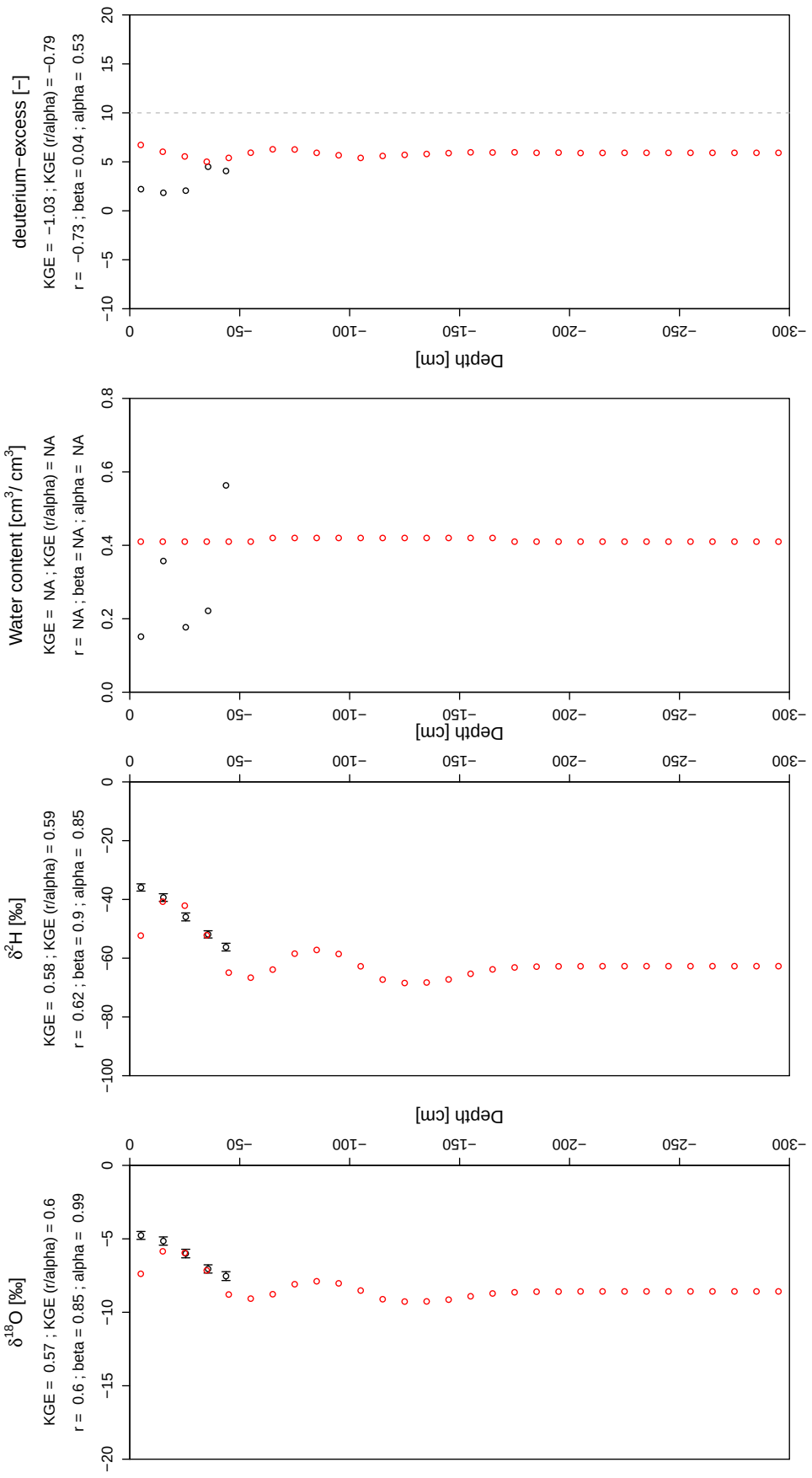

FIGURE C.20: Depth profile of observed (black) and modeled (red) $\delta^{18}O$, $\delta^{2}H$, volumetric water content and deuterium-excess values from best fit run of model step IV for profile 4 sampled in autumn 2014 in Buggingen.

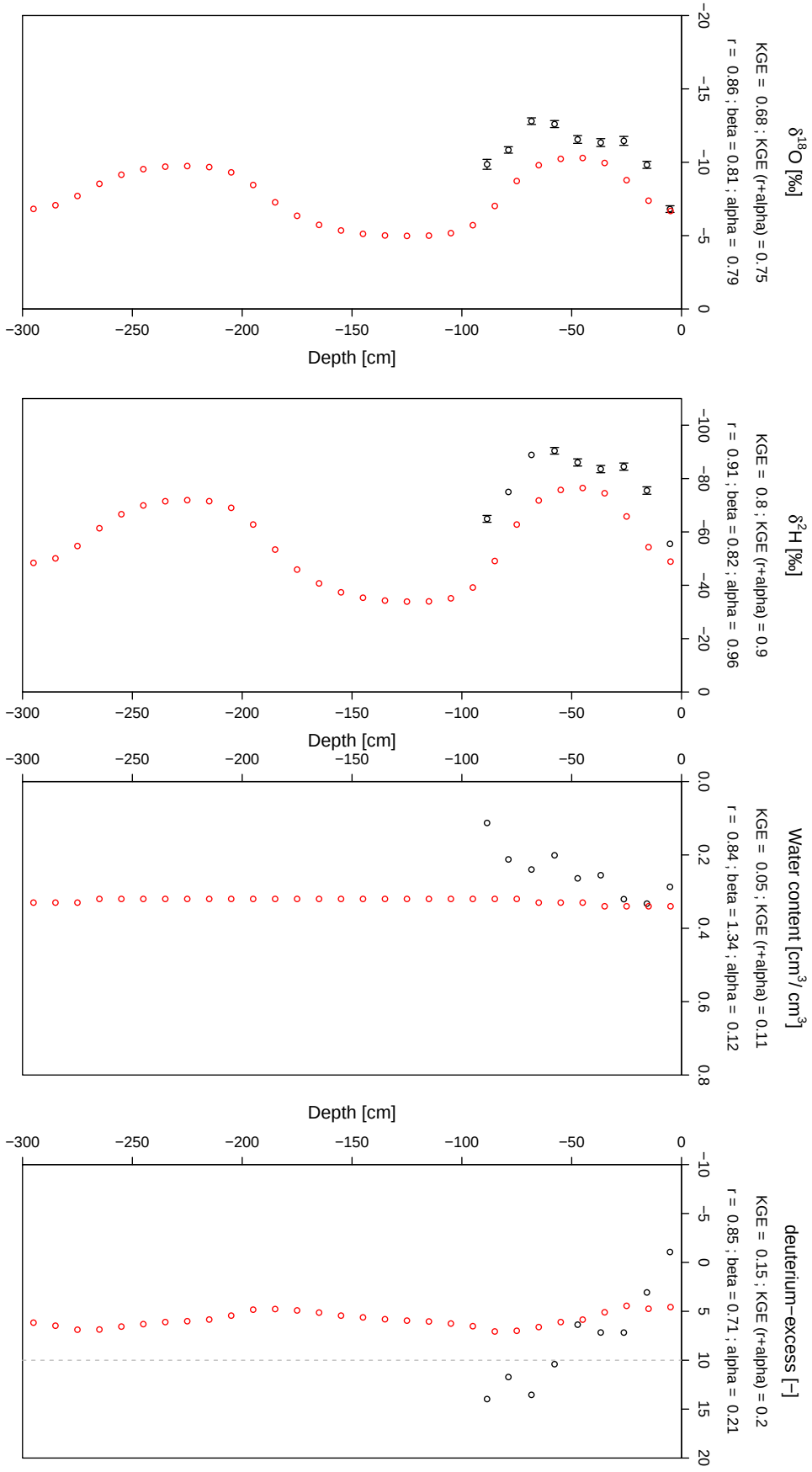

FIGURE C.21: Depth profile of observed (black) and modeled (red) $\delta^{18}O$, $\delta^{2}H$, volumetric water content and deuterium-excess values from best fit run of model step IV for profile 1 sampled in spring 2015 in Buggingen.

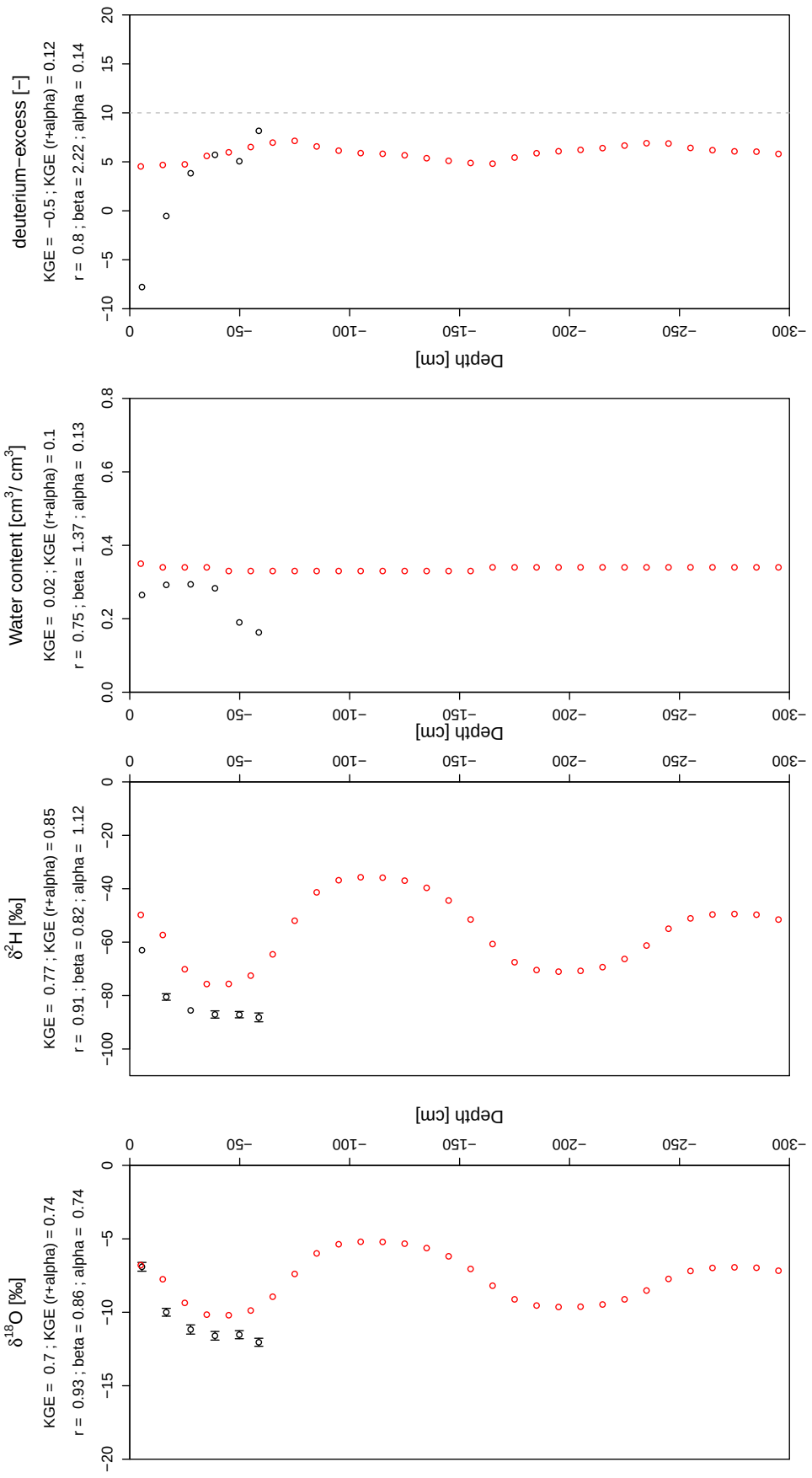

FIGURE C.22: Depth profile of observed (black) and modeled (red) $\delta^{18}O$, $\delta^{2}H$, volumetric water content and deuterium-excess values from best fit run of model step IV for profile 2 sampled in spring 2015 in Buggingen.

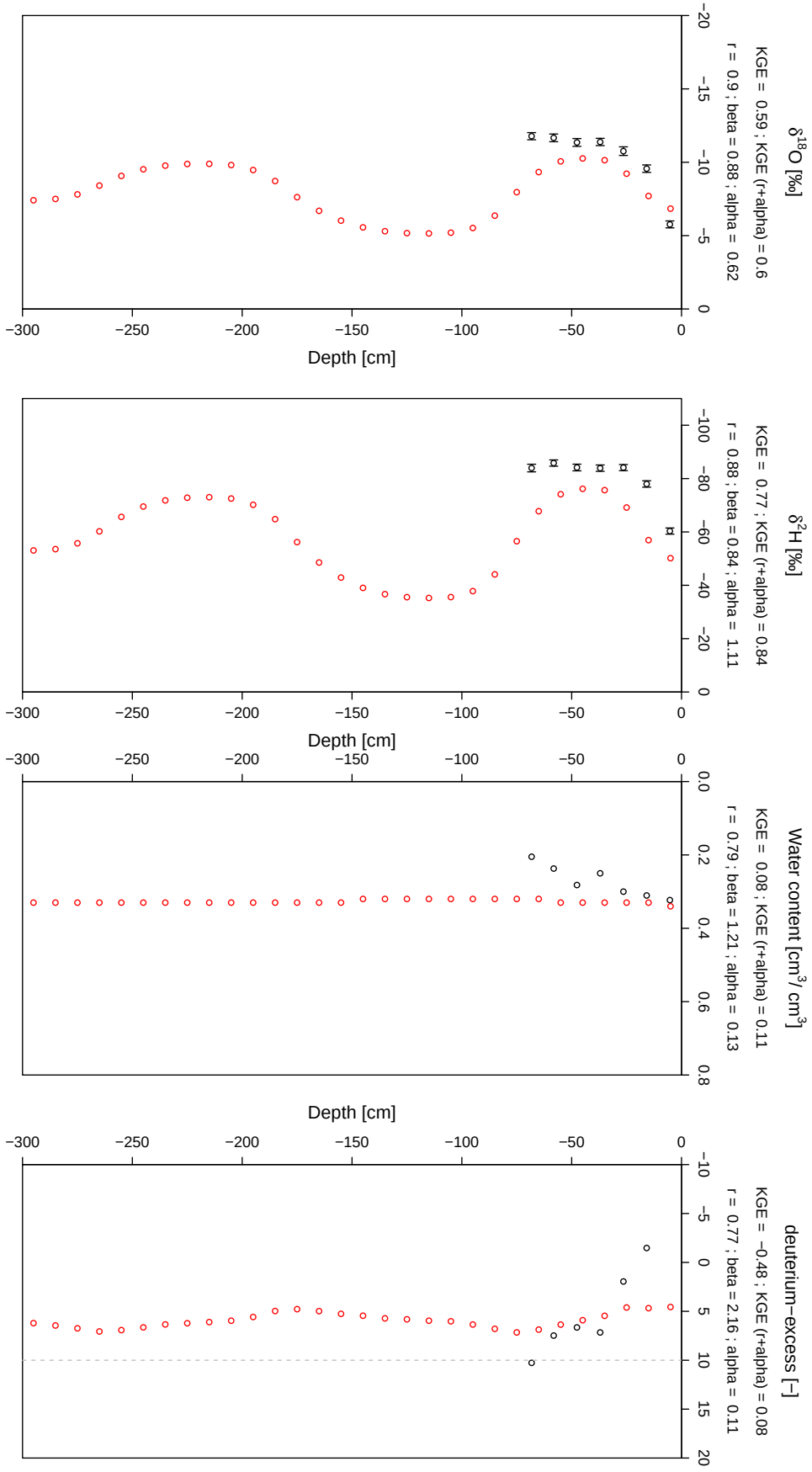

FIGURE C.23: Depth profile of observed (black) and modeled (red) $\delta^{18}O$, $\delta^{2}H$, volumetric water content and deuterium-excess values from best fit run of model step IV for profile 2 sampled in spring 2015 in Buggingen.

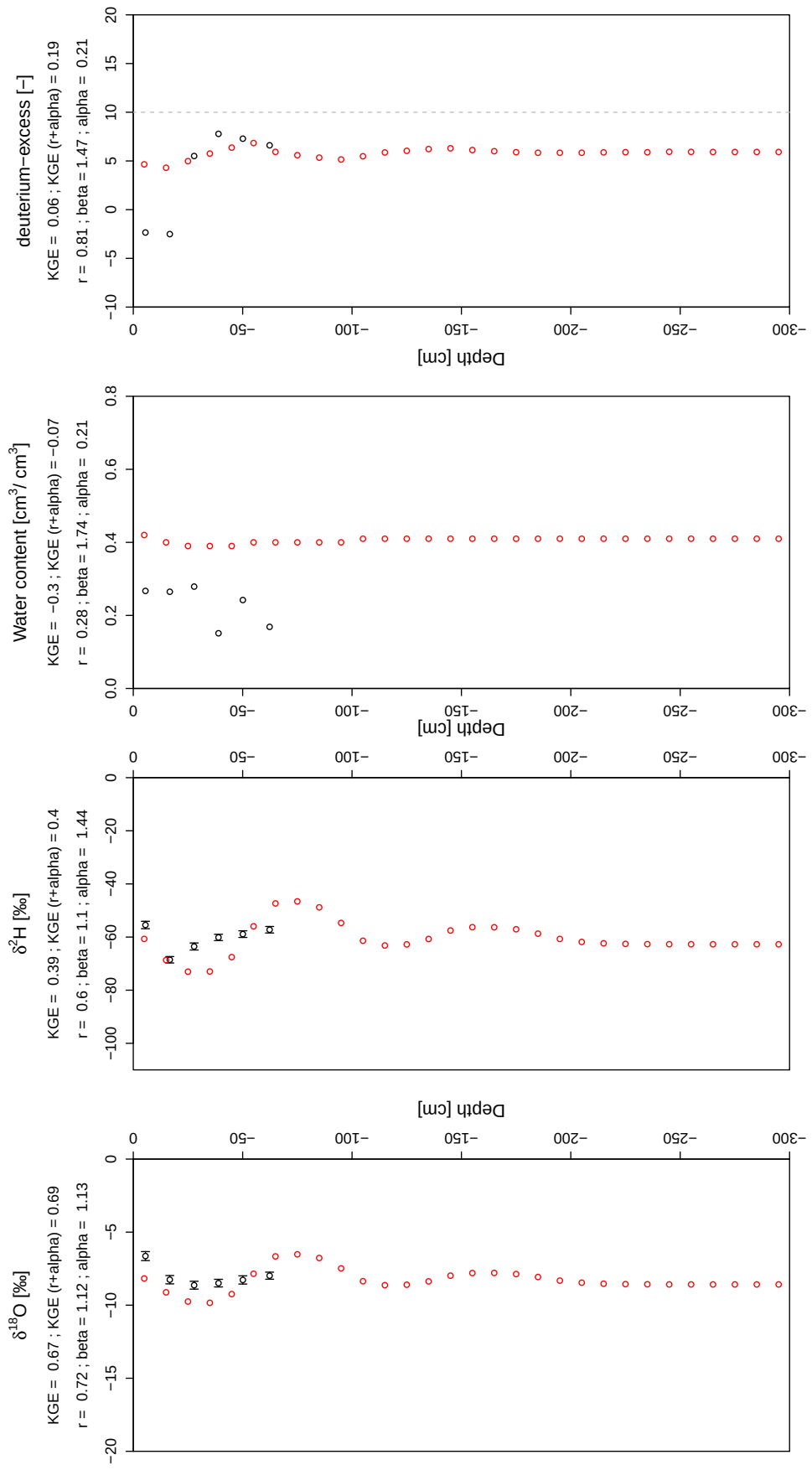

FIGURE C.24: Depth profile of observed (black) and modeled (red) $\delta^{18}O$, $\delta^{2}H$, volumetric water content and deuterium-excess values from best fit run of model step IV for profile 4 sampled in spring 2015 in Buggingen.

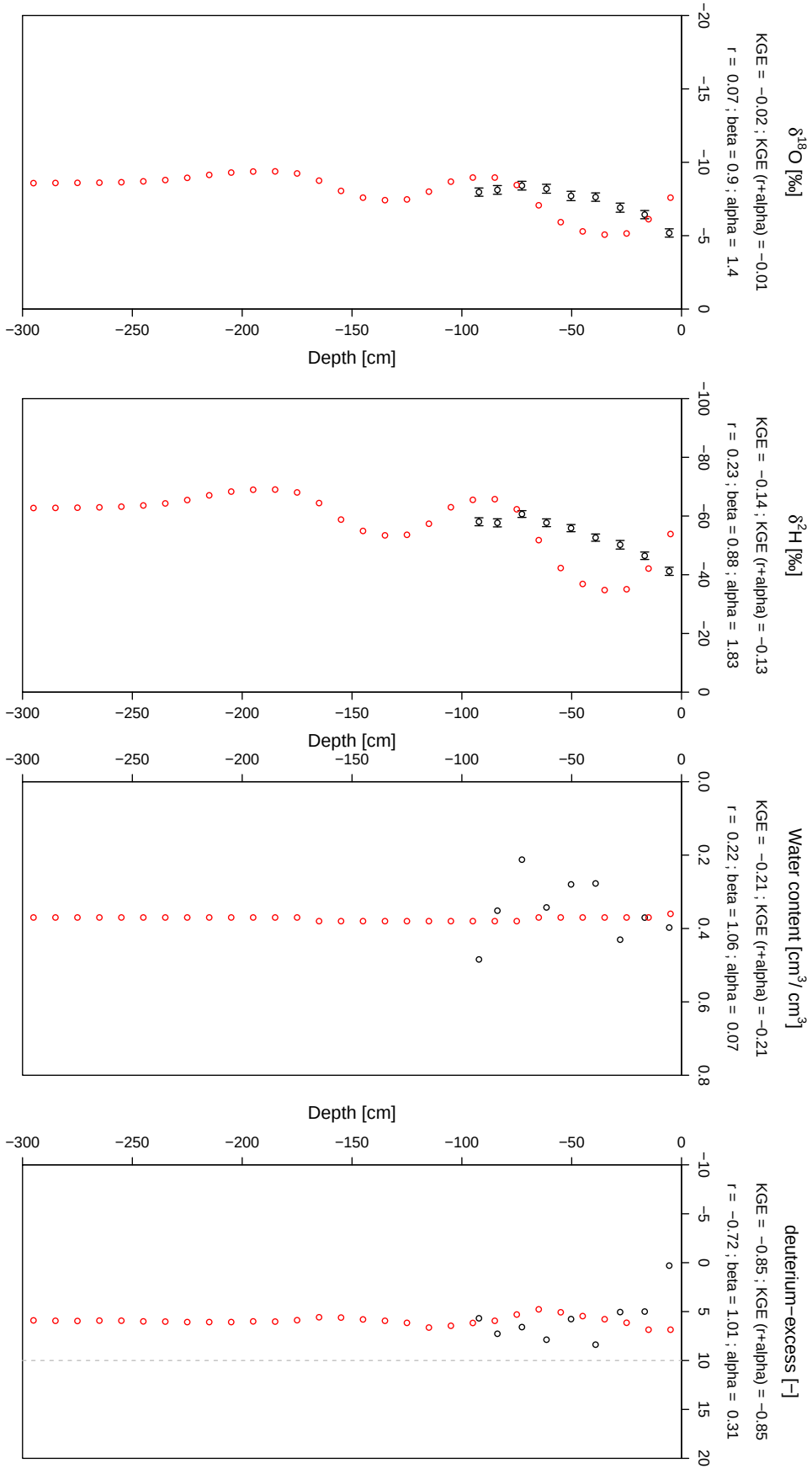

FIGURE C.25: Depth profile of observed (black) and modeled (red) $\delta^{18}O$, $\delta^{2}H$, volumetric water content and deuterium-excess values from best fit run of model step IV for profile 1 sampled in autumn 2014 in Laufen.

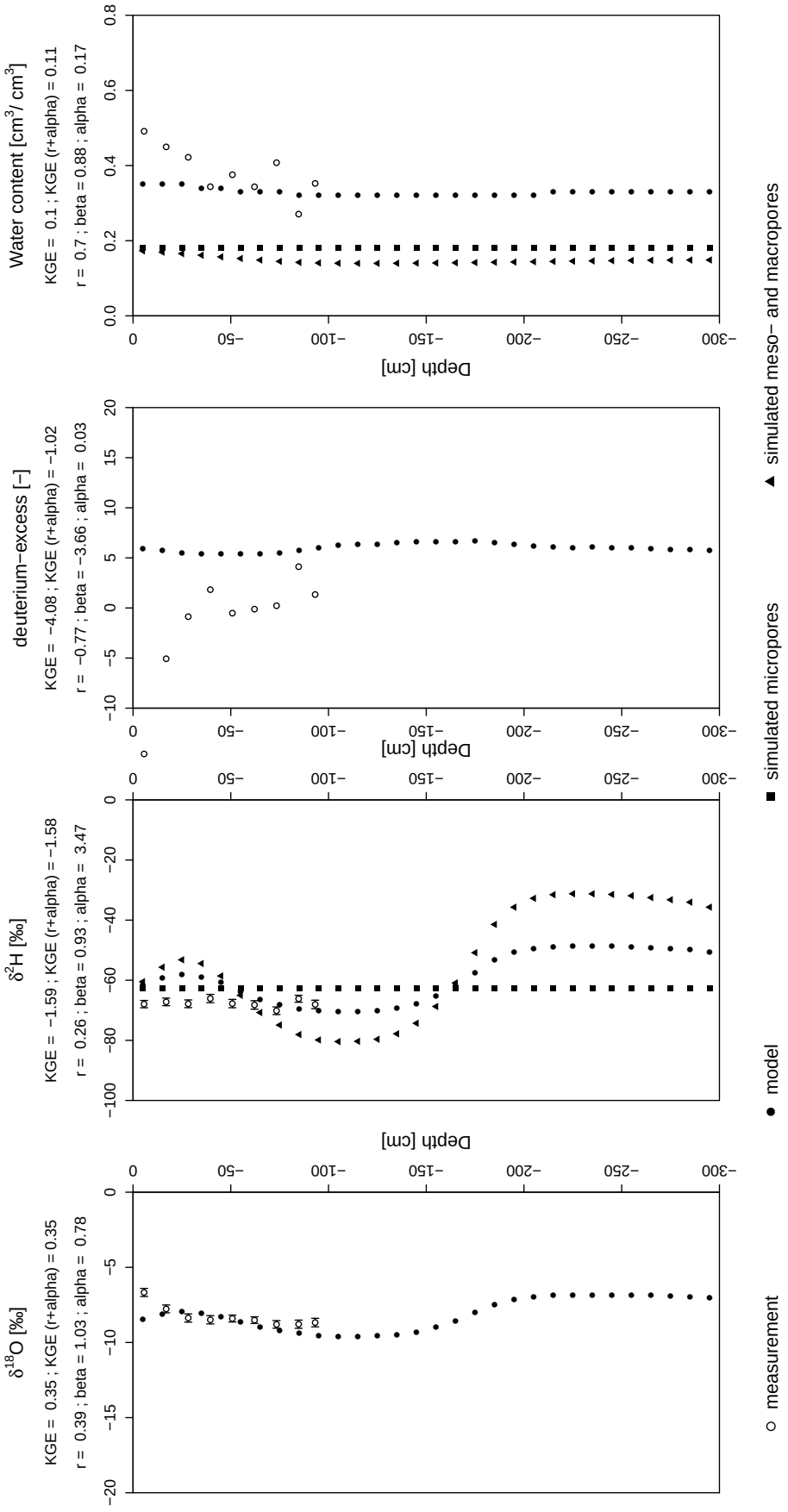

FIGURE C.26: Depth profile of observed and modeled $\delta^{18}O$, $\delta^{2}H$, volumetric water content and deuterium-excess values from best fit run of model step V for profile 1 sampled in 2015 in Laufen. Within model V water flow is calculated separately in micro-, meso- and macropores. Black model graph shows isotope signature resulting from a combination of both pore spaces; moreover, KGE is calculated from these simulations. For oxygen-18 the output of SWIS is only a combination of pore spaces.

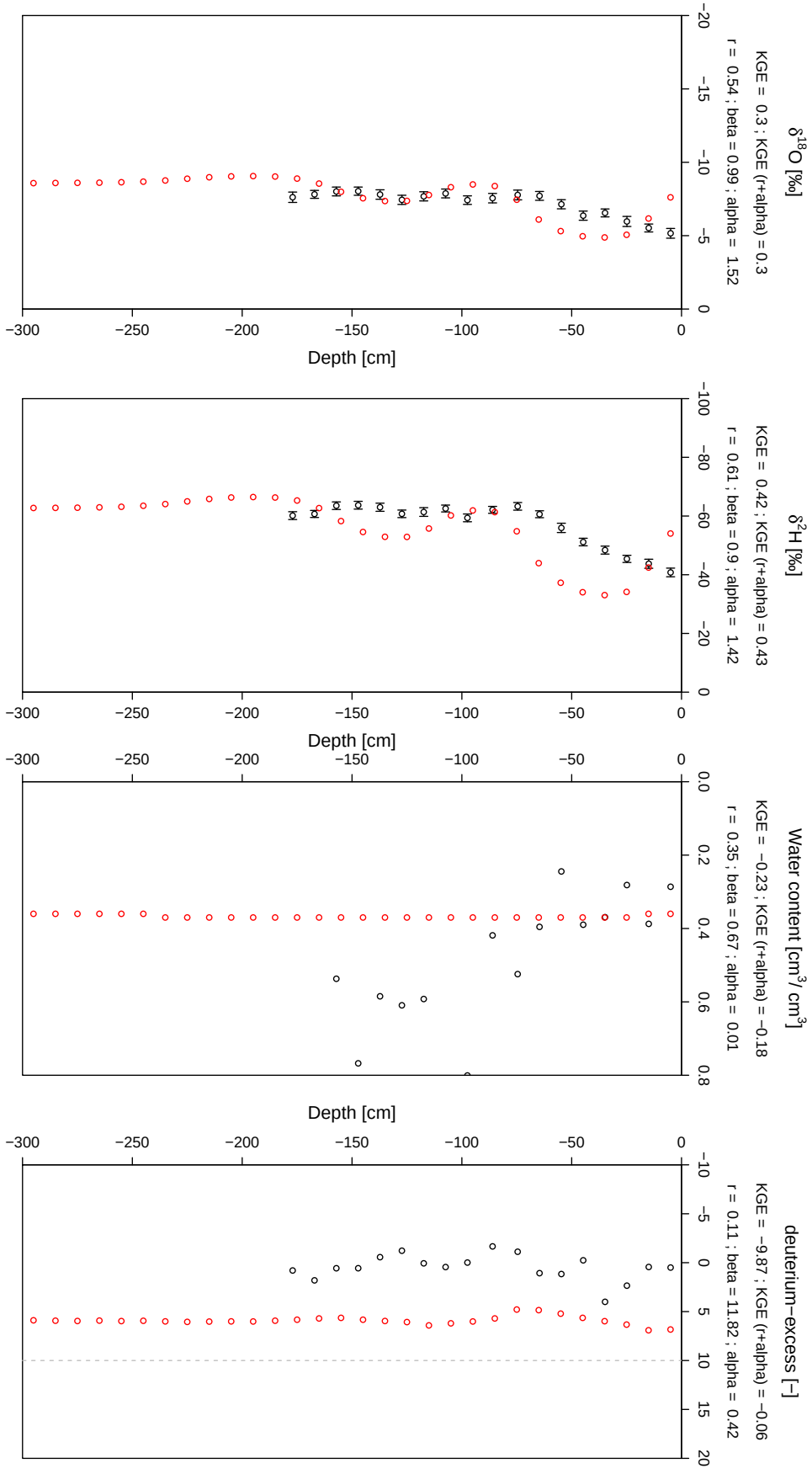

FIGURE C.27: Depth profile of observed (black) and modeled (red) $\delta^{18}O$, $\delta^{2}H$, volumetric water content and deuterium-excess values from best fit run of model step IV for profile 2 sampled in autumn 2014 in Laufen.

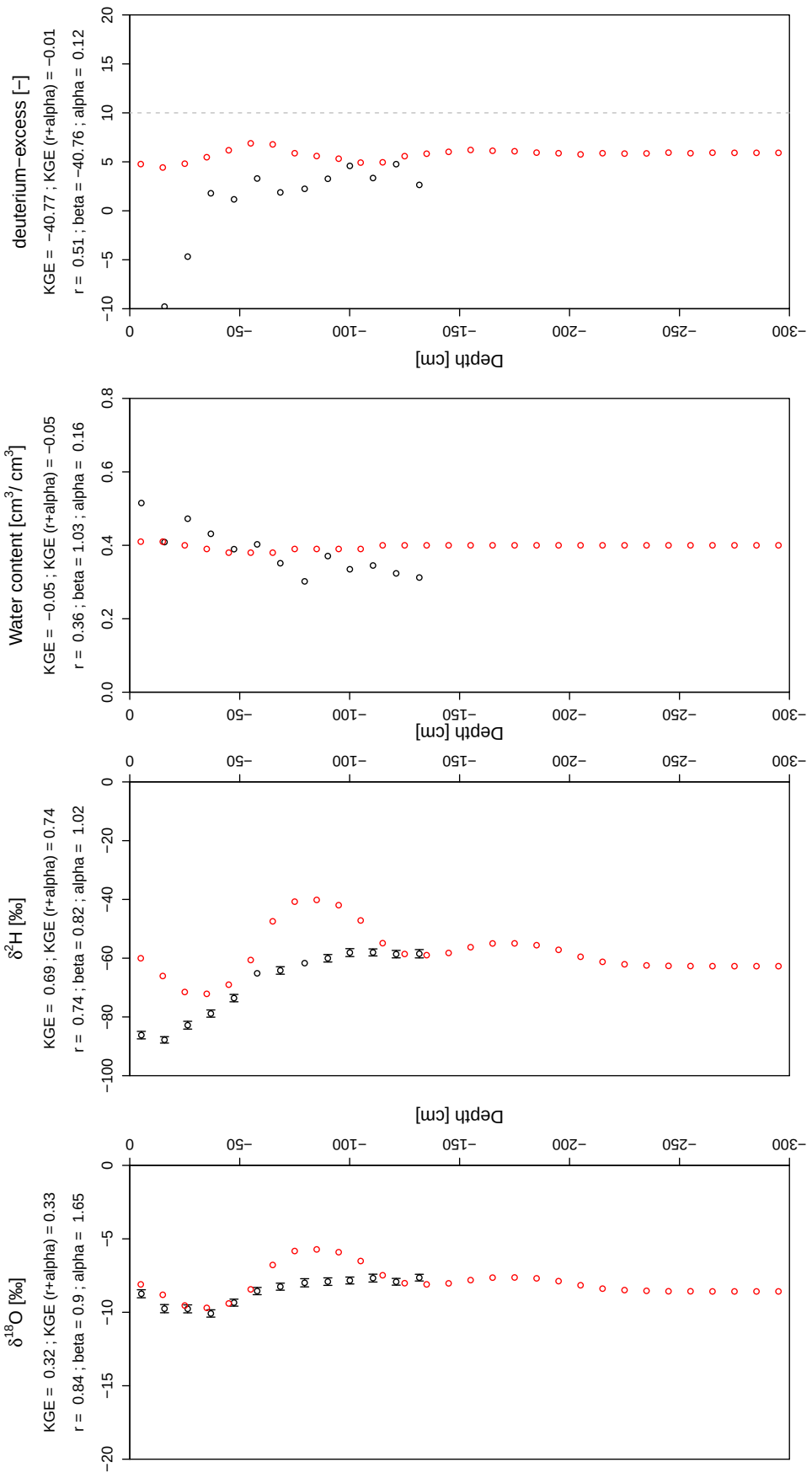

FIGURE C.28: Depth profile of observed (black) and modeled (red) $\delta^{18}O$, $\delta^{2}H$, volumetric water content and deuterium-excess values from best fit run of model step IV for profile 2 sampled in spring 2015 in Laufen.

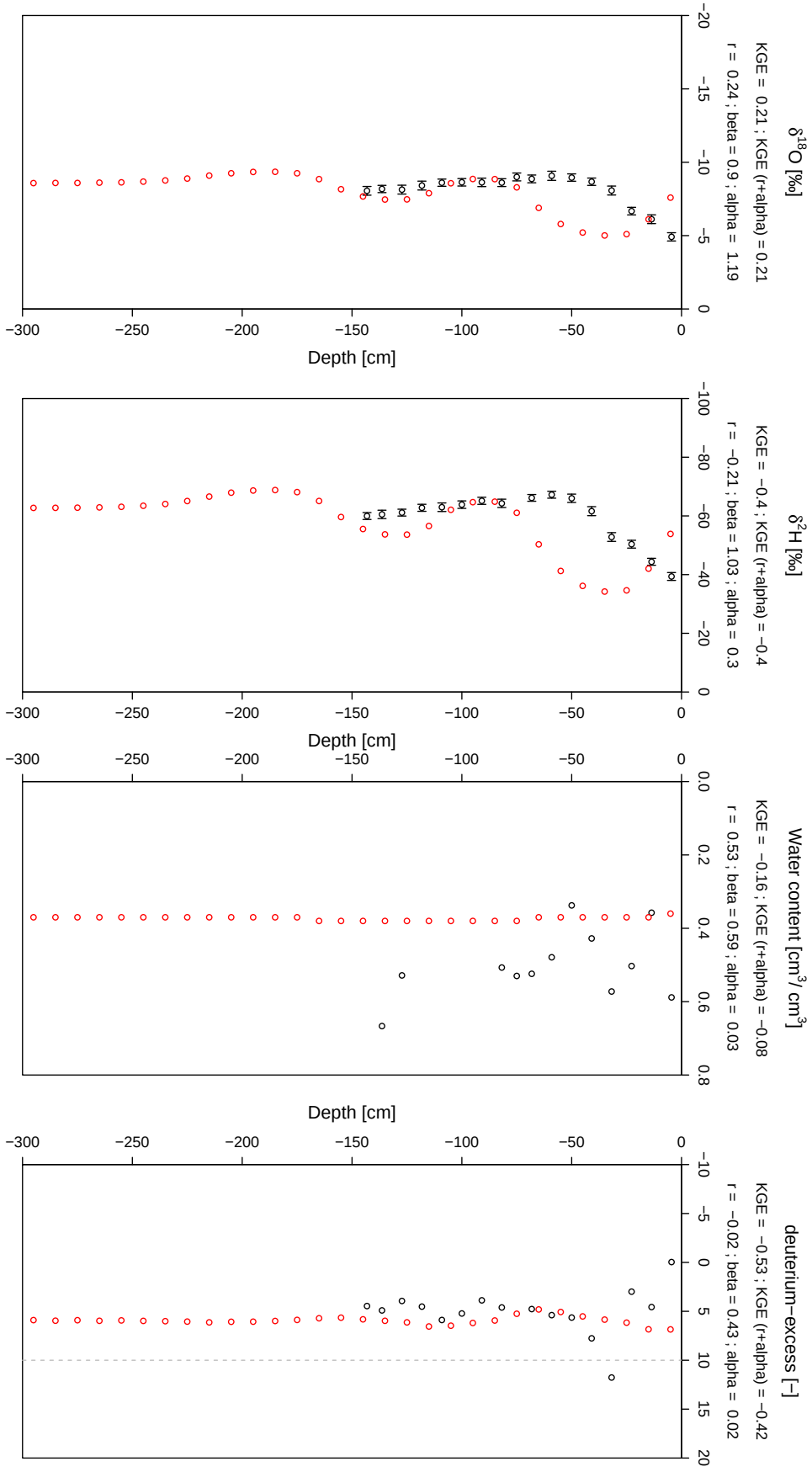

FIGURE C.29: Depth profile of observed (black) and modeled (red) $\delta^{18}O$, $\delta^{2}H$, volumetric water content and deuterium-excess values from best fit run of model step IV for profile 3 sampled in autumn 2014 in Laufen.

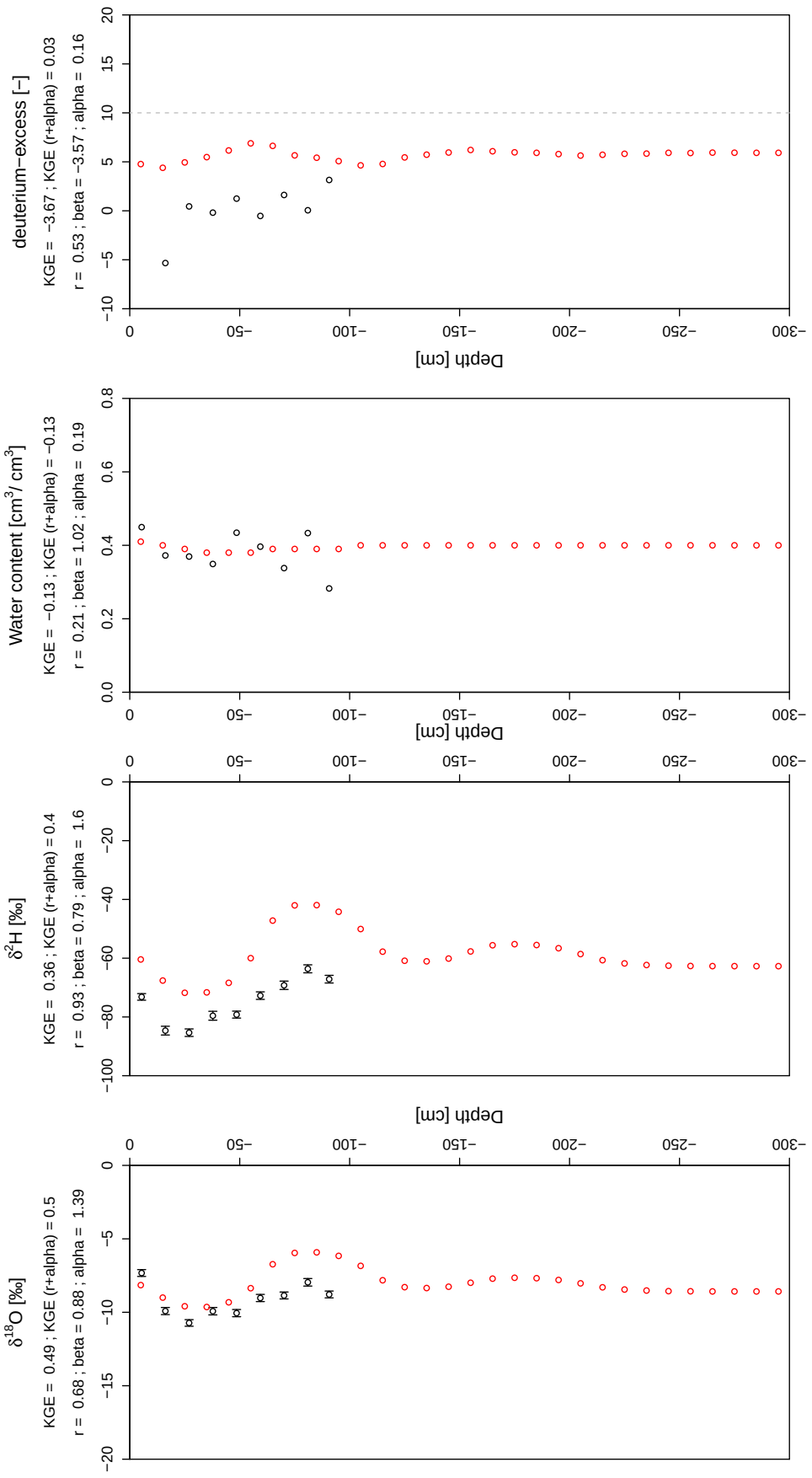

FIGURE C.30: Depth profile of observed (black) and modeled (red) $\delta^{18}O$, $\delta^{2}H$, volumetric water content and deuterium-excess values from best fit run of model step IV for profile 3 sampled in spring 2015 in Laufen.

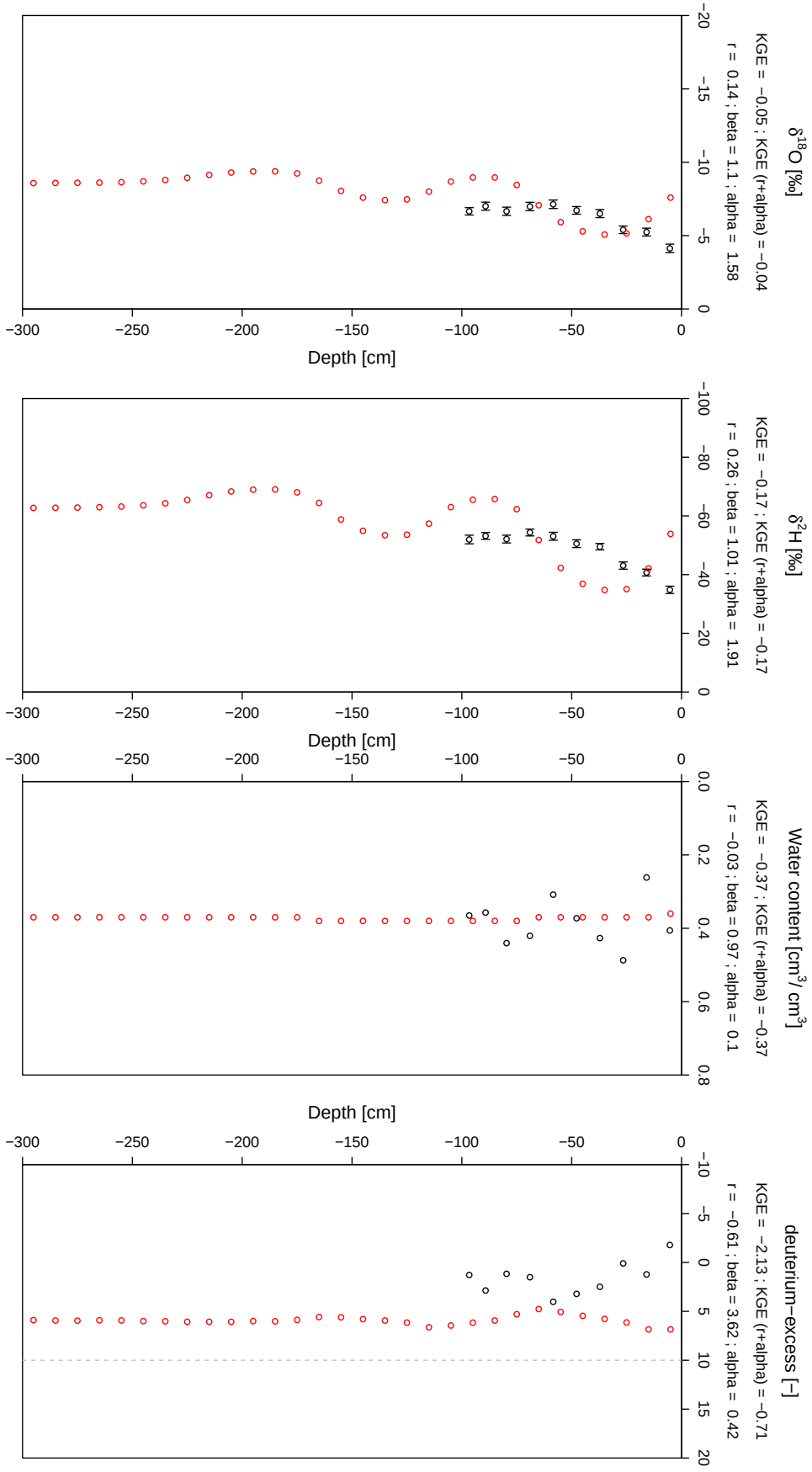

FIGURE C.31: Depth profile of observed (black) and modeled (red) $\delta^{18}O$, $\delta^{2}H$, volumetric water content and deuterium-excess values from best fit run of model step IV for profile 4 sampled in autumn 2014 in Laufen.

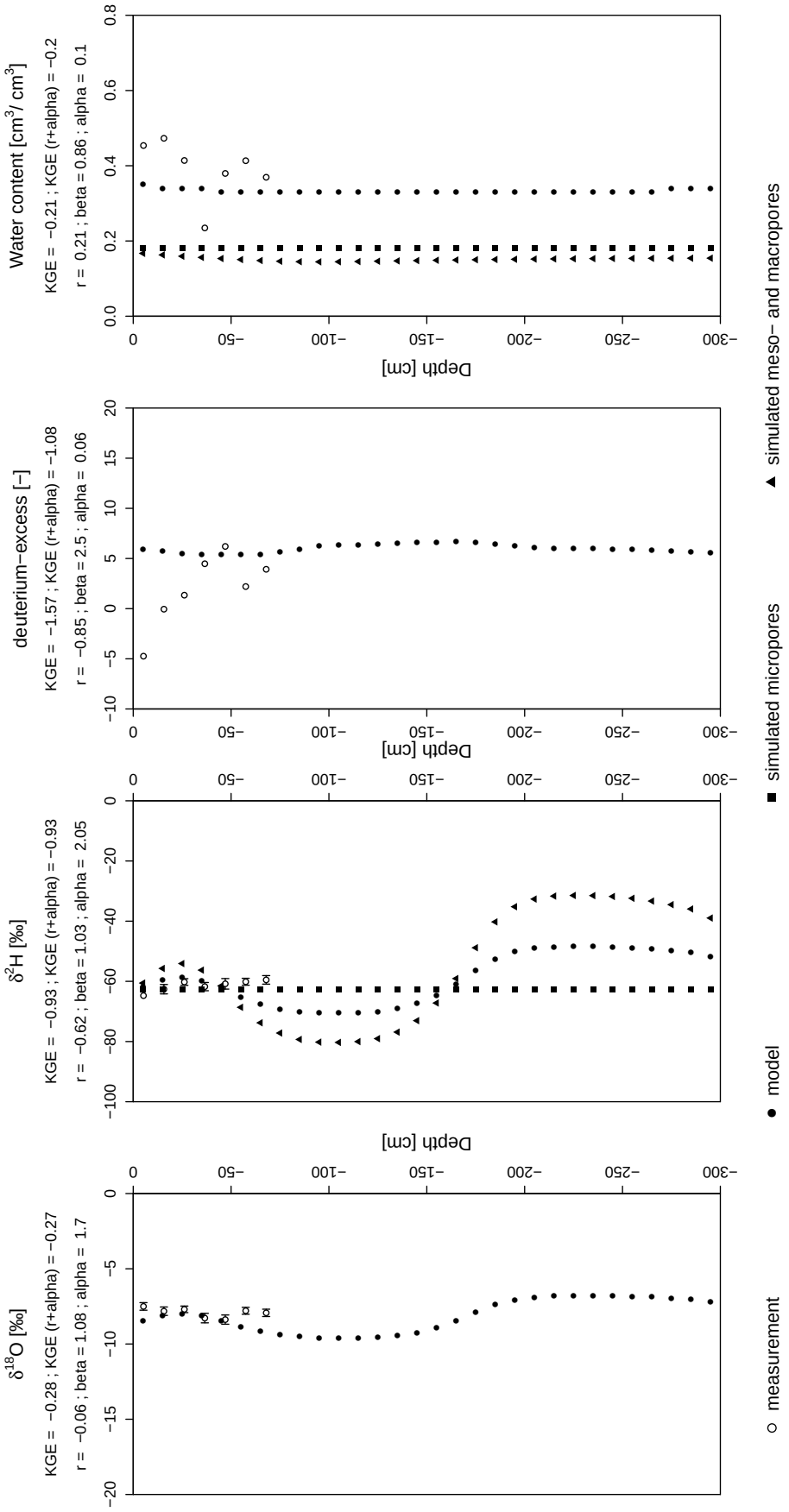

FIGURE C.32: Depth profile of observed and modeled $\delta^{18}O$, $\delta^{2}H$, volumetric water content and deuterium-excess values from best fit run of model step V for profile 4 sampled in 2015 in Laufen. Within model V water flow is calculated separately in micro-, meso- and macropores. Black model graph shows isotope signature resulting from a combination of both pore spaces; moreover, KGE is calculated from these simulations. For oxygen-18 the output of SWIS is only a combination of pore spaces.

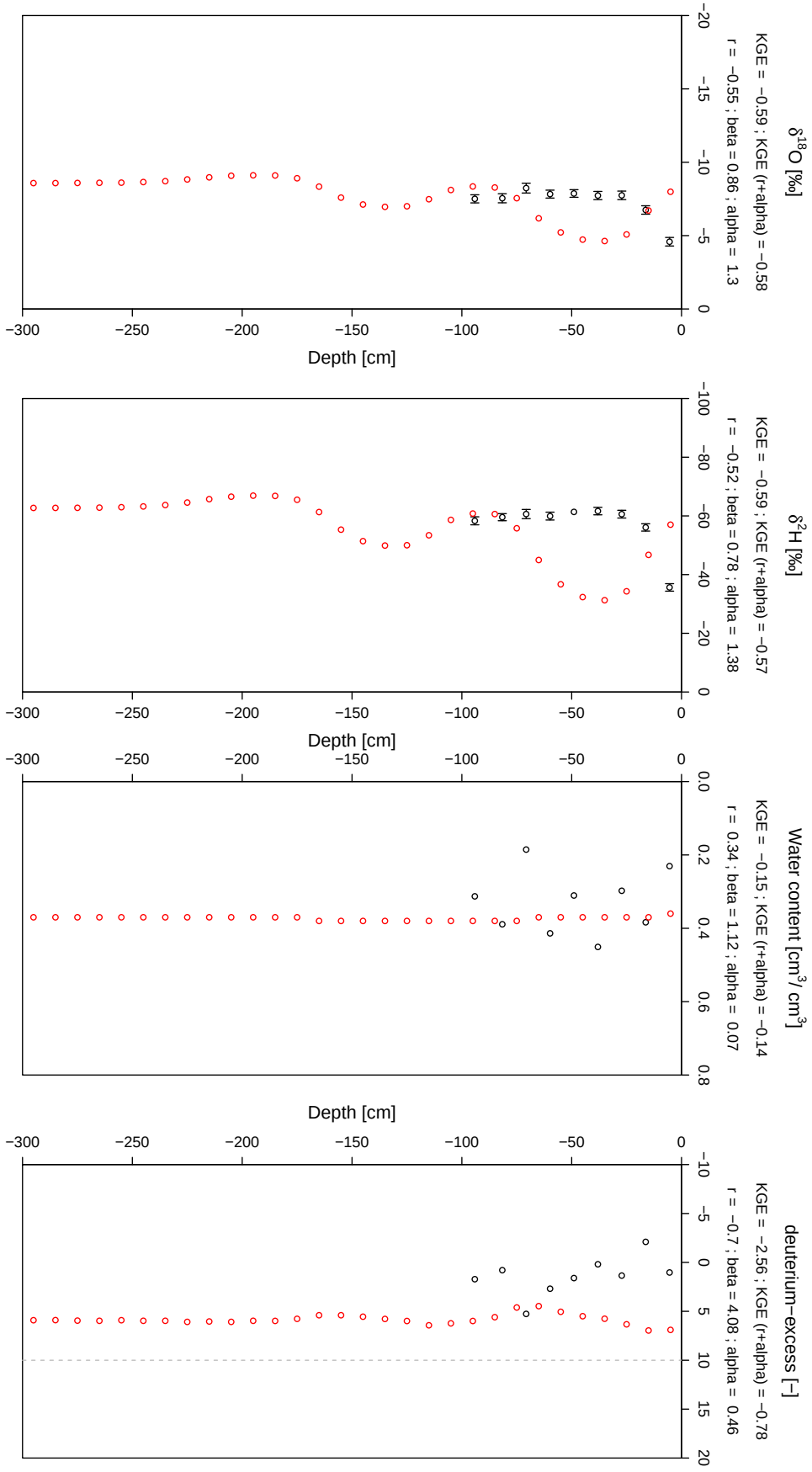

FIGURE C.33: Depth profile of observed (black) and modeled (red) $\delta^{18}O$, $\delta^{2}H$, volumetric water content and deuterium-excess values from best fit run of model step IV for profile 5 sampled in autumn 2014 in Laufen.

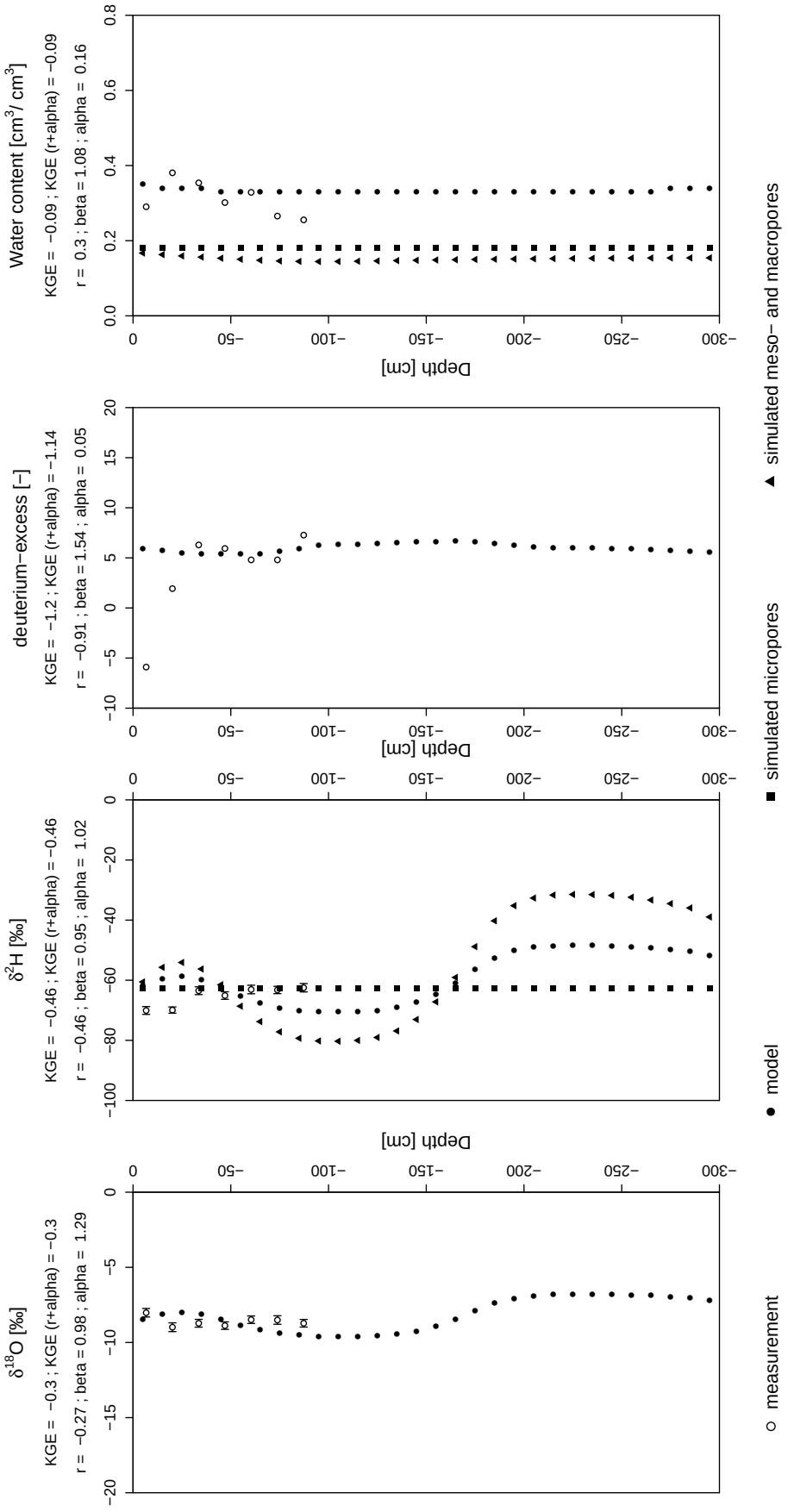

FIGURE C.34: Depth profile of observed and modeled $\delta^{18}O$, $\delta^{2}H$, volumetric water content and deuterium-excess values from best fit run of model step V for profile 5 sampled in 2015 in Laufen. Within model step V water flow is calculated separately in micro-, meso- and macropores. Black model graph shows isotope signature resulting from a combination of both pore spaces; moreover, KGE is calculated from these simulations. For oxygen-18 the output of SWIS is only a combination of pore spaces.

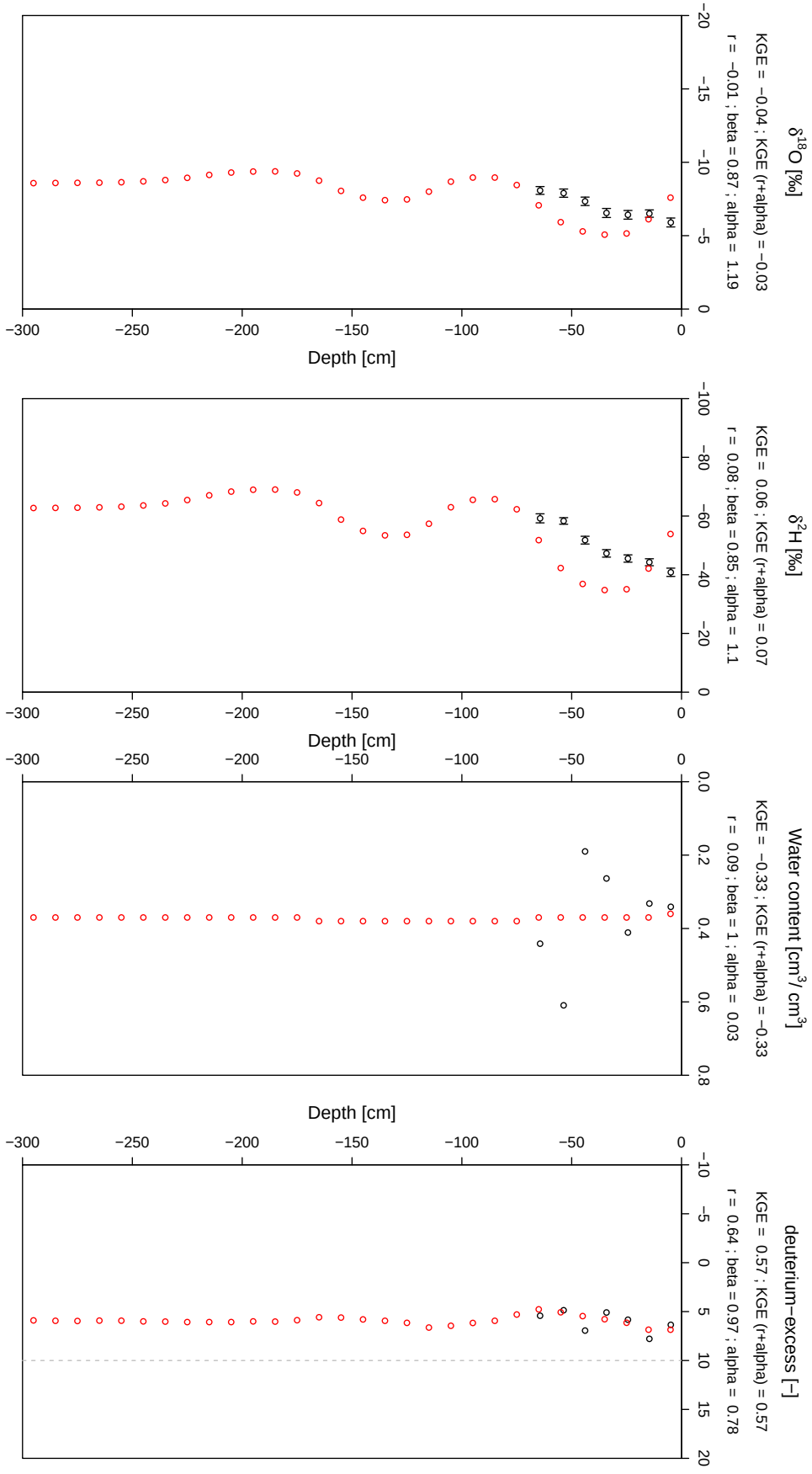

FIGURE C.35: Depth profile of observed (black) and modeled (red) $\delta^{18}O$, $\delta^{2}H$, volumetric water content and deuterium-excess values from best fit run of model step IV for profile 6 sampled in autumn 2014 in Laufen.

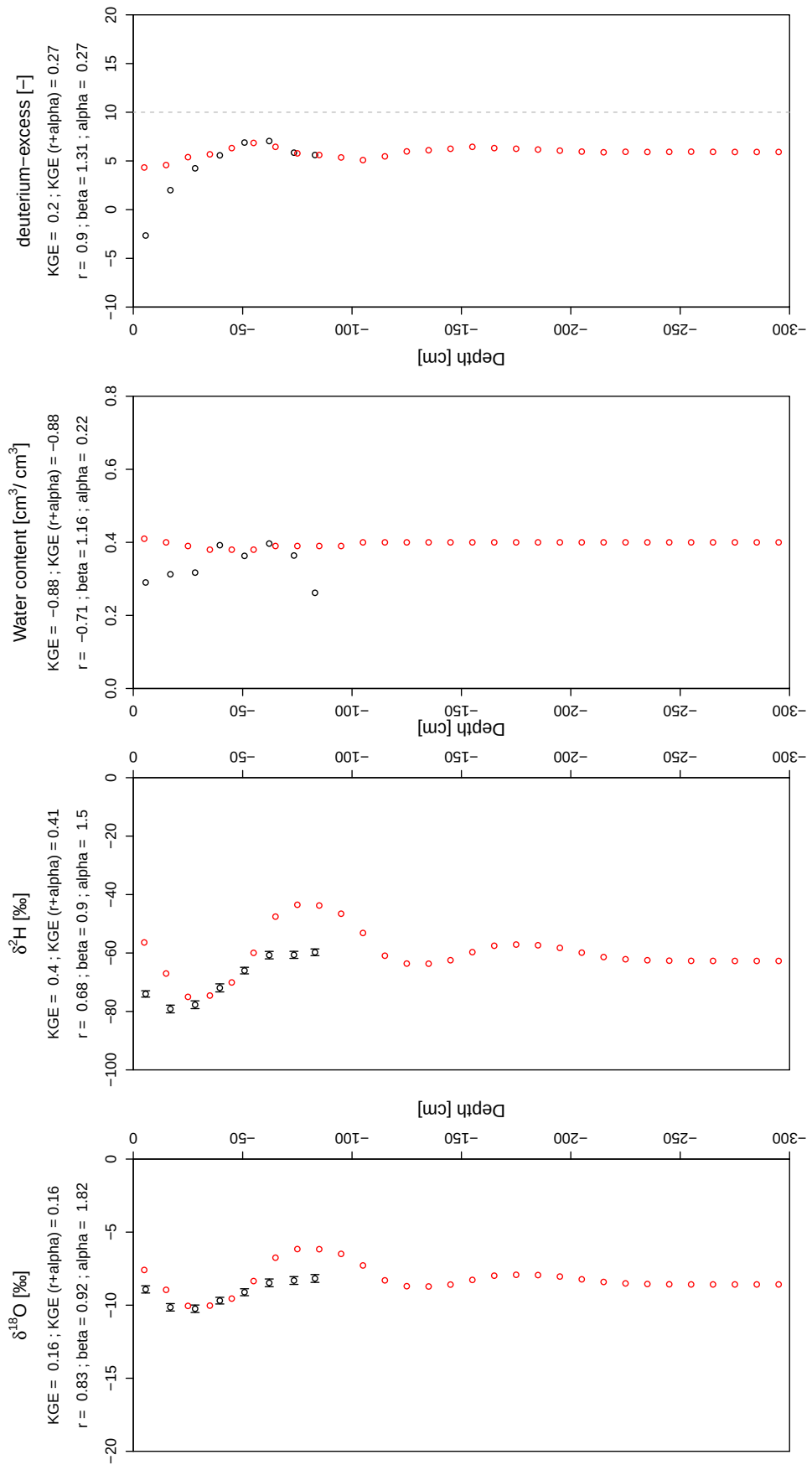

FIGURE C.36: Depth profile of observed (black) and modeled (red) $\delta^{18}O$, $\delta^{2}H$, volumetric water content and deuterium-excess values from best fit run of model step IV for profile 6 sampled in spring 2015 in Laufen.

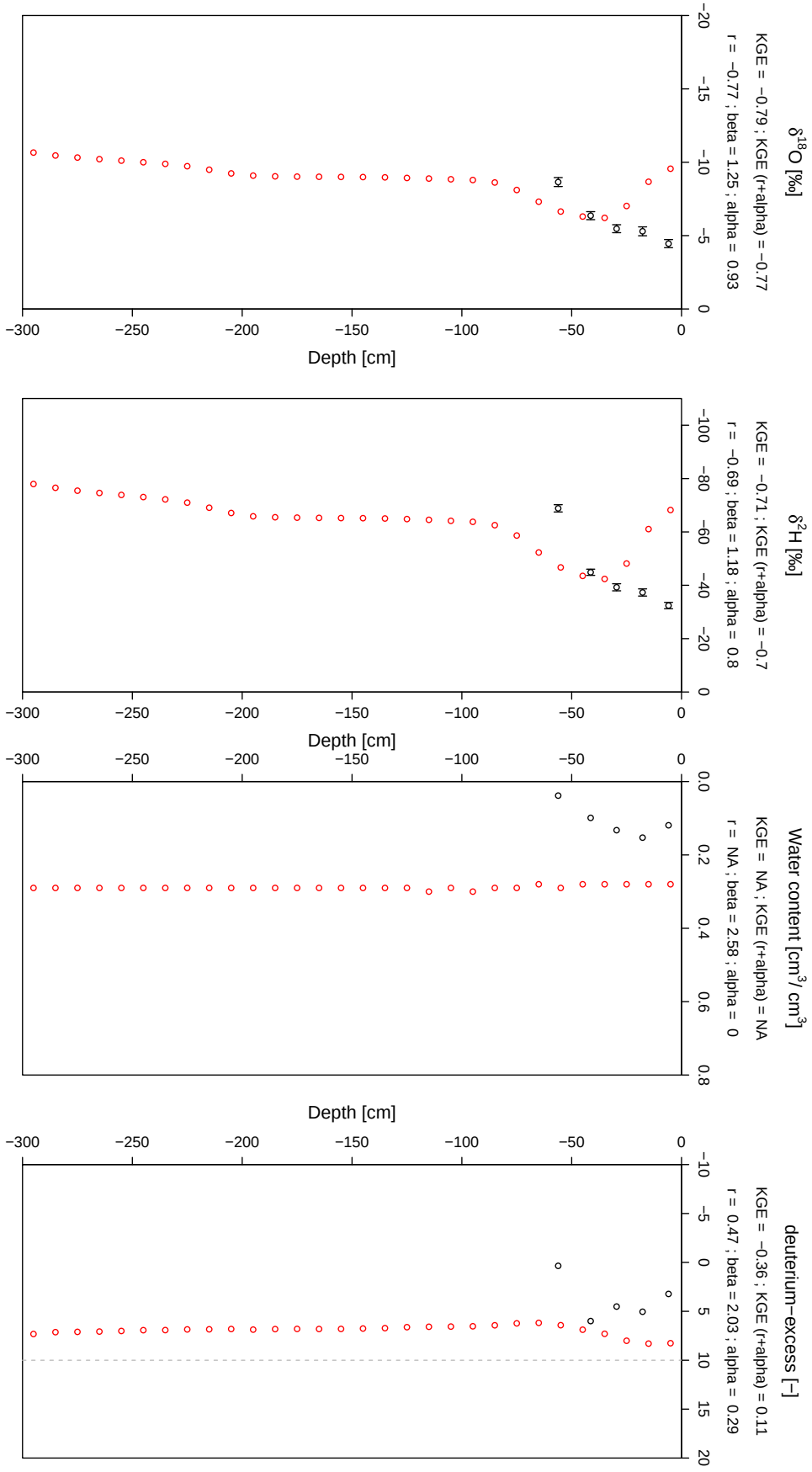

FIGURE C.37: Depth profile of observed (black) and modeled (red) $\delta^{18}O$, $\delta^{2}H$, volumetric water content and deuterium-excess values from best fit run of model step IV for profile 1 sampled in autumn 2015 in Welschingen.

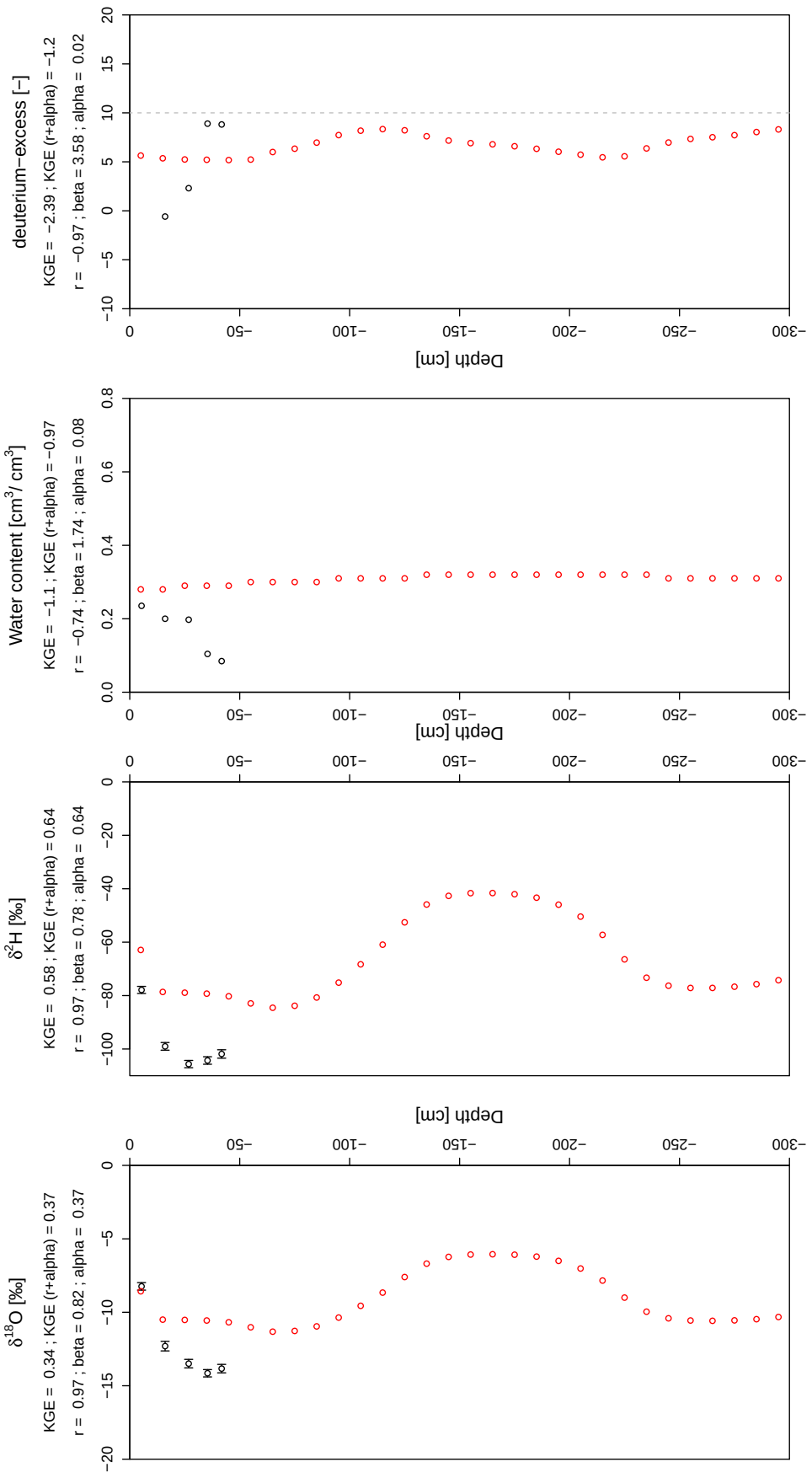

FIGURE C.38: Depth profile of observed (black) and modeled (red) $\delta^{18}O$, $\delta^{2}H$, volumetric water content and deuterium-excess values from best fit run of model step III for profile 1 sampled in spring 2015 in Welschingen.

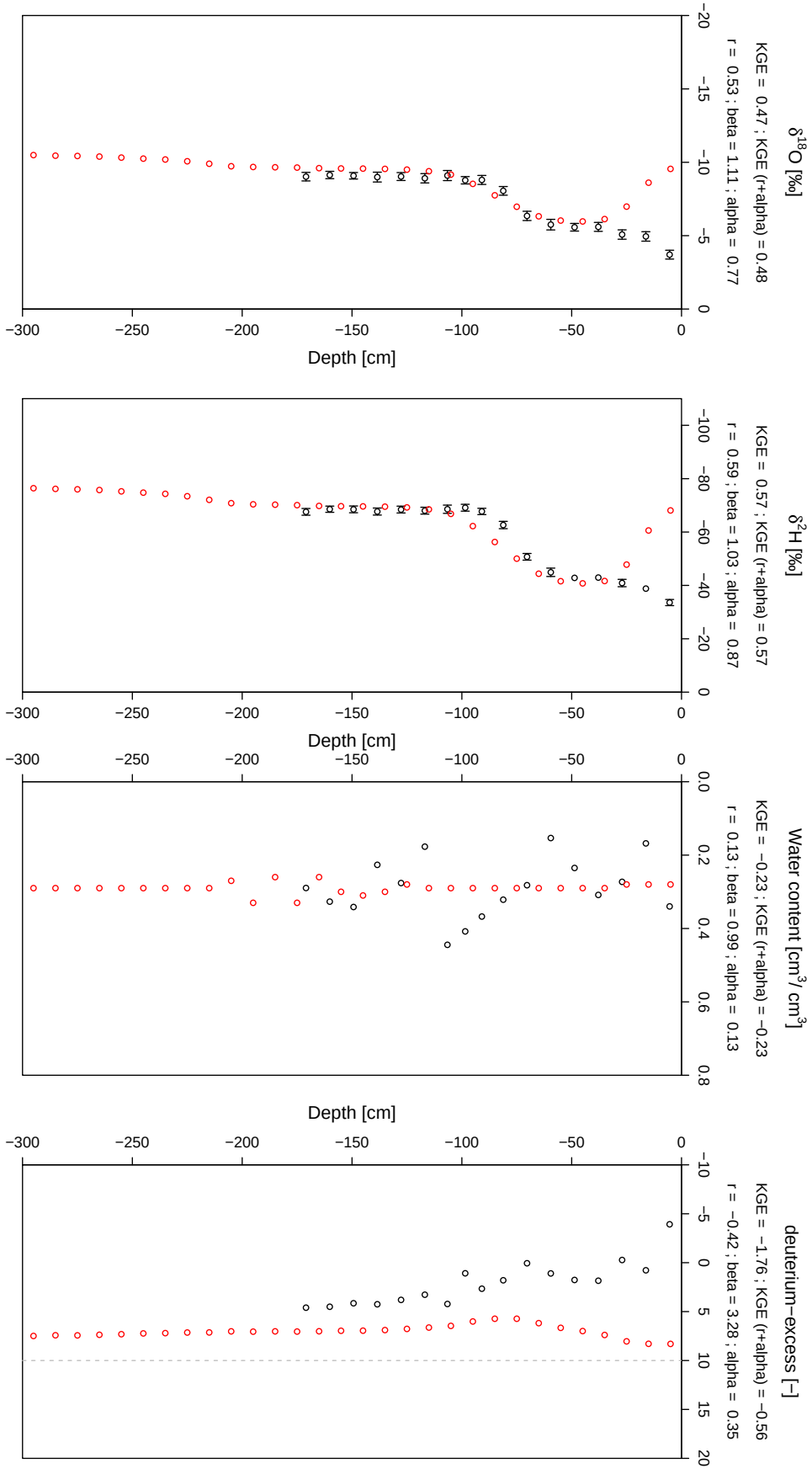

FIGURE C.39: Depth profile of observed (black) and modeled (red) $\delta^{18}O$, $\delta^{2}H$, volumetric water content and deuterium-excess values from best fit run of model step IV for profile 2 sampled in autumn 2014 in Welschingen.

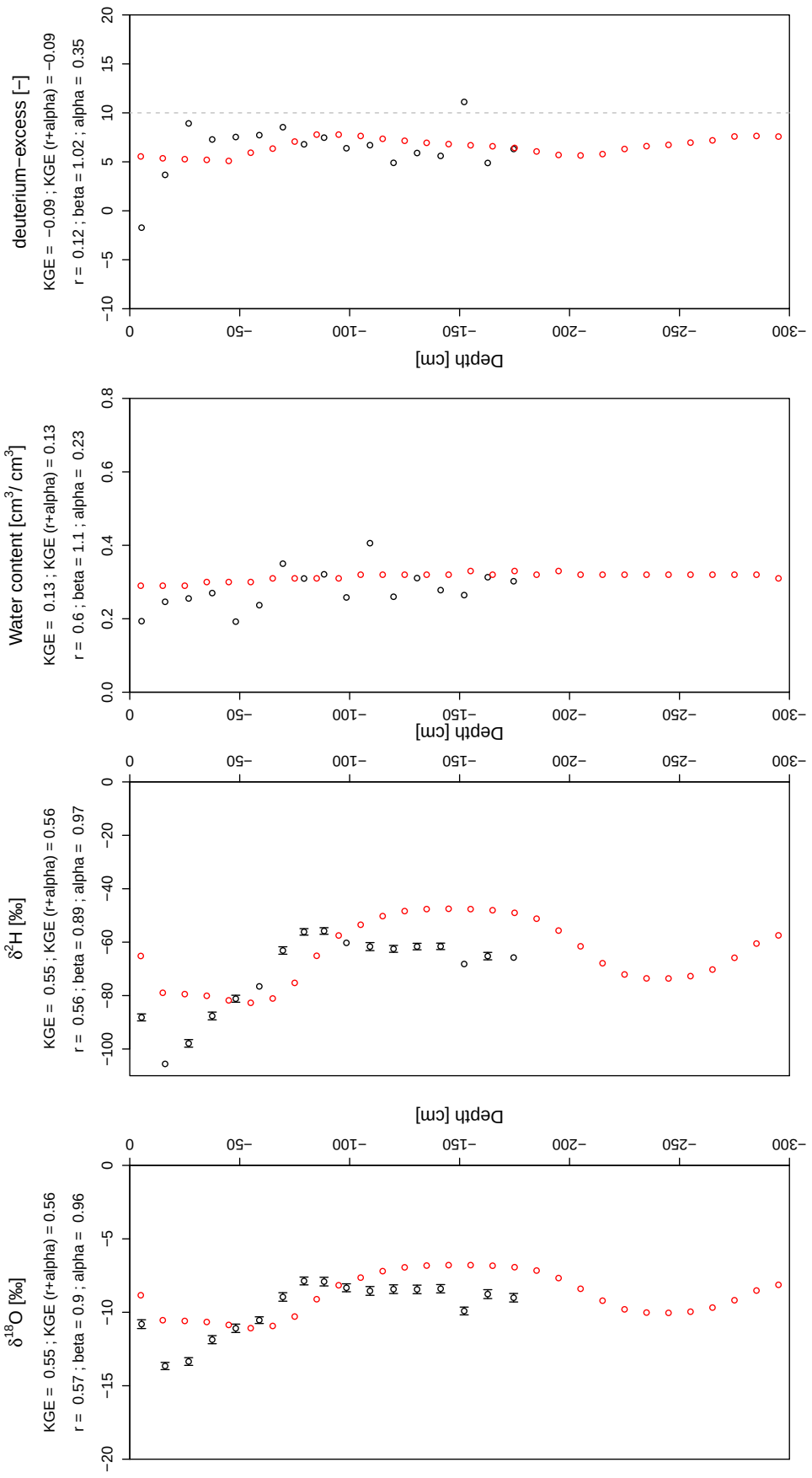

FIGURE C.40: Depth profile of observed (black) and modeled (red) $\delta^{18}O$, $\delta^{2}H$, volumetric water content and deuterium-excess values from best fit run of model step IV for profile 2 sampled in spring 2015 in Welschingen.

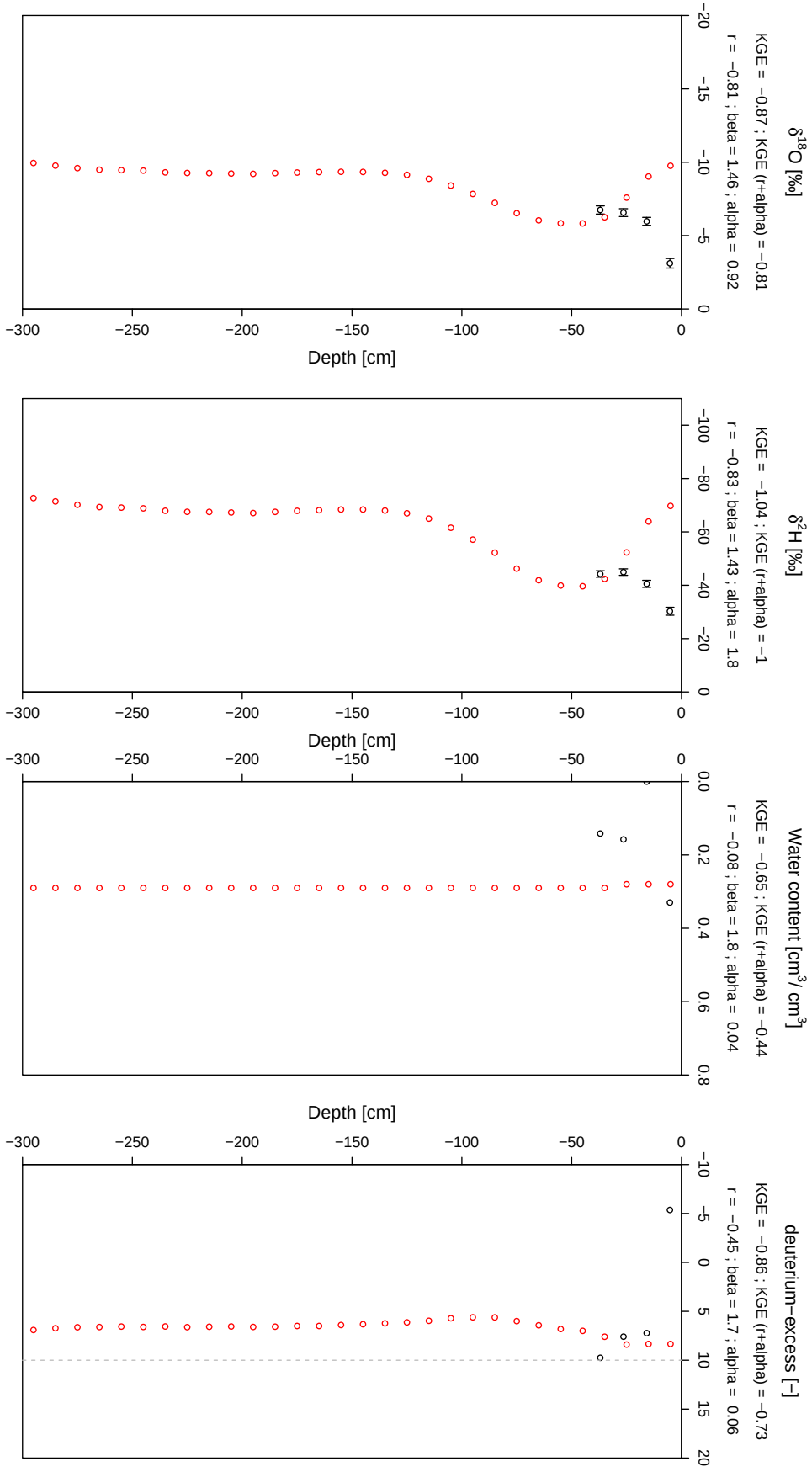

FIGURE C.41: Depth profile of observed (black) and modeled (red) $\delta^{18}O$, $\delta^{2}H$, volumetric water content and deuterium-excess values from best fit run of model step IV for profile 3 sampled in autumn 2015 in Welschingen.

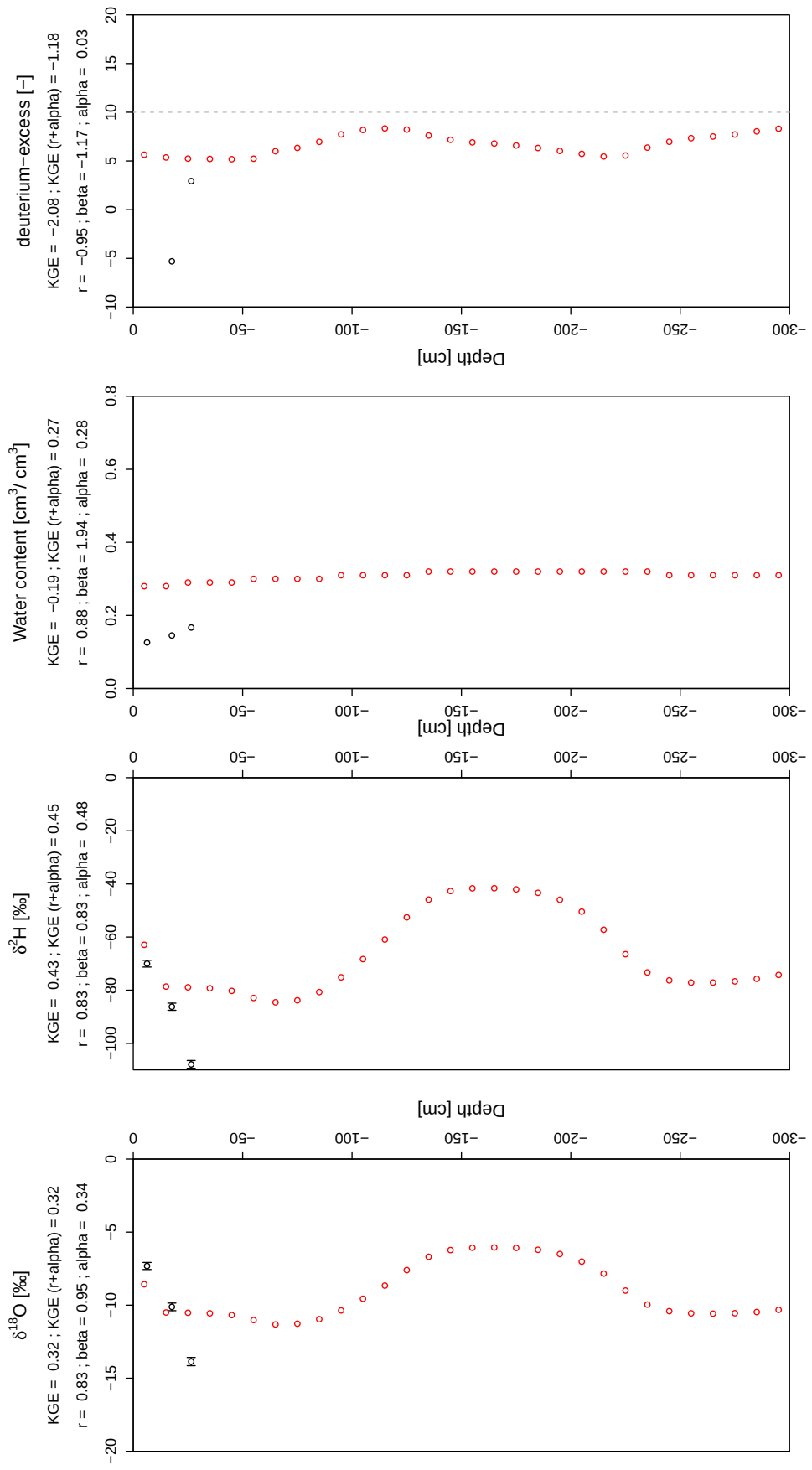

FIGURE C.42: Depth profile of observed (black) and modeled (red) $\delta^{18}O$, $\delta^{2}H$, volumetric water content and deuterium-excess values from best fit run of model step III for profile 3 sampled in spring 2015 in Welschingen.

Appendix D

Model step II - IV - selected sensitivity plots

In the following only a selection of sensitivity analysis plots is shown. Patterns of insensitive parameters are exemplified by transpiration depth in figure D.1. At the attached CD remaining sensitivity analysis plots are stored and can be viewed if necessary.

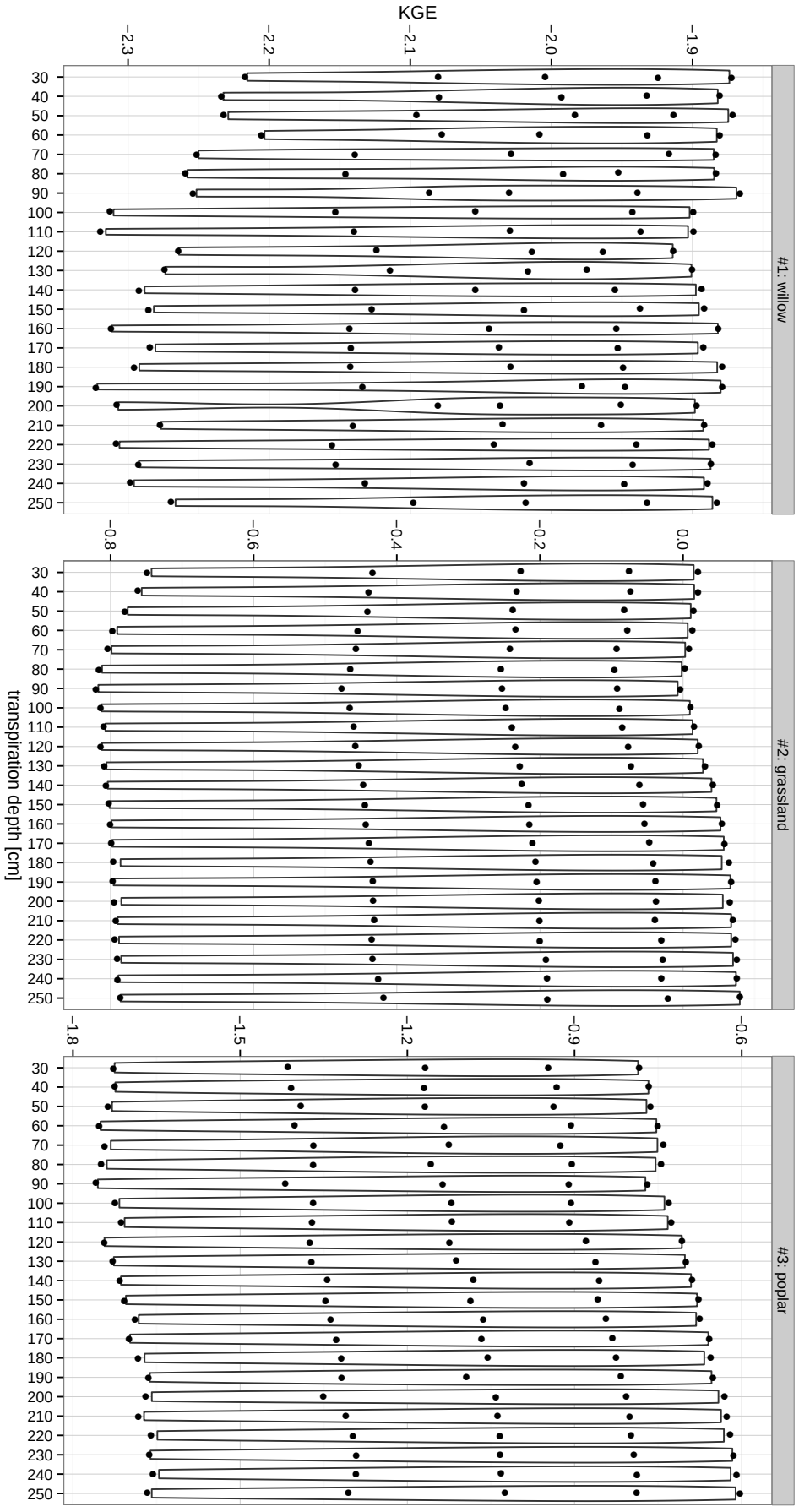

FIGURE D.1: Sensitivity analysis (Model Step III) of transpiration depth at Kupferzell. Model efficiency $KGE = KGE_{mean}$.

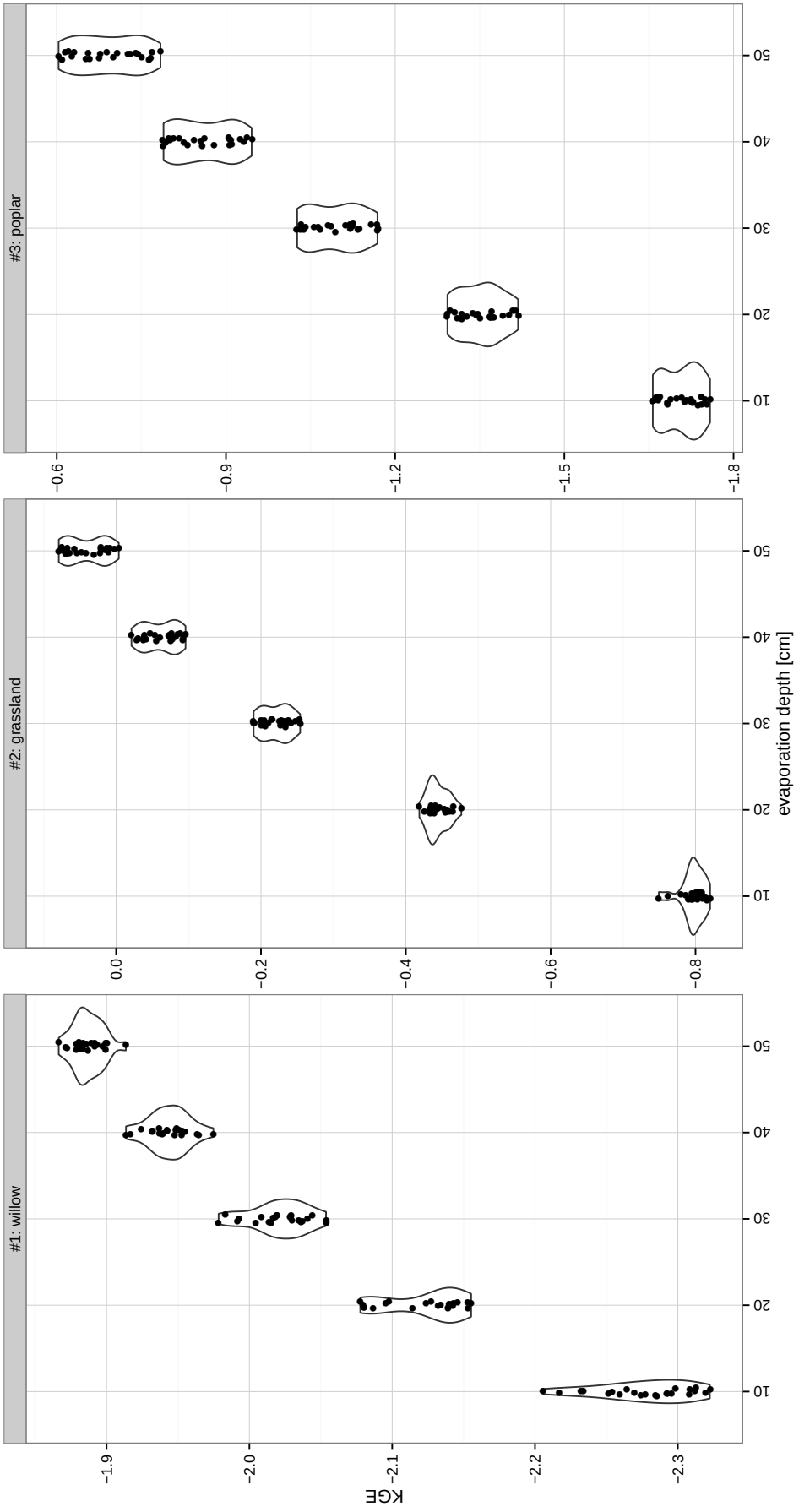

FIGURE D.2: Sensitivity analysis (Model Step III) of evaporation depth at Kupferzell. Model efficiency $KGE = KGE_{mean}$.

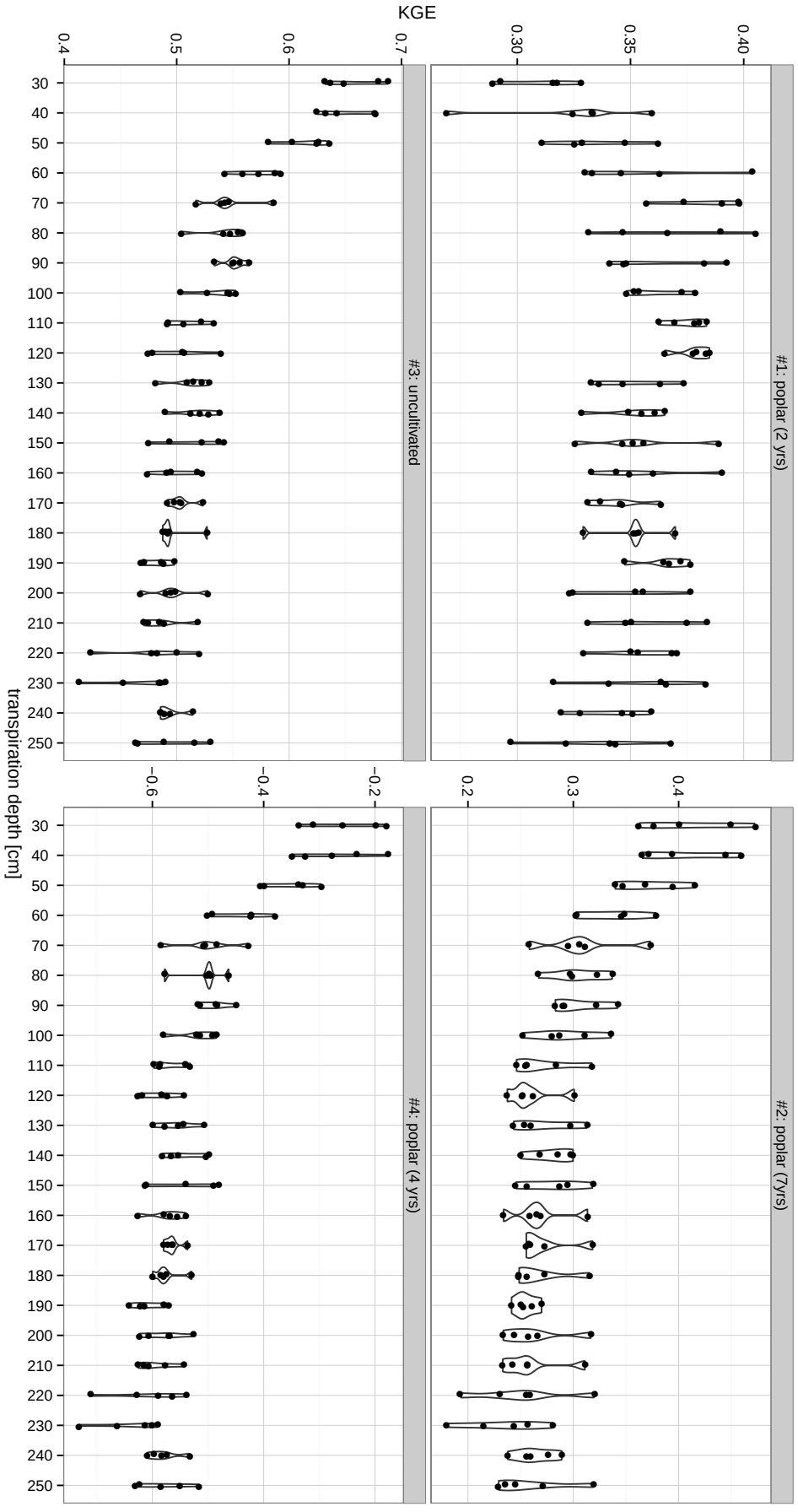

FIGURE D.3: Sensitivity analysis (Model Step III) of transpiration depth at Kraichtal. Model efficiency $KGE = KGE_{mean}$.

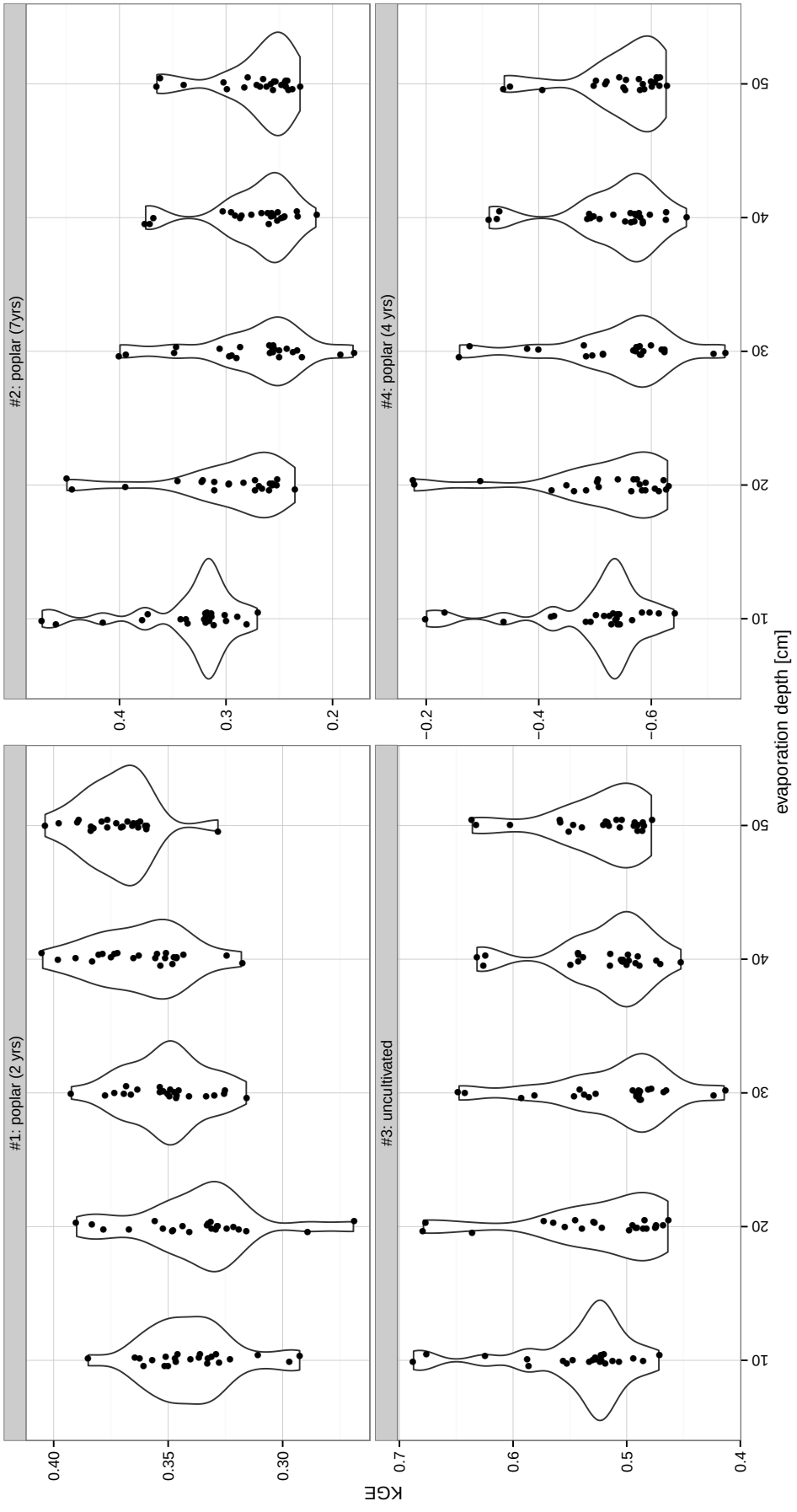

FIGURE D.4: Sensitivity analysis (Model Step III) of evaporation depth at Kraichtal. Model efficiency $KGE = KGE_{mean}$.

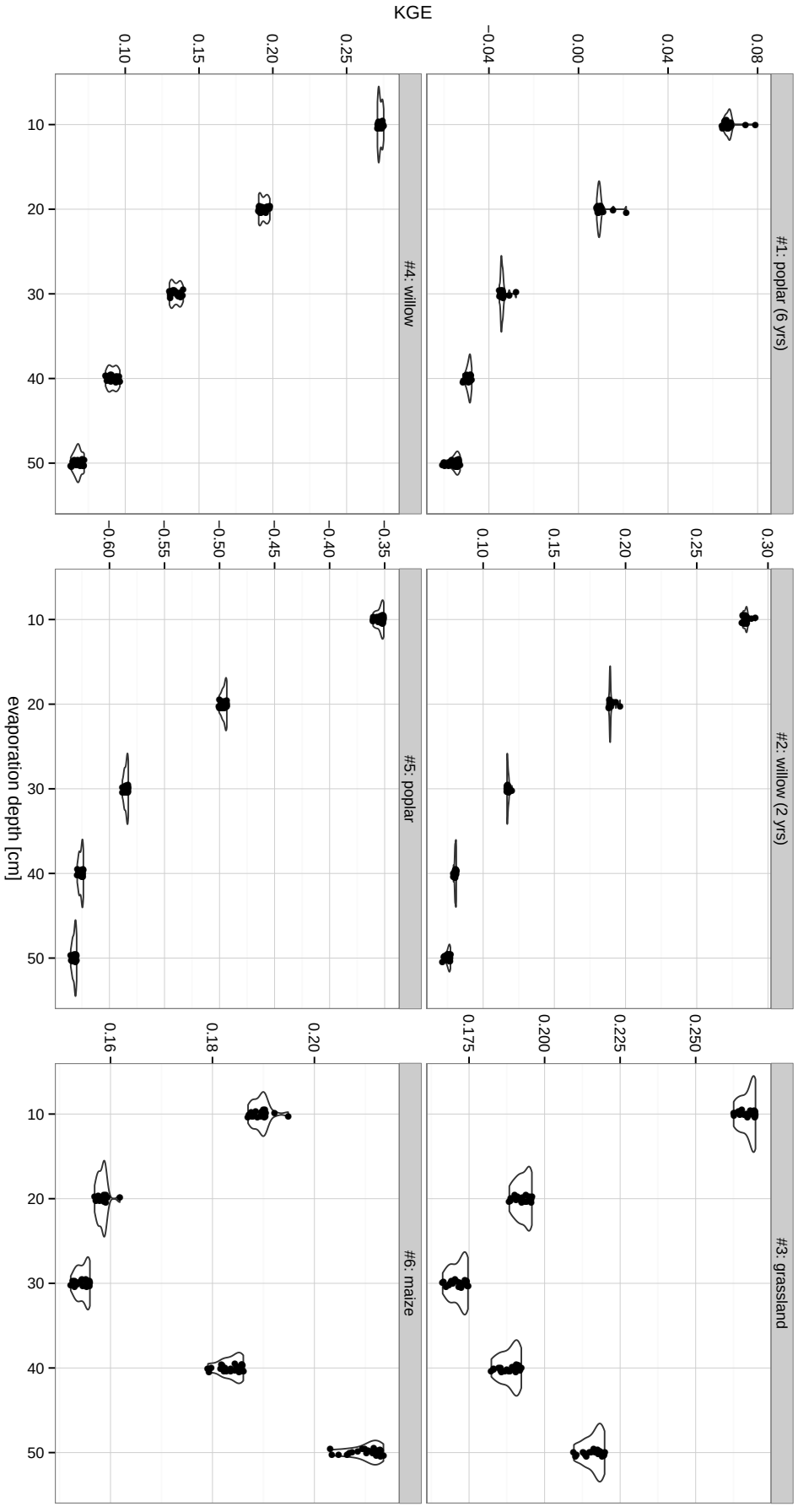

FIGURE D.5: Sensitivity analysis (Model Step III) of evaporation depth at Forchheim. Model efficiency $KGE = KGE_{mean}$.

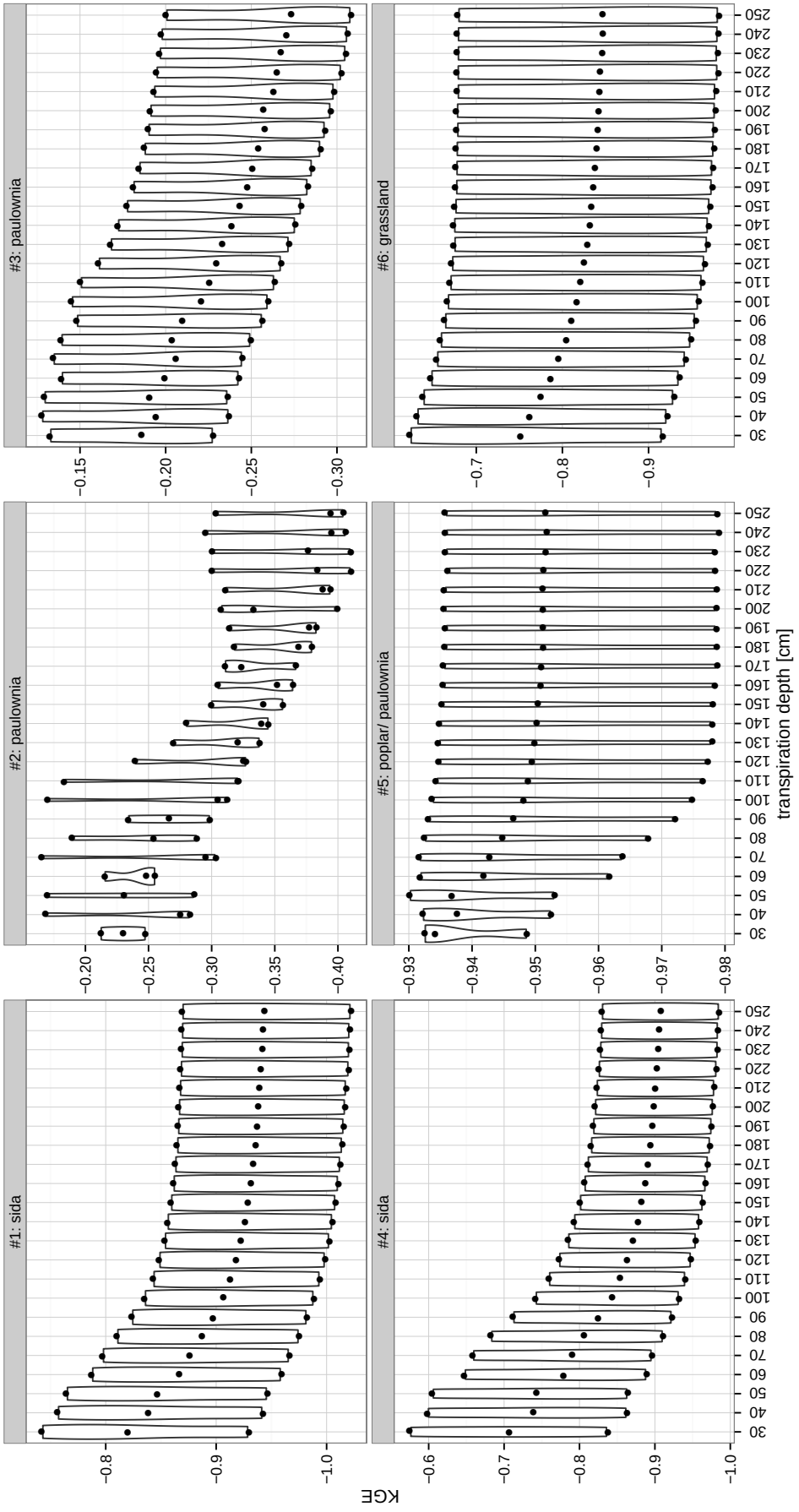

FIGURE D.6: Sensitivity analysis (Model Step III) of transpiration depth in Laufen 2014. Model efficiency $KGE = KGE_{mean}$.

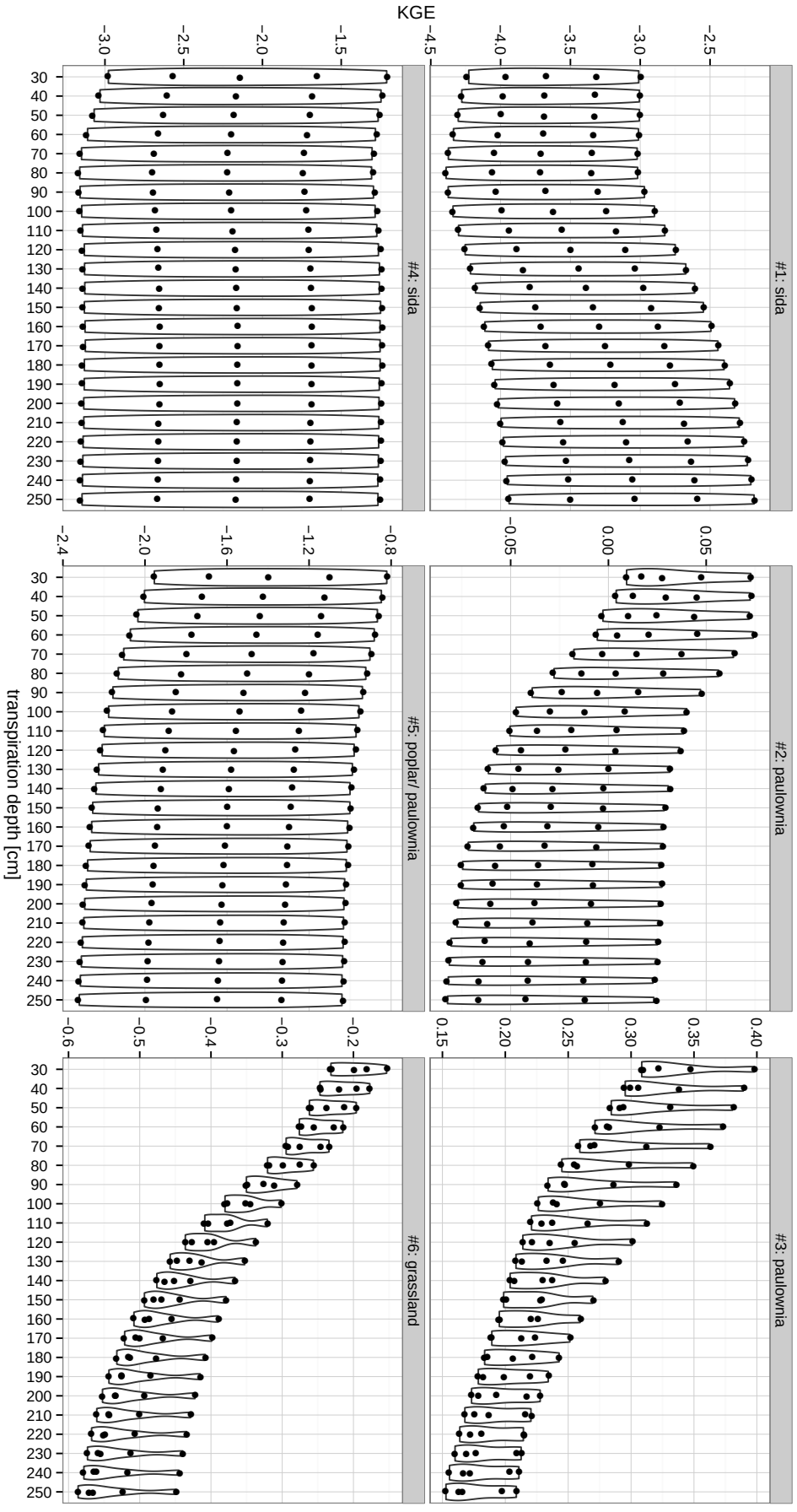

FIGURE D.7: Sensitivity analysis (Model Step III) of transpiration depth in Laufen 2015. Model efficiency $KGE = KGE_{mean}$.

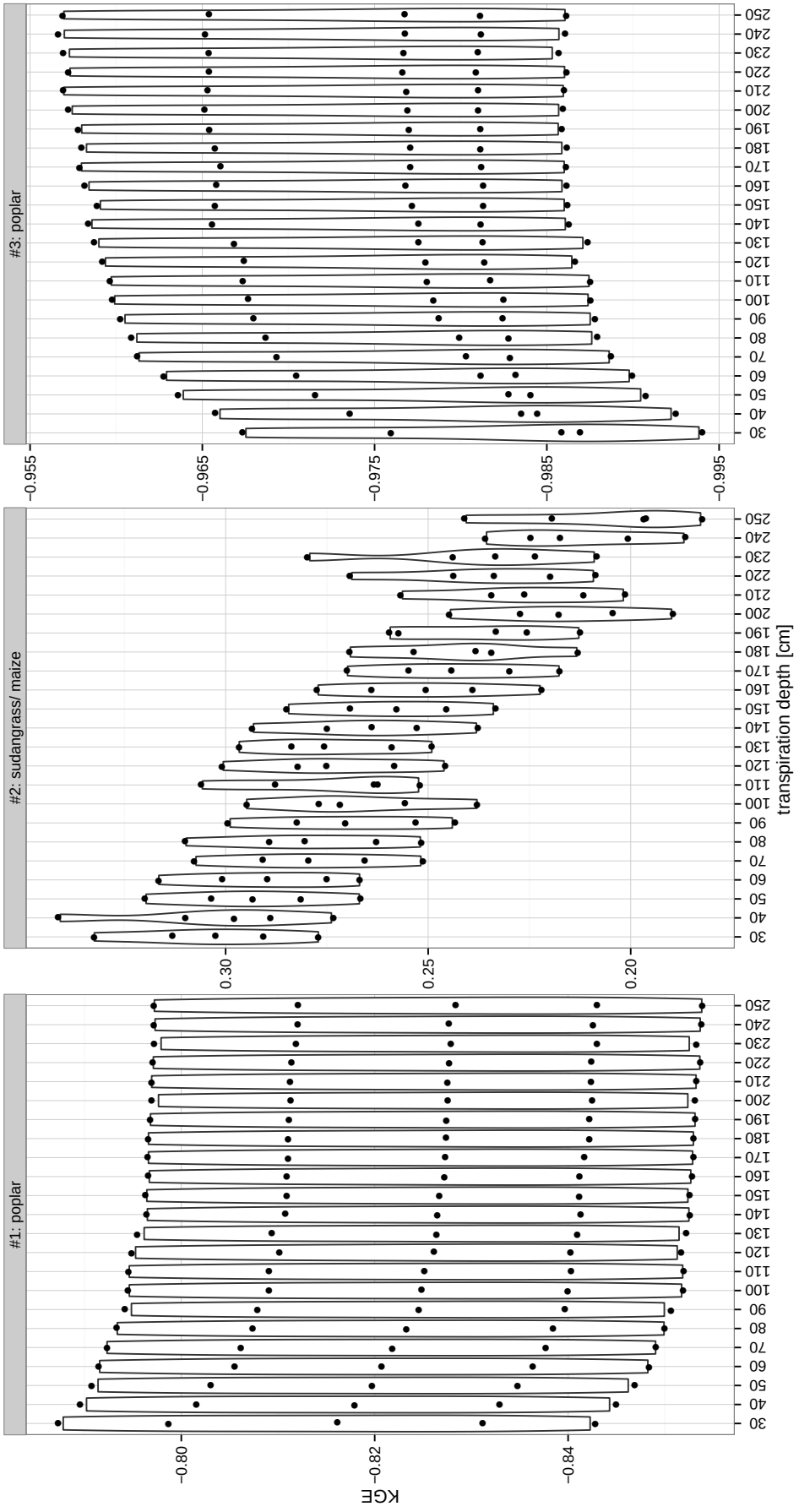

FIGURE D.8: Sensitivity analysis (Model Step III) of transpiration depth in Welschingen 2014. Model efficiency $KGE = KGE_{mean}$.

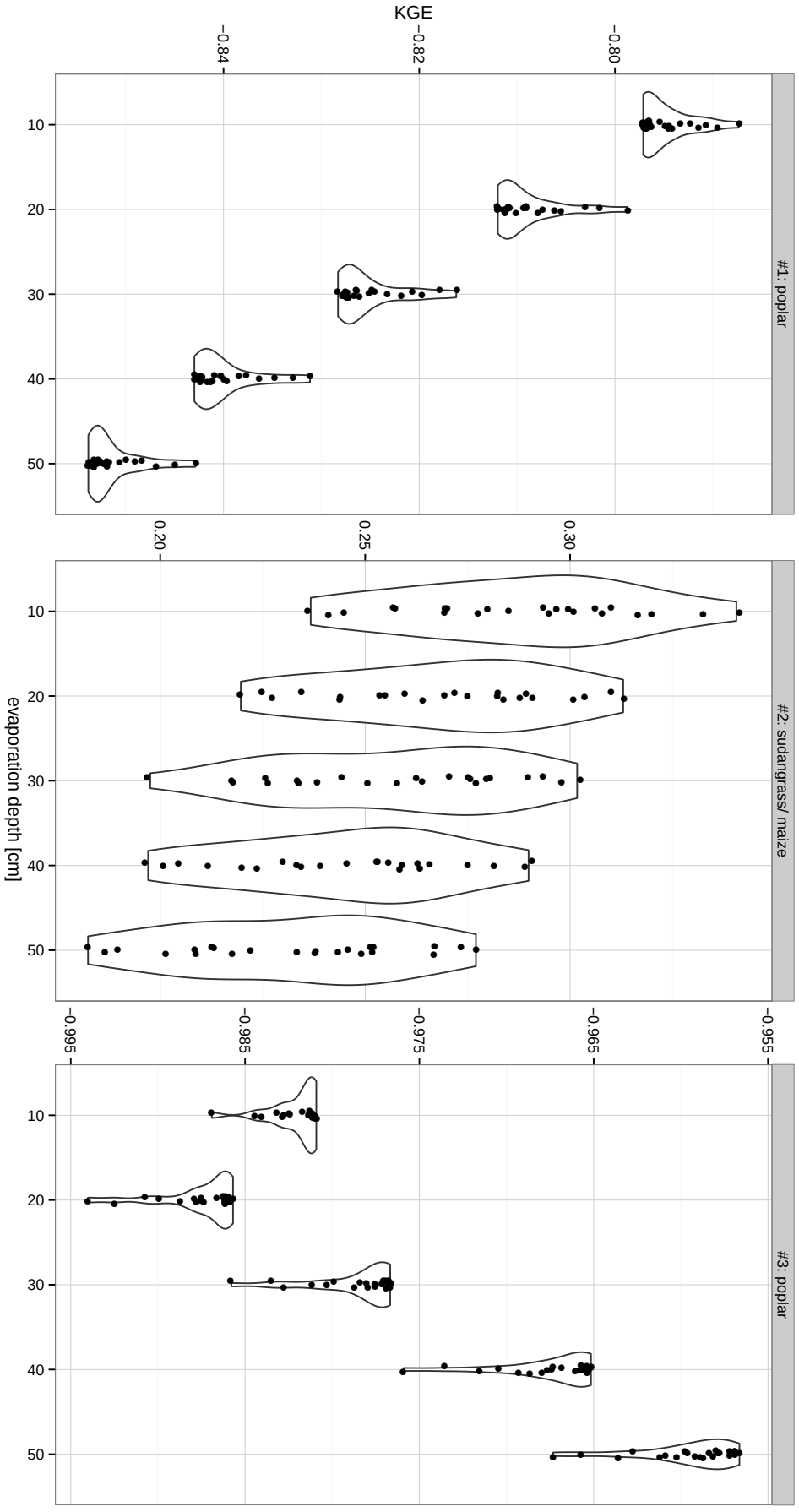

FIGURE D.9: Sensitivity analysis (Model Step III) of evaporation depth in Welschingen 2014. Model efficiency $KGE = KGE_{mean}$.